The Dissertation Committee for Siyuan Huang Certifies that this is the approved version of the following dissertation:

Application of Hot-melt Extrusion in the Manufacturing of Amorphous Solid Dispersions Containing Thermally Labile Drugs

Committee:

Robert O. Williams III, Supervisor

Feng Zhang

Hugh D. C. Smyth

James W. McGinity

Justin M. Keen

Application of Hot-melt Extrusion in the Manufacturing of Amorphous Solid Dispersions Containing Thermally Labile Drugs

by

Siyuan Huang, B.S.

Dissertation

Presented to the Faculty of the Graduate School of

The University of Texas at Austin

in Partial Fulfillment

of the Requirements

for the Degree of

Doctor of Philosophy

The University of Texas at Austin

January, 2017

Dedication

To my loving parents, Yong and Cheng, my wife and soul mate, Fan. Your unconditional support throughout this journey have made all of this possible.

Acknowledgements

First, I would like to thank Dr. Robert O. Williams III and Dr. Chuanbin Wu for introducing me to pharmaceutics and providing me the chance to spend the enjoyable four and a half years pursuing my Ph.D. degree here at the University of Texas at Austin which is halfway across the world from my hometown. I want to express my great appreciation to my supervisor Dr. Robert O. Williams III for his patience, mentorship, and encouragement throughout my Ph.D. study. I would also like to thank my committee members, Dr. Feng Zhang for his guidance on my research projects and career life, his broad knowledge and life experience significantly influence me both as a scientist and a person; Dr. Hugh D. C. Smyth for his valuable advice on my research plans and course designs; Dr. James W. McGinity for the deep talks on altitudes to be a qualified scientist, I am enlightened by his dedication to pharmaceutics industry; Dr. Justin M. Keen for his hands-on training and creative suggestions, his expertise helped me narrow my research goals.

I am also extremely fortunate to have Dr. Dave A. Miller, Dr. Chen Mao and Dr. Karthik Nagapudi as my mentors throughout my internships. Those internships significantly broaden my horizon, and prepared me for my post-graduate career. Also, I would like to express my appreciation to Dr. Kevin O'Donnell, Dr. James Dinunzio, Dr. Thiago Carvalho, Dr. Chris Brough, Dr. Bo Lang, and Dr. Jiping Liu for their constant help and constructive suggestions to my career development.

I would also like to thank my fellow graduate students in the College of Pharmacy. Especially Ms. Abbe Haser for all her assistance and our many hours of detailed scientific and non-scientific discussions which I will never forget. I would also like to acknowledge my other fellow graduate students for their assistance and friendship, including: Dr. Ryan Bennett, Dr. Matt Herpin, Dr. Simone Carvalho, Dr. Javier Morales, Dr. Yibo Wang, Dr. Youseff Naquib, Dr. Askan Yazdi, Dr. Justin LaFountaine, Dr. Leena Prasad, Dr. Soraya Hengsawas, Dr. Ju Du, Dr. Ping Du, Dr. Sha Liu, Dr. Alan Watts, Mr. Julien Maincent, Mr. Chaeho Moon, Mr. Zachary Warnken, Mr. Daniel Espinoza, Ms. Tania Bahamondez-Canas Ms. Tamara Tarbox, Mr. Daniel Ellenberger, Mr. Fan Meng, Mr. Xiangyu Ma, Mr. Sachin Thakkar, Mr. Tongzhou Liu, Mr. Xu Liu, Ms. Yajie Zhang, Ms. Sawittree Sahakijpijarn, Ms. Nada Kittikunakorn, Dr. Yuan Zhu, Dr. Yang Lu, Mr. Schott Jermain, Ms. Patrícia Martins, Dr. Masataka Hanada, Dr. Hiroyuki Takabe, Mr. Aaron Hong, Ms. Joana Silveira and Ms. Sophie M Delpon de Vaux. You were all great people to work with.

I also want to acknowledge the administrative staffs at the College of Pharmacy including Ms. Stephanie Crouch, Ms. Yolanda Camacho, Mr. John Reineke, Mr. Herman Schwarzer III, Mr. Jay Hamman, Ms. Belinda Gonzalez-Lehmkuhle.

Most importantly, I would like to thank my family members. My parents, Yong Huang and Cheng Li, who supported my decisions unconditionally throughout my life. My wife, Fan, for always being patient and taking care of our small home here in the US. My in-laws, Haiqin Lu and Yuesheng Fan, for all their encouragement. My grandparents for raising me when I was a kid. For the past eight years, I have not been around, but hopefully I can spend more family time with you in the future. Finally, my dearest paternal

grandmother, you left me 13 years ago, I wish you could be here sharing all the joys with me at this moment. Rest in peace, my guardian angel.

Application of Hot-melt Extrusion in the Manufacturing of Amorphous Solid Dispersions Containing Thermally Labile Drugs

Siyuan Huang, Ph.D.

The University of Texas at Austin, 2017

Supervisor: Robert O. Williams III

Hot-melt extrusion has gained favor over traditional pharmaceutical formulation techniques in bioavailability/solubility enhancement because it is a solvent-free and continuous operation process that does not require major downstream processing. However, the thermal and mechanical energy applied during the extrusion process can cause chemical degradation of drugs and polymeric carriers

In Chapter 1, different methods of preparing amorphous solid dispersions were reviewed. The amorphous solid dispersions generated by different methodologies were compared in terms of physical stability, chemical stability, and the in vivo/in vitro performance.

In Chapter 2, the solubility advantage of amorphous solid dispersions was investigated through the heterogeneous phase equilibria analysis. A thermodynamic model for the quantitative assessment of solubility advantage of amorphous solid dispersions was then presented. The thermodynamic model accounted for the chemical potential change as a result of (a) amorphization, (b) ASD formation, and (c) water partition. Experimental solubility advantages of amorphous solid dispersions containing indomethacin was studied by means of intrinsic dissolution measurement. The thermodynamic model allowed predicting the solubility advantage of amorphous solid dispersions.

In Chapters 3 and 4, the strategies used in hot-melt extrusion to facilitate manufacture of amorphous solid dispersions containing thermally labile drugs were investigated. Formulation screening based on Flory-Huggins theory, and the utilization of polymer designed for the extrusion process was evaluated in Chapter 3. With the selection of proper formulations, amorphous solid dispersions containing 30% (w/w) carbamazepine were manufactured without any degradation. Improved dissolution properties were also revealed with the final formulations. In Chapter 4, gliclazide was identified as a thermally labile drug with severe degradation by hydrolysis at elevated temperatures, especially when it existed in amorphous or solution form. After optimization of the hot-melt extrusion process, including improved screw design, machine setup, and processing conditions, gliclazide amorphous solid dispersion with ~95% drug recovery was achieved. This study demonstrated the importance of the following factors on drug degradation: (a) changing screw design to facilitate shorter amorphous (melt) residence time, (b) lowering processing temperature to avoid excess thermal exposure, and (c) minimizing processing parameters to reduce unnecessary mechanical energy input.

Table of Contents

List of Tables

List of Figures

Chapter 1: Effect of Preparation Process on Properties of Amorphous Solid Dispersions

1.1 ABSTRACT

The use of amorphous solid dispersions to improve bioavailability of active ingredients belonging to BCS II and IV classifications continues to gain interest in the pharmaceutical industry. Over the last decade, methods of generating amorphous solid dispersions have been well established in commercially available products and literature. However, the amorphous solid dispersions manufactured by different technologies differ in many aspects, such as chemical stability, physical stability, and in vitro/in vivo performance. This review will analyze the impact of manufacturing methods on those properties of amorphous solid dispersions. For example, the chemical stability of drugs and polymers can be influenced by the different level of thermal exposure during fusion- and solvent-based processes; the physical stability of amorphous content will vary based on the thermal history, particle morphology, and nucleation process of amorphous solid dispersions made by different methods; the in vitro/in vivo performance of the amorphous formulations will also be affected by the different particle morphology and molecular interactions caused by manufacturing methods. Additionally, the mechanism of manufacturing methods along with the thermodynamic theories related to amorphous formulations will be described in this review.

1.2 INTRODUCTION

High throughput screening techniques and combinational chemistry have been widely used in the pharmaceutical industry for drug candidate selection during the drug discovery phase, resulting in an increasing number of active pharmaceutical ingredients being discovered with relatively high molecular weight and lipophilicity (1, 2). These properties enable drugs to bind to their target receptors more effectively, but at the same time often reduce their solubility in water (3). It has been reported that about 70% of the newly developed active pharmaceutical ingredients exhibit poor water solubility (4).

The oral route of administration is the most common and preferred method of delivery due to the ease of administration and compliance by patients (5). For an orally administered drug to be absorbed from the gastrointestinal (GI) tract and exhibit a therapeutic effect, a sufficient amount of drug must be first dissolved in gastric and/or intestinal fluids and then permeate the membranes of the GI tract to reach systemic circulation. Therefore, a drug with poor aqueous solubility will typically exhibit solubility or dissolution rate limited absorption, causing poor bioavailability, and high absorption variability among patients (6).

Various techniques have been reported to enable the successful delivery of poorly water-soluble drugs (7, 8). These can be categorized into four strategies, namely drug solubilization, molecular modification, morphology modification, and intermolecular modification. In the case of drug solubilization, co-solvents, lipid vehicles, micelles

(surfactants) and complex formation are often employed. This formulation strategy has been widely reported in the production of liquid formulations (9). Molecular modification normally comprises the change of chemical structure. By adjusting the molecule's polarity, the solubility and permeability of the entire molecule will be altered, typically presenting a different pharmacokinetic behavior. Examples of molecular modification include pro-drug (10), twin-drug (11), salts (12), and co-crystals (13). For the morphology modification strategy, the goal is to increase the surface area of the particle by reducing the particle size, which according to the Noyes–Whitney equation (14), will enhance the drug dissolution rate and therefore bioavailability for drugs with dissolution rate limited absorption (15). Size reduction can be accomplished by either top-down or bottom-up methods, resulting in particles in the nano- to micron-size range (16). The intermolecular modification strategy, such as forming polymorphs or amorphous formulations, can be applied, when strong intermolecular interactions exist in between the drug molecules impacting the dissolution process (17). Among these four formulation strategies, intermolecular modification involving amorphous solid dispersion is a typically tried strategy to address solubility challenges, as evident by considering both approved commercial products and the literature (18, 19). Amorphous formulations not only provide improved drug dissolution rate and solubility, but also maintain the possibility of producing solid dosage form without changing the chemical structure of drug molecule (20).

Amorphous formulations are mainly manufactured by solvent- and fusion-based methods. For solvent-based method, drug and polymer are dissolved in a solvent (or solvent

combination), forming a homogeneous solution system. Different strategies can be used to rapidly remove (by evaporation or isolation) the solvent in the solution to form amorphous solid dispersion. Typically, the secondary drying process in a batch step is required to further remove the residual solvent. As for fusion-based methods, heat and shear are applied to soften or melt the polymer and drug. With the following mixing and cooling, the drug can be solubilized in the polymer and solidified into the amorphous solid dispersion. Therefore, amorphous solid dispersions made by different methods will be exposed to different conditions, resulting in various chemical stability, physical stability, and in vitro/in vivo performance.

This review will outline the advantages and challenges for amorphous formulations, together with a discussion of methods for generating amorphous solid dispersions. In addition, comparisons of chemical stability, physical stability, and in vitro/in vivo performance of ASDs manufactured by these methodologies will be reviewed with observations of current market trends.

1.3 AMORPHOUS SOLIDS AND AMORPHOUS SOLID DISPERSIONS

Amorphous solids differ from their crystalline polymorphic counterparts by the lack of long-range crystalline order. That is, molecules are completely randomly distributed and exist in various conformational states. Crystalline materials, on the other hand, have three-dimensional long-range symmetry operators over a domain of more than a thousand individual molecules. Due to the different packing arrangement compared to crystalline materials, amorphous solids lack sharp crystalline diffraction peaks, distinct melting point, and birefringence when analyzed by X-ray diffraction, differential scanning calorimetry, and polarized light microscope, respectively. Such diverse molecule arrangements also explain the different physicochemical properties between amorphous and crystalline solids, such as the density, hardness, and thermal properties.

1.3.1 Pure Amorphous Drug

Pure amorphous drugs represent the highest energy form of drugs in solid state. Thus, as mentioned before, benefits in solubility and dissolution rate are expected for pure amorphous drugs. Despite the mentioned advantages mentioned of amorphous solids, only few commercial products on the market containing pure amorphous drugs. Zafirlukast (Accolate®) was approved as a pure amorphous drug in 1999 by FDA (21). Crystalline zafirlukast is a poorly water-soluble drug [about 0.6 microgram/mL in FaSSIF (22)] with low oral bioavailability. When converted to the amorphous form in the commercial product, greater bioavailability is achieved (23). However, the pure amorphous zafirlukast recrystallizes into its monohydrate crystalline form in the presence of water, resulting in

decreased solubility and bioavailability (24). Some recent studies have shown that the incorporation of polymers (hydroxypropylmethyl cellulose acetate succinate, hypromellose, and polyvinylpyrrolidone) in the amorphous formulation can inhibit drug precipitation during the dissolution process, and increase drug concentration in the supersaturated state (22, 25). There are several other examples of marketed pure amorphous drugs, such as quinapril hydrochloride (Accupril®), cefuroxime axetil (Ceftin®), and nelfinavir mesylate (Viracept®). Due to the inherent high energy state of pure amorphous drug, these products have been reported to have thermodynamic instability issues leading to relaxation, nucleation, crystallization (26) and even chemical degradation (27) during storage or within the GI tract. Therefore, the application of pure amorphous drugs has been mainly limited to those reported mainly in lab-scale pre-formulation studies.

1.3.2 Amorphous Solid Dispersion

Amorphous solid dispersion (ASD) refers to a one-phase solid system containing amorphous drug molecularly dispersed in a polymeric carrier(s). Compared to pure amorphous drug, the addition of polymeric carriers improves the drug long-term storage and dissolution properties in different ways. These include interactions of the polymer with the drug to lower the energy state (chemical potential) of the amorphous drug and the polymer providing stereo-hindrance (local viscosity) to reduce the collision between amorphous drug molecules. Polymers are also known to help maintain desirable supersaturation conditions by delaying solvent-induced recrystallization to improve drug absorption. Moreover, hydrophilic polymers such as Kollidone®, Kollidone® VA64,

AFFINISOL™ HPMC HME (28), and METHOCEL™ are widely used in ASD formulation strategies, and the incorporation of highly water-soluble polymers also facilitates the water uptake during dissolution process and therefore increases the drug dissolution rate.

1.4 METHOD OF GENERATING AMORPHOUS SOLID DISPERSIONS

Generally speaking, based on the drug dissolution process in a polymer carrier, the methods of manufacturing amorphous solid dispersions can be categorized into two classes: (a) fusion-based methods; (b) solvent-based methods. Commercially available ASDs made by different methods are listed in Table 1.1.

1.4.1 Fusion-based Methods

Typical fusion-based methods of manufacturing ASDs consist of two major steps: (a) melting the drug within the carrier at elevated temperature; (b) rapid cooling of the molten material to solidify into a one-phase system (29). During the melting process, high temperature will be applied to the material, resulting in a high molecular mobility of the drug to fulfill the amorphous conversion (30). A common adaptation to the melting phase consists of suspending the active drug in a molten polymeric carrier to allow the dissolution of the drug instead of melting the drug and polymer together, which can help break the drug crystalline lattice at a reduced processing temperature (31). Different cooling methods can be used to provide various cooling rates, which can be used to control the crystalline growth inside the molten material (32, 33). However, a limitation of manufacturing ASDs using fusion-based methods is the high temperatures and shear conditions involved in the process, which may induce material chemical degradation.

1.4.1.1 Hot-melt Extrusion (HME)

HME technology is an industry-scale manufacturing method adapted from the plastics industry. A typical extruder consists of a feeder, an extrusion barrel, a screw shaft equipped with screw elements, a die, and potential downstream processing equipment (34), as shown in Figure 1.1. During the process, drug and polymer physical blend is fed into the extruder consistently, and the machine will perform the operations of conveying, melting, mixing, and condensing. The molten material is then shaped through a die and collected for downstream processing. During the melting and mixing, a homogenous system is formed, and after extrusion, the rapid cooling will result in a raise in system viscosity, which contributes to the kinetically stabilized ASD (35).

1.4.1.2 KinetiSol® Dispersing Technology (KSD)

KSD technology, also adapted from the thermo-kinetic mixer used in the plastics industry, is a new processing technology to manufacture ASD from a pharmaceutical perspective (36). As shown in Figure 1.2, the equipment consists of a processing chamber with rotating blades mounted at the center which rotate at high RPMs (typical thousands of RPMs) during the process. This high energy mixing technique utilizes the shear and thermal energy inputs generated by the fast rotating blades to process the drug and polymer blend for the production of homogeneous amorphous solids. Typical processing time is less than twenty seconds, and the materials being processed are exposed to elevated temperature conditions for less than five seconds before being ejected from the KSD unit and cooled down (36). In addition, the mechanical design of KSD machine enables the

processing of polymers with high melt-viscosity, which allows a wider selection of pharmaceutical excipients to be used (37).

1.4.2 Solvent-based Methods

Typical solvent-based ASD manufacturing methods consists of three major steps: (a) dissolving (or suspending) of the drug and carrier in a volatile solvent; (b) isolating majority solvent to get solids; (c) secondary drying to further remove residual solvent (38). Differences in solvent removal processes are related to the solvent isolation procedure, which usually includes vacuum drying (39), rotary evaporation (40), spray-drying (41), freeze-drying (42), co-precipitation (43), and the use of supercritical fluids (44). For solvent-based methods, the relatively lower processing temperature and/or cooling effect during solvent evaporation can help mitigate the thermal decomposition issue during the process (45). However, the use of organic solvents, the high preparation cost, and the difficulties in completely removing the solvent are some of the disadvantages associated with solvent-based manufacturing methods (38).

1.4.2.1 Spray Drying

Spray-drying is one of the most commonly-used solvent-based procedures in the production of ASDs. Three major components are involved in a spray dryer, namely feeding system (pump and spray nozzle), drying chamber, and collecting system (cyclone and collector) (46), as shown in Figure 1.3. A condensation system is required if organic solvents are used. For spray drying process, a molecular dispersed feed solution is first

achieved after dissolving the drug and polymer in the volatile solvent (such as ethanol, chloroform, acetone, or a solvent mixture). The feed solution is then pumped into the drying chamber through a spray nozzle, forming atomized droplets. Upon contacting the hot gas (air or nitrogen), solvent is then removed. Finally, the dried material is separated by a cyclone and collected in the collector for further process. Based on the solvent and processing conditions used, secondary drying may be required to further remove the residual solvent in the ASD.

1.4.2.2 Co-precipitation (Micro-precipitated Bulk Powder)

Another process is the co-precipitation method, which is based on solvent-antisolvent precipitation (47). As shown in Figure 1.4, the co-precipitation process starts from dissolving the drug an ionic polymer in nonvolatile solvent (such as dimethylacetamide, dimethylformamide, and dimethylsulfoxide). The solution is then transferred gradually into a pH-controlled and chilled aqueous media acting as an antisolvent to cause rapid co-precipitation (48). After the controlled co-precipitation process, the solids still contain relatively high amount of organic solvent which needs to be removed. Organic solvent removal is achieved by washing the solids with aqueous medium until residual organic solvent content is less than 0.1% (47). After washing with water, secondary drying process (forced air oven or fluid bed dryer) is required to remove the aqueous medium in the precipitates.

1.5 COMPARISON BETWEEN AMORPHOUS SOLID DISPERSIONS MANUFACTURED BY DIFFERENT METHODS

In the following sections, comparisons are made between solution-based and fusion-based manufacturing methods. To be more specifically, spray drying, co-precipitation, HME, and KSD.

1.5.1 Chemical Stability

Materials are subjected to various types of conditions during the conversion to amorphous form using different processing technologies. The elevated temperature and shear employed in the fusion process (e.g., HME and KSD), solution state in solvent drying process, and acidic or basic solution state in co-precipitation process can expose materials to chemical degradation. Moreover, the fact that amorphous drugs exist in a higher energy state makes them more vulnerable to chemical degradation compared to their crystalline counter-parts (49).

Spray drying has been known to be a mild processing technology for the generation of ASDs. Even though heat is induced during the process for the removing of solvent, the real temperature of the processed materials is normally low due to the solvent-evaporation cooling effect (50). However, the incompatibility of feed components in solution state can raise chemical stability issue for the spray drying technique. The application of novel-designed nozzle consisting of multiple liquid/gas pathways has been reported to allow spray drying of incompatible materials by separating the feed solution (51). A three-fluid

concentric nozzle was used in spray drying the acid labile drug omeprazole with the enteric-coating polymer Eudragit® L 100-55 (52). Component compatibility should also be addressed in co-precipitation technology since: (a) solution state is also involved during the co-precipitation process, (b) the amorphous MBP is formed by co-precipitation of drug and polymer in acidic (mostly) or basic media, (c) an estimation of several hours to several days of exposure in those conditions is expected for the whole process based on the scale of the manufacture (53). Therefore, it is critical to perform forced-degradation experiments in order to evaluate the component compatibility profile of the drug and polymer used in solution-based ASD manufacturing process.

Compared to solution-based methods, higher temperature and shear will be applied to material processed by fusion-based methods. According to the Arrhenius equation, elevated temperatures can significantly increase the degradation rate (54). Moreover, the shear energy input has also been shown to trigger chemical degradation for shear-sensitive materials (55). In a recent study (56), HME and spray drying were used to prepare albendazole ASD. Severe degradation (from 71.1% to 97.4%) was observed in the melt-extruded samples, while full recovery was achieved in ASD prepared by spray drying, and less than 1% degradation was observed in spray-dried ASD after 6-month storage at room temperature. The long residence time and high shear environment of the HME process exacerbated the thermal degradation of albendazole, resulted in low drug recovery. It should be noted though, the residence time and shear condition provided by HME have been shown to be adjustable through the application of different screw designs, machine

setup, and processing conditions (57). The thermally labile drug gliclazide was manufactured without severe degradation using HME after adapting the proper machine setup to reduce the processing pressure, applying the optimal screw design to minimize melt residence time, and selecting the optimized specific mechanical energy input to fulfill the amorphous conversion without providing excess shear force.

In the last decade, KSD, an emerging fusion-based manufacturing technology for production of ASDs, is recognized for being able to process materials at relatively lower temperatures with shorter periods of time compared to conventional fusion-based technology like HME (36). The chemical stability of a thermally labile drug and polymer during KSD process was recently reported (37). Ritonavir which was used as the thermally labile drug, undergoes hydrolytic degradation at elevated temperatures (58). A polymeric carrier (PVA 4-88) with high melt viscosity was chosen in the study bringing more challenges to thermal processing of ritonavir. HME process of PVA 4-88 requires either plasticizers or high processing temperatures (180 ℃) due to its semi-crystalline nature (59, 60), which will hamper the physical stability of the extruded ASD and the chemical stability of the drug being processed, respectively. In this case, HME process of ritonavir with PVA 4-88 without chemical degradation was not realistic since the lowest processing temperature of PVA 4-88 was 30 ℃ higher than the degradation onset temperature of ritonavir. With the help of KSD process, it has been shown that ASD containing ritonavir and PVA 4-88 can be successfully manufactured using. After proper KSD process optimization, ritonavir ASD was produced without any drug or polymer degradation.

Direct comparisons between the ability of processing thermally labile drug using HME and KSD has also been done in several publications (61-63), showing the unique ability of KSD for the processing of highly viscous polymers and thermally labile drugs.

The lower processing temperatures used in solution-based methods to manufacture ASDs relative to fusion-based methods benefit the chemical stability challenges of the processed materials by keeping the chemical degradation constant low. The chemical stability of ASDs made by fusion-based methods, however, can usually be addressed by optimizing the processing conditions of the solvent-free processes. In addition, KSD has been shown to result in ASDs with improved chemical stability, thus is used as an alternative strategy to manufacture ASDs.

1.5.2 Physical Stability

Physical stability of amorphous solid dispersions is a major concern in the industry (64). In order to maximize the benefits of ASDs, it is crucial to maintain the drugs in amorphous form during storage and following delivery. Formulation factors have been studied and reviewed, such as the selection of polymers as crystallization inhibitors (64) and the application of plasticizers as a processing aid (65). Besides the formulation factors, ASD preparation methods can also affect the physical stability of amorphous drugs through influences on thermal history, particle morphology, and nucleation process of ASDs.

1.5.2.1 Thermal History

It is widely accepted that the properties (e.g., solubility, physical and chemical stability) of formulations are closely related to the thermal history of the materials (65). For amorphous formulations, depending on the manufacturing processes used, materials will be exposed to different level of heat exposure, resulting in ASDs with different thermal histories. Amorphous molecules with different thermal histories have been reported to exhibit different molecular mobility which will further impact the crystallization propensity of the materials (66, 67).

As mentioned before, secondary drying process is required for solvent-based methods (e.g., freeze drying and spray drying), which can cause enthalpic relaxation leading to potential nucleation problems (68). For fusion-based methods (e.g., HME, KSD, and melt-quenching), however, temperature is dropped immediately upon melting the material to freeze the drug in amorphous state. To evaluate the effect of processing conditions on the physical stability of amorphous trehalose, four different methods, namely freeze drying, spray drying, dehydration, and melt quenching were used to manufacture amorphous trehalose (69). The thermal characterization revealed that processing technologies did not change the Tg and fragility of the amorphous materials. However, enthalpic relaxation, crystallization tendency, and water vapor sorption were influenced. In this case, secondary drying process was applied to freeze-drying process at 50 ℃ and 60 ℃ for a total of 48 hours. And, a relatively high outlet temperature (about 90 ℃) was used in the spray drying process. Also, the total exposure of material at about 100 ℃ for 24

hours was applied to dehydrate the drug. The different level of thermal exposures resulted in the different relaxations, as shown in Figure 1.5. The dehydrated sample exhibited the highest enthalpy relaxation, followed by spray-dried and freeze-dried samples, and melt-quenched sample underwent the least relaxation during preparation. The resistance to crystallization showed the same rank order as trehalose prepared by dehydration < freeze drying $\approx$ spray-drying < melt quenching. The impact of thermal history of ASDs on physical stability was also evaluated in another study (70). It was shown that the crystallization kinetics of amorphous trehalose was strongly correlated to the α-relaxation time, which was affected by the amorphous processing methods. As shown in Figure 1.6, in the sub-Tg region, spray-dried amorphous trehalose exhibited the longest α-relaxation time, followed by those made by freeze drying and dehydration, which was in agreement with rank order of the resistance to crystallization. Similar trend has also been reported in other literature (71-73). These results indicated that the preparation methods influenced physical stability by imparting different mobility states of the amorphous materials. Due to the exposure to elevated temperatures during the secondary drying process, amorphous materials produced by solvent-based methods exhibited more relaxation than fusion-based methods, causing higher crystallization tendency.

1.5.2.2 Particle Morphology

The effect of particle morphology on crystallization tendency has been evaluated from multiple aspects, including particle size (74), particle shape (75), and surface heterogeneities (76). In general, solvent-based manufacturing methods generate ASDs with

smaller particle size and relatively large surface area. For example, spray-dried particles exhibit inflated or collapsed sphere shape with porous structure, and based on processing conditions particle can be observed as a mixture of fractured spheres, broken and non-broken shells (77); MBP particles normally have a relatively smooth and round surface with a spongy network structure below the surface (78). Conversely, a low porosity material is generally achieved after fusion-based process (normally with intensive mixing, pressure, and or heat), due to the reduction of free space present in the polymer drug blends. Therefore, particle shape and size of the final products made by fusion technologies are typically irrelevant to the manufacturing process, but dependent on the milling process (79).

The presence of residual solvent and the relatively smaller particle size of the ASDs manufactured by solution-based methods have been proposed to negatively affect the physical stability in a study comparing physical stability of ASDs manufactured by HME and spray drying (80). The spray-dried ASD was achieved with the particle size of less than 10 microns, which was significantly smaller than the particle size HME ASD (> 250 microns), and the surface area of the spray-dried ASD was more than 22-fold higher than that of HME ASD, as shown in the Figure 1.7. The small particle size and high surface area significantly increased the surface energy of the spray-dried ASD, thus resulted in the higher crystallization rate. After being stored under accelerated conditions (40 ℃, 75% RH) for 8 weeks, spray-dried ASD started to show recrystallize peaks in X-ray diffraction. Similar result has been reported in another comparison study (81).

ASD made by another solvent-based method (co-precipitation) has also been reported to have reduced physical stability when compared to an HME ASD (43). Both HME and co-precipitated ASDs exhibited acceptable physical stability after storage at 40 ℃/75% RH for 3 months. However, the HME ASD was more stable than the co-precipitated ASD at accelerated conditions (aqueous suspension) due to the relatively smaller surface area.

These studies revealed that smaller particle size, larger surface area, and the potential residucal solvent of the ASDs made by solvent-based methods contributed to the higher surface energy, which can negatively affect physical stability.

1.5.2.3 Nucleation Process (converting power)

ASDs processing methods can affect product physical stability through impacting nucleation process. That is, different processing methods present different amorphous converting power, thus ASDs can be made containing not fully-converted crystalline drug. Due to the limitation of the typically-used characterization technologies (82), those small amount of trapped nuclei in the ASDs are difficult to detect, which can affect the crystallization tendency significantly (83). For example, at storage temperatures (below Tg), nuclei can act like seeds for crystal growth as glass can undergo α- or β-relaxation and molecules diffuse to the nuclei (84); or elevated temperature (above Tg), the nuclei will be exposed to the significantly enhanced crystalline growth rate causing crystallization (85).

The effect of spray drying and HME process of manufacturing ASDs on the kinetic miscibility of a poorly water-soluble drug miconazole and the graft copolymer polyethyleneglycol-co-vinylalcohol was investigated (86). The solid dispersions were prepared at different drug-polymer ratios (range from 4–43% w/w) using a lab-scale Büchi mini spray-dryer B-191 and a co-rotating mini twin screw extruder. The thermal analysis result showed that spray dried material with more than 12% w/w drug load exhibited an endothermic peak on top of the broad endothermic signal, pointing to the presence of a crystalline drug phase. HME products, on the other hand, the endothermic peak did not show up until 27% w/w drug load. Is has been shown that hot-melt extrusion results in a higher degree of mixing relative to the spray drying process. It was also confirmed in another publication comparing amorphous converting power between HME and spray drying, that HME provided sufficient energy for more intimate mixing to be achieved between drug and polymer, which could further improve physical stability of HME ASDs relative to spray-dried ASDs (87). In addition, it was proposed that spray drying allowed generation of ASDs with higher drug concentration than HME, but the FTIR results showed the existence of amorphous drug-rich domains within those high drug-loaded spray-dried samples, indicating phase separation. Interestingly, a recent publication addressed the difference in converting power between HME and spray drying through the relationship between the amorphous molecule mobility and viscosity (88). Crystallization occurs in two steps: nucleation and crystal growth (89), and the rates of both steps are related to transport frequency, which is inversely related to the solution viscosity. In addition, crystal growth rate is related to diffusion coefficient, which is also inversely

related to viscosity as described by the Stokes-Einstein Equation (90). Naproxen and PVP K25 were used in this study because naproxen is a fast crystallizer with strong interaction/miscibility with PVP K25 (91, 92). During HME process, naproxen was gradually dissolved in the melt PVP K25 at the processing temperature relying on the strong interaction of drug and polymer, since HME was conducted below the melting point of naproxen. And after the process, the product relied on the high viscosity of the formulation matrix to kinetically inhibit the crystallization of naproxen. Therefore, compared to the low viscosity environment naproxen experienced throughout the spray drying process, the viscosity during extrusion remains orders of magnitude higher, even with plasticization of PVP K25 from NPX during extrusion, ensuring that NPX has limited mobility. In summary, the physical stability difference caused by converting power between HME and spray drying is mainly caused by the fast recrystallization happened during the drying process due to the high molecular mobility.

Co-precipitation has similar recrystallization issue to spray drying during the process. Moreover, the relatively longer solvent exposure in co-precipitation process brings more physical stability challenges to the co-precipitation process (93). Therefore, the selection of drug and polymeric carriers are crucial to the success of stable co-precipitated ASD.

When comparing the amorphous converting power between fusion-based methods, the high shear rate inherent to KSD has been known to accelerate the dissolution kinetics

of drugs in molten polymeric carriers (36). Consequently, a high converting power is expected for this technique. ASDs were achieved at lower processing temperature with KSD where the processing of HME were not possible (37) or the extrudates came out with phase separation (94) with HME HAAKE Minilab II Micro compounder. However, it should be noted that the amorphous converting power of HME is highly dependent on the screw design, processing conditions, and the model of the extruder used (95). It has been demonstrated that ASDs made by the same extruder and screw design with two different screw speeds could result in completely different physical stability performances due to the homogeneity of the drug in the ASD system (96).

1.5.3 In vitro/In Vivo Performance

The ultimate goal of preparing ASD is to enhance the bioavailability of drug. Therefore, it is crucial to compare the in vitro/in vivo performances of ASDs made by different methods. It has been reported that several factors can affect the in vitro/in vivo performance of ASDs, such as particle size, system homogeneity, and intermolecular interactions (97). The effect of methods of manufacturing ASDs on the in vitro/in vivo performance will be discussed based on that.

As expected, ASDs made by different methods exhibited various particle sizes, which have been shown to cause different in vitro performances as shown in a study with a poorly water-soluble compound A (~0.2 microgram/mL in 50 mM pH 6.8 phosphate buffer) (43). ASDs with acceptable physical stability were prepared successfully with 40%

(w/w) compound A in HPMCAS-LF using both HME and co-precipitation methods. The ASDs manufactured by both methods exhibited similar true density (~ 1.30 g/cm3). But a much higher specific surface area of 6.19 m2/g was achieved for co-precipitated ASD compared with 0.13 m2/g for the HME product. The high surface area of co-precipitated ASD resulted in a faster dissolution rate, which was also observed in a comparison study between spray-dried ASD and HME ASD (98), confirming that the smaller particle size and the higher surface area generated by the solvent-based methods contributed to the faster dissolution rates of some poorly water-soluble drugs.

A challenge for ASDs is the ability to resist crystallization upon contacting the dissolution media. Rapid release of API in the supersaturation state certainly can be an advantage in improving absorption (97). However, it may be equally important for the polymer to provide stabilization against solvent-mediated crystallization by remaining in close contact with the drug. For example, in a comparison study of ASDs made by spray drying, HME, and ball milling technique with PVP and three poorly water-soluble compounds, namely carbamazepine, dipyridamole, and indomethacin (99), it was found that the dissolution rates of the spray-dried ASDs were the lowest for ASDs of all three drugs, even though smallest particle sizes were observed with the spray-dried ASDs. The slow dissolution rate was attributed to the rapid dissolution of the highly water soluble PVP, leaving behind amorphous drug without the intimate presence of the polymer, which likely caused in rapid recrystallization of the drug and would have certainly reduced the overall dissolution rate and wetting of the drug. Similar observations have also been

reported (100). Moreover, it was believed that the intermolecular interactions between drug and polymer would determine the dissolution rate. Namely, the stronger hydrogen bonding between indomethacin and PVP limited the rapid loss of PVP from the indomethacin spray-dried ASD due to the increase in hydrophobicity of PVP. Therefore, spray-dried indomethacin ASD showed comparable dissolution rate to ASDs prepared by the other two methods, while spray-dried carbamazepine ASD exhibited significantly slower dissolution rate due to the lack of intermolecular interaction with PVP.

The manufacturing method can influence the stabilization effect of polymers by generating ASD systems with different levels of homogeneity. As mentioned earlier, fusion-based technologies such as HME can provide more mixing of drug and polymer during ASD manufacturing, resulting in systems with better homogeneity relative to solution-based methods. The better homogeneity has also been shown to benefit the in vivo performance of ASDs (35). For example, ASDs of a poorly water-soluble Compound I (aqueous solubility of 0.03 mg/mL at pH 1, and < 0.003 mg/mL in the pH range of 3 to 9, pKa values of 2.9 and 10.0) were made by HME, spray drying, spray granulation, and rotary evaporation for solubility/bioavailability enhancement (101). The ASDs were prepared with 20% (w/w) Compound I, 70% PVP K30, and 10% Sorbitol, and then compared in a beagle dog study with a control formulation made of crystalline drug triturated with Poloxamer 188. The melt-extruded ASD provided a 7-fold greater bioavailability than the control crystalline formulation, followed by the ASD made by rotary evaporation. The spray-dried and spray-granulated solid dispersions produced

relatively lower bioavailability enhancement of 2- to 3-fold. The authors speculated that the degree of dispersion of the spray-dried and spray-granulated formulations as compared to that manufactured by HME, which had been exposed to high shear mixing. Another study comparing fusion-based method (KSD) and solvent-based method (rotary evaporation) also revealed that a more homogeneous ASD was generated by KSD as compared to the rotary evaporation method (102). Although faster dissolution rate was observed in a pH change non-sink dissolution test for the rotary-evaporated ASD with higher surface area as mentioned before, the ASD made by KSD exhibited better ability to prevent recrystallization in the dissolution. The difference was attributed to the higher degrees of thermodynamic stability in the ASD manufactured by rotary evaporation method than KSD. For further in vivo test, KSD samples were used due to the inferior physical stability performance compared to rotary-evaporated ASD, resulting in a 10-fold higher absorption than the crystalline drug in the Sprague–Dawley rat model.

Comparison between two fusion-based methods (KSD and HME) has also confirmed the importance of ensuring a homogeneous ASD system (94, 103). In one study (94), it was shown that both KSD and HME were capable of providing ASDs with improved dissolution behavior. However, as shown in Figure 1.8, KSD ASD provided a faster in vitro dissolution rate in comparison to the HME ASD processed by a HAAKE Minilab II extruder with no kneading element (low mixing ability). This observation supported the solid state characterization in this paper showing the increased amorphous homogeneity of KSD ASD. The oral bioavailability study using a Sprague–Dawley rat

model indicated ASDs from both processes exhibited enhanced AUC compared to crystalline drug, but a higher AUC value was observed with KSD ASD compared to that of HME ASD, which was also attributed to the improved homogeneity. Generally, if the active ingredient is not homogeneously distributed in the carrier, there will be drug-rich and polymer-rich zones, which may impact the drug release process. And for the ASD system containing poorly water-soluble drug (hydrophobic), a greater concentration of drug can negatively impact wetting and dissolution rate, therefore, a decrease in drug release would be anticipated from the system relative to a homogenous (evenly hydrophilic) system.

A reformulation of Zelboraf®, a marketed co-precipiated ASD product containing vemurafenib has been done recently with KSD (104). Vemurafenib is a poorly water-soluble drug, and due to its high melting point, poor solubility in low and moderate boiling temp organic solvents, common technologies of manufacturing ASD with vemurafenib are limited (105). It has been shown that similar supersaturation state was achieved with the KSD ASD and the commercial product in the in vitro dissolution study, demonstrating the versatility of KSD technology for the production of ASDs.

Due to the complexity of the in vitro/in vivo performance of ASDs, the ASD manufacturing methods can affect performance. Based on this review, solvent-based methods tend to generate ASDs with smaller particle sizes resulting in faster drug release rate; fusion-based methods, on the other hand, tend to generate more homogeneous ASDs

with better resistance to recrystallization in the dissolution media resulting in better in vivo absorption.

1.6 CONCLUSIONS

The application of ASDs for improving the bioavailability of poorly water-soluble drugs has gained interest in pharmaceutical industry. Fusion-based and solvent-based methods have been widely investigated and used to prepare ASDs. It has been shown that stability challenges involved in ASD formulations such as chemical stability, physical stability, and in vitro/in vivo performance vary based on the manufacturing method. Based on this review of the literature, solvent-based methods exhibit better chemical stability than fusion-based methods, however, residual solvent, high surface area, potential nuclei, and molecular relaxation during the secondary drying process may negatively impact the physical stability of ASDs manufactured by solvent-based methods. In vitro/in vivo performance depends on a number of factors including, the homogeneity of ASD systems, the intermolecular interactions between drug and polymer, and the morphology of the materials, which can be influenced by the manufacturing method. It should be noted though, besides the manufacturing methods, the overall performance of ASD also largely depends on the physicochemical properties of the drug and polymer. Therefore, selecting the right manufacturing method based on the properties of the materials is crucial to the success of the ASD.

1.7 REFERENCES

1. Lipinski CA, Lombardo F, Dominy BW, Feeney PJ. Experimental and computational approaches to estimate solubility and permeability in drug discovery and development settings. Advanced Drug Delivery Reviews. 2012;64, Supplement:4-17. doi: http://dx.doi.org/10.1016/j.addr.2012.09.019.

2. Keseru GM, Makara GM. The influence of lead discovery strategies on the properties of drug candidates. Nat Rev Drug Discov. 2009;8(3):203-12. doi: http://www.nature.com/nrd/journal/v8/n3/suppinfo/nrd2796_S1.html.

3. Lipinski CA. Drug-like properties and the causes of poor solubility and poor permeability. Journal of Pharmacological and Toxicological Methods. 2000;44(1):235-49. doi: http://dx.doi.org/10.1016/S1056-8719(00)00107-6.

4. Hauss DJ. Oral lipid-based formulations. Advanced Drug Delivery Reviews. 2007;59(7):667-76. doi: http://dx.doi.org/10.1016/j.addr.2007.05.006.

5. Morishita M, Peppas NA. Is the oral route possible for peptide and protein drug delivery? Drug Discovery Today. 2006;11(19–20):905-10. doi: http://dx.doi.org/10.1016/j.drudis.2006.08.005.

6. Amidon GL, Lennernäs H, Shah VP, Crison JR. A Theoretical Basis for a Biopharmaceutic Drug Classification: The Correlation of in Vitro Drug Product Dissolution and in Vivo Bioavailability. Pharmaceutical Research. 1995;12(3):413-20. doi: 10.1023/a:1016212804288.

7. Brough C, Williams Iii RO. Amorphous solid dispersions and nano-crystal technologies for poorly water-soluble drug delivery. International Journal of Pharmaceutics. 2013;453(1):157-66. doi: http://dx.doi.org/10.1016/j.ijpharm.2013.05.061.

8. Lang B, Liu S, McGinity JW, Williams RO. Effect of hydrophilic additives on the dissolution and pharmacokinetic properties of itraconazole-enteric polymer hot-melt extruded amorphous solid dispersions. Drug Development and Industrial Pharmacy. 2016;42(3):429-45. doi: 10.3109/03639045.2015.1075031.

9. Lee KWY, Porter CJH, Boyd BJ. The effect of administered dose of lipid-based formulations on the In Vitro and In Vivo performance of cinnarizine as a model poorly water-soluble drug. Journal of Pharmaceutical Sciences. 2013;102(2):565-78. doi: 10.1002/jps.23384.

10. Furfine ES, Baker CT, Hale MR, Reynolds DJ, Salisbury JA, Searle AD, et al. Preclinical pharmacology and pharmacokinetics of GW433908, a water-soluble

prodrug of the human immunodeficiency virus protease inhibitor amprenavir. Antimicrobial agents and chemotherapy. 2004;48(3):791-8.

11. Zhang T, Huang P, Shi L, Su Y, Zhou L, Zhu X, et al. Self-Assembled Nanoparticles of Amphiphilic Twin Drug from Floxuridine and Bendamustine for Cancer Therapy. Molecular Pharmaceutics. 2015;12(7):2328-36. doi: 10.1021/acs.molpharmaceut.5b00005.

12. Banik M, Gopi SP, Ganguly S, Desiraju GR. Cocrystal and Salt Forms of Furosemide: Solubility and Diffusion Variations. Crystal Growth & Design. 2016;16(9):5418-28. doi: 10.1021/acs.cgd.6b00902.

13. Childs SL, Kandi P, Lingireddy SR. Formulation of a Danazol Cocrystal with Controlled Supersaturation Plays an Essential Role in Improving Bioavailability. Molecular Pharmaceutics. 2013;10(8):3112-27. doi: 10.1021/mp400176y.

14. Noyes AA, Whitney WR. THE RATE OF SOLUTION OF SOLID SUBSTANCES IN THEIR OWN SOLUTIONS. Journal of the American Chemical Society. 1897;19(12):930-4. doi: 10.1021/ja02086a003.

15. Roberts AD, Zhang H. Poorly water-soluble drug nanoparticles via solvent evaporation in water-soluble porous polymers. International Journal of

Pharmaceutics. 2013;447(1–2):241-50. doi: http://dx.doi.org/10.1016/j.ijpharm.2013.03.001.

16. Mijatovic D, Eijkel J, Van Den Berg A. Technologies for nanofluidic systems: top-down vs. bottom-up—a review. Lab on a Chip. 2005;5(5):492-500.

17. Yang W, Johnston KP, Williams Iii RO. Comparison of bioavailability of amorphous versus crystalline itraconazole nanoparticles via pulmonary administration in rats. European Journal of Pharmaceutics and Biopharmaceutics. 2010;75(1):33-41. doi: http://dx.doi.org/10.1016/j.ejpb.2010.01.011.

18. Birtalan E, Hoelig P, Lindley DJ, Sanzgiri YD, Tong P. Melt-extruded solid dispersions containing an apoptosis-inducing agent. US 20120108590; 2012.

19. Baert LEC, Verreck G, Thoné D. Antifungal compositions with improved bioavailability. US 6509038; 2003.

20. Frank KJ, Rosenblatt KM, Westedt U, Hölig P, Rosenberg J, Mägerlein M, et al. Amorphous solid dispersion enhances permeation of poorly soluble ABT-102: True supersaturation vs. apparent solubility enhancement. International Journal of Pharmaceutics. 2012;437(1–2):288-93. doi: http://dx.doi.org/10.1016/j.ijpharm.2012.08.014.

21. Orange Book: Approved Drug Products with Therapeutic Equivalence Evaluations. US Food & Drug Administration. 2016.

22. Madsen CM, Boyd B, Rades T, Müllertz A. Supersaturation of zafirlukast in fasted and fed state intestinal media with and without precipitation inhibitors. European Journal of Pharmaceutical Sciences. 2016;91:31-9. doi: http://dx.doi.org/10.1016/j.ejps.2016.05.026.

23. Tawa M, Almarsson O, Remenar J. Pharmaceutical salts of zafirlukast. Google Patents; 2004.

24. Timko RJ, Bradway RJ, Clements A. Pharmaceutical agents. Google Patents; 1999.

25. Curatolo WJ, Niantic C. Solid pharmaceutical dispersions with enhanced bioavailability. EP 0901786 A2; 1999.

26. Raw AS, Furness MS, Gill DS, Adams RC, Holcombe Jr FO, Yu LX. Regulatory considerations of pharmaceutical solid polymorphism in Abbreviated New Drug Applications (ANDAs). Advanced Drug Delivery Reviews. 2004;56(3):397-414. doi: http://dx.doi.org/10.1016/j.addr.2003.10.011.

27. Guo Y, Byrn SR, Zografi G. Physical characteristics and chemical degradation of amorphous quinapril hydrochloride. Journal of Pharmaceutical Sciences.

2000;89(1):128-43. doi: 10.1002/(SICI)1520-6017(200001)89:1<128::AID-JPS13>3.0.CO;2-Z.

28. Huang S, O'Donnell KP, Keen JM, Rickard MA, McGinity JW, Williams RO. A New Extrudable Form of Hypromellose: AFFINISOL™ HPMC HME. AAPS PharmSciTech. 2016;17(1):106-19. doi: 10.1208/s12249-015-0395-9.

29. Vippagunta SR, Wang Z, Hornung S, Krill SL. Factors affecting the formation of eutectic solid dispersions and their dissolution behavior. Journal of Pharmaceutical Sciences. 2007;96(2):294-304. doi: 10.1002/jps.20754.

30. Feng T, Pinal R, Carvajal MT. Process induced disorder in crystalline materials: Differentiating defective crystals from the amorphous form of griseofulvin. Journal of Pharmaceutical Sciences. 2008;97(8):3207-21. doi: 10.1002/jps.21219.

31. Craig DQM. The mechanisms of drug release from solid dispersions in water-soluble polymers. International Journal of Pharmaceutics. 2002;231(2):131-44. doi: http://dx.doi.org/10.1016/S0378-5173(01)00891-2.

32. Sarode AL, Sandhu H, Shah N, Malick W, Zia H. Hot melt extrusion (HME) for amorphous solid dispersions: Predictive tools for processing and impact of drug–

polymer interactions on supersaturation. European Journal of Pharmaceutical Sciences. 2013;48(3):371-84. doi: http://dx.doi.org/10.1016/j.ejps.2012.12.012.

33. Timko RJ, Lordi NG. Thermal characterization of citric acid solid dispersions with benzoic acid and phenobarbital. Journal of Pharmaceutical Sciences. 1979;68(5):601-5. doi: 10.1002/jps.2600680523.

34. Breitenbach J. Melt extrusion: from process to drug delivery technology. European Journal of Pharmaceutics and Biopharmaceutics. 2002;54(2):107-17. doi: http://dx.doi.org/10.1016/S0939-6411(02)00061-9.

35. Qian F, Huang J, Hussain MA. Drug–polymer solubility and miscibility: Stability consideration and practical challenges in amorphous solid dispersion development. Journal of Pharmaceutical Sciences. 2010;99(7):2941-7. doi: 10.1002/jps.22074.

36. Miller DA, Keen JM. KinetiSol®-Based Amorphous Solid Dispersions. In: Shah N, Sandhu H, Choi DS, Chokshi H, Malick AW, editors. Amorphous Solid Dispersions: Theory and Practice. New York, NY: Springer New York; 2014. p. 567-77.

37. LaFountaine JS, Jermain SV, Prasad LK, Brough C, Miller DA, Lubda D, et al. Enabling thermal processing of ritonavir–polyvinyl alcohol amorphous solid

dispersions by KinetiSol® Dispersing. European Journal of Pharmaceutics and Biopharmaceutics. 2016;101:72-81. doi: http://dx.doi.org/10.1016/j.ejpb.2016.01.018.

38. Paudel A, Worku ZA, Meeus J, Guns S, Van den Mooter G. Manufacturing of solid dispersions of poorly water soluble drugs by spray drying: Formulation and process considerations. International Journal of Pharmaceutics. 2013;453(1):253-84. doi: http://dx.doi.org/10.1016/j.ijpharm.2012.07.015.

39. Chiang P-C, Ran Y, Chou K-J, Cui Y, Sambrone A, Chan C, et al. Evaluation of Drug Load and Polymer by Using a 96-Well Plate Vacuum Dry System for Amorphous Solid Dispersion Drug Delivery. AAPS PharmSciTech. 2012;13(2):713-22. doi: 10.1208/s12249-012-9795-2.

40. Broman E, Khoo C, Taylor LS. A comparison of alternative polymer excipients and processing methods for making solid dispersions of a poorly water soluble drug. International Journal of Pharmaceutics. 2001;222(1):139-51. doi: http://dx.doi.org/10.1016/S0378-5173(01)00709-8.

41. Alhalaweh A, Andersson S, Velaga SP. Preparation of zolmitriptan–chitosan microparticles by spray drying for nasal delivery. European Journal of

Pharmaceutical Sciences. 2009;38(3):206-14. doi: http://dx.doi.org/10.1016/j.ejps.2009.07.003.

42. Yang W, Tam J, Miller DA, Zhou J, McConville JT, Johnston KP, et al. High bioavailability from nebulized itraconazole nanoparticle dispersions with biocompatible stabilizers. International Journal of Pharmaceutics. 2008;361(1–2):177-88. doi: http://dx.doi.org/10.1016/j.ijpharm.2008.05.003.

43. Dong Z, Chatterji A, Sandhu H, Choi DS, Chokshi H, Shah N. Evaluation of solid state properties of solid dispersions prepared by hot-melt extrusion and solvent co-precipitation. International Journal of Pharmaceutics. 2008;355(1–2):141-9. doi: http://dx.doi.org/10.1016/j.ijpharm.2007.12.017.

44. Won D-H, Kim M-S, Lee S, Park J-S, Hwang S-J. Improved physicochemical characteristics of felodipine solid dispersion particles by supercritical anti-solvent precipitation process. International Journal of Pharmaceutics. 2005;301(1–2):199-208. doi: http://dx.doi.org/10.1016/j.ijpharm.2005.05.017.

45. Dobry DE, Settell DM, Baumann JM, Ray RJ, Graham LJ, Beyerinck RA. A Model-Based Methodology for Spray-Drying Process Development. Journal of Pharmaceutical Innovation. 2009;4(3):133-42. doi: 10.1007/s12247-009-9064-4.

46. Lowinger M, Baumann J, Vodak DT, Moser J. Practical Considerations for Spray Dried Formulation and Process Development. In: Templeton AC, Byrn SR, Haskell RJ, Prisinzano TE, editors. Discovering and Developing Molecules with Optimal Drug-Like Properties. New York, NY: Springer New York; 2015. p. 383-435.

47. Shah N, Sandhu H, Choi DS, Chokshi H, Iyer R, Malick AW. MBP Technology: Composition and Design Considerations. In: Shah N, Sandhu H, Choi DS, Chokshi H, Malick AW, editors. Amorphous Solid Dispersions: Theory and Practice. New York, NY: Springer New York; 2014. p. 323-50.

48. Sertsou G, Butler J, Scott A, Hempenstall J, Rades T. Factors affecting incorporation of drug into solid solution with HPMCP during solvent change co-precipitation. International Journal of Pharmaceutics. 2002;245(1–2):99-108. doi: http://dx.doi.org/10.1016/S0378-5173(02)00331-9.

49. Oguchi T, Yonemochi E, Yamamoto K, Nakai Y. Freeze-Drying of Drug-Additive Binary Systems. II. : Relationship between Decarboxylation Behavior and Molecular States of p-Aminosalicylic Acid. Chemical & Pharmaceutical Bulletin. 1989;37(11):3088-91. doi: 10.1248/cpb.37.3088.

50. Mujumdar AS. Handbook of industrial drying: Crc Press; 2014.

51. Mizoe T, Ozeki T, Okada H. Application of a Four-fluid Nozzle Spray Drier to Prepare Inhalable Rifampicin-containing Mannitol Microparticles. AAPS PharmSciTech. 2008;9(3):755-61. doi: 10.1208/s12249-008-9109-x.

52. Sunderland T, Kelly JG, Ramtoola Z. Application of a novel 3-fluid nozzle spray drying process for the microencapsulation of therapeutic agents using incompatible drug-polymer solutions. Archives of Pharmacal Research. 2015;38(4):566-73. doi: 10.1007/s12272-013-0261-9.

53. Shah N, Sandhu H, Choi DS, Chokshi H, Malick AW. Amorphous Solid Dispersions. Theory and Practice: Springer; 2014.

54. Hancock BC, Zografi G. Characteristics and significance of the amorphous state in pharmaceutical systems. Journal of Pharmaceutical Sciences. 1997;86(1):1-12. doi: 10.1021/js9601896.

55. Li M, Hasjim J, Xie F, Halley PJ, Gilbert RG. Shear degradation of molecular, crystalline, and granular structures of starch during extrusion. Starch - Stärke. 2014;66(7-8):595-605. doi: 10.1002/star.201300201.

56. Hengsawas Surasarang S, Keen JM, Huang S, Zhang F, McGinity JW, Williams RO. Hot melt extrusion versus spray drying: hot melt extrusion degrades

albendazole. Drug Development and Industrial Pharmacy. 2016:1-15. doi: 10.1080/03639045.2016.1220577.

57. Huang S, O'Donnell KP, Vaux SMDd, O'Brien J, Stutzman J, III ROW. Processing of a Thermally Labile Drug by Hot-Melt Extrusion. Submitted to International Journal of Pharmaceutics 2017.

58. Rao RN, Ramachandra B, Vali RM, Raju SS. LC–MS/MS studies of ritonavir and its forced degradation products. Journal of Pharmaceutical and Biomedical Analysis. 2010;53(4):833-42. doi: http://dx.doi.org/10.1016/j.jpba.2010.06.004.

59. Alexy P, Káchová D, Kršiak M, Bakoš D, Šimková B. Poly(vinyl alcohol) stabilisation in thermoplastic processing. Polymer Degradation and Stability. 2002;78(3):413-21. doi: http://dx.doi.org/10.1016/S0141-3910(02)00177-5.

60. De Jaeghere W, De Beer T, Van Bocxlaer J, Remon JP, Vervaet C. Hot-melt extrusion of polyvinyl alcohol for oral immediate release applications. International Journal of Pharmaceutics. 2015;492(1–2):1-9. doi: http://dx.doi.org/10.1016/j.ijpharm.2015.07.009.

61. Hughey JR, Keen JM, Brough C, Saeger S, McGinity JW. Thermal processing of a poorly water-soluble drug substance exhibiting a high melting point: The utility of

KinetiSol® Dispersing. International Journal of Pharmaceutics. 2011;419(1–2):222-30. doi: http://dx.doi.org/10.1016/j.ijpharm.2011.08.007.

62. Hughey JR, DiNunzio JC, Bennett RC, Brough C, Miller DA, Ma H, et al. Dissolution Enhancement of a Drug Exhibiting Thermal and Acidic Decomposition Characteristics by Fusion Processing: A Comparative Study of Hot Melt Extrusion and KinetiSol® Dispersing. AAPS PharmSciTech. 2010;11(2):760-74. doi: 10.1208/s12249-010-9431-y.

63. DiNunzio JC, Brough C, Miller DA, Williams Iii RO, McGinity JW. Applications of KinetiSol® Dispersing for the production of plasticizer free amorphous solid dispersions. European Journal of Pharmaceutical Sciences. 2010;40(3):179-87. doi: http://dx.doi.org/10.1016/j.ejps.2010.03.002.

64. Wegiel LA, Mauer LJ, Edgar KJ, Taylor LS. Crystallization of amorphous solid dispersions of resveratrol during preparation and storage—Impact of different polymers. Journal of Pharmaceutical Sciences. 2013;102(1):171-84. doi: 10.1002/jps.23358.

65. Ghebremeskel AN, Vemavarapu C, Lodaya M. Use of surfactants as plasticizers in preparing solid dispersions of poorly soluble API: Selection of polymer–surfactant combinations using solubility parameters and testing the processability.

International Journal of Pharmaceutics. 2007;328(2):119-29. doi: http://dx.doi.org/10.1016/j.ijpharm.2006.08.010.

66. Hancock BC, Shamblin SL, Zografi G. Molecular Mobility of Amorphous Pharmaceutical Solids Below Their Glass Transition Temperatures. Pharmaceutical Research. 1995;12(6):799-806. doi: 10.1023/a:1016292416526.

67. Shamblin SL, Tang X, Chang L, Hancock BC, Pikal MJ. Characterization of the Time Scales of Molecular Motion in Pharmaceutically Important Glasses. The Journal of Physical Chemistry B. 1999;103(20):4113-21. doi: 10.1021/jp983964+.

68. Surana R, Pyne A, Suryanarayanan R. Effect of Aging on the Physical Properties of Amorphous Trehalose. Pharmaceutical Research. 2004;21(5):867-74. doi: 10.1023/b:pham.0000026441.77567.75.

69. Surana R, Pyne A, Suryanarayanan R. Effect of Preparation Method on Physical Properties of Amorphous Trehalose. Pharmaceutical Research. 2004;21(7):1167-76. doi: 10.1023/B:PHAM.0000033003.17251.c3.

70. Bhardwaj SP, Suryanarayanan R. Molecular Mobility as an Effective Predictor of the Physical Stability of Amorphous Trehalose. Molecular Pharmaceutics. 2012;9(11):3209-17. doi: 10.1021/mp300302g.

71. Bhugra C, Rambhatla S, Bakri A, Duddu SP, Miller DP, Pikal MJ, et al. Prediction of the onset of crystallization of amorphous sucrose below the calorimetric glass transition temperature from correlations with mobility. Journal of Pharmaceutical Sciences. 2007;96(5):1258-69. doi: 10.1002/jps.20918.

72. Tsukushi I, Yamamuro O, Suga H. Heat capacities and glass transitions of ground amorphous solid and liquid-quenched glass of tri-O-methyl-ß-cyclodextrin. Journal of Non-Crystalline Solids. 1994;175(2):187-94. doi: http://dx.doi.org/10.1016/0022-3093(94)90010-8.

73. Yonemochi E, Inoue Y, Buckton G, Moffat A, Oguchi T, Yamamoto K. Differences in Crystallization Behavior Between Quenched and Ground Amorphous Ursodeoxycholic Acid. Pharmaceutical Research. 1999;16(6):835-40. doi: 10.1023/a:1018817801444.

74. Kestur US, Ivanesivic I, Alonzo DE, Taylor LS. Influence of particle size on the crystallization kinetics of amorphous felodipine powders. Powder Technology. 2013;236:197-204. doi: http://dx.doi.org/10.1016/j.powtec.2012.02.010.

75. Ho R, Naderi M, Heng JYY, Williams DR, Thielmann F, Bouza P, et al. Effect of Milling on Particle Shape and Surface Energy Heterogeneity of Needle-Shaped

Crystals. Pharmaceutical Research. 2012;29(10):2806-16. doi: 10.1007/s11095-012-0842-1.

76. Powell CT, Xi H, Sun Y, Gunn E, Chen Y, Ediger MD, et al. Fast Crystal Growth in o-Terphenyl Glasses: A Possible Role for Fracture and Surface Mobility. The Journal of Physical Chemistry B. 2015;119(31):10124-30. doi: 10.1021/acs.jpcb.5b05389.

77. Nandiyanto ABD, Okuyama K. Progress in developing spray-drying methods for the production of controlled morphology particles: From the nanometer to submicrometer size ranges. Advanced Powder Technology. 2011;22(1):1-19. doi: http://dx.doi.org/10.1016/j.apt.2010.09.011.

78. Shah N, Iyer RM, Mair H-J, Choi DS, Tian H, Diodone R, et al. Improved human bioavailability of vemurafenib, a practically insoluble drug, using an amorphous polymer-stabilized solid dispersion prepared by a solvent-controlled coprecipitation process. Journal of Pharmaceutical Sciences. 2013;102(3):967-81. doi: 10.1002/jps.23425.

79. Andrews GP, Abu-Diak O, Kusmanto F, Hornsby P, Hui Z, Jones DS. Physicochemical characterization and drug-release properties of celecoxib hot-melt

extruded glass solutions. Journal of Pharmacy and Pharmacology. 2010;62(11):1580-90. doi: 10.1111/j.2042-7158.2010.01177.x.

80. Mahmah O, Tabbakh R, Kelly A, Paradkar A. A comparative study of the effect of spray drying and hot-melt extrusion on the properties of amorphous solid dispersions containing felodipine. Journal of Pharmacy and Pharmacology. 2014;66(2):275-84. doi: 10.1111/jphp.12099.

81. Agrawal AM, Dudhedia MS, Patel AD, Raikes MS. Characterization and performance assessment of solid dispersions prepared by hot melt extrusion and spray drying process. International Journal of Pharmaceutics. 2013;457(1):71-81. doi: http://dx.doi.org/10.1016/j.ijpharm.2013.08.081.

82. Newman A, Zografi G. Critical Considerations for the Qualitative and Quantitative Determination of Process-Induced Disorder in Crystalline Solids. Journal of Pharmaceutical Sciences. 2014;103(9):2595-604. doi: 10.1002/jps.23930.

83. Bhugra C, Pikal MJ. Role of thermodynamic, molecular, and kinetic factors in crystallization from the amorphous state. Journal of Pharmaceutical Sciences. 2008;97(4):1329-49. doi: 10.1002/jps.21138.

84. Taylor LS. Physical Stability and Crystallization Inhibition. harmaceutical Sciences Encyclopedia: John Wiley & Sons, Inc.; 2010.

85. Schroers J, Masuhr A, Johnson WL, Busch R. Pronounced asymmetry in the crystallization behavior during constant heating and cooling of a bulk metallic glass-forming liquid. Physical Review B. 1999;60(17):11855-8.

86. Guns S, Dereymaker A, Kayaert P, Mathot V, Martens JA, Van den Mooter G. Comparison Between Hot-Melt Extrusion and Spray-Drying for Manufacturing Solid Dispersions of the Graft Copolymer of Ethylene Glycol and Vinylalcohol. Pharmaceutical Research. 2011;28(3):673-82. doi: 10.1007/s11095-010-0324-2.

87. Tian Y, Caron V, Jones DS, Healy A-M, Andrews GP. Using Flory–Huggins phase diagrams as a pre-formulation tool for the production of amorphous solid dispersions: a comparison between hot-melt extrusion and spray drying. Journal of Pharmacy and Pharmacology. 2014;66(2):256-74. doi: 10.1111/jphp.12141.

88. Haser A, Cao T, Lubach J, Listro T, Acquarelo L, Zhang F. The Effect of Processing Methods on the Stability of Naproxen Amorphous Solid Dispersions Prepared by Melt Extrusion and Spray Drying Submitted to International Journal of Pharmaceutics 2017.

89. Andronis V, Zografi G. Crystal nucleation and growth of indomethacin polymorphs from the amorphous state. Journal of Non-Crystalline Solids. 2000;271(3):236-48. doi: http://dx.doi.org/10.1016/S0022-3093(00)00107-1.

90. Zhou D, Zhang GGZ, Law D, Grant DJW, Schmitt EA. Thermodynamics, Molecular Mobility and Crystallization Kinetics of Amorphous Griseofulvin. Molecular Pharmaceutics. 2008;5(6):927-36. doi: 10.1021/mp800169g.

91. Paudel A, Van Humbeeck J, Van den Mooter G. Theoretical and Experimental Investigation on the Solid Solubility and Miscibility of Naproxen in Poly(vinylpyrrolidone). Molecular Pharmaceutics. 2010;7(4):1133-48. doi: 10.1021/mp100013p.

92. Paudel A, Nies E, Van den Mooter G. Relating Hydrogen-Bonding Interactions with the Phase Behavior of Naproxen/PVP K 25 Solid Dispersions: Evaluation of Solution-Cast and Quench-Cooled Films. Molecular Pharmaceutics. 2012;9(11):3301-17. doi: 10.1021/mp3003495.

93. Shah N, Sandhu H, Phuapradit W, Pinal R, Iyer R, Albano A, et al. Development of novel microprecipitated bulk powder (MBP) technology for manufacturing stable amorphous formulations of poorly soluble drugs. International Journal of

Pharmaceutics. 2012;438(1–2):53-60. doi: http://dx.doi.org/10.1016/j.ijpharm.2012.08.031.

94. DiNunzio JC, Brough C, Miller DA, Williams RO, McGinity JW. Fusion processing of itraconazole solid dispersions by kinetisol® dispersing: A comparative study to hot melt extrusion. Journal of Pharmaceutical Sciences. 2010;99(3):1239-53. doi: 10.1002/jps.21893.

95. Lang B, McGinity JW, Williams RO. Dissolution Enhancement of Itraconazole by Hot-Melt Extrusion Alone and the Combination of Hot-Melt Extrusion and Rapid Freezing—Effect of Formulation and Processing Variables. Molecular Pharmaceutics. 2014;11(1):186-96. doi: 10.1021/mp4003706.

96. Qian F, Huang J, Zhu Q, Haddadin R, Gawel J, Garmise R, et al. Is a distinctive single Tg a reliable indicator for the homogeneity of amorphous solid dispersion? International Journal of Pharmaceutics. 2010;395(1–2):232-5. doi: http://dx.doi.org/10.1016/j.ijpharm.2010.05.033.

97. Newman A, Knipp G, Zografi G. Assessing the performance of amorphous solid dispersions. Journal of Pharmaceutical Sciences. 2012;101(4):1355-77. doi: 10.1002/jps.23031.

98. Javeer SD, Patole R, Amin P. Enhanced solubility and dissolution of simvastatin by HPMC-based solid dispersions prepared by hot melt extrusion and spray-drying method. Journal of Pharmaceutical Investigation. 2013;43(6):471-80. doi: 10.1007/s40005-013-0092-1.

99. Patterson JE, James MB, Forster AH, Lancaster RW, Butler JM, Rades T. Preparation of glass solutions of three poorly water soluble drugs by spray drying, melt extrusion and ball milling. International Journal of Pharmaceutics. 2007;336(1):22-34. doi: http://dx.doi.org/10.1016/j.ijpharm.2006.11.030.

100. Patterson JE, James MB, Forster AH, Rades T. Melt Extrusion and Spray Drying of Carbamazepine and Dipyridamole with Polyvinylpyrrolidone/Vinyl Acetate Copolymers. Drug Development and Industrial Pharmacy. 2008;34(1):95-106. doi: 10.1080/03639040701484627.

101. Lakshman JP, Cao Y, Kowalski J, Serajuddin ATM. Application of Melt Extrusion in the Development of a Physically and Chemically Stable High-Energy Amorphous Solid Dispersion of a Poorly Water-Soluble Drug. Molecular Pharmaceutics. 2008;5(6):994-1002. doi: 10.1021/mp8001073.

102. Bennett RC, Brough C, Miller DA, O'Donnell KP, Keen JM, Hughey JR, et al. Preparation of amorphous solid dispersions by rotary evaporation and KinetiSol

Dispersing: approaches to enhance solubility of a poorly water-soluble gum extract. Drug Development and Industrial Pharmacy. 2015;41(3):382-97. doi: 10.3109/03639045.2013.866142.

103. DiNunzio JC, Brough C, Hughey JR, Miller DA, Williams Iii RO, McGinity JW. Fusion production of solid dispersions containing a heat-sensitive active ingredient by hot melt extrusion and Kinetisol® dispersing. European Journal of Pharmaceutics and Biopharmaceutics. 2010;74(2):340-51. doi: http://dx.doi.org/10.1016/j.ejpb.2009.09.007.

104. Miller DA, Keen JM, Brough C, Kucera SU, Ellenberger DJ. Improved formulations of vemurafenib and methods of making the same WO 2016073421 A1; 2016.

105. Zelboraf EMA assessment report WC500124400; 2011.

106. Hughey JR, McGinity JW. Emerging Technologies to Increase the Bioavailability of Poorly Water-Soluble Drugs. In: Williams Iii RO, Watts AB, Miller DA, editors. Formulating Poorly Water Soluble Drugs. New York, NY: Springer New York; 2012. p. 569-602.

107. European Medicines Agency. Public Assessment Reports. 2016.

1.8 LIST OF FIGURES

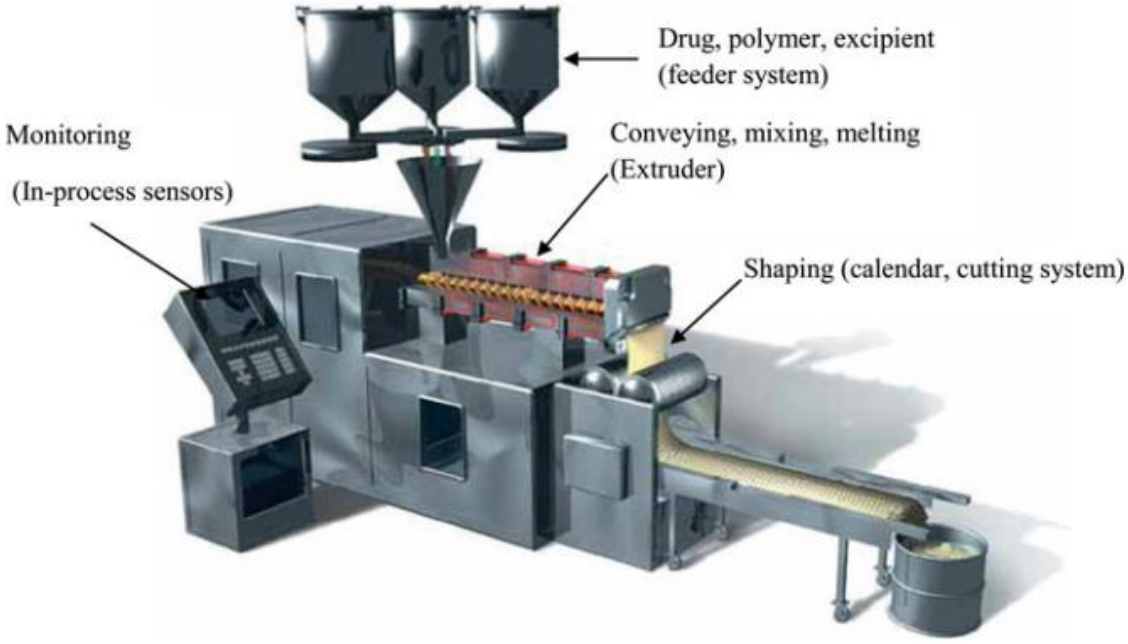

Figure 1.1 Schematic representation of a typical pharmaceutical twin-screw extruder. Reproduced with permission from (34).

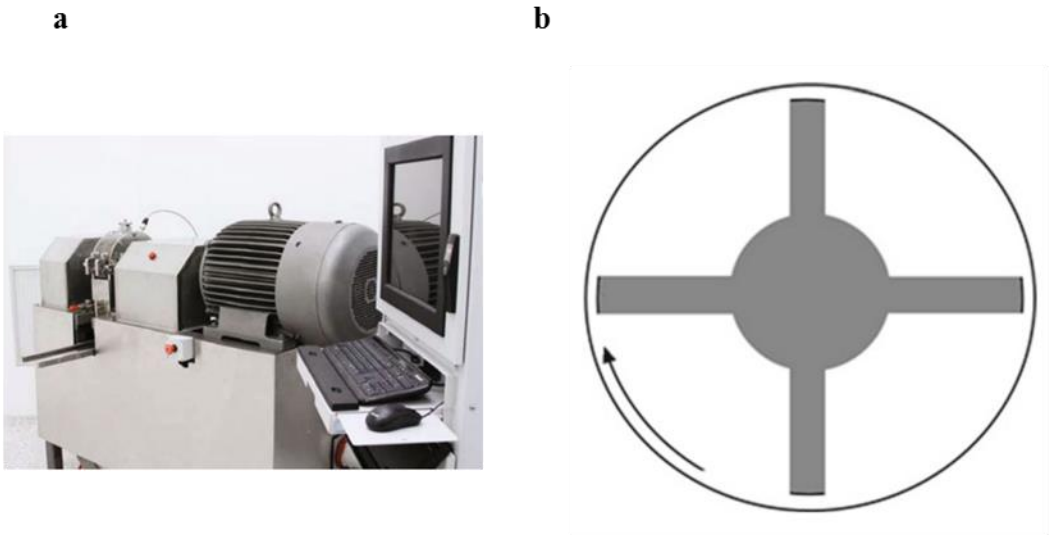

Figure 1.2 (a) Batch-mode GMP KSD compounder model TC-254B; (b) Cross-sectional view of the KSD processing chamber. Reproduced with permission from (36, 106).

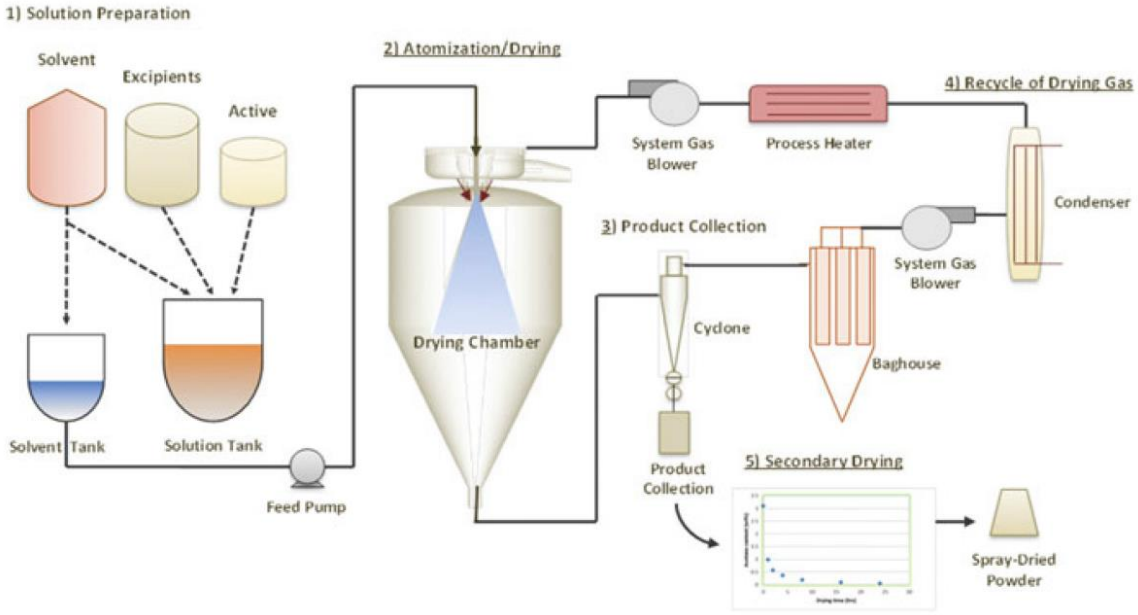

Figure 1.3 Overview of the spray drying process key operations. Reproduced with permission from (46).

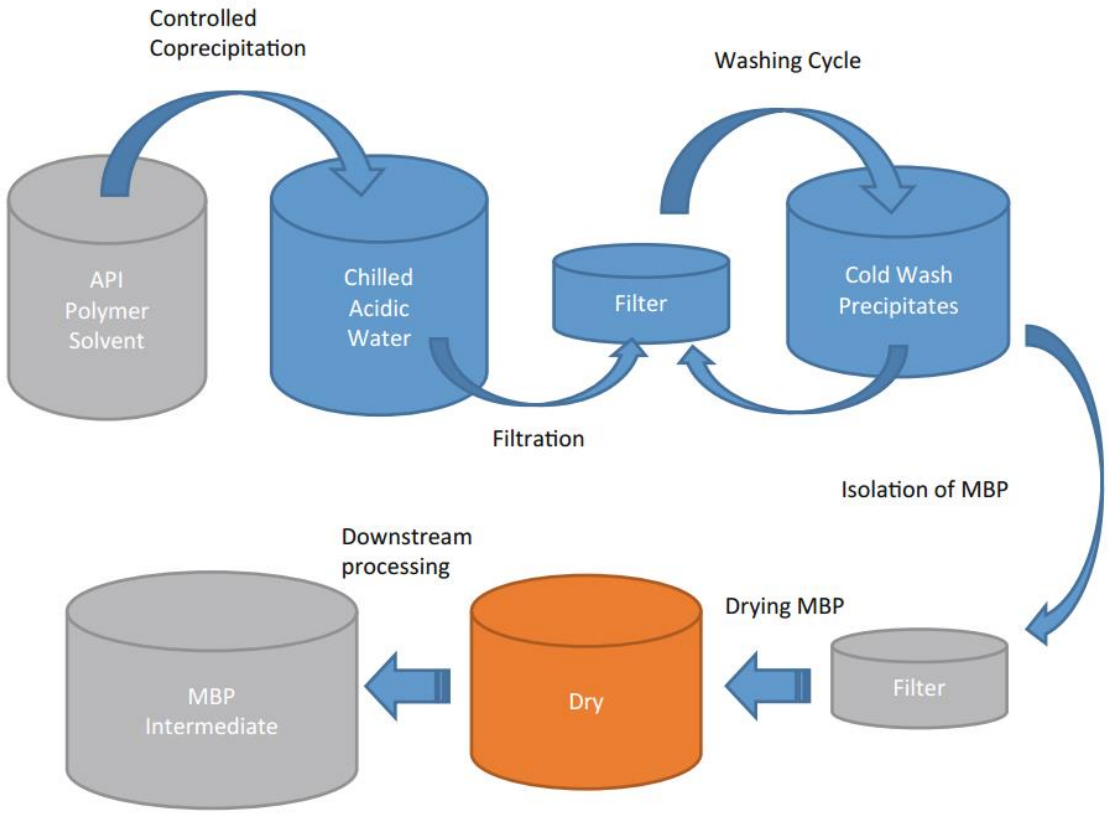

Figure 1.4 Schematic of co-precipitation process. Co-precipitation is comprised of several unit operations including stock solution preparation, controlled co-precipitation, filtration, washing cycles, isolation of co-precipitation, drying, and downstream processing. Reproduced with permission from (47).

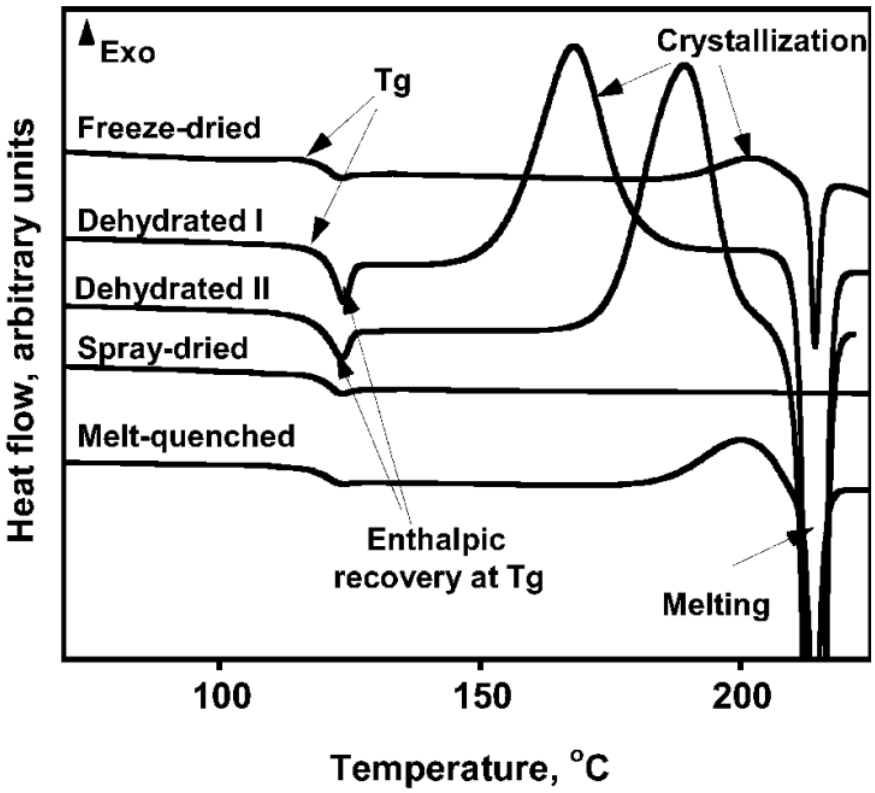

Figure 1.5 DSC heating scans of amorphous trehalose prepared by different methods. Following drying at 60 ℃ the samples were cooled to room temperature and heated to 230 ℃ at 10 ℃/min. The glass transition, enthalpic recovery, crystallization and melting events are shown. Reproduced with permission from (69).

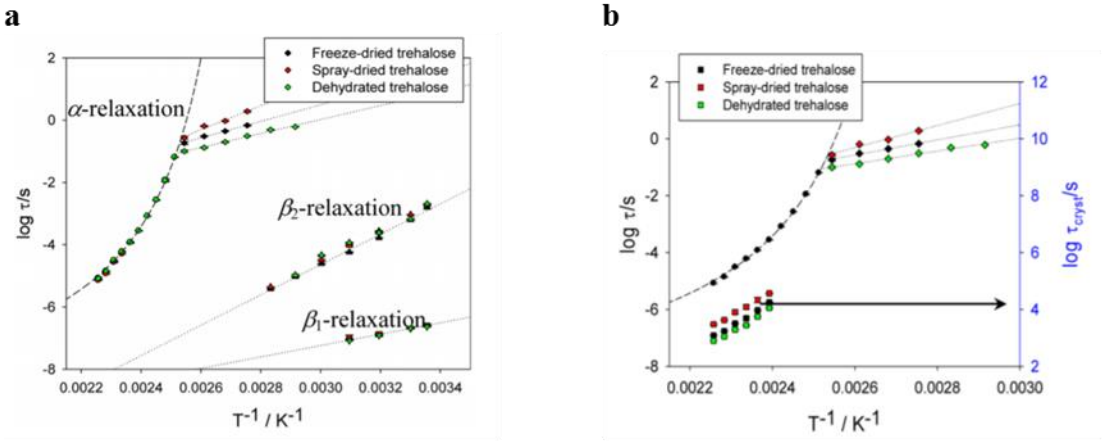

Figure 1.6 Temperature dependence of (a) relaxation in amorphous trehalose prepared by freeze-drying (black), spray-drying (red) and dehydration of trehalose dihydrate (green). Circles, diamonds, triangles and inverted triangles represent, respectively, α-relaxation time above Tg, α-relaxation time below Tg, β2-relaxation time and β1-relaxation time. Dashed line represents VTF fit while dotted lines represent Arrhenius fit (every data point is the mean of 3 determinations; in many cases, the error bar was smaller than the symbol size). In the supercooled liquid region, since the relaxation times were independent of the preparation method, only one symbol is readily visible; (b) crystallization time (squares; plotted on the right y-axis) and α-relaxation time (circles at temperatures above Tg and diamonds below Tg; plotted on the left y-axis) for trehalose prepared by different methods. Reproduced with permission from (70).

Dispersion type	True density (g/cm^3)	Surface area (m^2/g)	Bulk density (g/ml)	Tap density (g/ml)	Carr index (%)
Spray dried dispersion (slugged and milled)	1.285	1.485	0.42	0.64	34
Hot melt extruded dispersion (milled)	1.268	0.066	0.53	0.71	26

Figure 1.7 True density, surface area and powder flow for slugged and milled spray dried and milled hot melt extruded dispersion (above). Scanning electron microscopy images for spray dried dispersion and hot melt extruded dispersion (below). Reproduced with permission from (81).

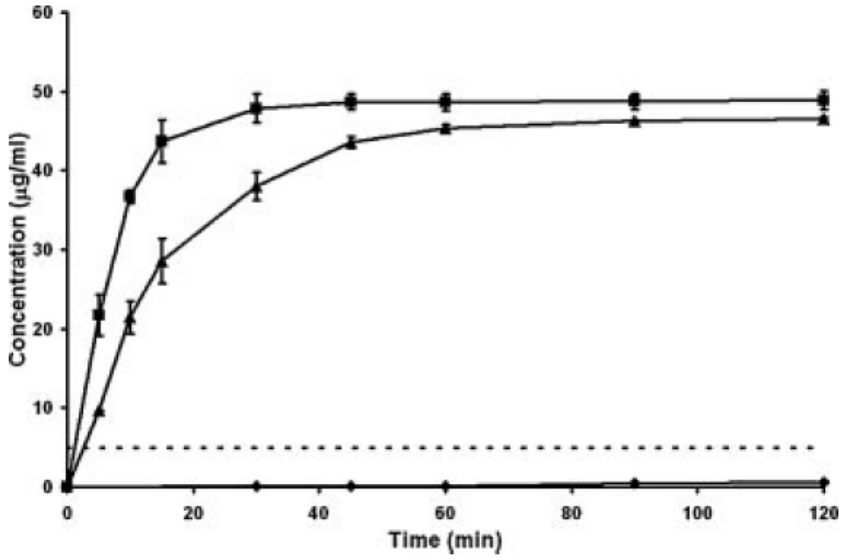

Figure 1.8 Supersaturated dissolution profile of HME (solid triangle) and KSD (solid square) processed solid dispersions. Each vessel (n = 3) contained 50.0 mg/mL ITZ equivalent corresponding to 10 times the equilibrium solubility of ITZ in the acid phase. Testing was conducted for 2 h in 900 mL of 0.1 N HCl. Reproduced with permission from (94).

1.9 LIST OF TABLES

	Preparation method	Drug	Year of Approval
Fusion-based methods	**Hot melt-extrusion**	Gris-PEG	1982 [a]
		Isoptin SR-E SR-E	1987 [a]
		NuvaRing	2001 [a]
		Kaletra	2007 [a]
		Eucreas	2007 [b]
		Onmel	2010 [a]
		Norvir	2010 [a]
		Noxafil	2013 [a]
		Harvoni	2014 [a]
		Viekira PAK	2014 [a]
		Belsomra	2014 [a]
		Venclexta	2016 [a]
Solvent-based methods	**Spray drying**	Sporanox	1992 [a]
		Prograf	1998 [a]
		Crestor	2003 [a]
		Fenoglide	2007 [a]
		Modigraf	2009 [b]
		Zortress	2010 [a]
		Incivek	2011 [a]
		Intelence	2012 [a]
		Kalydeco	2012 [a]
		Orkambi	2016 [a]
	Co-precipitation	Zelboraf	2011 [a]

(a) Based on FDA approval (21).
(b) Based on EMA approval (107).

Table 1.1 Commercially available amorphous solid dispersions manufactured by different methods.

Chapter 2: Solubility Advantage (and Disadvantage) of Pharmaceutical Amorphous Solid Dispersions[1]

2.1 ABSTRACT

The solubility of a drug is ultimately governed by its chemical potential as it is present in the undissolved solute. For a pharmaceutical amorphous solid dispersion (ASD), its solubility depends on the state and composition of the undissolved solute when the ASD is equilibrated with water. Concerning the undissolved solute phase which can contain up to three components (drug, polymer, and water), we develop a complete thermodynamic model to calculate the chemical potential of a drug in the multi-component, amorphous system. This approach enables the estimation of the true solubility advantage of ASD from calorimetric measurements and moisture sorption isotherms. Both theoretical estimation and experimental studies, using indomethacin/Eudragit E ASD systems, show that the solubility advantage of the amorphous indomethacin is significantly reduced through ASD formation and water partitioning. For the ASD with 70% drug loading, the solubility of indomethacin is lower than its crystalline counterpart. Our results show that stabilization through the ASD formation and water sorption can be manifested by the lowering of drug solubility, and demonstrate that the core property in ASD development is the drug chemical

[1] Huang, S., Mao, C., Williams, R. O., Yang, C. Y. Solubility Advantage (and Disadvantage) of Pharmaceutical Amorphous Solid Dispersions. Journal of Pharmaceutical Sciences 105, 3549-3561. I am the primary author of this work.

potential, which is essentially the thermodynamic driving force and can be quantitated using the model presented in this work.

2.2 INTRODUCTION

In today's pharmaceutical development, delivering molecules through the preparation of an amorphous solid dispersion (ASD) has become a routine practice for small molecule drugs exhibiting poor aqueous solubility. Since the idea of the ASD was accepted into to the mainstream of pharmaceutical industry at the turn of the century (1, 2), substantial advances have been made regarding the preparation, characterization, stabilization, and biopharmaceutical performance of the ASD systems, which have been well elaborated in a diverse array of review articles (3-6).

One of the main purposes of an ASD formulation is to improve the drug exposure in humans through the elevation of the apparent drug solubility. Nevertheless, the answer to a highly germane question to this end: "What is the true solubility advantage of the ASD system over that of crystalline drug?", still remains elusive. Numerous experiments have been carried out to evaluate the maximum solubility or supersaturation an ASD system can sustain (7-10), but attempts to estimate the true solubility advantage of ASD have been scarce.

Unlike ASDs, the estimation of the solubility advantage of neat amorphous drugs was extensively studied separately by Hancock et al and Murdande et al. (11-14). In both

studies, the true solubility advantage of the amorphous drug compared to its crystalline counterpart was assessed by evaluating the free energy difference between the two forms through the measurement of their thermal properties. Both studies treated the amorphous drug as a supercooled liquid form. Additionally, through the work of the Murdande et al., corrections were made to account for the solubility change due to water sorption and the difference in solution ionization status, and this exercise led to close proximity between the estimated and experimental solubility values, particularly for drugs that remained in their amorphous state for a prolonged period of time in water (12-14).

Similar to the neat amorphous drug, the solubility advantage of a drug in the form of an ASD is also determined by the free energy. In a more precise term, provided that an ASD is a miscible 1-phase, multi-component system, the solubility advantage is governed by the partial molar free energy, or chemical potential of the drug. Because of the presence of extra components in the system, the free energy of the drug is not equivalent to its neat amorphous counterpart, and we believe this will lead to a considerable difference in their corresponding solubility advantage.

Another effect one must consider is the fate of the ASD upon exposure to water. A common perception in the current literature is that once an ASD is in contact with water, the highly hydrophilic, soluble polymer will dissolve away, leaving the amorphous drug present as the undissolved solute in the super-saturated condition, and the dissolved polymer could potentially act to retard the drug crystallization. From the phase equilibria

standpoint, this conception may be an over-simplification. An ASD in equilibrium with water is a ternary system, containing three components (drug, polymer and water). At constant temperature and pressure, the phase rule permits the coexistence of up to three phases, and the phase behavior depends largely on the mutual solubilities of the three components. Take co-crystals as an example (like ASD, it is also a 1-phase, 2-component system), the coexistence of three phases is extremely common for co-crystals in equilibrium with water (a solution phase, a co-crystal phase, and either the drug or coformer phase) (15, 16). In fact, the phase behavior for the ASD-water system can be more sophisticated because, unlike in co-crystals, significant water partitioning can take place in the ASDs, potentially enabling the coexistence of multiple 3-component phases (this phenomenon is not possible for co-crystals because crystal does not absorb significant amount of water into its lattice).(17) There have been many reports on "amorphous-amorphous" phase separation when an ASD is exposed to elevated humidity.(18-20) In essence, the case of "ASD in high humidity" is not fundamentally different from the situation where an ASD is equilibrated with bulk water. It simply represents different positions in the same drug-polymer-water ternary phase diagram, which ultimately dictates the number of phases present and their respective compositions.

In principle, the solubility of a drug is essentially governed by the chemical potential of the drug in the undissolved solute. The complication concerning ASD solubility therefore stems from the fact that the undissolved solute is no longer the neat drug, but rather a multi-component phase containing up to three components including the

drug. Application of this concept to ASDs implicates that in order to contemplate the issue of ASD solubility, two sequential topics must be addressed: 1) the state of the undissolved solute and its quantitative composition, and 2) quantitative determination of the chemical potential of the drug in such undissolved solute. In this study, we aim to address these two fundamental questions, so that the mechanism of solubility enhancement of ASD (or the lack thereof) can be elucidated, both qualitatively and quantitatively. To achieve this objective, we present a full thermodynamic model to enable the estimation of the chemical potential of a drug, by considering all processes involved in ASD formation and dissolution, i.e. drug amorphization, mixing with polymer, and water partitioning. As verification, experimental solubility advantages of model ASD systems were also obtained through intrinsic dissolution studies. Through this work, we hope to emphasize that a highly critical thermodynamic property of an ASD system is the drug's chemical potential, of which the solubility is a manifestation. Because our model allows for the mapping of the drug chemical potential in the ASD, this approach can also be used to estimate the thermodynamic driving force for various ASD systems under different storage conditions, a vital attribute for the physical stability evaluation.

2.3 THEORY: CALCULATION OF SOLUBILITY ADVANTAGE AND DISADVANTAGE OF DRUGS IN AMORPHOUS SOLID DISPERSIONS

The solubility enhancement of a drug in an amorphous state is solely the consequence of increasing chemical potential (μ), or thermodynamic activity (a), of the drug. Consider, under constant temperature and pressure, the saturated solutions each

equilibrated with the crystalline or with the amorphous drug. Because the activity of the undissolved solute is equal to the activity of the dissolved solute, the evaluation of solubility ratio between the amorphous and crystalline drug is made possible by assessing their chemical potential difference:

$$\Delta\mu_{A-X} = RT\ln\frac{a_{A,undissolved}}{a_{X,undissolved}} = RT\ln\frac{a_{A,dissolved}}{a_{X,dissolved}} = RT\ln\frac{X_A\gamma_A}{X_X\gamma_X} \quad (1)$$

The symbol X_A and X_X represent the molar fraction of amorphous and crystalline drug in a saturated solution (a.k.a, solubility), respectively; R is the gas constant and T is the temperature in Kelvin. Under infinite dilution assumption (which holds true for poorly water soluble drugs), the activity coefficient of the amorphous and crystalline drugs are considered equal: $\gamma_A = \gamma_X$. Thus the solubility ratio between the amorphous and crystalline drug can be determined by rearranging equation 1 as:

$$\frac{X_A}{X_X} = \exp(\frac{\Delta\mu_{A-X}}{RT}) \quad (2)$$

As shown in equation 2, the theoretical solubility ratio between the amorphous and crystalline drug can be calculated by measuring the chemical potential differences between these two states. The ensuing sections delineate the approaches to estimate the chemical potential changes resulting from the processes which transform a neat crystalline drug to the drug mixed within an ASD system, and from the water sorption into the ASD system. Specifically, the following three processes are considered:

1. Chemical potential change of the drug due to amorphization, i.e., chemical potential difference of the *neat* drug between the amorphous state and crystalline state;

2. Chemical potential change of the drug as a result of mixing with a polymeric component, or ASD formation;

3. Chemical potential change of the drug resulting from water partitioning into the ASD when it is in equilibrium with water.

Assuming identical solution properties (e.g., the same ionization and complexation status in solution state) and free of water-mediated crystallization, the consideration of the above effects, combined, is adequate to provide a quantitative measure of the drug solubility in an ASD, as compared with the neat amorphous or crystalline state.

2.3.1 Chemical Potential Difference between the Neat Amorphous and Crystalline Drug States

The calculation of the chemical potential difference between the amorphous and crystalline states of drugs has been described in the articles by Hancock and Parks (11), and by Murdande et al. (12). Notably, in both papers, the calculation was presented by taking the supercooled liquid, rather than glass, as the reference amorphous state. While it was believed that the thermodynamic properties of the supercooled liquid and glass states, relevant to the solubility evaluation, are very similar,(12) we nevertheless present the

equations by referring the amorphous state as both a glass and supercooled liquid, so as to provide a quantitative comparison over these two assumptions.

Regardless of the choice of amorphous state, the derivation follows the same principle: the chemical potential is calculated by designing hypothetical process paths, which allow for the determination of enthalpy and entropy differences between crystalline and amorphous states at the temperature of interest using measureable thermal properties (such as heat or heat capacity).

When the supercooled liquid is assumed as the reference amorphous state, the enthalpy and entropy difference between the amorphous and crystalline state can be determined via a hypothetical path including: 1) heating the crystalline phase from temperature of interest to melting temperature, 2) fusion, and 3) cooling the liquid phase back to the temperature of interest (illustrated in Figure 2.1A). The equations representing this hypothetical path are therefore as follows:

$$\Delta H_{A-X}(T) = \Delta H_m - \int_T^{T_m}(C_{p,L} - C_{p,X})dT \tag{3}$$

$$\Delta S_{A-X}(T) = \frac{\Delta H_m}{T_m} - \int_T^{T_m}\frac{C_{p,L}-C_{p,X}}{T}\,dT \tag{4}$$

where ΔH_m and T_m are the heat of fusion and melting temperature; $C_{p,L}$ and $C_{p,X}$ are the heat capacity of the liquid and crystal, respectively. The chemical potential

difference (which is interchangeable with free energy, *G,* for one component system) is therefore:

$$\Delta G_{A-X}(T) = \Delta H_{A-X}(T) - T\Delta S_{A-X}(T)$$
$$= \Delta H_m \left(\frac{T_m - T}{T_m}\right) - \int_T^{T_m}(C_{p,L} - C_{p,X})dT + T\int_T^{T_m}\frac{C_{p,L}-C_{p,X}}{T}dT \quad (5)$$

Since all properties at the right hand side of equation 5 are available through direct measurement or extrapolation from measurable thermal quantities, the chemical potential difference can readily be evaluated through calorimetric analysis. Note that because the glass is not the reference amorphous state, this approach does not take into account the glass transition process.

Alternatively, when the glass is assumed as the reference amorphous state, the glass transition needs to be included in the hypothetical process path designed for the calculation of chemical potential difference. The path therefore includes the following steps: 1) heating the crystalline phase from temperature of interest to melting temperature, 2) fusion, and 3) cooling the liquid phase back to the glass transition temperature, 4) glass transition (from liquid to glassy state), and 5) cooling the glass from the glass transition temperature to the temperature of interest (illustrated in Figure 2.1B). Following this path, the enthalpy, entropy, and free energy difference are given as follows:

$$\Delta H_{A-X}(T) = \Delta H_m - \int_T^{T_g}(C_{p,G} - C_{p,X})dT - \int_{T_g}^{T_m}(C_{p,L} - C_{p,X})dT \quad (6)$$

$$\Delta S_{A-X}(T) = \frac{\Delta H_m}{T_m} - \int_T^{T_g} \frac{C_{p,G} - C_{p,X}}{T} dT - \int_{T_g}^{T_m} \frac{C_{p,L} - C_{p,X}}{T} dT \quad (7)$$

$$\Delta G_{A-X}(T) = \Delta H_m \left(\frac{T_m - T}{T_m}\right) - \left[\int_T^{T_g} (C_{p,G} - C_{p,X}) dT + \int_{T_g}^{T_m} (C_{p,L} - C_{p,X}) dT\right] + T\left[\int_T^{T_g} \frac{C_{p,G} - C_{p,X}}{T} dT + \int_{T_g}^{T_m} \frac{C_{p,L} - C_{p,X}}{T} dT\right] \quad (8)$$

where $C_{p,G}$ is the heat capacity of glass and T_g is the glass transition temperature. The solubility ratio between the amorphous and crystalline state of a neat drug can therefore be assessed by combining equation 2 with equation 5 (using supercooled liquid as reference amorphous state), or with equation 8 (using glass as reference amorphous state).

2.3.2 Chemical Potential Change of Drug Resulting from ASD Formation

The formation of a fully miscible ASD is in essence a mixing process giving rise to a one-phase, two-component system. Because pharmaceutical ASDs typically involve a small molecule drug and a polymeric component, the system is pertinently described by the Flory-Huggins equation originally used to study polymer-solvent miscibility.(21) Based on the Flory-Huggins formalism, the free energy of mixing ΔG_{mix} for the ASD system is:

$$\Delta G_{mix} = RT\left(\emptyset_{drug} \ln \emptyset_{drug} + \frac{\emptyset_{poly}}{r} \ln \emptyset_{poly} + \chi \emptyset_{drug} \emptyset_{poly}\right) \quad (9)$$

where $\emptyset_{drug}$ and $\emptyset_{poly}$ are the volume fraction of the drug and polymer, respectively. The symbol r is the volume ratio of polymer and drug ($r = V_{poly}/V_{drug}$), and χ is the interaction parameter.

It's important to note that the Flory-Huggins equation (equation 9) assesses the free energy of the ASD *system* only, whereas the component of interest is in fact the *drug*. To consider the change of chemical potential, or *partial molar free energy*, of the drug in the ASD system, one is to take the partial derivative of ΔG_{mix} with respect to the molar quantity of the drug ($\Delta\mu_{drug} = \left.\frac{\partial \Delta G_{mix}}{\partial n_{drug}}\right|_{P,T,n_{poly}}$). The derivation leads to (22):

$$\frac{\Delta\mu_{drug}}{RT} = \ln\emptyset_{drug} + \left(1 - \frac{1}{r}\right)\emptyset_{poly} + \chi\emptyset_{poly}^{\,2} \tag{10}$$

Equation 10 describes the chemical potential change of an amorphous drug when it is mixed with a polymeric component to form the miscible ASD. Because the volume fraction and size difference of two components are readily available from the drug loading and the molecular properties of individual components, the effect of ASD formation on the chemical potential of the drug can be quantitatively evaluated as long as the interaction parameter χ, representing the enthalpic contribution of the drug-polymer interaction, is known.

2.3.3 Chemical Potential Change of Drug in ASD Resulting from Water Partition

Unlike the crystalline drug, which does not take up a significant amount of water in its lattice, amorphous systems are characterized by stronger moisture absorption in an environment with high water activity. For a saturated aqueous solution equilibrated with ASD, water partition into the undissolved solute during water equilibration will take place and will effectively lower the activity of the drug.(23) Namely, the chemical potential of the drug in an ASD will be further reduced as the result of water partitioning, when the ASD is exposed to water.

The impact of water sorption on chemical potential of the *neat* drug was previously investigated in a number of articles (12, 13, 24, 25) following the Gibbs-Duhem equation. Unlike the neat drug, a total of 3 components must be accounted for regarding the ASD-water system. At constant temperature and pressure, the Gibbs-Duhem equation therefore takes the following form:

$$x_{drug}d\mu_{drug} + x_{poly}d\mu_{poly} + x_{water}d\mu_{water} = 0 \quad (11)$$

Rearranging equation 11 and integrating from zero to complete water saturation gives:

$$\Delta\mu_{drug} + \frac{x_{poly}}{x_{drug}}\Delta\mu_{poly} = -\int_0^{\mu^0_{water}} \frac{x_{water}}{x_{drug}} d\mu_{water} \quad (12)$$

Because $\mu_{water} = \mu^0_{water} + RT\ln a_{water}$, where μ^0_{water} is the chemical potential of water at standard state, and a_{water} is the water activity, and assuming $\frac{x_{poly}}{x_{drug}}$ remains unchanged regardless of the extent of water sorption in ASD, equation 12 can be re-written as:

$$\Delta\mu_{drug} + \frac{x_{poly}}{x_{drug}}\Delta\mu_{poly} = -RT\int_0^1 \left(\frac{x_{water}}{x_{drug}}\right)\frac{1}{a_{water}}da_{water} \quad (13)$$

If we make an assumption that the ASD is a homogenous 1-phase system, and that the interaction of water with drug and with polymer are identical, such that $\Delta\mu_{drug} = \Delta\mu_{poly}$, then the chemical potential of the drug in ASD becomes:

$$\frac{\Delta\mu_{drug}}{RT} = -\left(\int_0^1 \left(\frac{x_{water}}{x_{drug}}\right)\frac{1}{a_{water}}da_{water}\right) / \left(1 + \frac{x_{poly}}{x_{drug}}\right) \quad (14)$$

The evaluation of $\Delta\mu_{drug}$ from standard dynamic vapor sorption experiment is thus enabled by equation 14. The vapor sorption isotherm of the ASD, covering the relative humidity of 0% to 100%, can be integrated following equation 14 to obtain the quantitative estimation of the chemical potential change of the drug resulting from water partition into the ASD.

2.3.4 Drug Solubility Ratio: ASD vs. Neat Crystalline or Amorphous Drug

By accounting for the process of amorphization, ASD formation, and water partition, one can estimate the solubility ratio between the drug in ASD and the drug in neat crystalline state, $\frac{X_A^{ASD}}{X_X}$. Specifically, the solubility ratio is obtained by combining equations 2, 5 (or 8), 10, and 14 as:

$$\ln\frac{X_A^{ASD}}{X_X} = \left\{\frac{\Delta H_m}{R}\left(\frac{1}{T}-\frac{1}{T_m}\right) - \frac{1}{RT}\int_T^{T_m}(C_{p,L}-C_{p,X})dT + \frac{1}{R}\int_T^{T_m}\frac{C_{p,L}-C_{p,X}}{T}dT\right\} + \left\{\ln\emptyset_{drug} + \left(1-\frac{1}{r}\right)\emptyset_{poly} + \chi\emptyset_{poly}{}^2\right\} - \left\{\left(\int_0^1\left(\frac{x_{water}}{x_{drug}}\right)\frac{1}{a_{water}}da_{water}\right)/\left(1+\frac{x_{poly}}{x_{drug}}\right)\right\} \quad (15)$$

Equation 15 assumes that the supercooled liquid is reference amorphous state, or:

$$\ln\frac{X_A^{ASD}}{X_X} = \left\{\frac{\Delta H_m}{R}\left(\frac{1}{T}-\frac{1}{T_m}\right) - \frac{1}{RT}\left[\int_T^{T_g}(C_{p,G}-C_{p,X})dT + \int_{T_g}^{T_m}(C_{p,L}-C_{p,X})dT\right] + \frac{1}{R}\left[\int_T^{T_g}\frac{C_{p,G}-C_{p,X}}{T}dT + \int_{T_g}^{T_m}\frac{C_{p,L}-C_{p,X}}{T}dT\right]\right\} + \left\{\ln\emptyset_{drug} + \left(1-\frac{1}{r}\right)\emptyset_{poly} + \chi\emptyset_{poly}{}^2\right\} - \left\{\left(\int_0^1\left(\frac{x_{water}}{x_{drug}}\right)\frac{1}{a_{water}}da_{water}\right)/\left(1+\frac{x_{poly}}{x_{drug}}\right)\right\} \quad (16)$$

Equation 16 assumes that the glass is the amorphous reference state.

The three curly brackets on the right hand side of equations 15 and 16 represent the contributions from the process of amorphization, ASD formation, and water partitioning, respectively.

The derivation also allows for the estimation of solubility ratio between the drug in ASD and the drug in neat amorphous state, $\frac{X_A^{ASD}}{X_A^{neat}}$. Although the drug remains amorphous in both conditions, their chemical potentials (and thereby solubilities) are different due to the mixing process from the ASD formation, as well as the difference in their ability to absorb water upon water exposure. $\frac{X_A^{ASD}}{X_A^{neat}}$ is expressed by combining equations 2, 10, and 14:

$$\ln\frac{X_A^{ASD}}{X_A^{neat}} = \left[\ln\emptyset_{drug} + \left(1-\frac{1}{r}\right)\emptyset_{poly} + \chi\emptyset_{poly}{}^2\right] - \left[\left(\int_0^1\left(\frac{x_{water}}{x_{drug}}\right)\frac{1}{a_{water}}da_{water}\right)/\left(1+\frac{x_{poly}}{x_{drug}}\right)\right]_{ASD} + \left[\int_0^1\left(\frac{x_{water}}{x_{drug}}\right)\frac{1}{a_{water}}da_{water}\right]_{neat} \quad (17)$$

The subscripts "ASD" and "neat" on the right hand side of equation 17 indicate the water absorption with the ASD and with the neat amorphous drug, respectively.

Collectively, equations 15, 16, and 17 establish the full thermodynamic treatment of the solubility advantage (and disadvantage) of the drug in the form of an ASD, as compared to its crystalline and amorphous counterparts.

2.4 MATERIALS AND METHODS

2.4.1 Materials

Crystalline indomethacin (IMC) was purchased from Acros Organics (Fisher Scientific, Waltham, WA). EUDRAGIT® E PO (EPO) was obtained from Evonik (Evonik Industries, Piscataway, NJ). Phosphoric acid and HPLC grade acetonitrile were purchased from Fisher Scientific (Fisher Scientific, Houston, TX). All other chemicals used in this study were of American Chemical Society (ACS) grade.

2.4.2 Methods

2.4.2.1 Preparation of Amorphous Drug and Amorphous Solid Dispersions

Amorphous IMC and IMC/EPO ASDs with IMC loadings of 30%, 50%, and 70% w/w were prepared by quench cooling the molten raw crystalline IMC (γ-form) or the IMC/EPO physical blends. Specifically, the crystalline IMC or IMC/EPO physical blends were kept in a scintillation vial in an oven set at 175 ℃ until they were visually 100% molten. The vial was then stored in the oven for an additional 5 minutes. The molten materials were then quench-cooled by immersion into liquid nitrogen and further milled using pre-chilled mortar and pestle in a dry glove box to avoid moisture condensation.

The resulting melt-quenched samples were confirmed to be fully amorphous by the absence of birefringence under cross polarized microscopy, the absence of a crystalline diffraction pattern by powder x-ray diffraction, and by the presence of a glass transition

and absence of melting endotherm by differential scanning calorimetry. All amorphous samples were analyzed by reverse phase HPLC (high-performance liquid chromatography) to assess their chemical purity after melting and quench cooling. All amorphous compounds were determined to have > 99% purity relative to the original crystalline sample. Amorphous samples were stored in a desiccator over phosphorus pentoxide and were presented for analysis as powders of between 74 (200 US mesh) and 125 μm (120 US mesh). The water content of each of these samples was found to be less than 0.2% w/w by Karl-Fisher titration.

2.4.2.2 Intrinsic Dissolution

To evaluate the true solubility advantage of ASDs, intrinsic dissolution tests were carried out as an alternative to the equilibrium solubility measurements to minimize the likelihood of potential water-mediated crystallization (26, 27). For a diffusion-controlled dissolution process, the intrinsic dissolution rate (dm/dt) is governed by the Noyes-Whitney equation:

$$\frac{dm}{dt} = A\frac{D}{h}(C_s - C_0) \tag{18}$$

where A is the surface area, D is the diffusion coefficient, h is the thickness of the diffusion layer, and C_s and C_0 are the concentration at the inner boundary of the diffusion layer (or saturated solubility) and in the bulk, respectively. As far as IMC is concerned, when the intrinsic dissolution tests of the IMC/EPO ASDs (including the

IMC/EPO physical mixtures) are conducted with identical surface area, under sink conditions, and with identical hydrodynamics, the solubility of the IMC (C_s) is linearly proportional to its intrinsic dissolution rate (dm/dt). The solubility advantage of ASDs can therefore be obtained by comparing the intrinsic dissolution rate of an ASD with the corresponding IMC/EPO physical mixture of the same drug loading.

A custom-made system, modified from the traditional Wood's design (28), was used for the intrinsic dissolution testing. For each run, 75 mg of ASD powder between 74 to 125 μm in size were compressed into compact in an 8-mm round die using a Carver press. For the intrinsic dissolution testing of IMC/EPO physical mixtures, the two components were co-ground using mortar and pestle to achieve intimate mixing before compressing into compact. The compact was produced at the compression force of 1.5 metric ton and the dwell time of 3 second to ensure that a highly smooth compact surface was produced. The compact was then ejected against a smooth metal surface so that the bottom face of the compact was fully exposed. No phase transformation or chemical degradation was observed due to compression.

The compact-die assembly was placed at the center of a 500-mL beaker containing 200 mL 50 mM, pH 6.0 citrate buffer pre-warmed at 25 °C. A paddle was placed 1 inch above the exposed compact surface and stirred at a rate of 50 RPM. Dissolution medium samples were collected at predetermined time points and analyzed using HPLC. Only the data from the samples collected at early time points (below 10 min), which fit well into a

straight line in the concentration-time profile, were used for dissolution rate analysis. The pH of the dissolution medium was found to remain unchanged during the course of the dissolution run. For tests where ASDs or the neat amorphous drug were used as specimen, the remaining compacts were collected at the end of the run and subjected to powder X-ray diffraction analysis to confirm the lack of crystallization. At least three separate measurements were carried out for each material. To ensure identical surface area and hydrodynamic conditions, the exact same experimental setup and accessory parts, including the beaker, were used for all measurements.

2.4.2.3 Heat Capacity Measurement

The calorimetric analysis of IMC, EPO and ASDs were measured by a TA Q2000 differential scanning calorimeter (DSC) equipped with a refrigerated cooling system (TA Instruments, New Castle, DE). Dry nitrogen gas at a flow rate of 40 mL/min throughout the testing was used to purge the cell. For heat capacity measurement, the standard ASTM method was adopted (29). Firstly, empty hermetic pans with lids (without crimping) was heated from 25 °C to 105 °C at the heating rate of 20 °C/min and then cooled to -20 ° C, followed by a 5 minutes isothermal hold. The pans were then heated back to 180 °C at the heating rate of 20 °C/min. Secondly, the accurately weighed (±0.001 mg) disc-shape sapphire standard were loaded into the same sample pan and subjected to the identical "heat-cool-heat" cycle. Thirdly, the sapphire standard disc was removed from the same sample pan and replaced by the specimen. The same thermal cycle was performed again. The heat capacity of the specimen was calculated from the heat flow data and by

referencing the heat capacity data of the sapphire standard, following the ASTM method (30).

2.4.2.4 Melting Point Depression Analysis

The interaction parameter of the IMC/EPO system was determined by the melting point depression analysis. Physical IMC/EPO mixtures containing 0, 5, 10, 15, 20, and 25% wt of EPO (w/w) were prepared by geometric mixing. These mixtures were stored in desiccator over phosphorous pentoxide until use. The melting temperature of the IMC in the presence of EPO was measured with the TA Q2000 DSC equipped with a refrigerated cooling system at a scan rate of 1 ℃/min. The extrapolated onset melting temperature was used for the data analysis. The details of the method is described elsewhere.(31)

2.4.2.5 Dynamic Vapor Sorption Analysis

The water sorption isotherm of amorphous IMC and ASDs were determined at 25 ℃ using a DVS2000 dynamic vapor sorption apparatus (Scientific Measurement Systems, Manchester, UK). The sample (about 10 mg) was transferred to the quartz holder where they were dried at 25 ℃, 0.4% relative humidity (RH) until a constant mass was attained. The moisture sorption isotherm was measured by increasing percent RH at the step size of 5% and covered the entire (0-100%) RH range. A maximum of 6 hours of equilibration time was given for each RH step, unless the rate of weight gain dropped to below 0.005% wt per 10 min. At the end of the sorption runs, samples were retrieved and subjected to the

polarized light microscopy and powder X-ray diffractometry to verify the absence of moisture-mediated crystallization.

2.5 RESULTS AND DISCUSSIONS

2.5.1 What is the Undissolved Solute When an ASD is in Equilibrium with Water?

We start the discussion by asking the question: What exactly is the undissolved solute when an ASD is in equilibrium with water? This is a critical question because it is the activity of drug in the undissolved solute that governs the solubility. The answer for the question lies in the understanding of the phase behavior of the ternary system, which consists of three components (drug, polymer, and water) and up to three phases at constant temperature and pressure, as permitted by the phase rule.

Most pharmaceutical ASDs share some common features: they are the binary system containing a poorly water soluble drug, and a polymer component which is hydrophilic and possesses high solubility with both water and the drug (such as PVP, PVPVA, or HPMC etc.). Because the water-equilibrated ASD exists as the supercooled liquid state due to significant water partitioning (see discussion in ensuing sections), the phase equilibria in the pharmaceutical drug-polymer-water system is analogous to the "polymer"-solvent-nonsolvent (P-S-N) system commonly encountered in the polymer industry (the quotation mark is used to distinguish from pharmaceutical polymers used in ASD) (32-34). Here, the pharmaceutical polymer is analogous to the solvent because the

polymer is miscible with both water and drug; the water is analogous to nonsolvent, and the drug to “polymer”. Just as the “polymer” is not soluble in nonsolvent, neither is the drug soluble in water.

The simplest phase equilibria of the pharmaceutical ASD in water are demonstrated in the schematic ternary phase diagram shown in Figure 2.2. In the diagram, point A represents the state of a typical ASD solubility study, where a small quantity of ASD (assuming 50% drug loading here, corresponding to point D) is placed in a large amount of water. Like the P-S-N system, there is a miscibility gap that extends from the drug-water side into the ternary system. Because point A is located inside the miscibility gap, the ASD-water system in equilibrium contains two phases, and their respective compositions are revealed through the tie line BC which extends through point A. The measured drug solubility in water can therefore be determined from point C, the phase where water is the prevalent component. Similarly, the final equilibrating ASD (or undissolved solute) corresponds to point B, the phase where the drug and polymer are the prevalent components. Figure 2.2 shows that the final equilibrating ASD in water has much higher drug loading (point F) than the original ASD (point D). The analysis on the simple version of the schematic ternary phase diagram indicates that the ASD solubility is a rather complicated issue. The apparent aqueous drug solubility of an ASD not only depends on the size and shape of the miscibility gap, which could be evaluated under the framework of the Flory-Huggins theory, it also depends on the initial ASD drug loading, as well as the amount of ASD added in water (because they control where the tie line is drawn).

To the question: What is the undissolved solute when an ASD is equilibrated with water? A possible answer by following Figure 2 is: as the first step, a 1-phase, 3-component system containing drug, polymer and water (such as point B in Figure 2.2), and the compositions of this solute may be different from the original ASD compositions. A subsequent crystallization step could occur if the chemical potential of the drug in this solute is higher than the free energy of the neat crystal. But even without crystallization, we may not expect the predicted solubility advantage, calculated on the basis of the initial drug loading and moisture sorption isotherm of the "dry" ASD, to be identical to the experimental data. However, if the compositions of the undissolved solute are known, then the drug solubility of ASD, relative to the neat form, can be calculated. The following sections center on the quantitative estimation of the effect of polymer and water on drug solubility, as they are inevitably present in the undissolved solute in the ASD-water system.

2.5.2 Solubility Advantage of Amorphous Drug Can be Reduced Through ASD Formation

The impact of ASD formation on IMC drug solubility is presented in Table 2.1 and Table 2.2. The tables list the experimental and predicted solubility ratio of IMC in the form of ASD, versus the neat crystalline form ($\frac{X_A^{ASD}}{X_X}$) and versus the neat amorphous form ($\frac{X_A^{ASD}}{X_A^{neat}}$), respectively. The calculations were carried out by following equations 15 and 17, using the molecular properties of IMC and EPO given in Table 2.3. The experimental solubility ratios ($\frac{X_A^{ASD}}{X_X}$ and $\frac{X_A^{ASD}}{X_A^{neat}}$) were determined through the intrinsic dissolution rate obtained at

the early phase of the dissolution process, using the respective materials, i.e. IMC/EPO ASD, physical mixture of crystalline IMC and EPO, and physical mixture of amorphous IMC and EPO, all with the same drug loading (Figure 2.3). The intrinsic dissolution was used as an alternative to the equilibrium solubility measurement to minimize the potential confounding effect of water-mediated crystallization (see Materials and Methods section).

The experimental data in Table 2.1 show that the solubility advantages of IMC in IMC/EPO ASD systems over the crystalline form are rather limited. The highest solubility ratio ($\frac{X_A^{ASD}}{X_X}$) observed is 1.27, and for the ASD with 70% drug loading, the solubility of IMC is lower than that of its crystalline counterpart! As verification, our experimental solubility ratio of the neat amorphous IMC vs neat crystalline IMC at 25 ºC, also through intrinsic dissolution measurements, is 3.4, close to the literature data (between 4.4-4.9).(11, 12) These ASD solubility data demonstrate that: *for an amorphous drug, the ASD formation could be a process of strong thermodynamic stabilization, leading to marked decrease in its chemical potential, which can be manifested by the lowering of its solubility*. In order to capture this phenomenon, we purposely selected EPO as the polymeric component for the ASD, and conducted the dissolution experiments at pH 6.0, where EPO exhibits low solubility. Additionally, we determined the intrinsic dissolution rate using the data points collected in the first few minutes, so as to minimize any potential phase separation or phase transformation upon exposure of ASD to water.

The stabilization effect of ASD formation is equally evident from the experimental solubility ratio of IMC in the form of ASD vs. neat amorphous IMC ($\frac{X_A^{ASD}}{X_A^{neat}}$) (Table 2.2). In all ASD systems tested, the solubility of IMC in the form of ASD is lower than the neat amorphous form; value of $\frac{X_A^{ASD}}{X_A^{neat}}$ as low as 21% is observed. These data suggest that, for a small molecule drug, its solubility advantage gained through amorphization can take a significant loss when the drug is mixed with another component to form a stable ASD system, even though the amorphous structure of the ASD is maintained.

The solubility-reducing effect underlying the ASD formation can be understood through examining the theoretical calculations. As shown in Table 2.1 and 2.2, the ASD formation plays a significant role in lowering the predicted drug solubility. Quantitatively, the extent of solubility reduction through ASD formation is expressed by equation 10: $\Delta \ln X_A^{ASD} = \frac{\Delta \mu_{drug}}{RT} = \ln \emptyset_{drug} + \left(1 - \frac{1}{r}\right) \emptyset_{poly} + \chi \emptyset_{poly}{}^2$. Equation 10 indicates that the magnitude of chemical potential or solubility change of a drug in ASD depends primarily on two factors: 1) drug loading, and 2) drug-polymer interaction parameter χ. Using IMC/EPO ASD system as an example, the impact from these two factors is exhibited in Figure 2.4, where the solubility advantage of ASD over the crystal, $\frac{X_A^{ASD}}{X_X}$, and ASD-driven chemical potential change are plotted as the function of drug loading. To demonstrate the effect of drug-polymer interaction, Figure 2.4 also contains several curves calculated using the properties of the IMC/EPO ASD system but with hypothetical χ values. The water

partitioning effect was not included in the calculation, so that Figure 2.4 focuses solely on the effect of ASD formation.

Figure 2.4 shows that in the actual IMC/EPO ASD system (χ = -0.58), the value of $\frac{X_A^{ASD}}{X_X}$ and the chemical potential of the drug decrease monotonically with decreasing drug loading. For this ASD system, the negative χ value means the IMC-EPO mixing is an exothermic event. Thus, for as far as the IMC is concerned, its dilution with EPO is both entropically and enthalpically favored in a monotonic manner. In other words, for any ASD systems where the mixing is athermal or exothermal ($\chi \leq 0$), the solubility and chemical potential of the drug will decrease with decreasing drug loading. This relationship is evident in Figure 2.4 for all the ASDs with zero or negative interaction parameter. It is only in the systems where $\chi \geq 0$ (endothermic mixing) can the chemical potential of a drug rise with decreasing drug loading. Such ASD systems are nevertheless enthalpically disfavored and are usually not fully miscible in the long term.

The interaction parameter χ also has profound impact on the IMC solubility and chemical potential. By definition, χ is the term to account for the non-athermal mixing in the Flory-Huggins formalism.(35) A large, negative χ value translates to highly exothermic drug-polymer mixing and hence stronger attractive interactions. As shown in Figure 2.4, ASD systems possessing more negative χ values exhibit more precipitous decrease in drug solubility and chemical potential with decreasing drug loading, indicating greater

stabilization effect. For these systems, the chemical potential or solubility of a drug can be depressed to below that of its crystalline counterpart! For example, for the "IMD/EPO ASD" with a hypothetical χ value of -5 in Figure 2.4, the chemical potential and the solubility of the drug become lower than that of the crystalline form (represented as the horizontal line in Figure 2.4), when the drug loading drops to below 25%. The interaction parameter of this level has shown to be realistic in pharmaceutical ASDs both by computation and by experiments.(36,37). To summarize, the formation of *an enthalpically favored, low drug loading ASD is a highly efficient means to reduce the chemical potential of an amorphous drug.* If sufficient amount of polymer is present in the equilibrated undissolved solute, it will act as a strong thermodynamic stabilizer, which will be reflected by the significant decrease of the drug solubility.

2.5.3 Solubility Advantage of Amorphous Drug Can be Further Reduced by Water Partitioning in ASD

The deleterious effect of water partitioning on the solubility of neat amorphous materials has been described by Sacchetti and by Murdande et al.(12, 13, 24, 25) according to the Gibbs-Duhem equation. For ASD systems, the same principle applies, but because the undissolved solute in the ASD-water system is a 3-component phase, the Gibbs-Duhem equation must be presented as a ternary system (instead of binary system), comprising drug, polymer and water (see equation 14). The hydrophilic polymers employed in the pharmaceutical ASD typically exhibit greater hygroscopicity than the neat amorphous drug (such is the case for IMC/EPO system, see Figure 2.5), and are therefore capable of

absorbing more water. Essentially, the use of hydrophilic polymers facilitates water partitioning into the solid phase, and serves to further reduce the chemical potential of both the drug and polymer components.

The impact of water partitioning on drug solubility in an ASD is significant. In Figure 2.6, the estimated solubility ratio $\frac{X_A^{ASD}}{X_X}$, with and without the correction on water partition, is shown for IMD/EPO ASD systems with different drug loadings. As expected, solubility reduction resulting from the water partitioning is not negligible across all ASD systems, including the neat amorphous IMC. It is more pronounced at low drug loading, owing to the higher level of water sorption for low drug loading ASDs (Figure 2.5). The smallest effect is on neat amorphous IMC, with 23% of decrease in $\frac{X_A^{ASD}}{X_X}$; the greatest effect is on ASD with lowest (30%) drug loading, with 67% of decrease in $\frac{X_A^{ASD}}{X_X}$. Combined with the previous section, this study shows that the solubility advantage of a drug in ASD can be very sensitively to drug loading. Lowering the drug loading leads to chemical potential decrease by means of two mechanisms: 1) greater level of polymer dilution and 2) more water partitioning. These mechanisms contribute synergistically to removing the solubility advantage of the drug originally gained from the process of amorphization.

It is worth noting that we carried out the quantitative analysis by making an assumption that the drug-water interaction and polymer-water interaction are identical, so that $\Delta\mu_{drug} = \Delta\mu_{poly}$ (see Theoretical section). We made this assumption because for the

ASD-water system, the Gibbs-Duhem equation contains three terms and cannot be resolved without a known relationship between $\Delta\mu_{drug}$ and $\Delta\mu_{poly}$. While the relationship $\Delta\mu_{drug}$ and $\Delta\mu_{poly}$ is not readily assessed in the miscible system, literature data are available for individual components. It was shown that for water partitioning into an amorphous drug or polymer, the solid phase usually undergoes a negative deviation from the ideal behavior (i.e. greater reduction in chemical potential than predicted by Raoult's law),(24, 38) and that the hydrophilic polymers, such as PVP or microcrystalline cellulose, exhibit more negative deviation than indomethacin. If this observation also holds true for the 1-phase system, then the relationship becomes: $\Delta\mu_{poly} = k\Delta\mu_{drug}$ where $k > 1$. Equation 14 can therefore be re-written as $\frac{\Delta\mu_{drug}}{RT} = -\left(\int_0^1 \left(\frac{x_{water}}{x_{drug}}\right)\frac{1}{a_{water}} da_{water}\right) / \left(1 + k\frac{x_{poly}}{x_{drug}}\right)$, indicating that our data regarding drug solubility advantage loss due to water partition could be an over-estimate, predicting the worst-case scenario.

2.5.4 The State of Undissolved Solute: Glass or Supercooled Liquid?

For solubility assessment of ASDs, a pertinent question to consider is the state of the undissolved solute in equilibrium with water, as drug solubility is dictated by the activity of the drug in the undissolved solute. As discussed in the preceding section, significant water partitioning, with a minimum of a few percent by weight, will occur in pharmaceutical ASDs upon exposure to water. Because water is a strong plasticizer and possesses a much lower molecular weight than ASD components, the water sorption of this magnitude will inevitably depress the T_g to below the temperature of practical interests

(e.g. between 0 – 37 ºC).(19, 39) Therefore, we believe that for a pharmaceutical ASD in equilibrium with water, the undissolved solute is presented as the supercooled liquid. Additionally, as proposed Murdande et al.,(12) because supercooled liquid is a quasi-equilibrium state,(40) any prior thermal history gathered by the glassy ASD will be erased upon equilibration with water. For this reason, the solubility estimation in foregoing sections was carried out by treating the ASD as a supercooled liquid.

We complete this question by providing a quantitative comparison of the supercooled liquid form and the glass form of IMC, regarding their energy state and solubility advantage over crystal. This assessment was carried out following equations 5 and 8, using the heat capacity data of crystalline, glass, and liquid state of IMC (see Theoretical section for details). In Figure 2.7, the estimated solubility ratio between the neat amorphous IMC and crystalline IMC, $\frac{X_A}{X_X}$, using either the supercooled liquid or glass as reference amorphous state, is provided over a range of temperatures below T_g (approximately 44 ºC). As the temperature is reduced below T_g, the two solubility ratios depart, with the glass showing an increasingly higher solubility advantage than the supercooled liquid (Figure 2.7). This phenomenon is valid because the glass, being a thermodynamically arrested state, always exhibits higher entropy *S* than the supercooled liquid (as demonstrated in Figure 2.1). Because the slope of the *G*-*T* curve is –*S*, the rate of free energy increase with decreasing temperature in the glass must be higher than that of the supercooled liquid. The lower the temperature away from T_g, the greater this discrepancy. However, for IMC, since the temperature of our solubility measurements (25

^{o}C) is very close to T_g, the difference between the solubility advantages calculated using either glass or supercooled liquid are negligible ($\frac{X_A}{X_X} = 48.6$ for glass vs. 47.1 for supercooled liquid). Yet, for materials possessing a much higher T_g, the difference is expected to be significant if the solubility or free energy is estimated at the ambient temperature.

2.5.5 Discrepancy between Predicted and Experimental Solubilities

Our model predicts that the solubility advantages of IMC in the IMC/EPO ASD systems are much less than the estimation based merely on the free energy elevation due to amorphization (Table 2.1 and 2.2). This conclusion is corroborated by our experimental data showing rather moderate solubility advantage, if at all, of the IMC/EPO ASDs over the IMC crystal. Still, the calculated solubility ratios using our model remain as an over-estimate in comparison with the experimental data (predicted $\frac{X_A^{ASD}}{X_X}$ values of 6.2-25.8 vs. experimental values of 1.27-0.95). Most notably, our model indicates that the solubility advantage decreases with decreasing drug loading, whereas the experimental data show precisely the opposite.

As stated in the preceding section, we do not expect the experimental solubility to be identical to the predicted value, because the final composition of the undissolved solute can be different from the original ASD (though we attempted to retard the water-mediated phase separation by using an ASD comprising a poorly water soluble polymeric

component). Another main contributor to this discrepancy is the evaluation of the interaction parameter χ. In this study, χ was measured using the common melting point depression approach.(41) The method is known to suffer several limitations, one of which is the negligence of its temperature and composition dependence.(42) Due to the nature of the method, we assigned a single χ value to all ASDs regardless of their composition, though χ was reported to vary significantly with composition.(43) In our measurements, the melting point data were collected with up to 25% EPO in the mixture, and the resulting melting points are distant from the ambient temperature. The use of these data at the ambient temperature, and for compositions containing a maximum of 70% EPO, could lead to substantial deviation. Furthermore, Sun et al.(37) suggest that the typical DSC scanning rate for the melting point depression study (such as the rate used in our measurement: 1 ^{o}C/min) could be too fast to attain the solubility equilibrium, so that the apparent melting temperature is higher than the value at which the solubility equilibrium would actually be arrived. By adding a lengthy annealing step at an elevated temperature to achieve solubility equilibrium, Sun et al. obtained χ values which are up to one order of magnitude more negative than the original approach. This could mean that we significantly under-estimated the negativity of the χ values for the IMC/EPO ASD systems, and hence over-estimated the solubility advantage of the ASDs.

One evidence appearing to support this hypothesis is the T_g of the IMC/EPO ASDs relative to the theoretical values calculated using Gordon-Taylor equation, derived on the assumption of volume additivity and ideal mixing behavior.(44) As shown in Figure 2.8,

there is a strongly positive deviation from the theoretical T_g for the ASD with high drug loading (70%), and negative deviation for the ASD with low drug loading (30%). A positive deviation from the theoretical T_g is usually attributed to strong intermolecular interactions, and vice versa.(45, 46) While this notion may be an over-simplification and exceptions exist,(3) the substantial composition-dependence of T_g deviation of the IMC/EPO system agrees with the this hypothesis. Namely, the ASD with high drug loading possesses much stronger drug-polymer interaction than the ASD with low drug loading, and the actual χ value at higher drug loading is more negative than at lower drug loading. Consequently, the greater polymer dilution brought about by lower drug loading could be offset by the weaker drug-polymer interactions, and the difference in solubility for the ASD with different drug loadings would be less pronounced than our original estimate assuming a constant χ value.

2.5.6 Pharmaceutical Significance

Like any solubility study, the activity (or chemical potential) of the drug in the undissolved solute is the governing factor for drug solubility. A prerequisite to understanding the ASD solubility is to analyze the phase behavior of the drug-polymer-water ternary system; in particular, the composition of the undissolved solute when the ASD is in equilibrium with water. This information should be valuable for pharmaceutical ASD development seeking superior solubility and dissolution behavior. To this end, we propose that, as a simplest case, the following phenomena could be expected when a pharmaceutical ASD is exposed to water:

1) A miscibility gap may exist in the drug-polymer-water system, which gives rise to phase separation upon exposure of ASD to water;

2) The final undissolved solute may be a 1-phase, 3-component system containing drug, polymer, and water, and its composition could be different from that of the original ASD;

3) For a stable ASD, both the polymer and water present in the undissolved solute serve to reduce the solubility advantage of the drug;

4) The undissolved solute is in the supercooled liquid state;

5) If only two phases are present in the ASD-water system, the ASD solubility will be dependent on the initial ASD drug loading and the amount of ASD and water used for equilibration, due to the extra degree of freedom permitted by the phase rule. Namely, the apparent solubility of ASD depends on how the experiments are carried out.

If the equilibrium composition of the undissolved solute is known, then the solubility advantage of the drug in the ASD can be quantitatively determined. In light of this, the working equations are fully derived and discussed throughout the preceding sections.

Furthermore, we believe the pharmaceutical significance of this study goes beyond the ASD solubility evaluation. What is presented in this article is essentially the quantitative mapping of the chemical potential change of the drug as the result of amorphization, ASD preparation and water sorption. This approach, as a whole, also addresses questions relating to the thermodynamics of ASD, with solubility being just one of them.

A fundamental question remaining in pharmaceutical ASD development is the mechanism by which the ASD stabilizes amorphous drugs and prevents their crystallization. *The model presented in this article enables the actual quantitation of the chemical potential difference between the drug in ASD and the neat crystalline form, which is, by definition, the thermodynamic driving force*. Through thermodynamic calculations and solubility experiments, we showed that this thermodynamic driving force can actually be determined, and under certain circumstances (such as low drug loading, highly exothermic drug-polymer mixing, and high moisture sorption), the driving force can become negative, meaning that the ASD stabilizes the drug to the extent that the chemical potential of the drug falls below its crystalline counterpart, essentially eliminating any possibility for crystallization. We also notice that the key to this practice is an accurate estimation of the drug-polymer interaction parameter. With such information available, we believe that the method presented in this article is useful for any pharmaceutical ASD screening process, as it informs scientists, quantitatively, the extent of thermodynamic stabilization for different polymer candidates and with different drug loading.

2.6 CONCLUSIONS

Although amorphous solid dispersions (ASDs) have long entered the mainstream of pharmaceutical development arena as an approach to improve bioavailability, quantitative studies of its mechanism on solubility enhancement have been scarce. In this article, we provided a quantitative answer to the question of ASD solubility advantage, through the investigation of the drug-polymer-water system by means of heterogeneous phase equilibria analysis.

We started by emphasizing that the ASD solubility is solely governed by the activity (or equivalently, chemical potential) of the drug in the undissolved solute in equilibrium with water, and the first question to answer in light of the ASD solubility is the phase behavior of the drug-polymer-water ternary system. We proposed that the state of pharmaceutical ASD in equilibrium with water resembles the polymer-solvent-nonsolvent systems encountered in the polymer industry and that in a simplest case, a miscibility gap could be present. This miscibility gap will lead to phase separation, and the final undissolved solute in equilibrium with water is a 1-phase, 3-component material, containing drug, polymer, and water. The composition of this undissolved solute can be different from the composition of the original ASD.

We then presented the full thermodynamic model for the quantitative assessment of solubility advantage of such ASDs. Specifically, the method accounts for the solubility change as the result of 1) amorphization, 2) ASD formation, and 3) water partitioning.

Experimentally, we measured the solubility advantage of ASDs, by means of intrinsic dissolution measurements, using indomethacin/EPO ASD as the model system. Both the theoretical and experimental results showed that the solubility advantage of ASD can be significantly lower than the neat amorphous drug, due to the effect of polymer dilution and water sorption, both of which contributed to the lowering of the drug chemical potential. Particularly, for highly stable ASD systems characterized by low drug loading and strong drug-polymer interactions, the solubility advantage of ASD can be fully eliminated, leading to an apparent ASD solubility lower than that of the neat crystalline forms. We also showed that the key to the estimation of the ASD solubility is the ability to accurately assess the drug-polymer interaction parameters by accounting for its temperature and composition dependence.

Finally, we noted that the study presented in this article is essentially on mapping out the chemical potential landscape of the drug in an ASD system containing one phase and three components. The chemical potential of the drug is the primary thermodynamic property that not only governs the drug solubility, but also affects the behaviors relating to physical stability, such as drug-polymer miscibility and crystallization. The method presented in this article can therefore be used in the effort to find the most optimal pharmaceutical ASD, i.e., a predictable drug-polymer phase with the lowest possible drug chemical potential to minimize the risk of crystallization and phase separation, and a predictable phase separation upon exposure to water to form an undissolved solute exhibiting higher drug chemical potential and favorable solubility advantage.

2.7 REFERENCES

1. Leuner C, Dressman J. Improving drug solubility for oral delivery using solid dispersions. European Journal of Pharmaceutics and Biopharmaceutics. 2000;50(1):47-60.

2. Serajuddin ATM. Solid dispersion of poorly water-soluble drugs: Early promises, subsequent problems, and recent breakthroughs. Journal of Pharmaceutical Sciences. 1999;88(10):1058-66.

3. Baird JA, Taylor LS. Evaluation of amorphous solid dispersion properties using thermal analysis techniques. Advanced Drug Delivery Reviews. 2012;64(5):396-421.

4. Janssens S, Van den Mooter G. Review: physical chemistry of solid dispersions. Journal of Pharmacy and Pharmacology. 2009;61(12):1571-86.

5. Newman A, Knipp G, Zografi G. Assessing the performance of amorphous solid dispersions. Journal of Pharmaceutical Sciences. 2012;101(4):1355-77.

6. Vasconcelos T, Sarmento B, Costa P. Solid dispersions as strategy to improve oral bioavailability of poor water soluble drugs. Drug Discovery Today. 2007;12(23–24):1068-75.

7. Babu NJ, Nangia A. Solubility Advantage of Amorphous Drugs and Pharmaceutical Cocrystals. Crystal Growth & Design. 2011;11(7):2662-79.

8. Konno H, Handa T, Alonzo DE, Taylor LS. Effect of polymer type on the dissolution profile of amorphous solid dispersions containing felodipine. European Journal of Pharmaceutics and Biopharmaceutics. 2008;70(2):493-9.

9. Sun DD, Lee PI. Probing the mechanisms of drug release from amorphous solid dispersions in medium-soluble and medium-insoluble carriers. Journal of Controlled Release. 2015;211:85-93.

10. Van den Mooter G. The use of amorphous solid dispersions: A formulation strategy to overcome poor solubility and dissolution rate. Drug Discovery Today: Technologies. 2012;9(2):e79-e85.

11. Hancock BC, Parks M. What is the True Solubility Advantage for Amorphous Pharmaceuticals? Pharmaceutical Research.17(4):397-404.

12. Murdande SB, Pikal MJ, Shanker RM, Bogner RH. Solubility advantage of amorphous pharmaceuticals: I. A thermodynamic analysis. Journal of Pharmaceutical Sciences. 2010;99(3):1254-64.

13. Murdande SB, Pikal MJ, Shanker RM, Bogner RH. Solubility Advantage of Amorphous Pharmaceuticals: II. Application of Quantitative Thermodynamic Relationships for Prediction of Solubility Enhancement in Structurally Diverse Insoluble Pharmaceuticals. Pharmaceutical Research. 2010;27(12):2704-14.

14. Murdande SB, Pikal MJ, Shanker RM, Bogner RH. Solubility advantage of amorphous pharmaceuticals, part 3: Is maximum solubility advantage experimentally attainable and sustainable? Journal of Pharmaceutical Sciences. 2011;100(10):4349-56.

15. Childs SL, Rodriguez-Hornedo N, Reddy LS, Jayasankar A, Maheshwari C, McCausland L, et al. Screening strategies based on solubility and solution composition generate pharmaceutically acceptable cocrystals of carbamazepine. CrystEngComm. 2008;10(7):856-64.

16. Jayasankar A, Reddy LS, Bethune SJ, Rodríguez-Hornedo N. Role of Cocrystal and Solution Chemistry on the Formation and Stability of Cocrystals with Different Stoichiometry. Crystal Growth & Design. 2009;9(2):889-97.

17. Petit S, Coquerel G. The amorphous state. In: Hilfiker R, editor. Polymorphism. Weinheim, Germany: Wiley-VCH; 2006. p. 259-85.

18. Marsac PJ, Rumondor ACF, Nivens DE, Kestur US, Stanciu L, Taylor LS. Effect of temperature and moisture on the miscibility of amorphous dispersions of felodipine and poly(vinyl pyrrolidone). Journal of Pharmaceutical Sciences. 2010;99(1):169-85.

19. Rumondor ACF, Marsac PJ, Stanford LA, Taylor LS. Phase Behavior of Poly(vinylpyrrolidone) Containing Amorphous Solid Dispersions in the Presence of Moisture. Molecular Pharmaceutics. 2009;6(5):1492-505.

20. Rumondor ACF, Taylor LS. Effect of Polymer Hygroscopicity on the Phase Behavior of Amorphous Solid Dispersions in the Presence of Moisture. Molecular Pharmaceutics. 2010;7(2):477-90.

21. Flory PJ. Principles of polymer chemistry. Ithaca, New York, NY: Cornell University Press; 1953.

22. Olabisi O, Robeson LM, Shaw MT. Polymer-polymer miscibility. New York, NY: Academic Press; 1979.

23. Yalkowsky SH, Banerjee S. Aqueous Solubility: methods of estimation for organic compounds. New York, NY: Marcel Dekker; 1992.

24. Sacchetti M. Thermodynamic analysis of moisture sorption isotherms. Journal of Pharmaceutical Sciences. 1998;87(8):982-6.

25. Sacchetti M. The General Form of the Gibbs-Duhem Equation for Multiphase/Multicomponent Systems and Its Application to Solid-State Activity Measurements. Journal of Chemical Education. 2001;78(2):260.

26. Kim M-S, Jin S-J, Kim J-S, Park HJ, Song H-S, Neubert RHH, et al. Preparation, characterization and in vivo evaluation of amorphous atorvastatin calcium nanoparticles using supercritical antisolvent (SAS) process. European Journal of Pharmaceutics and Biopharmaceutics. 2008;69(2):454-65.

27. Law D, Schmitt EA, Marsh KC, Everitt EA, Wang W, Fort JJ, et al. Ritonavir–PEG 8000 amorphous solid dispersions: In vitro and in vivo evaluations. Journal of Pharmaceutical Sciences. 2004;93(3):563-70.

28. Wood JH, Syarto JE, Letterman H. Improved holder for intrinsic dissolution rate studies. Journal of Pharmaceutical Sciences. 1965;54(7):1068-.

29. Patterson JE, James MB, Forster AH, Lancaster RW, Butler JM, Rades T. Preparation of glass solutions of three poorly water soluble drugs by spray drying,

melt extrusion and ball milling. International Journal of Pharmaceutics. 2007;336(1):22-34.

30. ASTM. E1269-11. Standard test method for determining specific heat capacity by differential scanning calorimetry. West Conshohocken, PA, USA: ASTM International.

31. Marsac PJ, Li T, Taylor LS. Estimation of Drug–Polymer Miscibility and Solubility in Amorphous Solid Dispersions Using Experimentally Determined Interaction Parameters. Pharmaceutical Research. 2008;26(1):139-51.

32. West DRF, Saunders N. Ternary Phase Diagrams in Materials Science. London, UK: Maney Publishing; 2002.

33. Cohen C, Tanny GB, Prager S. Diffusion-controlled formation of porous structures in ternary polymer systems. Journal of Polymer Science: Polymer Physics Edition. 1979;17(3):477-89.

34. Soh YS, Kim JH, Gryte CC. Phase behaviour of polymer/solvent/ non-solvent systems. Polymer. 1995;36(19):3711-7.

35. Flory PJ. Thermodynamics of high polymer solutions. Journal of Chemical Physics. 1942;10:51-61.

36. Pajula K, Taskinen M, Lehto V-P, Ketolainen J, Korhonen O. Predicting the Formation and Stability of Amorphous Small Molecule Binary Mixtures from Computationally Determined Flory–Huggins Interaction Parameter and Phase Diagram. Molecular Pharmaceutics. 2010;7(3):795-804.

37. Sun Y, Tao J, Zhang GGZ, Yu L. Solubilities of crystalline drugs in polymers: An improved analytical method and comparison of solubilities of indomethacin and nifedipine in PVP, PVP/VA, and PVAc. Journal of Pharmaceutical Sciences. 2010;99(9):4023-31.

38. Hancock BC, Zografi G. The Use of Solution Theories for Predicting Water Vapor Absorption by Amorphous Pharmaceutical Solids: A Test of the Flory–Huggins and Vrentas Models. Pharmaceutical Research.10(9):1262-7.

39. Crowley KJ, Zografi G. Water vapor absorption into amorphous hydrophobic drug/poly(vinylpyrrolidone) dispersions. Journal of Pharmaceutical Sciences. 2002;91(10):2150-65.

40. Stillinger FH. A topographic view of supercooled liquid and glass formation. Science. 1995;267:1935-9.

41. Nishi T, Wang TT. Melting Point Depression and Kinetic Effects of Cooling on Crystallization in Poly(vinylidene fluoride)-Poly(methyl methacrylate) Mixtures. Macromolecules. 1975;8(6):909-15.

42. Koningsveld R, Stockmayer WH, Nies E. Polymer Phase Diagrams. New York, NY, USA: Oxford University Press; 2001.

43. Lu X, Weiss RA. Relationship between the glass transition temperature and the interaction parameter of miscible binary polymer blends. Macromolecules. 1992;25(12):3242-6.

44. Gordon M, Taylor JS. Ideal copolymers and the second-order transitions of synthetic rubbers. i. non-crystalline copolymers. Journal of Applied Chemistry. 1952;2(9):493-500.

45. Nair R, Nyamweya N, Gönen S, Martínez-Miranda LJ, Hoag SW. Influence of various drugs on the glass transition temperature of poly(vinylpyrrolidone): a thermodynamic and spectroscopic investigation. International Journal of Pharmaceutics. 2001;225(1–2):83-96.

46. Taylor LS, Zografi G. Sugar–polymer hydrogen bond interactions in lyophilized amorphous mixtures. Journal of Pharmaceutical Sciences. 1998;87(12):1615-21.

2.8 LIST OF FIGURES

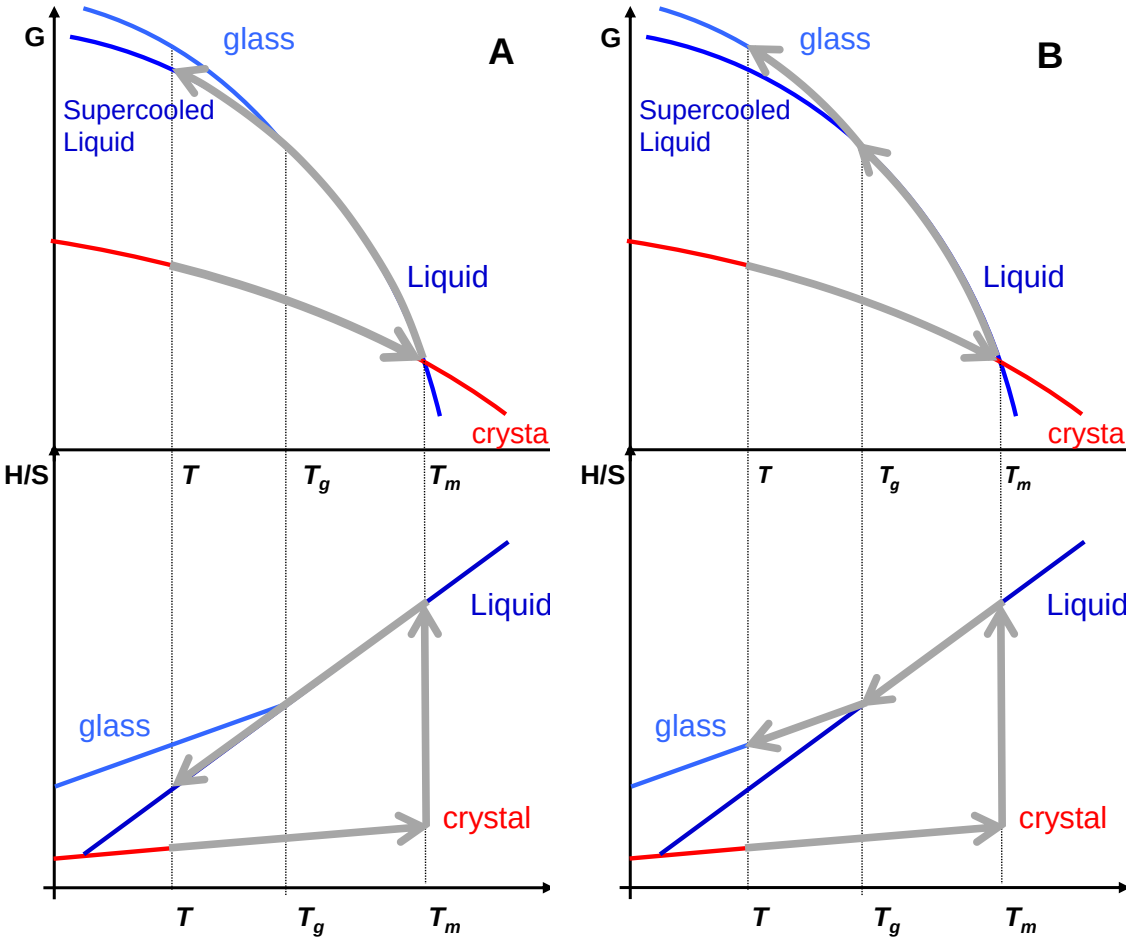

Figure 2.1 Schematic G-T and H/S-T diagrams showing the hypothetical process paths used to calculate the free energy difference between the amorphous and crystalline states of a neat drug. A: reference amorphous state is supercooled liquid; B: reference amorphous state is glass.

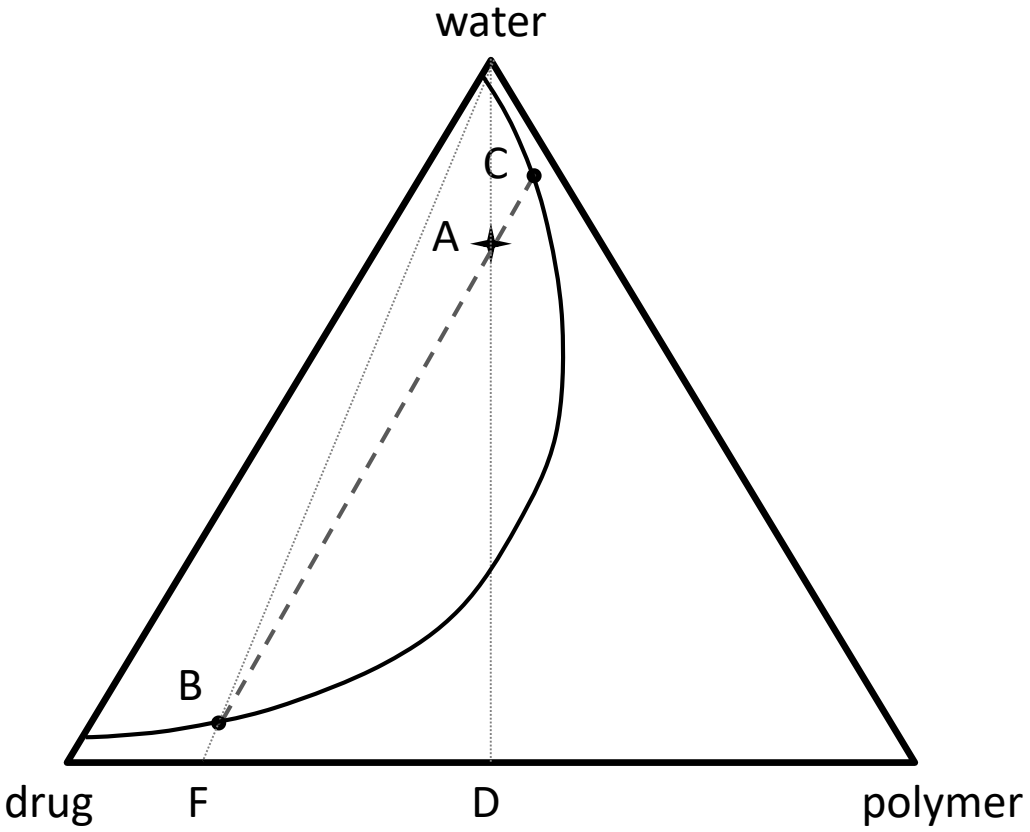

Figure 2.2 Schematic drug-polymer-water ternary phase diagram showing the phase behavior of ASD in equilibrium with water (ASD drug loading is 50%).

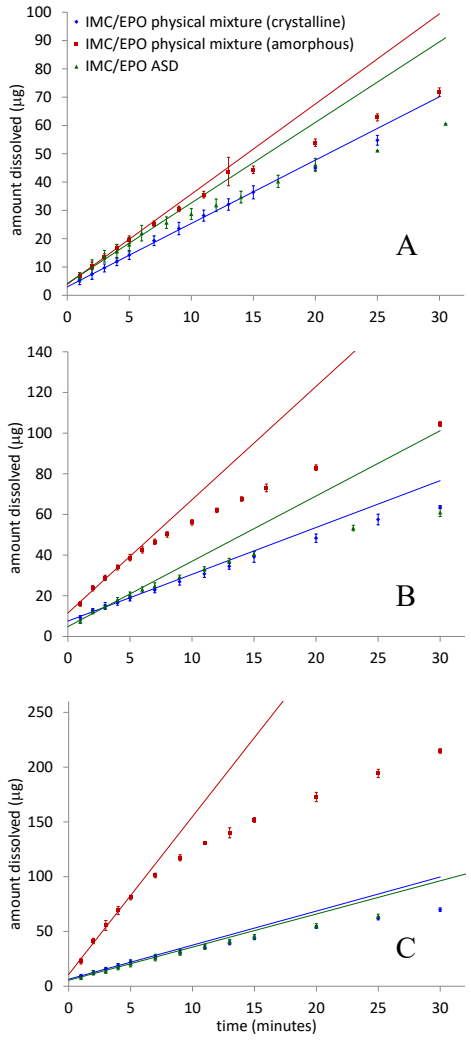

Figure 2.3 Overlay of intrinsic dissolution results of the IMC/EPO physical mixture (crystalline IMC), IMC/EPO physical mixture (amorphous IMC), and the IMC/EPO ASD. (A: 30% drug loading; B: 50% drug loading; C: 70% drug loading). The intrinsic dissolution rates were determined by linear regression of early time points which fit well into straight lines (shown in Figure).

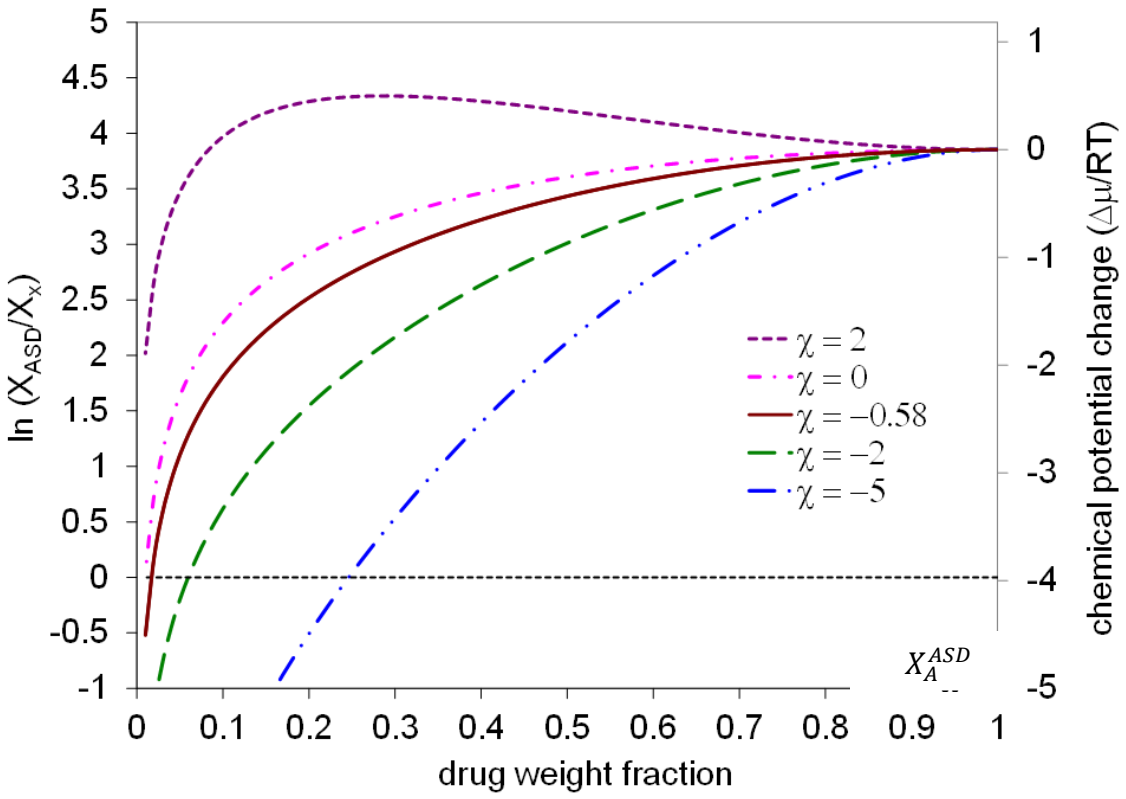

Figure 2.4 Estimated solubility ratio $\frac{X_A^{ASD}}{X_X}$ and chemical potential change $(\frac{\Delta\mu}{RT})$ of IMC as the function of drug loading for the IMC/EPO ASD systems, including curves calculated using hypothetical values of the interaction parameter χ.

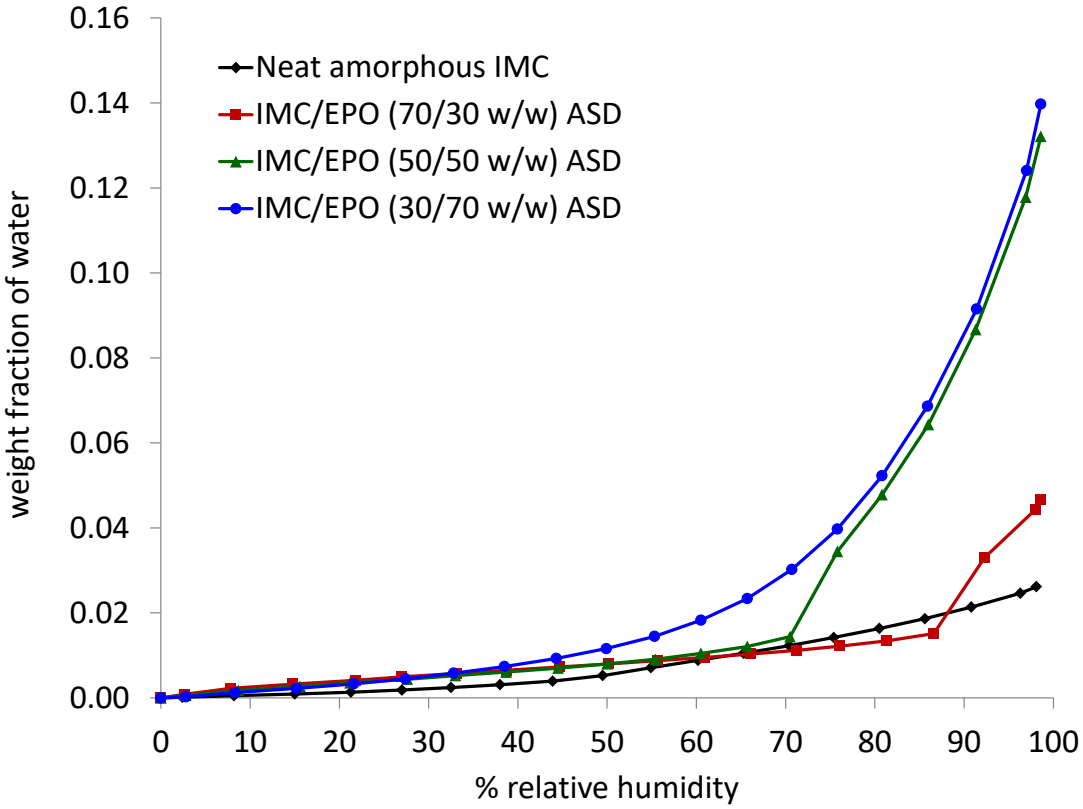

Figure 2.5 Moisture sorption isotherms of amorphous IMC and IMC/EPO ASDs with different drug loading.

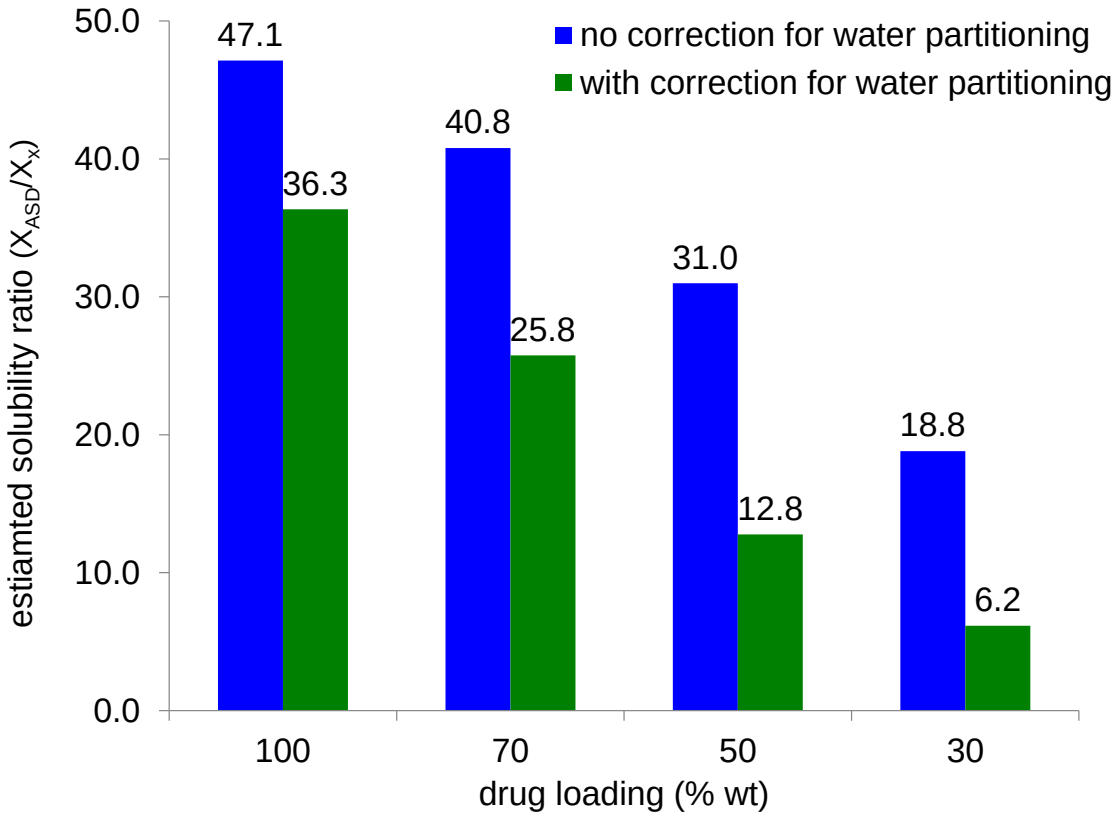

Figure 2.6 Estimated solubility ratio $\frac{X_A^{ASD}}{X_X}$ for the amorphous IMC and the IMC/EPO ASD systems with different drug loading, with and without the correction for water partition.

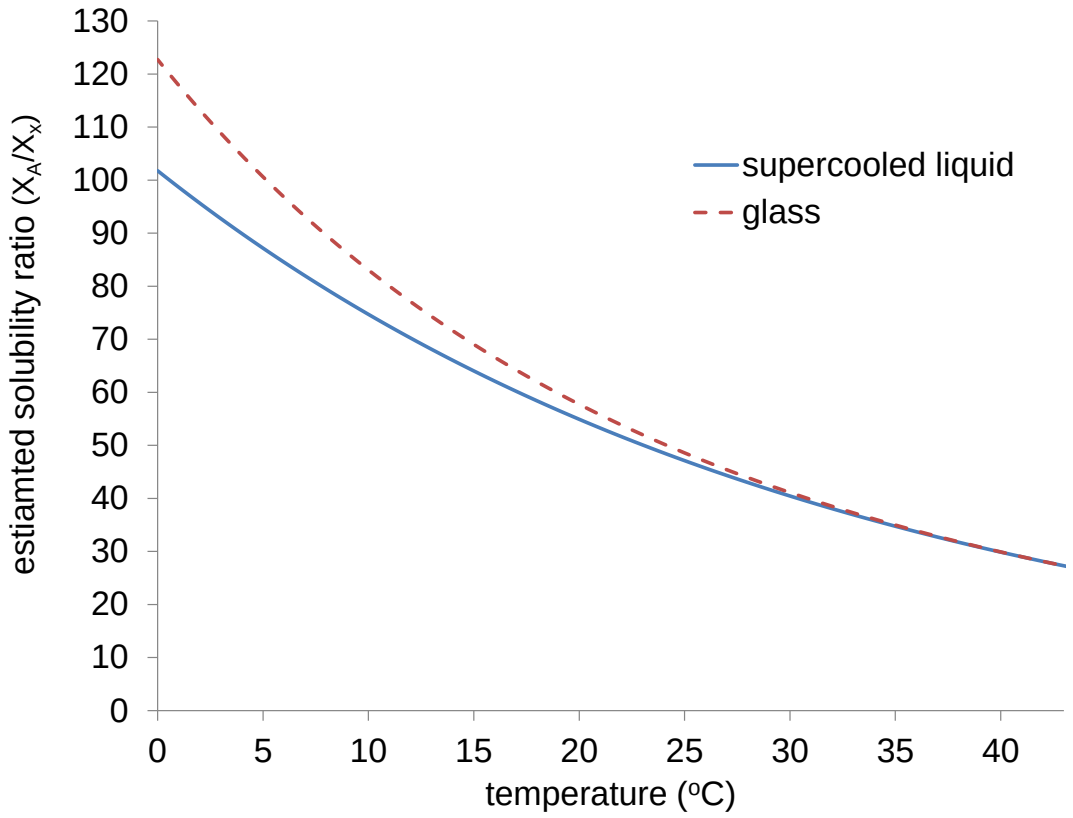

Figure 2.7 Estimated solubility ratio between the amorphous and crystalline IMC, $\frac{X_A}{X_X}$, as the function of temperature, using supercooled liquid or glass as the reference amorphous state.

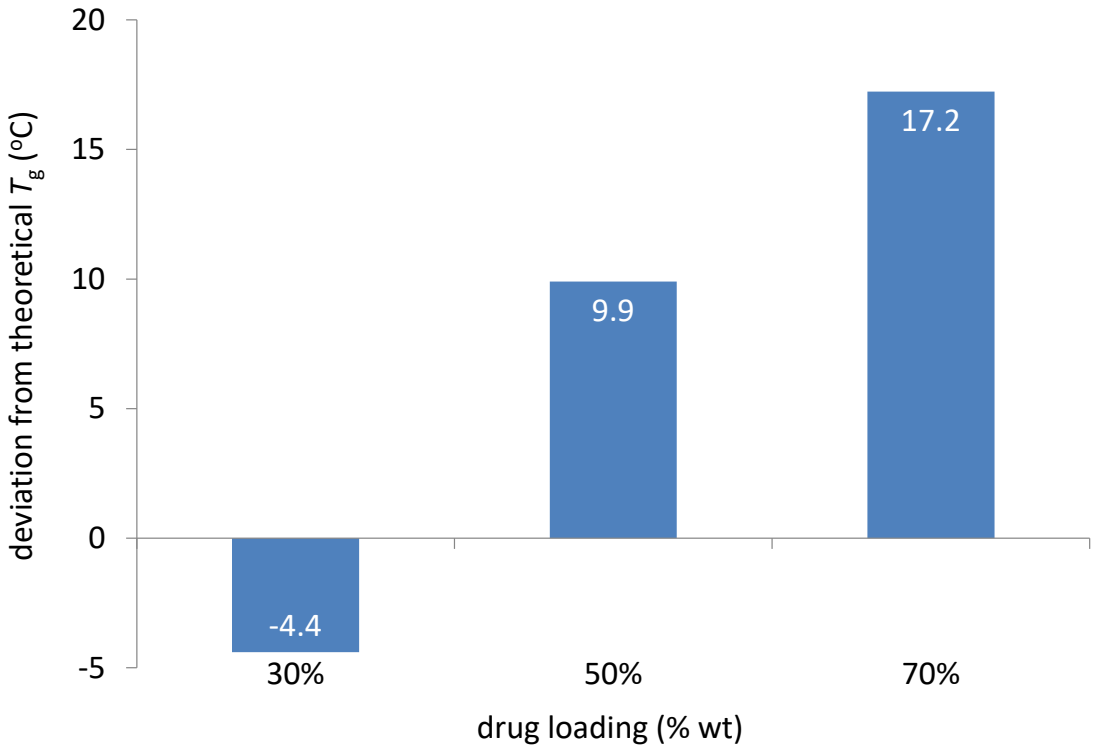

Figure 2.8 Deviation from the theoretical T_g values calculated based on Gordon-Taylor equation, for IMC/EPO ASD systems of different drug loading.

2.9 LIST OF TABLES

ASD drug loading (% wt)	Experimental Solubility Ratio	Predicted Solubility Ratio		
		Amorphization Only	Amorphization + ASD formation	Amorphization + ASD formation + water partitioning
30	1.27	47.1	18.8	6.2
50	1.40	47.1	31.0	12.8
70	0.95	47.1	40.8	25.8

Table 2.1 Experimental and predicted solubility ratio for indomethacin: IMC/EPO ASD versus neat crystalline form: ($\frac{X_A^{ASD}}{X_X}$). T = 25 ℃.

ASD drug loading (%wt)	Experimental Solubility Ratio	Predicted Solubility Ratio	
		ASD formation only	ASD formation + water partitioning
30	0.89	0.40	0.17
50	0.58	0.66	0.35
70	0.21	0.87	0.71

Table 2.2 Experimental and predicted solubility ratio for indomethacin: IMC/EPO ASD versus neat amorphous form: $(\frac{X_A^{ASD}}{X_A^{neat}})$. T = 25 ℃.

Material	M_w (g/mol)	M_w repeating unit (g/mol)	True Density (g/cm^3)	Molecular Volume (cm^3/mol)	Volume Ratio
Indomethacin	357.79	N/A	1.11	267.4	157.7
Eudragit EPO	47000	570.4	1.34	42175.2	

Table 2.3 Molecular properties of indomethacin and EPO used to calculate the solubility ratios.

Chapter 3: A New Extrudable Form of Hypromellose: AFFINISOL™ HPMC HME[2]

3.1 ABSTRACT

Hypromellose is a hydrophilic polymer widely used in immediate and modified release oral pharmaceutical dosage forms. However, currently available grades of hypromellose are difficult, if not impossible, to process by hot-melt extrusion (HME) because of their high glass transition temperature, high melt viscosity, and low degradation temperature. To overcome these challenges, a modified grade of hypromellose, AFFINISOL™ HPMC HME, was recently introduced. It has a significantly lower glass transition temperature and melt-viscosity as compared to other available grades of hypromellose. The objective of this paper is to assess the extrudability and performance of AFFINISOL™ HPMC HME (100LV and 4M) as compared to other widely used polymers in HME, including HPMC 2910 100cP (the currently available hypromellose), Soluplus®, Kollidon® VA 64 and EUDRAGIT® E PO. Formulations containing polymer and carbamazepine (CBZ) were extruded on a co-rotating 16mm twin-screw extruder, and the effect of temperature, screw speed and feed rate was investigated. The performance of the solid dispersions was evaluated based on Flory-Huggins modeling, and characterized by differential scanning calorimetry (DSC), X-ray powder diffraction (XRD), Raman

---

[2] Huang S, O'Donnell KP, Keen JM, Rickard MA, McGinity JW, Williams RO. A New Extrudable Form of Hypromellose: AFFINISOL™ HPMC HME. AAPS PharmSciTech. 2016;17(1):106-19. doi: 10.1208/s12249-015-0395-9.
I am the primary author of this work.

spectroscopy, Fourier-transform infrared (FTIR) spectroscopy, and dissolution. All formulations extruded well except for HPMC 2910 100 cP, which resulted in over-torqueing the extruder (machine overloading because motor cannot provide efficient energy to rotate the shaft). Among the HME extrudates, only the EUDRAGIT® E PO formulation was crystalline as confirmed by DSC, XRD and Raman, which agreed with predictions from Flory-Huggins modeling. Dissolution testing was conducted under both sink and non-sink conditions. Sink dissolution testing in neutral media revealed that amorphous CBZ in the HME extrudates completely dissolved within 15 minutes, which was much more rapid than the time for complete dissolution of bulk CBZ (60 minutes) and EUDRAGIT® E PO solid dispersion (more than 6 hours). Non-sink dissolution in acidic media testing revealed that only CBZ contained in the AFFINISOL™ HPMC HME and EUDRAGIT® E PO solid dispersions rapidly supersaturated after 15 minutes, reaching a 2-fold drug concentration compared to the CBZ equilibrium solubility. In summary, AFFINISOL™ HPMC HME 100LV and AFFINISOL™ HPMC HME 4M are useful in the pharmaceutical HME process to increase wetting and dissolution properties of poorly water-soluble drugs like CBZ.

3.2 INTRODUCTION

Applying high throughput screening in discovery and synthesis of small-molecule drugs has dramatically increased the number of poorly water-soluble compounds (1). The absorption of poorly water-soluble drugs into systemic circulation is highly dependent upon their aqueous solubility and therefore increasing the solubility/dissolution properties of poorly water-soluble drugs for oral delivery is a mandatory and challenging task in dosage form development. Solid dispersions are considered an attractive approach to increase solubility, dissolution and bioavailability of poorly soluble drugs (2). Solid dispersions have been prepared by various approaches such as HME, KinetiSol® technique, co-evaporation, hot spin mixing, roll-mixing or co-milling, thin film-freezing (i.e., ultra-rapid freezing), spray drying and supercritical fluid processing (3-7).

HME was originally adapted from the plastics industry, first used for pharmaceutical formulations in 1971 by El-Egakey et al., and refined in later years by various research groups (8-11). HME technology has gained favor over traditional pharmaceutical formulation techniques in solubility enhancement because it is a solvent-free and continuous operation process that does not require major downstream processing (9, 12). By selecting a suitable exit die and processing parameters, a variety of solid dosage forms including granules, pellets, tablets, suppositories, implants, stents, transdermal and transmucosal systems, and ophthalmic inserts can be produced using HME (9, 13). As for the quality of the extruded material (i.e., the extrudate), carrier (polymer) properties such as the glass transition temperature (i.e., T_g; the temperature at which the polymer starts to

soften), the solubility of the drug in the softened or molten polymer and the stability of the polymer are crucial to forming a homogeneous composition (11).

Hypromellose is a hydrophilic polymer widely used in pharmaceutical dosage forms, including immediate release and modified release formulations. It is an amorphous polymer that typically exhibits a broad glass transition temperature from about 160 to 210 °C. The polymer has a comparatively low decomposition temperature, showing significant degradation at temperatures in the range of 200 to 250 °C, depending upon the substitution (14). This high glass transition temperature and low degradation temperature together with the high melt viscosity make it challenging to process hypromellose by HME. Current techniques reported to improve the processability of hypromellose require the use of high levels of plasticizer and other processing aids (15), which for certain amorphous systems, including solid dispersions, may result in crystallization of the drug during storage and during imbibition of water as the dosage form travels through the gastrointestinal tract leading to a subsequent reduction in dissolution and absorption (e.g., decrease in bioavailability). Hypromellose has been shown to be an effective recrystallization inhibitor in stabilizing amorphous drugs which can enhance the bioavailability of poorly soluble compounds (16). Therefore, it is highly desirable to incorporate hypromellose into a HME formulation without the use of plasticizers. Although some recent studies suggest the possibility of extrusion of existing commercial grades of hypromellose at high temperatures (17, 18), it is very challenging to apply these conditions to most drug candidates due to thermal degradation of the drug itself. A modified hypromellose,

AFFINISOL™ HPMC HME was recently introduced by The Dow Chemical Company. It is produced using traditional HPMC manufacturing methods to result in a different substitution architecture, which makes AFFINISOL™ HPMC HME exhibit a significantly lower T_g (117-128 ℃) (19) and melt-viscosity than presently available grades of hypromellose making it more suitable to thermal processing.

The purpose of this study was to compare the extrudability of two different grades of AFFINISOL™ HPMC HME 4M (552.8 kDa) and 100 LV (179.3 kDa) to currently available HPMC as well as alternative extrusion polymers. Additionally, the ability to generate and the performance of amorphous solid dispersions with the selected polymers was studied using carbamazepine as a poorly soluble model API. Flory-Huggins modeling was used to predict the initial experimental conditions and drug load.

3.3 MATERIALS AND METHODS

3.3.1 Materials

Crystalline carbamazepine (CBZ) was purchased from Letco Medical (Decatur, AL). The Dow Chemical Company (Midland, MI) kindly donated AFFINISOL™ HPMC HME 4M and 100 LV (AFF4000 or AFF100) and HPMC 2910 100cP (HPMC100). BASF Corporation (Florham Park, NJ) kindly donated Soluplus® (Soluplus) and Kollidon® VA 64 (VA64). Evonik (Piscataway, NJ) kindly donated EUDRAGIT® E PO (EPO). HPLC

grade acetonitrile and water were purchased from Fisher Scientific Co. (Houston, TX). All other chemicals used in this study were of American Chemical Society (ACS) grade.

3.3.2 Methods

3.3.2.1 Modeling Based on Flory–Huggins Theory

Phase diagrams for CBZ and polymer systems were generated using Flory–Huggins Theory as previously described (20-26). Briefly speaking, the Gibbs free energy of mixing function that results from application of the Flory–Huggins model is dependent on the volume fraction of the drug, ϕ, a constant indicative of the relative size of the polymer in relation to the drug, m, and the interaction parameter, χ

$$\frac{\Delta G_{mix}}{RT} = \phi \ln \phi + \frac{(1-\phi)}{m} \ln(1-\phi) + \phi(1-\phi)\chi \quad (1)$$

DSC experiments was used to determine the melting enthalpy of the drug, ΔH, and either the melting temperature (22, 23), onset of melting (24) or ending of melting (25) have been applied by various authors to determine χ, which is a function of temperature (27). For CBZ and polymer systems, melting temperature was selected based on the reproducibility of this value in experimental trials. The temperature dependency of χ at room temperature can be calculated with the application of solubility parameters (24). Calculation of the solubility parameters, along with the molar volume per Flory–Huggins

lattice size, were performed using Molecular Modeling Pro software (Chem SW Inc., Fairfield, CA)

For our analysis, χ is assumed to only be a function of temperature. Any dependency on composition is neglected, and this assumption is in line with that reported previously (22, 25). With the χ value at different temperatures being calculated by the linear equation predicted by the two points (χ at room temperature and T_m), a Gibbs free energy diagram at selected temperatures can be produced.

Setting the second derivative of Equation 1 equal to 0, and determining ϕ as a function of χ allows for the determination of the boundary between unstable and metastable regions, or referred to as the spinodal curve. Furthermore, constructing the common tangents between the minima on the free energy diagram can form the boundary between the metastable and stable regions called bimodal curve. This corresponds to points in which the chemical potentials of the two phases are in equilibrium. The binodal curve which is solved numerically will intersect the spinodal curve at the critical point, the third derivative of Equation 1.

3.3.2.2 Hot Melt Extrusion and Milling

HME studies were conducted on a co-rotating Leistritz Nano-16 twin-screw extruder (American Leistritz Extruder Corp. USA, Somerville, NJ) equipped with screws containing two kneading elements (30 degree and 60 degree) were used in each screwand

a 3 mm strand die. A single screw feeder set on top of the barrel feed zone provided an accurate 5 grams/ minute feed rate of the powder blend. Polymer drug blend with 15% and 30% CBZ loading were extruded by Leistritz extruder at different temperature ranging from 120 °C to 180 °C, screw speed at 100, 150 and 200 rpm. Extrudates were cooled to room temperature before milling. A Fitzmill L1A hammer mill (Fitzpatrick) operating at 9000 RPM with knives side forward and a 0.020" screen installed in the chamber was used to mill the extrudates. The powder fraction retained between 60 mesh and 100 mesh screens was collected for further analysis.

3.3.2.3 High Performance Liquid Chromatography (HPLC)

CBZ was detected by a Dionex HPLC system (Thermo Fisher Scientific Inc., Waltham, MA) equipped with a Phenomenex® Luna 250 mm C18 (5 μm, 4.6×250 mm) column. The composition of HPLC mobile phase was 60:40 acetonitrile:water. Prior to use, the mobile phase was filtered through a 0.45 micron filter, and then degassed under vacuum with sonication. The mobile phase flow rate was 1 mL/min. The retention time of CBZ was approximately 4.2 min. The detection wavelength was 263 nm.

3.3.2.4 X-ray Powder Diffraction (XRD)

XRD studies were conducted on a Philips 1710 X-ray diffractometer with a copper target and a nickel filter (Philips Electronic Instruments, Inc., Mahwah, NJ). The voltage and current of the equipment were set to 40 KV and 40 mA, respectively. Prior to analysis, the sample was placed in the quartz slot of a zero background XRD sample holder, and

flattened with a glass slide. The 2-theta angle, step size, and dwell time were set to 10-50°, 0.05°, and 2 s, respectively. In order to obtain XRD patterns, the raw data was processed using Jade 5.0 software (Materials Data, Inc., Livermore, CA).

3.3.2.5 Modulated Differential Scanning Calorimetry (mDSC)

To characterize the thermal behavior of the samples, modulated DSC equipped with a DSC refrigerated cooling system (DSC 2920, TA Instruments, New Castle, DE) was employed. Dry nitrogen gas at a flow rate of 40 mL/min throughout the testing was used to purge the DSC cell. Samples were accurately weighed in aluminum sample pan kits (PerkinElmer Inc., Waltham, MA) and crimped before analysis. Samples were heated from 50°C to 220°C with a heating rate of 10°C/min using a 0.5°C/40 s modulation program. TA Universal Analysis 2000 software was used to process the raw data.

3.3.2.6 Spectroscopy

3.3.2.6.1 Raman Spectroscopy

Raman spectra were collected with a Raman RXN1 microscope (Kaiser Optical Systems, Inc.) equipped with a 785 nm Invictus laser. The laser was focused on the sample with an Mk II probe and a 50x microscope objective (≈ 30 mW at sample), and the back-scattered light was collected with the same optics. The total acquisition time of each spectrum was sixty seconds. The Raman shift axis was calibrated with the 801.8 cm^{-1} band of cyclohexane (28). The amorphous form of carbamazepine was prepared by heating the

material on a hot stage until it was completely melted and then quench cooling it in liquid nitrogen.

3.3.2.6.2 Fourier-Transform Infrared Spectroscopy (FTIR)

Attenuated total reflectance (ATR) infrared spectra were acquired with a Perkin Elmer Spectrum One FT-IR and Universal ATR Sampling Accessory at a resolution of 4 cm^{-1}. Sixteen scans (≈ 90 second acquisition time) were collected for each spectrum in the wavelength region between 300 and 4000 cm^{-1}. The Universal ATR Sampling Accessory was equipped with a single bounce diamond/ZnSe crystal.

3.3.2.7 Dissolution Testing

3.3.2.7.1 Dissolution Testing at Sink Conditions

A VanKel VK 7000 dissolution system (Varian, Inc., Palo Alto, CA) with the corresponding paddle was utilized to perform the testing according to USP 29 apparatus II. The paddle speed and temperature were set to 100 rpm and 37±0.5°C, respectively. Before testing, 1000 mL of DI water was pre-heated to 37 °C in each dissolution vessel. Milled extrudates containing 100 mg CBZ equivalent (n=6) were pre-wetted in a 20 mL scintillation vial using dissolution media for 10 seconds; the time at which the material was pre-wetted was considered the 0 minute time point. The wetted sample was then added immediately to the dissolution vessel. At time points of 15 min, 30 min, 45 min, 1 hr, 1 hr 30 min, and 2 hr, a 1 mL sample was pulled and filtered through a 0.2 µm 13 mm PVDF

membrane filter. A 200 µL aliquot of filtered solution was diluted with 1.4 mL HPLC grade acetonitrile and the concentration of CBZ in the diluted sample was measured using HPLC.

3.3.2.7.2 Dissolution Testing at Non-sink Conditions

Dissolution testing was also conducted at non-sink conditions in acidic media using 200 mL vessels and corresponding paddles. 100 mL of 0.1 N HCl solution was pre-heated to 37 °C in each dissolution vessel. Milled extrudate containing 100 mg CBZ equivalent (n=6) was pre-wetted in a 20 mL scintillation vial using dissolution media for 10 seconds; the time at which the material was pre-wetted was considered the 0 minute time point. The wetted sample was then added immediately to the dissolution vessel. At time points of 15 min, 30 min, 45 min, 1 hr, 1 hr 30 min, 2 hr, 6 hr, a 1mL sample was taken and filtered through a 0.2 µm 13 mm PVDF membrane filter. Sample dilution and HPLC quantification were the same as the sink condition dissolution testing above.

3.3.2.8 Statistical Analysis

Data are presented as mean ± standard deviation. The data were analyzed through paired t-test and one way-ANOVA using the JMP® 11 software. For the paired t-test, $p < 0.05$ was set as the significance threshold for the differences within groups. For one-way ANOVA, $p < 0.05$ was set as the significance threshold for differences between groups.

3.4 RESULTS

3.4.1 Polymer – CBZ Miscibility Based on Flory–Huggins Theory

The Flory–Huggins interaction parameter, χ, was calculated based on the linear equation predicted by the experimentally determined χ at melting point of each polymer and drug mixture and solubility parameters estimated χ at 25 ℃. Substitution of χ value into Equation 1 yields the free energy of mixing versus drug composition plot which is shown in Figure 3.1A. As shown in Figure 3.1A, the free energy of mixing is convex at elevated temperatures (200 ℃), and homogeneous mixtures of CBZ and all polymers were stable for all compositions at this temperature and above. For all systems except AFF100 and AFF4000, χ decreased at elevated temperatures, which indicated mixing of CBZ and polymer became more favorable with increasing temperature. The results shown in Figure 3.1B, which were generated by solving the free energy relationship (Equation 1) at specific temperatures, further highlight this relationship. To the contrary, for AFF100 and AFF4000 systems, χ was negative at all temperatures between -200 ℃ to 200 ℃. Moreover, χ increased with increasing temperature for those two systems. Therefore, no unstable zone of CBZ was observed in Figure 3.1B unless at high drug load and temperature.

3.4.2 Hot Melt Extrusion

Hypromellose (2910 100cP) having the comparable viscosity in aqueous as AFF100 exhibited different properties when processed at elevated temperature by a twin-screw melt extruder (Figure 3.2). Both AFF100 and HPMC100 were processed at 140°C,

100 rpm, however at that condition it was not possible to extrude the HPMC100 formulation due to machine over-torqueing. To decrease the viscosity of HPMC100, the processing temperature and screw speed were increased to 160°C, 150 rpm. As seen in the figure, the AFF100 extrudate at 140°C, 100 rpm (Figure 3.2A) was slightly less yellow and clear than AFF100 extruded at 160°C, 150 rpm (Figure 3.2B). On the other hand, the higher temperature and shear force helped facilitate HPMC100 extrusion because the torque created during the extrusion process decreased enabling the machine to operate. However, after being exposed to a higher temperature for a long period of time (approximately 15 minutes), together with more energy input caused by a higher rpm, the extrudate was burned as observed upon exiting (Figure 3.2C). The results demonstrated that at similar HME process conditions, currently available HPMC was difficult to extrude while the newly designed AFFINISOL™ HPMC HME was much more amendable to processing by HME.

Moreover, Soluplus, VA64, EPO, and another grade of AFFINISOL™ HPMC HME with a higher viscosity (AFF4000) were used in HME as comparisons. As shown in Figure 3.3, except for the EPO formulation (white rod), all other extrudates were clear and transparent, indicating a good mixing between drug and polymers that concurred with the miscibility predicted by Flory–Huggins Theory.

3.4.3 X-ray Powder Diffraction (XRD)

XRD diffractograms of the unprocessed powders (polymers and CBZ) are shown in Figure 3.4. Bulk CBZ powder showed characteristic crystalline peaks at 2θ = 15.2, 15.8 and 27.4°, which agreed with the CBZ P-monoclinic form III pattern (29). No crystalline peaks were observed in the patterns of the extrudates except for the EPO extrudate which exhibited characteristic crystalline peaks at 2θ =12.8, 18.9, and 19.6°, corresponding to CBZ form I (29). Therefore, within these extrudates CBZ was confirmed to be in the amorphous or molecular state, or, the crystallinity was too low to be detected by XRD.

3.4.4 Modulated Differential Scanning Calorimetry (mDSC)

The thermograms of bulk CBZ and CBZ-polymer extrudates are shown in Figure 3.5. Bulk CBZ, EPO, AFF100, and AFF4000 extrudates exhibited endothermic peaks that indicated the existence of crystalline CBZ. For bulk CBZ, three events were observed as described in previous reports (29, 30): 1) the endothermic peak observed at 175.4 ℃ was attributed to the melting of CBZ form III (P-monoclinic), 2) a very small exothermic peak was observed at 181.7 ℃ because form I CBZ crystal generates during heating process, 3) the third event observed at 195.7°C is attributed to the melting of form I (Triclinic). For EPO, AFF100 and AFF4000, however, the observed melting points did not match the endothermic peak of bulk CBZ. Soluplus and VA64 extrudates were amorphous due to the lack of any observed endothermic peak.

3.4.5 Raman and FTIR Spectroscopy

Raman spectra of crystalline (form III) and amorphous CBZ are shown in Figure 3.6. There are substantial changes in the frequencies, intensities and peak shapes of bands at 253, 374, 723, 768, 873, 987, 1222, 1250, 1412 and 1566 cm^{-1} from the crystalline to the amorphous form. The Raman spectra of CBZ extrudates in AFF100, AFF4000, EPO and VA64 were dominated by bands from CBZ (data not shown). An overlay of the 1600 cm^{-1} region (Figure 3.7) illustrates the spectral changes among crystalline CBZ, amorphous CBZ and CBZ-polymer extrudates. The Raman spectra of CBZ-polymer extrudates were not consistent with either crystalline (form III) CBZ or amorphous CBZ, which indicated that all of the polymers had substantial interactions with CBZ.

Infrared spectra of CBZ in EPO (Figure 3.8) were consistent with these observations. From the IR spectrum, the 30% CBZ formulation was partially crystalline (form I, bands at 3486 cm^{-1} and 1393 cm^{-1}) (29), which was in agreement with the DSC and XRD results. However, the 15% CBZ formulation was amorphous. The carbonyl stretch of CBZ (31) occurs at 1674, 1681, 1686 and 1685 cm^{-1} in crystalline (form III) CBZ, amorphous CBZ, 15% CBZ in EPO and 30% CBZ in EPO, respectively. The $\approx$ 12 cm^{-1} frequency increase from bulk CBZ to the CBZ-polymer extrudates indicated that there was less hydrogen bonding to the carbonyl group of CBZ in the EPO formulations.

3.4.6 Dissolution testing

3.4.6.1 Dissolution Testing at Sink Conditions

The dissolution profiles for bulk CBZ and CBZ-polymer extrudates are shown in Figure 3.9. The dissolution rate of bulk CBZ was slow, 90% release was achieved after about 60 minutes, due to poor wettability and agglomeration. The dissolution rates of the CBZ-polymer extrudates were faster than that of bulk CBZ, except for the crystalline drug-EPO extrudate; all other drug-polymer extrudates achieved at least 90% release by 15 minutes. For the CBZ-EPO extrudate, a much slower release rate (40% release at 2 hr) was observed. CBZ-polymer extrudates except for CBZ-EPO were well dispersed and gradually swelled and dissolved during the dissolution process. For CBZ-EPO extrudate, due to the low solubility of Eudragit® E PO at neutral pH, particles stayed at the bottom of the vessel and were not dissolved in the dissolution study.

3.4.6.2 Dissolution Testing at Non-sink Conditions

The results of dissolution testing at non-sink conditions are presented in Figure 3.10. The CBZ-EPO extrudate exhibited the most rapid dissolution rate with approximately 55% of CBZ released in solution at 15 min., and the concentration was maintained through 360 minutes. Meanwhile, CBZ-AFF100, and CBZ-AFF4000 extrudates, as well as the CBZ -EPO physical mixture released 45% CBZ by 15 minutes and reached 50% after 45 minutes; the super-saturation state did not change after that. However, CBZ-VA64 and CBZ-Soluplus extrudates dissolved remarkably more slowly than CBZ-AFF100, CBZ-

AFF4000 and CBZ-EPO extrudates, and by the end of the study reached approximately the same drug release amount as bulk CBZ. Because of the limited volume of dissolution media, CBZ-AFFs (both AFF100 and AFF4000), CBZ-Soluplus and CBZ-VA64 extrudates clumped at the beginning of the dissolution test, and were not fully dissolved at the final sampling time point. CBZ-EPO extrudate, however, was dispersed fast and homogeneously in the dissolution vessel due to the solubility of Eudragit® E PO at acidic conditions. Towards the end of the test, the dissolution media became a stable white suspension.

To provide a more quantitative examination of these dissolution results, the area under the dissolution curve (AUDC) for the non-sink condition dissolution test in acidic environment was calculated by the linear trapezoidal method. These values are presented in Table 3.1. The AUDC values further indicated the significantly superiority of the CBZ-AFFINISOL HPMC HME (both AFF100 and AFF4000) extrudates which exhibited 157, 182, and 163% mean AUDC total values of bulk CBZ, CBZ-VA64, and CBZ-Soluplus extrudates, respectively. The AUDC of CBZ-EPO extrudate was 12% greater (not significantly) than CBZ-AFF (both AFF100 and AFF4000) extrudates.

3.5 DISCUSSIONS

For HME applications in pharmaceutical industry, it is crucial to successfully develop amorphous dispersions without degrading drug and other ingredients in the formulation. Therefore, identifying drug loadings and processing temperatures become necessary to ensure chemical and physical stability of the final formulation. In our study, the phase diagram obtained through Flory-Huggins modeling shown in Figure 3.1B indicated that at 15% CBZ drug load, amorphous systems would be obtained at processing temperatures below 150 ℃ for all polymers. However, modeling result suggested that 30% CBZ concentration systems would be challenging to formulate, first because 30% CBZ systems require much higher energy input to achieve the amorphous state compared to 15% CBZ systems, and secondly, when extrudates are cooled, 30% CBZ systems will fall within the spinodal curve which refers to the unstable region (24). Based on the modeling results, 15% and 30% drug loadings were chosen to compare the performance of different polymers. As for processing temperature, the upper boundary allowing the amorphous system to be generated without heat-induced drug degradation was determined by the thermal stability of CBZ. In forced-degradation study (exposure to heat for 6 minutes), CBZ was observed to be thermally stable at temperatures lower than 190 ℃ (T_m =192 ℃). When 30% (w/w) CBZ was mixed with 70% (w/w) polymers, CBZ degradation beyond 0.5% was observed at temperatures greater than 170 ℃ (data not shown). Both CBZ by itself and CBZ polymer mixtures showed increasing rate of decomposition as temperature increased. Meanwhile, polymer decomposition temperatures have also been reported such as Soluplus at 250 ℃ (32), EPO at 200 ℃ (33), VA64 at 230 ℃ (32), HPMC at 200-250 ℃

(34). According to these results, the processing temperature should be controlled below 170 ℃ and other conditions like screw speed and screw design should be optimized based on the extrusion outcomes.

To avoid drug degradation, HME was performed at 160 ℃, 150 rpm with 30% CBZ in AFF100 using the screw design in Figure 3.11 at 3 grams/min feed rate (F1). However, as shown in Table 3.2, at this condition, F1 only provided 85.46% drug recovery according to the HPLC result. From F1 to F3, increasing screw speeds were used. Inspection of CBZ recovery and extrudate appearance in Table 3.2, decrease in CBZ recovery rate and significant darkening of extrudate colors were observed due to more shear force being transferred to the materials (9, 35). For CBZ, according to forced-degradation studies (Figure 3.12), drug degradation happened at 170 ℃ and above with only heat applied to the sample. However, about 15% drug degradation was observed in F3 at 160 ℃, 200 rpm. It has been previously reported that significant heat will be generated inside the extruder chamber by shear and pressure at kneading elements that cannot be detected by the thermal sensors effectively, since sensors are normally built in the chamber wall which are not detecting material real temperature (on the screw) directly (36). As shown in Figure 3.11, two mixing elements (30 degree and 60 degree) were used in each screw, high shear and hot spots might occur at those areas. Moreover, unvented system was applied throughout the extruder, which helped keep heat inside. In other words, the actual temperature the samples were experiencing can be much higher than the set temperature for the extrusion process (36). Therefore, we believed that the degradation was attributed to localized hot

spots generated by shear and pressure. For further process optimization, 100 rpm was chosen instead of a higher speed to avoid drug degradation. From F4 to F7, the effect of barrel temperature was investigated. The opaque appearance of F4 processed at 120 °C as well as its XRD pattern shown in Figure 3.13 indicated that CBZ was not molecularly dispersed in the polymer during the extrusion process. Considering heat is one of the most important energy in-puts of the extrusion process to ensure complete mixing (36), it was determined that temperatures above 120 ℃ were necessary to generate an amorphous system. Moreover, for F4, the low temperature resulted in high melt viscosity of polymer, which provided higher energy transfer efficiency (10), thus more shear was transferred to CBZ causing degradation and low recovery. However, even with the increased melt viscosity at this low temperature (120 ℃), AFFINISOL™ HPMC HME did not result in operational failure. As for F8 and F9, different feed rates were tested. The results indicated that a faster feed rate can help increase CBZ recovery primarily because of a shorter residence time and thus less thermal and shear exposure. Ultimately, 100% CBZ recovery was achieved using 140 ℃, 100 rpm, at 5 g/min feed rate, and this condition was applied to all other formulations.

The DSC thermogram (Figure 3.5) for 30% CBZ-polymer extrudates, showed a distinct endothermic peak in the CBZ-EPO formulation at 177.6 °C; this incomplete amorphicity was predicted by our Flory-Huggins model. The XRD (Figure 3.4) and FTIR results (Figure 3.8) indicated that after extrusion CBZ in EPO recrystallized into Form I (Triclinic) crystalline form, with the melting point of approximately 180°C (29). The 3 °C

difference in observed T_m and literature data was attributed to the molecular interaction between EPO and CBZ at elevated temperature (27), which was also predicted in our modeling result. The DSC results for VA64 and Soluplus formulations matched the information obtained from the XRD study, which showed that CBZ exists in amorphous form in those systems. Preparing of CBZ-VA64 and CBZ-Soluplus amorphous solid dispersions by HME has also been reported previously in literature (37). In contrast to our result, Djuris et al. reported immiscibility between Soluplus and carbamazepine at 30% drug load (38). However, that study was performed on a melt-fusion product instead of an HME product. For the Soluplus extrudate herein, CBZ dissolved to a higher degree in the polymer because of the shear provided by extruder, thus the final DSC thermogram did not show any endothermic peak. Small endothermic peaks at approximately 170 °C were also observed in AFF100 and AFF4000 formulations. As mentioned before, the depression of those two peaks compared with CBZ form III (P-monoclinic) (T_m approximately 175 °C) was also due to the strong interaction between AFF and CBZ. In Figure 3.4, however, the existence of crystalline CBZ in the AFF extrudates was not detected by XRD or Raman. Considering that Raman and FTIR have good sensitivity detecting crystalline material, we believe that the endothermic peaks detected in the DSC result are because that CBZ miscibility in both AFF100 and AFF4000 decreased at elevated temperature as predicted by the Flory-Huggins modeling results.

Dissolution testing at sink conditions (Figure 3.9) showed significant enhancement of the drug dissolution rate in amorphous formulations. It has been widely reported (39,

40) that the strong interaction between drug and polymer in amorphous solid dispersions can increase dissolution rate. Raman spectroscopy was used in this research to characterize the interactions between CBZ and polymers. Subsets of the Raman bands that were reasonably strong and had little or no interference from the polymers were examined in greater detail. The positions of these bands in the 30% CBZ formulations and the frequency shifts from crystalline CBZ are shown in Table 3.3 and Figure 3.14. The frequency shifts are generally consistent with the amorphous form except for the 374 cm^{-1} (lattice vibration) and 1160 cm^{-1} (C-C ring stretch/C-N-C asymmetric stretch) bands. In these cases, the shifts are substantially greater than the amorphous form, which indicated that the polymers had substantial interactions with CBZ. These interactions may include contributions from both hydrogen bonding and dipole-dipole forces. But unlike amorphous formulations, CBZ-EPO extrudate showed a decreased dissolution rate compared to bulk CBZ. This is first attributed to CBZ still existing in crystalline form in the CBZ-EPO extrudate; second, EPO is not soluble but swellable and permeable at neutral pH condition according to the USP monograph, therefore the matrix fromed by EPO can prevent crystalline CBZ from dissolving into the dissolution media; thirdly, during the dissolution process, CBZ in the CBZ-EPO extrudate (form I) changes to its less soluble di-hydrate form more rapidly than bulk CBZ (form III) (41).

In non-sink dissolution testings (Figure 3.10), the significant dissolution rate improvement of CBZ-AFF extrudates was also observed and is because of the fact that cellulose-based polymers are excellent drug recrystallization inhibitors in amorphous

systems by lowering the thermodynamic tendency of drugs toward recrystallization (42, 43). As for CBZ-Soluplus and CBZ-VA64 extrudates, CBZ dissolved rapidly because it existed in its high energy form. However, neither was able to reach supersaturation, despite being amorphous. From the Flory-Huggins modeling result of CBZ-VA64 and CBZ-Soluplus systems shown in Figure 3.1, both extrudates were in the unstable state with low system mobility (within spinodal curve and below T_g of the CBZ-polymer system) when cooled down to room temperature after extrusion. In that state, phase separation is highly favorable (27). However, the reason why CBZ was amorphous may be because of the low mobility of these systems providing resistance to drug recrystallization (44). When calculating χ at room temperature, instead of using an experimental method such as the melting point depression to estimate the interaction parameter χ at elevated temperature (25), the solubility parameters were used. The limitation of using the solubility parameter method in this model is that it overlooks the interactions between polymer and CBZ (45). These interactions, however, were well represented at elevated temperatures using the experimental methods (23). Therefore, the F-H modeling results of CBZ-VA64 and CBZ-Soluplus might not be accurate at room temperature.

Once the CBZ-VA64 and CBZ-Soluplus extrudates mixed with the dissolution media, the incorporation of water into CBZ-VA64 and CBZ-Soluplus extrudates initiates drug crystallization due to the decrease of system T_g, which can provide necessary system mobility for CBZ to recrystallize (46). Moreover, water dominating H-bonds and dipole forces with water-soluble polymers like VA64 and Soluplus will also result in

thermodynamic driving forces for drug crystallization (47). It is known that the dissolution advantage of amorphous solids can be negated either by crystallization of the amorphous solid on contact with the dissolution medium or through rapid crystallization of the supersaturated solution (2). Therefore, CBZ-Soluplus and CBZ-VA64 extrudate lose the ability to reach supersaturation conditions as shown in Figure 3.10. It should be noted that the presence of CBZ with a T_g as low as 52 ℃ (48) may contribute to considerable T_g depression in the formulations. Therefore, system made by carrier with a higher T_g such as AFFINISOL™ HPMC HME (115 ℃) was more beneficial to improve physical stability of CBZ during storage and dissolution by preventing drug recrystallization or phase separation (49) compared to Soluplus® (70 ℃), Kollidon® VA 64 (101 ℃) (32). The difference in dissolution performance between CBZ-AFF, CBZ-Soluplus, and CBZ-VA64 at non-sink condition can also be attributed to the gelification of HPMC-based polymer slowing down diffusion of water to the solid dispersion, which also decrease CBZ recrystallization rate (50).

Surprisingly, the CBZ-EPO extrudate enabled CBZ to supersaturate in acidic dissolution media and maintain supersaturation over 6 hours (Figure 3.10). Based on the structure of CBZ and EPO, it is hypothesized that this result is due to cation-π interactions between CBZ and ionized EPO polymer. The most studied cation-π interactions involve binding between an aromatic π-system and an alkali metal or nitrogenous cation. Numerous studies have shown the existence of cation–π interactions in protein structures (51), protein–ligand (52), and protein-DNA complexes (53). It has been revealed that the

preferential localization of amine groups are close to aromatic rings (54). In particular, it is found that the positive charge of amines groups make favorable interactions with the π-electron cloud of aromatic side chains. The optimal interaction geometry places the cation in Van der Waals contact with the aromatic ring, centered on top of the π face along the 6-fold axis (55). This cation–π interaction, electrostatic in nature, is calculated to be more stabilizing than analogous salt-bridge interactions and comparable with hydrogen bonding (56, 57). Based on these literature studies, when ionized, EPO will generate the nitrogenous cation that can interact with the aromatic π-system in CBZ. Moreover, EPO does not ionize above pH 5.0 (58), therefore the cation-π interaction does not exist at neutral conditions. Thus slow release rate of CBZ from the EPO extrudate in neutral media (Figure 3.9) also supports this cation-π interaction hypothesis. On the other hand, it was also found that CBZ-EPO extrudate showed a higher dissolution rate of CBZ compared to the other extrudates. Besides the interaction between EPO and CBZ mentioned above, CBZ-EPO extrudate was better dispersed in acidic condition as observed in the experiment, which contributed to the higher dissolution rate as well.

3.6 CONCLUSIONS

In this study, a co-rotating twin-screw extruder was used to evaluate the modified grades of hypromellose AFFINISOL™ HPMC HME 100LV and AFFINISOL™ HPMC HME 4M. The results revealed that these polymers are readily processed by HME without plasticizers and act as effective precipitation inhibitors of drug. Different extrusion conditions were tested on these new polymers, demonstrating that these modified HPMC polymers can serve as excellent carriers (polymers) for HME solid dispersions over a broad temperature range. Moreover, the newly developed HPMC made extruding viscous HPMC polymer possible (AFFINISOL™ HPMC HME 4M), and therefore has the potential of being used as a sustained release excipient in a HME process.

Acknowledgements

The authors would like to thank The Dow Chemical Company for sponsoring this work, Jamie Stanley for collecting for the Raman spectra and Professor Ben Liu (Medicinal Chemistry) for his help confirming the cation–π interactions between CBZ and ionized EPO.

3.7 REFERENCES

1. Keseru GM, Makara GM. The influence of lead discovery strategies on the properties of drug candidates. Nat Rev Drug Discov. 2009;8(3):203-12. doi: 10.1038/nrd2796

2. Alonzo D, Zhang GZ, Zhou D, Gao Y, Taylor L. Understanding the Behavior of Amorphous Pharmaceutical Systems during Dissolution. Pharm Res. 2010;27(4):608-18. doi: 10.1007/s11095-009-0021-1.

3. Serajuddin ATM. Solid dispersion of poorly water-soluble drugs: Early promises, subsequent problems, and recent breakthroughs. Journal of Pharmaceutical Sciences. 1999;88(10):1058-66. doi: 10.1021/js9804031.

4. Chauhan B, Shimpi S, Paradkar A. Preparation and characterization of etoricoxib solid dispersions using lipid carriers by spray drying technique. AAPS PharmSciTech. 2005;6(3):E405-E9. doi: 10.1208/pt060350

5. Shah N, Sandhu H, Phuapradit W, Pinal R, Iyer R, Albano A, et al. Development of novel microprecipitated bulk powder (MBP) technology for manufacturing stable amorphous formulations of poorly soluble drugs. International Journal of Pharmaceutics. 2012;438(1–2):53-60. doi: 10.1016/j.ijpharm.2012.08.031.

6. O'Donnell KP, Cai Z, Schmerler P, Williams RO, 3rd. Atmospheric freeze drying for the reduction of powder electrostatics of amorphous, low density, high surface area pharmaceutical powders. Drug Development and Industrial Pharmacy. 2012;39(2);205-17. doi:10.3109/03639045.2012.669385.

7. Hughey J, DiNunzio J, Bennett R, Brough C, Miller D, Ma H, et al. Dissolution Enhancement of a Drug Exhibiting Thermal and Acidic Decomposition Characteristics by Fusion Processing: A Comparative Study of Hot Melt Extrusion and KinetiSol® Dispersing. AAPS PharmSciTech. 2010;11(2):760-74. doi: 10.1208/s12249-010-9431-y

8. El-Egakey MA, Soliva M, Speiser P. Hot extruded dosage forms. I. Technology and dissolution kinetics of polymeric matrices. Pharmaceutica Acta Helvetiae. 1971;46(1):31-52.

9. Breitenbach J. Melt extrusion: from process to drug delivery technology. European Journal of Pharmaceutics and Biopharmaceutics. 2002;54(2):107-17. doi: 10.1016/S0939-6411(02)00061-9.

10. Prodduturi S, Urman K, Otaigbe J, Repka M. Stabilization of hot-melt extrusion formulations containing solid solutions using polymer blends. AAPS PharmSciTech. 2007;8(2):E152-E61. doi: 10.1208/pt0802050.

11. Crowley MM, Zhang F, Repka MA, Thumma S, Upadhye SB, Kumar Battu S, et al. Pharmaceutical Applications of Hot-Melt Extrusion: Part I. Drug Development and Industrial Pharmacy. 2007;33(9):909-26. doi:10.1080/03639040701498759.

12. Forster A, Hempenstall J, Rades T. Characterization of glass solutions of poorly water-soluble drugs produced by melt extrusion with hydrophilic amorphous polymers. Journal of Pharmacy and Pharmacology. 2001;53(3):303-15. doi: 10.1211/0022357011775532.

13. Swarbrick J, Boylan JC. Encyclopedia of Pharmaceutical Technology: Volume 20-Supplement 3: CRC Press; 2000.

14. Jani R, Patel D. Hot melt extrusion: An industrially feasible approach for casting orodispersible film. Asian Journal of Pharmaceutical Sciences, 2015;10(4):292–305. doi:10.1016/j.ajps.2015.03.002

15. Bennett R, Keen J, Bi Y, Porter S, Dürig T, McGinity J. Investigation of the interactions of enteric and hydrophilic polymers to enhance dissolution of griseofulvin following hot melt extrusion processing. Journal of Pharmacy and Pharmacology. 2015:67(7):918-38. doi: 10.1111/jphp.12388

16. Konno H, Handa T, Alonzo D, Taylor L. Effect of polymer type on the dissolution profile of amorphous solid dispersions containing felodipine. European journal of pharmaceutics and biopharmaceutics, 2008:70(2): 493-9. doi:10.1016/j.ejpb.2008.05.023

17. Six K, Berghmans H, Leuner C, Dressman J, Van Werde K, Mullens J, et al. Characterization of solid dispersions of itraconazole and hydroxypropylmethylcellulose prepared by melt extrusion, part II. Pharm Res. 2003;20(7):1047-54. doi: 0724-8741/03/0700-1047/0

18. Verreck G, Six K, Van den Mooter G, Baert L, Peeters J, Brewster ME. Characterization of solid dispersions of itraconazole and hydroxypropylmethylcellulose prepared by melt extrusion—part I. International journal of pharmaceutics. 2003;251(1):165-74. doi: 0378-5173/02

19. O'Donnell, K. P. and W. H. H. Woodward. Dielectric spectroscopy for the determination of the glass transition temperature of pharmaceutical solid dispersions. Drug Development and Industrial Pharmacy. 2014: 1-10.

20. Flory PJ. Thermodynamics of High Polymer Solutions. The Journal of Chemical Physics. 1942;10(1):51-61. doi:10.1063/1.1723621.

21. Huggins ML. THERMODYNAMIC PROPERTIES OF SOLUTIONS OF LONG-CHAIN COMPOUNDS. Annals of the New York Academy of Sciences. 1942;43(1):1-32. doi: 10.1111/j.1749-6632.1942.tb47940.x.

22. Marsac P, Li T, Taylor L. Estimation of Drug–Polymer Miscibility and Solubility in Amorphous Solid Dispersions Using Experimentally Determined Interaction Parameters. Pharm Res. 2009;26(1):139-51. doi: 10.1007/s11095-008-9721-1.

23. Lin D, Huang Y. A thermal analysis method to predict the complete phase diagram of drug–polymer solid dispersions. International Journal of Pharmaceutics. 2010;399(1–2):109-15. doi: 10.1016/j.ijpharm.2010.08.013.

24. Zhao Y, Inbar P, Chokshi HP, Malick AW, Choi DS. Prediction of the thermal phase diagram of amorphous solid dispersions by flory–huggins theory. Journal of Pharmaceutical Sciences. 2011;100(8):3196-207. doi: 10.1002/jps.22541.

25. Tian Y, Booth J, Meehan E, Jones DS, Li S, Andrews GP. Construction of Drug–Polymer Thermodynamic Phase Diagrams Using Flory–Huggins Interaction Theory: Identifying the Relevance of Temperature and Drug Weight Fraction to Phase Separation within Solid Dispersions. Molecular Pharmaceutics. 2012;10(1):236-48. doi: 10.1021/mp300386v.

26. Bellantone RA, Patel P, Sandhu H, Choi DS, Singhal D, Chokshi H, et al. A method to predict the equilibrium solubility of drugs in solid polymers near room temperature using thermal analysis. Journal of Pharmaceutical Sciences. 2012;101(12):4549-58. doi: 10.1002/jps.23319.

27. Marsac P, Shamblin S, Taylor L. Theoretical and Practical Approaches for Prediction of Drug–Polymer Miscibility and Solubility. Pharm Res. 2006;23(10):2417-26. doi: 10.1007/s11095-006-9063-9.

28. Fountain AW, Vickers TJ, Mann CK. Factors that Affect the Accuracy of Raman Shift Measurements on Multichannel Spectrometers. Appl Spectrosc. 1998;52(3):462-8. doi: 0003-7028 / 98 / 5203-0462$2.00 / 0

29. Grzesiak AL, Lang M, Kim K, Matzger AJ. Comparison of the four anhydrous polymorphs of carbamazepine and the crystal structure of form I. Journal of Pharmaceutical Sciences. 2003;92(11):2260-71. doi: 10.1002/jps.10455.

30. Naima Z, Siro T, Juan-Manuel G-D, Chantal C, René C, Jerome D. Interactions between carbamazepine and polyethylene glycol (PEG) 6000: characterisations of the physical, solid dispersed and eutectic mixtures. European Journal of Pharmaceutical Sciences. 2001;12(4):395-404. doi: 10.1016/S0928-0987(00)00168-8.

31. Rustichelli C, Gamberini G, Ferioli V, Gamberini MC, Ficarra R, Tommasini S. Solid-state study of polymorphic drugs: carbamazepine. Journal of Pharmaceutical and Biomedical Analysis. 2000;23(1):41-54. doi: 10.1016/S0731-7085(00)00262-4.

32. Kolter K, Karl M, Gryczke A, Ludwigshafen am Rhein B. Hot-melt extrusion with BASF pharma polymers: extrusion compendium: BASF; 2012.

33. McGinity JW, Felton LA. Aqueous polymeric coatings for pharmaceutical dosage forms: CRC Press; 2013.

34. Coppens K, Hall M, Larsen P, Mitchell S, Nguyen P, Read M, et al., editors. Thermal and rheological evaluation of pharmaceutical excipients for hot melt extrusion. AAPS Annual Meeting and Exposition, Baltimore, MD; 2004.

35. Hughey JR, Keen JM, Miller DA, Brough C, McGinity JW. Preparation and characterization of fusion processed solid dispersions containing a viscous thermally labile polymeric carrier. International Journal of Pharmaceutics. 2012;438(1–2):11-9. doi: 10.1016/j.ijpharm.2012.08.032.

36. Martin C. Twin Screw Extrusion for Pharmaceutical Processes. In: Repka MA, Langley N, DiNunzio J, editors. Melt Extrusion: Springer New York; 2013. p. 47-79.

37. Liu J, Cao F, Zhang C, Ping Q. Use of polymer combinations in the preparation of solid dispersions of a thermally unstable drug by hot-melt extrusion. Acta Pharmaceutica Sinica B. 2013;3(4):263-72. doi: 10.1016/j.apsb.2013.06.007.

38. Djuris J, Nikolakakis I, Ibric S, Djuric Z, Kachrimanis K. Preparation of carbamazepine–Soluplus® solid dispersions by hot-melt extrusion, and prediction of drug–polymer miscibility by thermodynamic model fitting. European Journal of Pharmaceutics and Biopharmaceutics. 2013;84(1):228-37. doi: 10.1016/j.ejpb.2012.12.018.

39. Miller DA, McConville JT, Yang W, Williams RO, McGinity JW. Hot-melt extrusion for enhanced delivery of drug particles. Journal of Pharmaceutical Sciences. 2007;96(2):361-76. doi: 10.1002/jps.20806.

40. Leuner C, Dressman J. Improving drug solubility for oral delivery using solid dispersions. European Journal of Pharmaceutics and Biopharmaceutics. 2000;50(1):47-60. doi: 10.1016/S0939-6411(00)00076-X.

41. Kobayashi Y, Ito S, Itai S, Yamamoto K. Physicochemical properties and bioavailability of carbamazepine polymorphs and dihydrate. International Journal of Pharmaceutics. 2000;193(2):137-46. doi: 10.1016/S0378-5173(99)00315-4.

42. Tanno F, Nishiyama Y, Kokubo H, Obara S. Evaluation of Hypromellose Acetate Succinate (HPMCAS) as a Carrier in Solid Dispersions. Drug Development and Industrial Pharmacy. 2004;30(1):9-17. doi: 10.1081/DDC-120027506.

43. Mehuys E, Vervaet C, Gielen I, Van Bree H, Remon JP. In vitro and in vivo evaluation of a matrix-in-cylinder system for sustained drug delivery. Journal of Controlled Release. 2004;96(2):261-71. doi: 10.1016/j.jconrel.2004.01.023.

44. Matsumoto T, Zografi G. Physical Properties of Solid Molecular Dispersions of Indomethacin with Poly(vinylpyrrolidone) and Poly(vinylpyrrolidone-co-vinyl-acetate) in Relation to Indomethacin Crystallization. Pharm Res. 1999;16(11):1722-8. doi: 10.1023/A:1018906132279.

45. Barton AFM. Solubility parameters. Chemical Reviews. 1975;75(6):731-53. doi: 10.1021/cr60298a003.

46. Hancock B, Zografi G. The Relationship Between the Glass Transition Temperature and the Water Content of Amorphous Pharmaceutical Solids. Pharm Res. 1994;11(4):471-7. doi: 10.1023/A:1018941810744.

47. Crowley KJ, Zografi G. Water vapor absorption into amorphous hydrophobic drug/poly(vinylpyrrolidone) dispersions. Journal of Pharmaceutical Sciences. 2002;91(10):2150-65. doi: 10.1002/jps.10205.

48. Murphy D, Rodríguez-Cintrón F, Langevin B, Kelly RC, Rodríguez-Hornedo N. Solution-mediated phase transformation of anhydrous to dihydrate carbamazepine and the effect of lattice disorder. International Journal of Pharmaceutics. 2002;246(1–2):121-34. doi: 10.1016/S0378-5173(02)00358-7.

49. Sotthivirat S, McKelvey C, Moser J, Rege B, Xu W, Zhang D. Development of amorphous solid dispersion formulations of a poorly water-soluble drug, MK-0364. International Journal of Pharmaceutics. 2013;452(1–2):73-81. doi: 10.1016/j.ijpharm.2013.04.037.

50. Goddeeris C, Willems T, Van den Mooter G. Formulation of fast disintegrating tablets of ternary solid dispersions consisting of TPGS 1000 and HPMC 2910 or PVPVA 64 to improve the dissolution of the anti-HIV drug UC 781. European

Journal of Pharmaceutical Sciences. 2008;34(4–5):293-302. doi: 10.1016/j.ejps.2008.05.005.

51. Minoux H, Chipot C. Cation–π Interactions in Proteins: Can Simple Models Provide an Accurate Description? Journal of the American Chemical Society. 1999;121(44):10366-72. doi: 10.1021/ja990914p.

52. Meyer EA, Castellano RK, Diederich F. Interactions with Aromatic Rings in Chemical and Biological Recognition. Angewandte Chemie International Edition. 2003;42(11):1210-50. doi: 10.1002/anie.200390319.

53. Wintjens R, Liévin J, Rooman M, Buisine E. Contribution of cation-π interactions to the stability of protein-DNA complexes1. Journal of Molecular Biology. 2000;302(2):393-408. doi: 10.1006/jmbi.2000.4040.

54. Crowley PB, Golovin A. Cation–π interactions in protein–protein interfaces. Proteins: Structure, Function, and Bioinformatics. 2005;59(2):231-9. doi: 10.1002/prot.20417.

55. Tsuzuki S, Yoshida M, Uchimaru T, Mikami M. The Origin of the Cation/π Interaction: The Significant Importance of the Induction in Li+ and Na+

Complexes. The Journal of Physical Chemistry A. 2001;105(4):769-73. doi: 10.1021/jp003287v.

56. Gallivan JP, Dougherty DA. A Computational Study of Cation−π Interactions vs Salt Bridges in Aqueous Media: Implications for Protein Engineering. Journal of the American Chemical Society. 2000;122(5):870-4. doi: 10.1021/ja991755c.

57. Zhong W, Gallivan JP, Zhang Y, Li L, Lester HA, Dougherty DA. From ab initio quantum mechanics to molecular neurobiology: A cation–π binding site in the nicotinic receptor. Proceedings of the National Academy of Sciences. 1998;95(21):12088-93. doi: 10.1073/pnas.95.21.12088.

58. Jung J-Y, Yoo SD, Lee S-H, Kim K-H, Yoon D-S, Lee K-H. Enhanced solubility and dissolution rate of itraconazole by a solid dispersion technique. International Journal of Pharmaceutics. 1999;187(2):209-18. doi: 10.1016/S0378-5173(99)00191-X.

59. O'Brien LE, Timmins P, Williams AC, York P. Use of in situ FT-Raman spectroscopy to study the kinetics of the transformation of carbamazepine polymorphs. Journal of Pharmaceutical and Biomedical Analysis. 2004;36(2):335-40. doi: 10.1016/j.jpba.2004.06.024.

3.8 LIST OF FIGURES

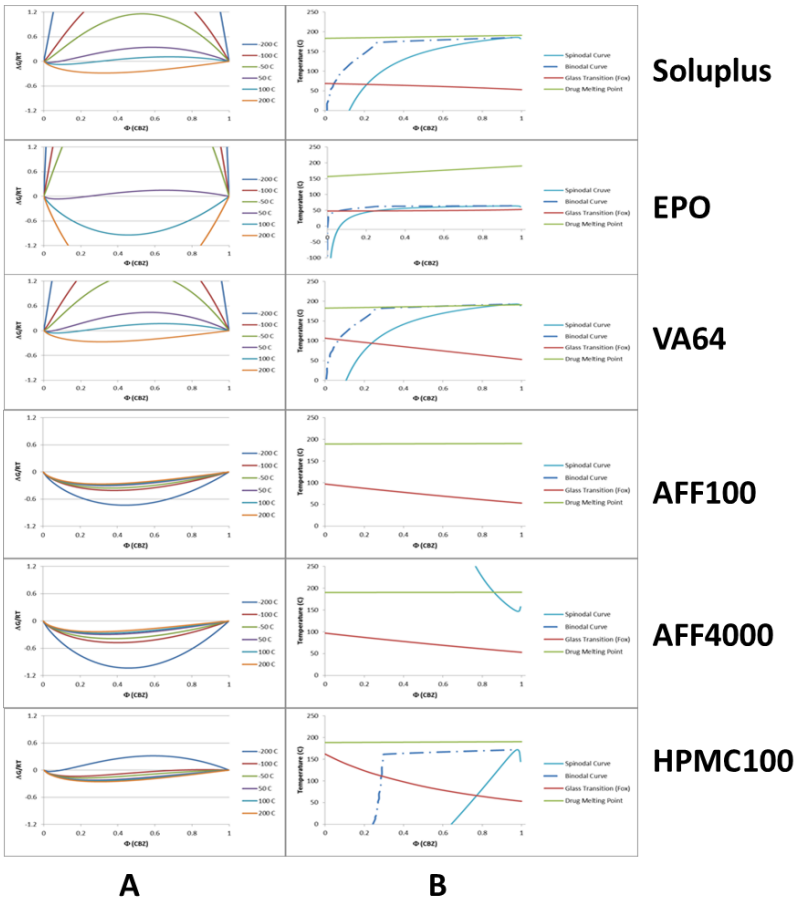

Figure 3.1 Free energy and phase diagrams. (A) Free energy diagram of the CBZ/polymers system as determined using Flory–Huggins Theory. (B) Thermal phase diagram of the CBZ/polymers representing the boundaries between thermodynamically unstable, metastable and stable regions as bounded by the spinodal and binodal curves along with the glass transition boundary. [Soluplus® (Soluplus), Kollidon® VA 64 (VA64), EUDRAGIT® E PO (EPO), HPMC 2910 100cP (HPMC100), and AFFINISOL™ HPMC HME 4000 (AFF4000) or 100 (AFF100)]

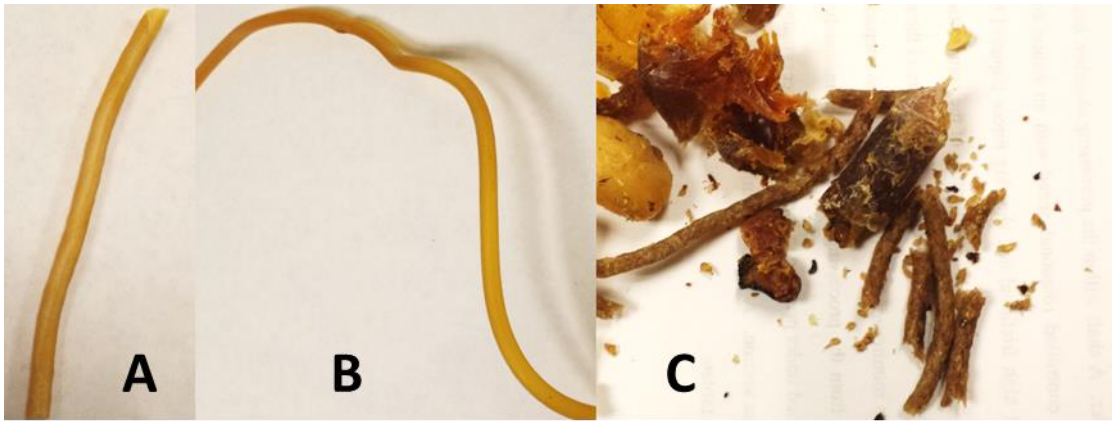

Figure 3.2 Extrudate of 30% CBZ and 70% (A) AFF100 at 140°C, 100 rpm, (B) AFF100 and (C) HPMC100 at 160°C, 150 rpm, using Leistritz Nano-16.

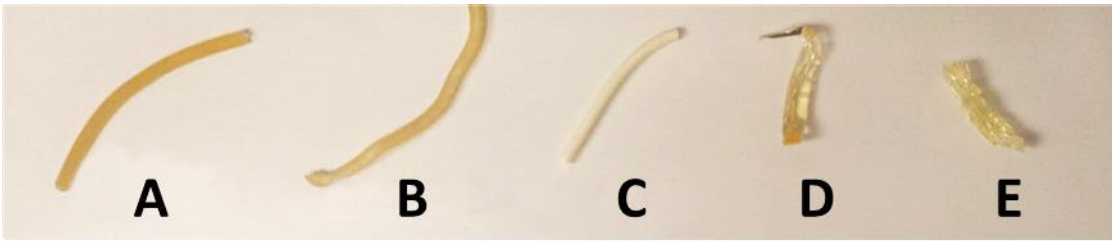

Figure 3.3 Extrudate of 30% CBZ and 70% (A) AFF100, (B) AFF4000, (C) EPO, (D) VA64, (E) Soluplus, at 140°C, 100 rpm using Leistritz Nano-16.

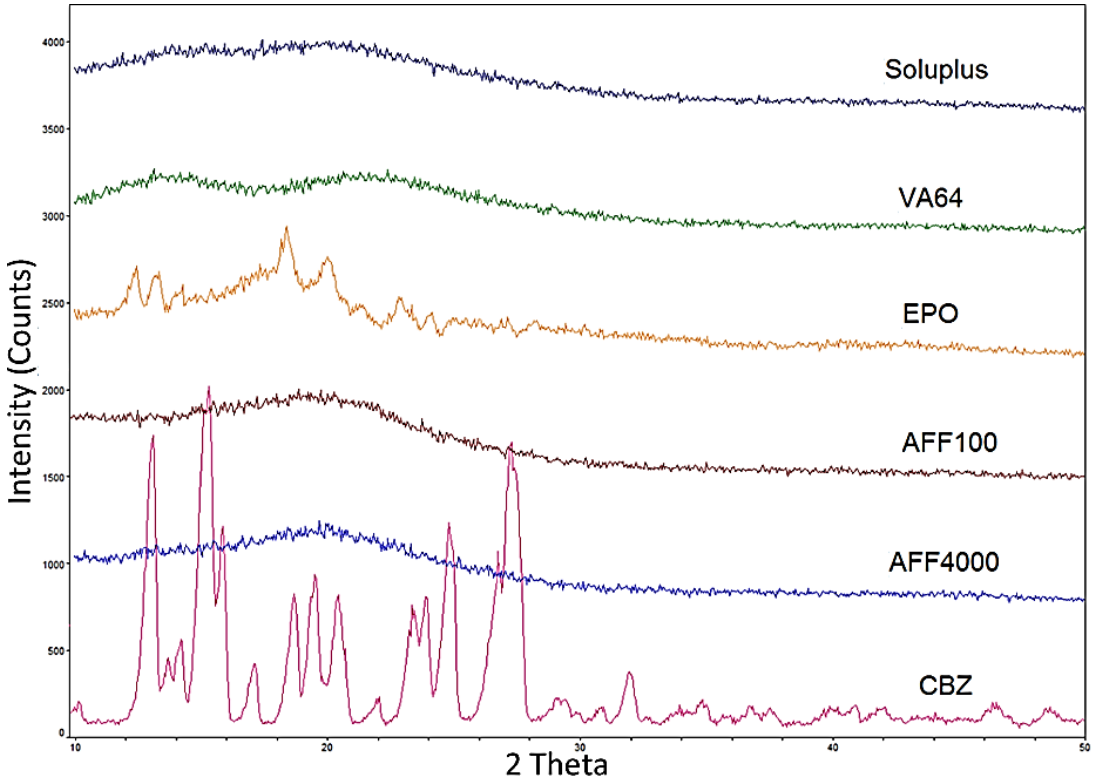

Figure 3.4 XRD patterns of extrudate containing 30% CBZ and 70% polymer (listed above each XRD signal line See legend in Figure 3.1 for abbreviations of extrudates).

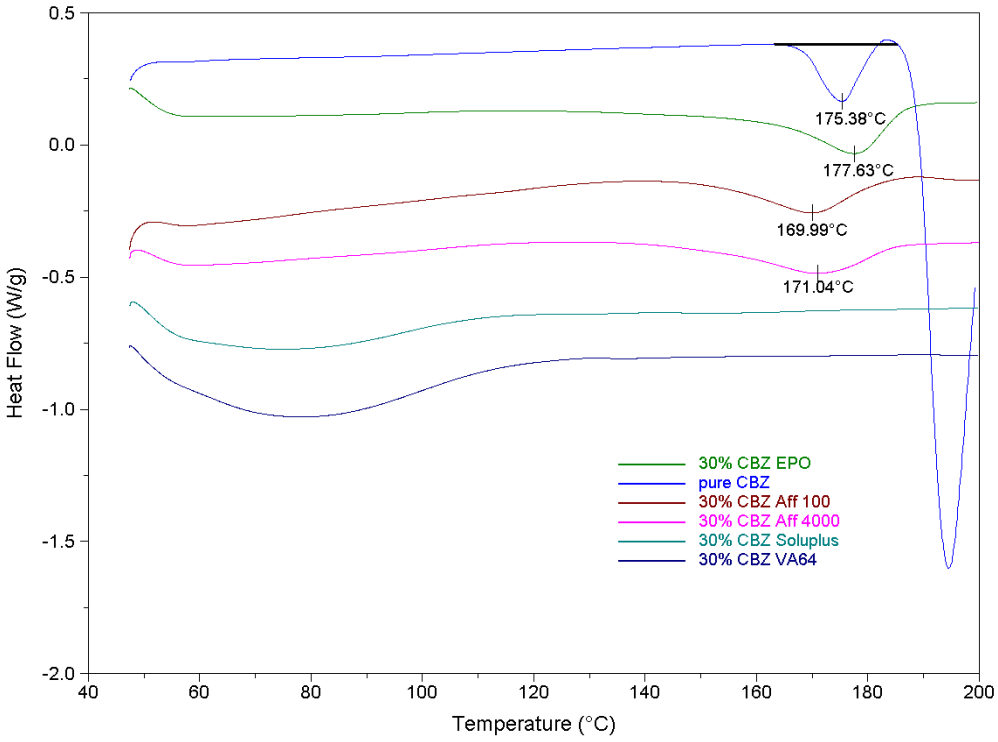

Figure 3.5 DSC thermograms of CBZ and extrudates containing 30% CBZ and 70% polymer (See legend in Figure 3.1 for abbreviations of extrudates).

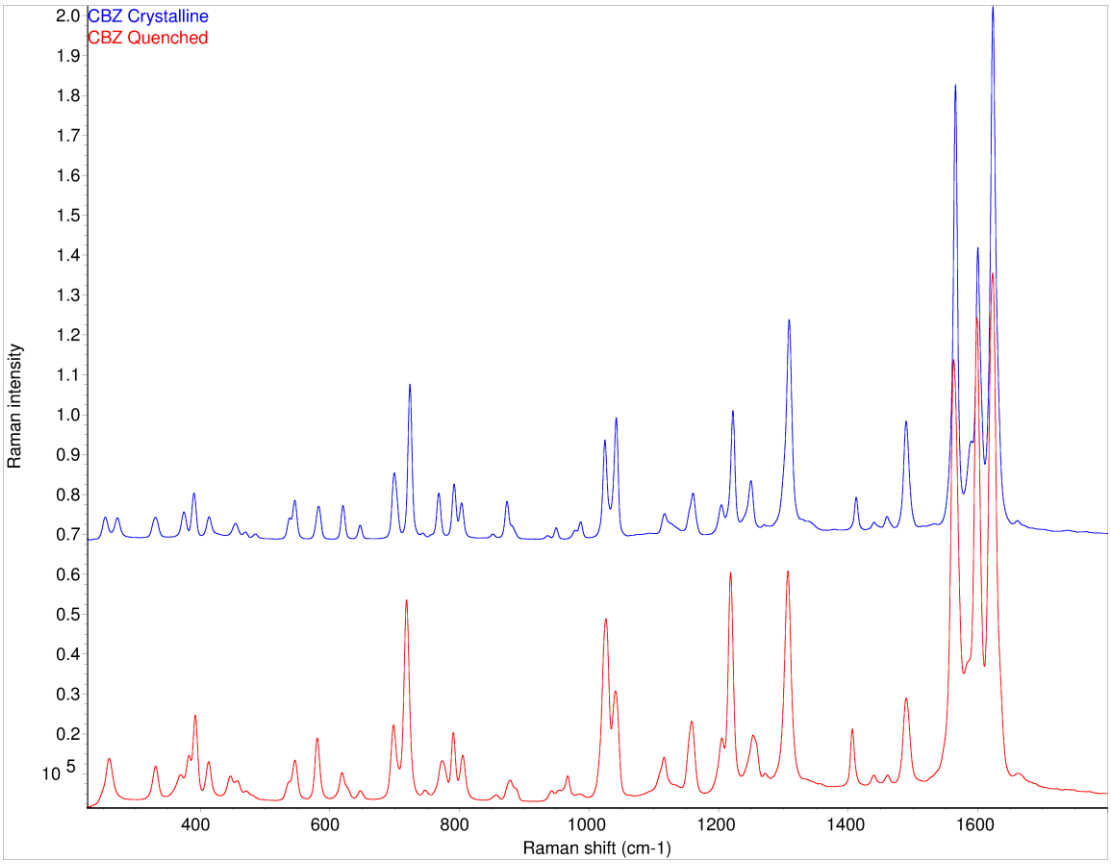

Figure 3.6 Raman spectra of crystalline (top) and amorphous CBZ (bottom).

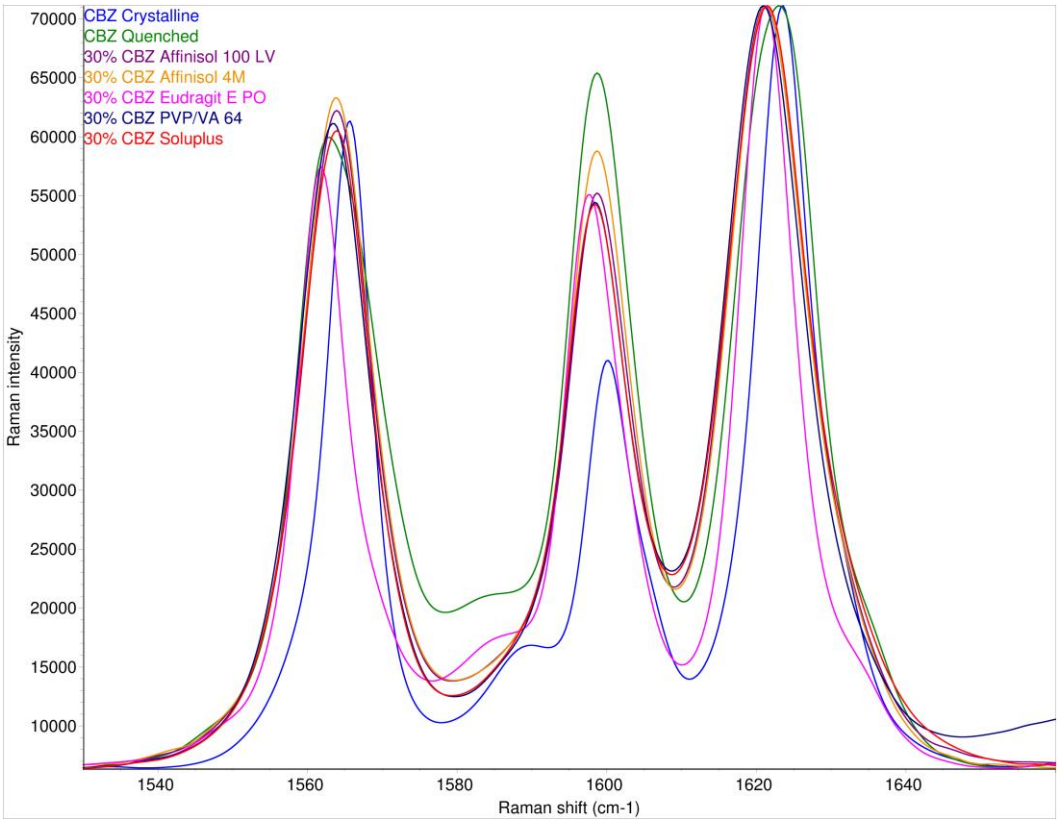

Figure 3.7 Raman spectra of the 1600 cm-1 region of crystalline CBZ (blue), amorphous CBZ (green) and 30% CBZ in AFF100 (purple), AFF4000 (orange), EPO (pink), VA 64 (dark blue) and Soluplus (red). The spectra are scaled to the strongest band for comparison. (See legend in Figure 3.1 for abbreviations of extrudates).

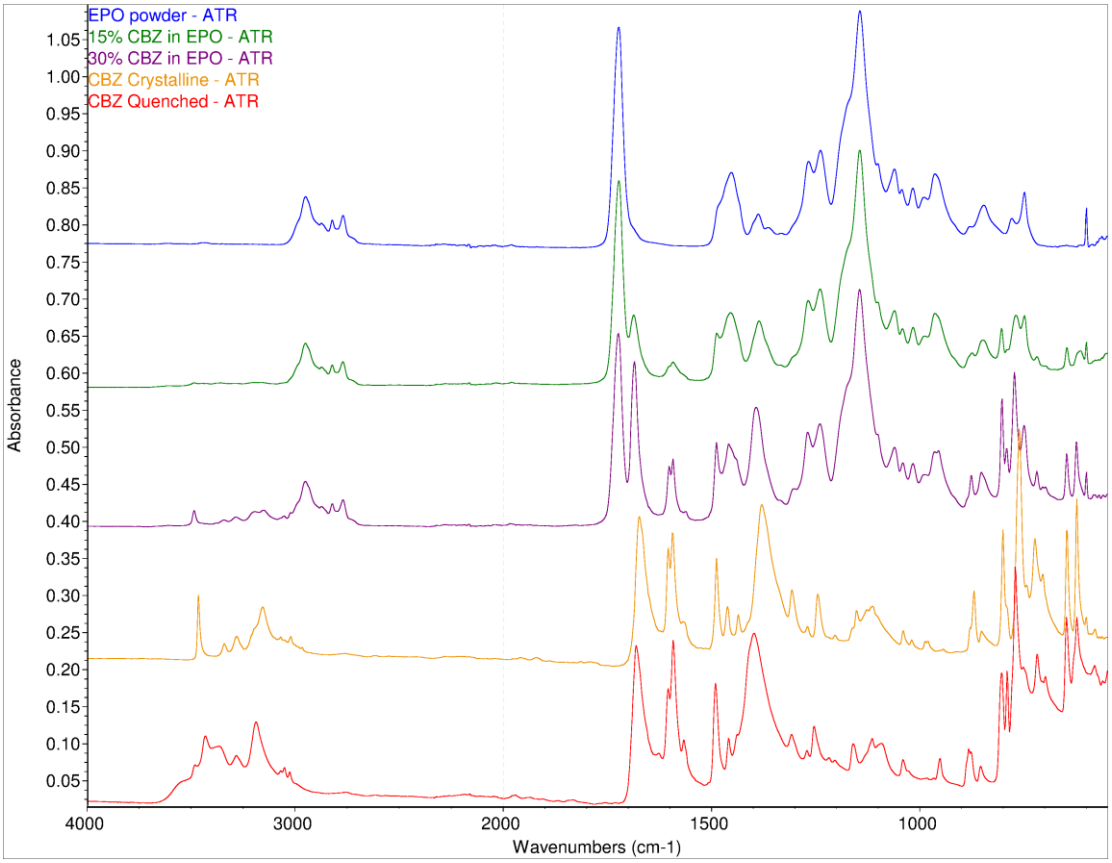

Figure 3.8 ATR FTIR spectra of EPO (blue), 15% CBZ in EPO (green), 30% CBZ in EPO (purple), crystalline CBZ (orange) and amorphous CBZ (red).

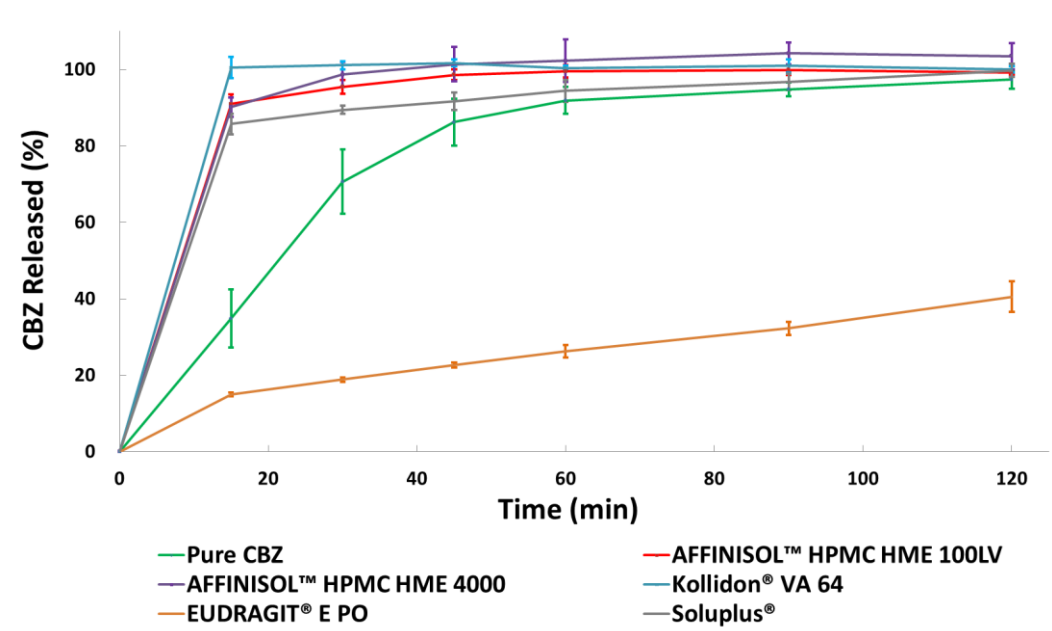

Figure 3.9 Sink condition dissolution test of extrudates and bulk CBZ containing 100 mg CBZ in 1000 mL DI water (n=3) (See legend in Figure 3.1 for abbreviations of extrudates).

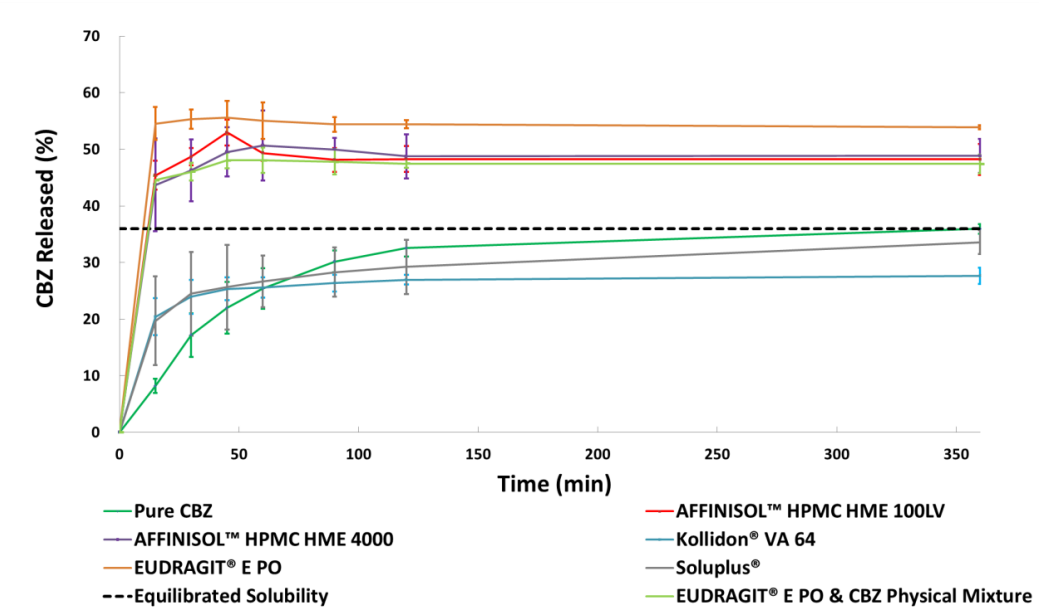

Figure 3.10 Non-sink condition dissolution test of extrudates and bulk CBZ containing 100 mg CBZ in 100 mL 0.1 HCl (n=3) (See legend in Figure 3.1 for abbreviations of extrudates).

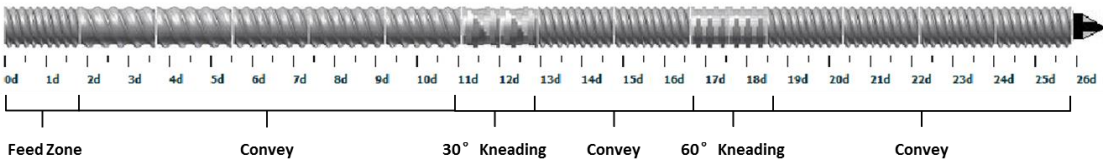

Figure 3.11 Screw design for all formulations processed (Leistritz Nano-16).

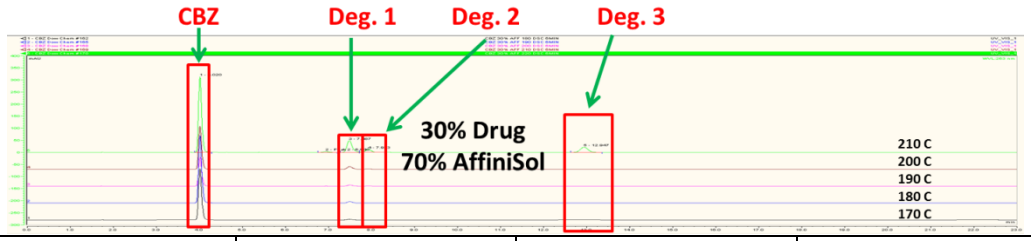

	Deg. 1 RRT (1.862)	Deg. 2 RRT (1.973)	Deg. 3 RRT (3.221)
Room Temperature	0	0	0
170	1.2%	<1%	<1%
180	2%	<1%	<1%
190	2.2%	<1%	<1%
200	2.9%	<1%	<1%
210	3.2%	<1%	<1%

Figure 3.12 Forced-degradation study of CBZ and AFF100 (peaks over 0.5% are marked in the figure).

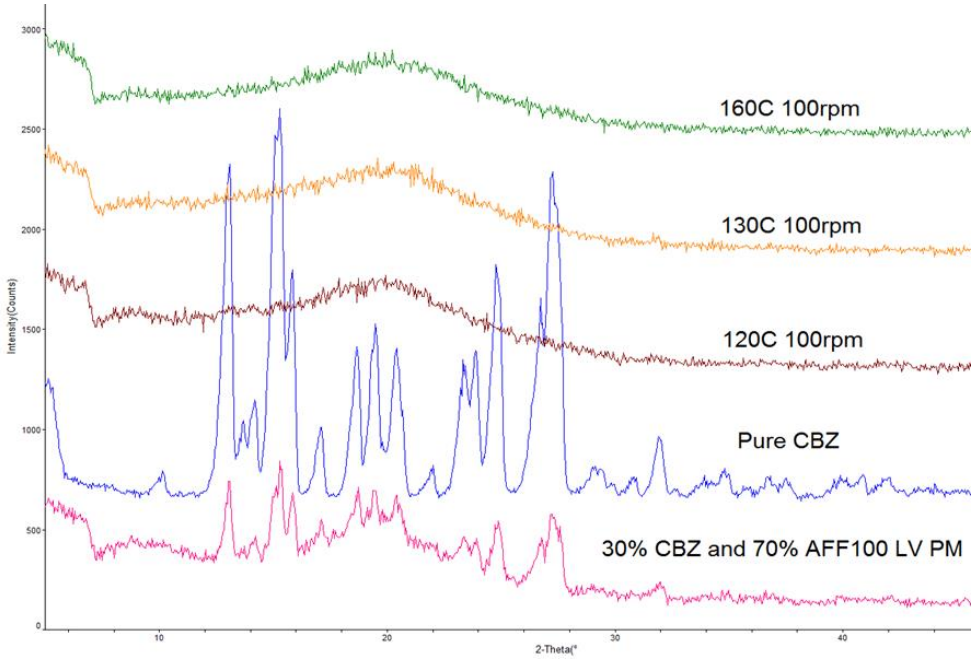

Figure 3.13 XRD patterns of extruded material using different temperature.

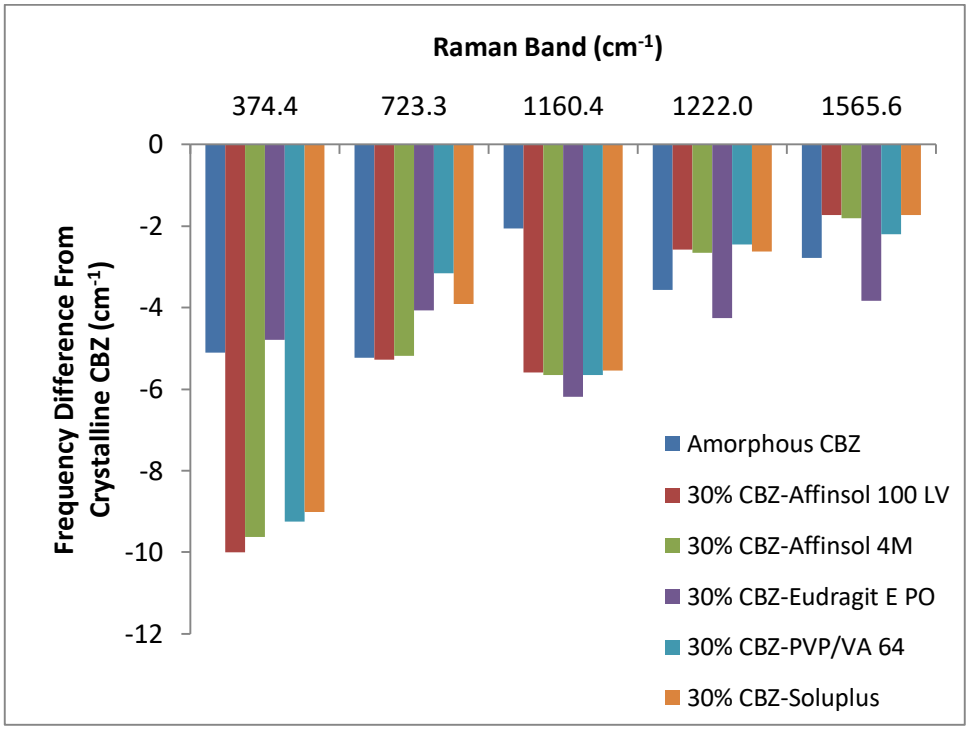

Figure 3.14 Frequency shifts of selected Raman bands from crystalline CBZ (See legend in Figure 3.1 for abbreviations of extrudates).

3.9 LIST OF TABLES

	EPO	AFF100	AFF4000
AUC (mg·min)	19164 ± 157	17064 ± 451	17174 ± 628
	Bulk CBZ	VA64	Soluplus
AUC (mg·min)	10894 ± 252	9371 ± 282	10467 ± 594

Table 3.1 Area under the dissolution curve (AUDC) values for non-sink dissolution testing in 0.1N HCl.

Formulation	Temperature (℃)	Screw Speed (rpm)	Feed Rate (g/min)	CBZ Recovery (%)	Appearance
1	160	150	3	85.46	
2	160	100	3	87.66	
3	160	200	3	82.53	
4	120	100	3	89.76	
5	130	100	3	92.23	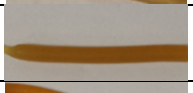
6	140	100	3	91.42	
7	180	100	3	82.88	
8	140	100	4	95.97	
9	140	100	5	99.81	

Table 3.2 Processing conditions optimization using AFF100-CBZ formulations and screw design shown in Figure. 4.11.

	Raman Frequency (cm^{-1})						
Raman Band Assignment (59)	**Crystalline CBZ**	**Amorphous CBZ**	**CBZ-AFF100**	**CBZ-AFF4000**	**CBZ-EPO**	**CBZ-VA 64**	**CBZ-Soluplus**
Lattice vibration	374.4	369.3	364.4	364.8	369.7	365.2	365.4
C-N-C stretch	723.4	718.1	718.1	718.2	719.3	720.2	719.4
C-C ring stretch/C-N-C asymmetric stretch	1160.4	1158.4	1154.8	1154.8	1154.2	1154.8	1154.9
C-N stretch (amide III)	1222.0	1218.4	1219.4	1219.4	1217.8	1219.6	1219.4
C=C ring stretch	1565.6	1562.8	1563.9	1563.8	1561.8	1563.4	1563.9
Mean Difference From Crystalline CBZ		-3.7	-5.0	-5.0	-4.6	-4.5	-4.6

Table 3.3 Frequencies of selected Raman bands for the crystalline, amorphous and formulated forms of CBZ. For each formulation, the Raman spectrum of the neat polymer was subtracted from the Raman spectrum of the 30% CBZ/polymer formulation.

Chapter 4: Processing of a Thermally Labile Drug by Hot-Melt Extrusion

4.1 ABSTRACT

The formation of molecularly dispersed amorphous solid dispersions by the hot-melt extrusion technique relies on the thermal and mechanical energy inputs provided by the extruder, which can cause chemical degradation of drugs and polymeric carriers. Additionally, drug degradation may be exacerbated as drugs convert from a more stable crystalline form to a higher energy amorphous form during the HME process. Therefore, it is imperative to minimize drug degradation caused by HME, especially for thermally labile drugs. In this work, gliclazide was used as a model thermally labile drug to evaluate the benefits of optimizing extruder screw designs, machine setup, and processing conditions. Preformulation studies were conducted using differential scanning calorimetry, thermogravimetric analysis, and liquid chromatography–mass spectroscopy to identify drug degradation pathways and to determine initial extrusion conditions. Formulations containing 10% drug and 90% AFFINISOL™ HPMC HME 100LV were then extruded using a twin screw extruder, and the extrudates were characterized using X-ray powder diffraction, modulated dynamic scanning calorimetry, and potency testing to evaluate physicochemical properties. For comparison, gliclazide amorphous solid dispersions were prepared using a spray drying technique for the degradation kinetics study, and the energies of activation for both amorphous gliclazide, crystalline gliclazide, and gliclazide solution were calculated using the Arrhenius equation to further guide the extrusion optimization

process. Results from the preformulation studies indicated that the 10% gliclazide blend was stable after holding at or below 140 °C for 4 min. At higher temperatures, the gliclazide blend started to degrade, and two hydrolysis degradation pathways of gliclazide were proposed. The activation energy study indicates a significantly higher degradation rate for the amorphous gliclazide compared to the crystalline form. After optimization of the hot-melt extrusion process, including improved screw designs, machine setup, and processing conditions, we achieved gliclazide amorphous solid dispersion with ~95% drug recovery. This study clearly demonstrates the importance of the following factors on drug degradation: (a) changing screw design to facilitate shorter amorphous (melt) residence time, (b) lowering processing temperature to avoid excess thermal exposure, and (c) minimizing processing parameters to reduce unnecessary mechanical energy input. The ability to process thermally labile drugs and polymers using hot-melt extrusion will significantly expand the possible applications of this manufacturing process.

4.2 INTRODUCTION

The hot-melt extrusion (HME) technique has gained increasing popularity in the pharmaceutical industry due to its widespread applications as a drug delivery option, including device shaping (1), taste-masking (2), controlled release (3), and solubility enhancement (4). In particular, the manufacture of amorphous solid dispersions (ASDs) to improve the bioavailability of BCS Class II and Class IV drugs has been widely studied and has been commercially proven as an effective formulation strategy (5). However, during extrusion the conversion of the drug from the crystalline to amorphous form relies

on thermal and mechanical energy inputs from the extruder, and this energy input can degrade the active ingredient or excipients (6). Therefore, the application of HME with thermally labile materials is challenging. Thermal energy input during the extrusion process is normally supplied by heat conduction from the barrel and the friction of the material against the kneading elements and interior wall of the extruder barrel (7). Thermally induced chemical degradation has been widely reported to occur during HME process (8-10). Moreover, mechanical energy input is also supplied by the machine motor, and it is delivered through the interaction of the screw elements and the extruded materials (11). Part of the mechanical energy can be converted to thermal energy, especially in large-scale extruders. However, when kneading elements are used, the relatively high-shear energy generated can still result in degradation of shear-sensitive materials (12).

Due to the wide diversity of drugs and excipients, many may be susceptible to different degradation pathways during the extrusion process, including hydrolysis, oxidation, dehydration, isomerization, and photo-degradation (13). Among the different pathways, oxidation (14) and hydrolysis (15) are considered the most common degradation reactions. Chemical degradation can be triggered by some of the conditions involved in HME, such as elevated temperature (16), excipient incompatibility (17), the presence of oxygen (18), moisture (19), and pH level (20). Temperature, which is an important processing parameter in HME, is well known to significantly affect chemical degradation kinetics as predicted by the Arrhenius equation (21). Moreover, because of the high

molecular mobility of amorphous materials, amorphous drugs are more prone to chemical degradation compared to their crystalline counter-parts (22, 23).

In general, extrusion involves melting and mixing of the materials. The melting process is highly influenced by the degree of filling, the material residence time, and the level of heat conduction from the barrel of co-rotating twin-screw extruders (24). The mixing performance depends significantly on the shear stress and stress duration of the mixing process. Therefore, it is important to find the optimum balance between providing enough energy for amorphous conversion and generating excess energy that triggers chemical degradation (25). Some formulation approaches such as decreasing the melting point, viscosity, and mixing temperature of the extruded materials (26, 27) have been used to achieve a milder extrusion conditions. Processing approaches, on the other hand, have also shown some success in minimizing degradation by optimizing barrel temperature, screw speed, machine throughput, and screw geometry (9, 28, 29). However, these studies do not provide a sufficiently detailed explanation of how and where drug degradation took place during the process, or a systematic strategy to solve the degradation problem during HME.

The aim of this study was to investigate the cause of degradation of an ASD of gliclazide (GLZ) during the HME process and to investigate the degradation kinetics of different forms of GLZ. This information was then used to further optimize the extrusion process in order to minimize the chemical degradation of GLZ, which has not been

addressed previously in the thermal process of GLZ (30). In this paper, it was hypothesized that the screw design and processing condition optimization based on the degradation studies would reduce GLZ degradation during the HME manufacturing of an ASD.

4.3 MATERIALS AND METHODS

4.3.1 Materials

Crystalline GLZ and AFFINISOL™ HPMC HME 100LV were donated by The Dow Chemical Company (Midland, MI). Soluplus® (Soluplus) and Kollidon® VA 64 (PVP VA64) were donated by BASF Corporation (Florham Park, NJ). Indigo carmine was obtained from Acros Organics (Geel, Belgium). HPLC–grade acetonitrile and water were purchased from Fisher Scientific Co. (Houston, TX). All other chemicals used in this study were of American Chemical Society (ACS) grade. All percentages are based on w/w unless otherwise noted.

4.3.2 Methods

4.3.2.1 Hot Melt Extrusion and Milling

HME processing was conducted on a co-rotating Leistritz Nano-16 twin-screw extruder (American Leistritz Extruder Corp., Somerville, NJ, USA) with a twin-screw volumetric feeder (Brabender Technology, Duisburg, Germany). Three screw designs were used to provide different levels of shear input. Blends with 10% GLZ loading were processed at temperatures ranging from 100–160 °C and with screw speeds set at 100 rpm,

200 rpm, and 300 rpm with or without a die. Extrudates were cooled to room temperature before milling. A Fitzpatrick L1A Fitzmill (Fitzpatrick, Inc., Elmhurst, IN, USA) operating at 9,000 rpm in the impact configuration with a 0.033-inch screen was used to mill HME materials. Powders retained between 37 μm (400 US mesh) and 44 μm (325 US mesh) were collected and stored in a desiccator over phosphorus pentoxide for further analysis.

4.3.2.2 Residence Time Studies

The residence time of GLZ formulations at different processing conditions was determined after the processing torque was stable. The time at which 0.2 g of indigo carmine was charged into the extruder feed port and into the sampling port was denoted as t = 0. The time at which colored extrudate emerged from the die was noted as the residence time. A calibrated timer was utilized to determine the time.

4.3.2.3 High-Performance Liquid Chromatography (HPLC)

GLZ content was analyzed with a Dionex Ultimate 3000 HPLC system (Thermo Fisher Scientific Inc., Waltham, MA) equipped with a Waters Spherisorb® ODS-2 250 mm (5 μm, 4.6 mm × 250 mm) column. The HPLC system also included an Ultimate 3000 autosampler to consistently inject 20 μL samples, an Ultimate RS variable wavelength detector extracting at a wavelength of 235 nm, and dual Ultimate 3000 pumps. The system was operated under isocratic flow at 1 mL/min using a mobile phase consisting of 60% ammonium acetate buffer (0.025 M, with pH adjusted to 3.1 using acetic acid) and 40% acetonitrile. The mobile phase was filtered through a 0.45-micron filter and degassed under

vacuum with sonication before use. The column was kept at 30 °C. Chromeleon Version 6.80 software (Thermo Fisher Scientific Inc., Waltham, MA) was used to process all chromatography data.

Finely ground powder samples were accurately weighed to 20.0 ± 1.0 mg and transferred directly into a 20-mL scintillation vial. Measured powder samples were dissolved using 20 mL 1:1 acetonitrile:water diluent solution. Samples were then filtered using 13-mm 0.2-micron PTFE filters (Wheaton, Millville, NJ) and transferred into HPLC vials for analysis (Phenomenex, Torrance, CA) for analysis.

4.3.2.4 X-Ray Powder Diffraction (XRD)

XRD studies were performed with a Rigaku Miniflex 600 (Rigaku, Tokyo, Japan) X-Ray Diffractometer equipped with Cu Kα radiation at 40 kV, 15 mA. Data were collected in a scan mode with a step size of 0.02° and a step time of 2 s over a 2θ range of 5–50°. Data analysis was performed with Bruker DIFFRACplus EVA diffraction software, version 15.0 (Billerica, MA, USA).

4.3.2.5 Liquid Chromatography-Mass Spectroscopy (LC–MS)

Analytes were analyzed using an Agilent 1290 Infinity binary liquid chromatograph and a 6538 UHD Accurate-Mass quadruple time of flight (QTOF) mass spectrometer (Santa Clara, CA). Analyte solutions were subjected to liquid separation on an Agilent Atlantis dC18 4.6 mm x 150 mm (3 μm particle size) column at a flow rate of 0.7 mL/min.

Mobile phases were composed of 0.1% formic acid (aqueous) and 0.1% formic acid in acetonitrile (organic). Starting conditions were held at 2% organic for 4 minutes and then ramped to 95% over 20 minutes, and the organic was held at 95% for 10 minutes. Analyte effluent was analyzed using electrospray ionization in the positive and negative ion modes. Mass spectra were subjected to an external calibration during the MS analysis to generate accurate mass assignments within +/−1 mDa. Agilent MassHunter Qualitative Analysis software (version B.03.01) was used to interpret the collected results.

4.3.2.6 Modulated Differential Scanning Calorimetry (MDSC)

MDSC analysis was performed with a TA Instruments Model Auto Q20 DSC (TA Instruments, New Castle, DE, USA). Samples were placed into Tzero® pans and crimped using a press. Raw materials were heated to 105 ℃ for 5 min to remove residual moisture and then equilibrated at −20 ℃, followed by heating to 250 ℃ at a ramp rate of 5 ℃/min with a modulation amplitude and period of 1 ℃ and 60 s, respectively. Processed samples were equilibrated at −20 ℃, followed by heating to 250 ℃ at a ramp rate of 5 ℃ /minute with a modulation amplitude and period of 1 ℃ and 60 s, respectively. During analyses, high-purity nitrogen flowed through the sample chamber at a rate of 50 mL/min. Data analysis was performed with TA Universal Analysis 2000 software.

4.3.2.7 Thermogravimetric Analysis

A Mettler Thermogravimetric Analyzer, Model TGA/DSC 1 (Mettler Toledo, Columbus, OH, USA) was utilized to evaluate the thermal stability of the drug. Samples

were weighed into individual 70-microliter alumina crucibles. Sample mass was monitored as the temperature ramped to 300 °C at 10 °C/min under 65 mL/min nitrogen or air purging conditions. Weight loss (percentage) was analyzed using STARe software (Mettler Toledo, Columbus, OH, USA). Moreover, the thermogravimetric analyzer was also used to thermally treat the drug. Samples were also weighed in the 70-microliter alumina crucibles, and placed under 65 mL/min nitrogen or air purging conditions. Crucibles were heated to set temperature ranges from 100–200 °C with 10 °C intervals using the jump mode. Crucibles were then held for 4 min before being removed for HPLC drug potency analysis. Weight loss and HPLC analysis results were compared to determine the initial extrusion condition.

4.3.2.8 Energy of Activation Study

4.3.2.8.1 Spray Drying

The amorphous solid dispersion of 10% GLZ in AFFINISOL™ HPMC HME 100LV was prepared by spray drying to avoid thermal degradation. The drug and the polymer were dissolved in ethanol:dichloromethane (1:1) at a total solids load of 2% (w/v). This solution was then spray-dried using a Buchi B-290 (Buchi Corporation, Flawil, Switzerland) mini-spray dryer with an inlet temperature of approximately 67–69 °C, 100% nitrogen gas aspirator rate (about 475 L/h), −10 °C condenser temperature, and a feed solution infusion rate of approximately 5 mL/min. The stable outlet temperature was about 42 °C. Following spray drying, the powder was secondarily dried in a vacuum oven (0.1

mPa) at ambient temperature for one week to remove the residual solvent. The size of the resulting spray-dried particles was approximately 40 μm.

4.3.2.8.2 Forced-Degradation of Samples

Samples of crystalline, ASD, and a 1 mg/mL DMSO solution of GLZ were weighed into 20-mL amber serum vials. Dried nitrogen gas was used to fill the vials before they were capped with bromobutyl stoppers and crimped with aluminum seals. The samples were then transferred to ovens pre-equilibrated at different temperatures ranging from 30–120 °C depending on the materials contained in the vial. At designated sampling points, vials were taken out of the oven and stored in a freezer at −20 °C until they were tested. Samples were thawed and dissolved with 10 mL diluent (acetonitrile:water = 1:1) before HPLC measurement. The energy of activation values for the hydrolysis reactions of GLZ were obtained from a linear regression analysis of the degradation constants at different temperatures.

4.4 RESULTS

4.4.1 Preformulation Studies

Thermogravimetric analysis results were used to study the thermal behavior of GLZ and its physical blends with polymers. As shown in Figure 4.1A, GLZ was stable up to approximately 165 °C, which corresponds with the onset of GLZ melting measured by DSC as shown in Figure 4.2A. The weight loss of GLZ in both air and nitrogen conditions

was less than 10% between 165 ℃ and 240 ℃; however, when measured by HPLC, about 10% of GLZ degradation was observed after holding at 170 ℃ for 4 min under air purging. For physical mixtures of GLZ and polymers, an initial 1% weight loss (water) was observed up to 100 ℃, as shown in Figure 4.1B. The onset temperature of GLZ degradation was depressed to about 140 ℃, which is also reflected in the depressed onset of GLZ melting measured by DSC (Figure 4.2B). The DSC result of the physical mixture of GLZ and polymer also confirmed the water loss by showing an apparent endothermic peak below 100 ℃.

Solid-state characterization of GLZ by XRD and MDSC were shown in Supplemental Figure S4.1. Besides the melting point shown in Figure 4.2A, a clear glass transition temperature at 39.95 ℃ was observed in the second heating cycle of the pure GLZ sample. In the XRD test, crystalline GLZ also showed characteristic diffraction peaks at 2θ = 10.42°, 14.90°, 17.00°, 18.12°, 20.72°, 21.96°, 25.22°, and 26.18°. Furthermore, 1% crystalline GLZ was spiked into polymers, and the blend was mixed homogeneously before testing. Both XRD and MDSC exhibited the crystalline GLZ (data not shown), which indicates the capability of detecting small amounts of crystalline GLZ using both DSC and XRD methods.

The origin of GLZ degradation and the resulting degradants were identified using LC–MS. Several samples were analyzed, including unheated and heated GLZ, extruded polymers without GLZ, and extruded polymers containing 10% GLZ. The unheated GLZ

sample was first subjected to reversed-phase LC–MS and subsequent ion activation through tandem mass spectrometry (MS/MS) to characterize GLZ and potential degradants. Both reversed-phase liquid chromatography and the positive ion mode total ion chromatogram (TIC) of the unheated GLZ drug generated elution of GLZ at approximately 18.5 min (see Supplemental Figure S4.2). Positive mode MS analysis of the 18.5 min peak generated an ion signal at m/z 324.1378, which was consistent with the singly protonated form of GLZ (i.e., [C15H21N3O3S + H]+). No major degradants were identified in the LC–MS analysis of the unheated GLZ. Next, the extruded 10% GLZ and polymer blends were subjected to LC–MS analysis to determine any major degradants as a result of direct exposure to elevated temperatures. Upon LC–MS analysis of the extrudates, the LC/UV chromatogram generated a dominant peak at 13.3 min, while the signal from GLZ at 18.5 min was absent in the chromatogram regardless of polymer chemistry (Figure 4.3ABC). MS analysis of the 13.3 min peak generated ion responses at m/z 172.0427 and 189.0695, which is consistent with singly protonated and ammoniated cations of the empirical formula C7H9NO2S. The empirical formula, C7H9NO2S, is consistent with the sulfonamide structure in Figure 4.3A. Further MS analysis of the positive mode TIC identified other non-UV active GLZ degradants. For instance, the MS peak at 14.8 min with ion responses at m/z 279.2183 and 301.1995 (Figure 4.3DEF) is consistent with the singly protonated and sodiated cations with the empirical formula C15H27N4O. Structures for the additional degradants are illustrated in Figure 4.3D. Samples of GLZ heated at 200 °C for 4 min were also subjected to LC–MS analysis (data

not shown), and showed similar results as the extrudates of 10% GLZ in AFFINISOL™ HPMC HME 100LV, Soluplus, and PVP VA64.

4.4.2 Processing and Characterization

Five HME Runs, each comprising multiple batches at different conditions, were performed to improve the drug potency in the extruder, and the screw designs and machine setups are shown in Figure 4.4. Processing conditions, processing measurements, potency tests are summarized in Table 4.1.

4.4.2.1 Run 1

As shown in Figure 4.4, four sets of kneading elements were used to ensure sufficient mixing. During the run at 130 °C, processing torque was 1,700–2,100 Gm, which was close to the limit of the machine. Also, die pressure was about 600 psi. Therefore, lower temperatures were not used in Run 1 in order to prevent machine over-torque failure. Total residence time (from port A to D) was about 12.6 min, and melt residence time (from port C to D) was 9.0 min, which indicated that the accumulation of material occurred toward the end of the extruder. The melt temperature of the material inside the extruder, measured at the die, was about 20 °C higher than the set processing temperature of the barrels. The drug potency in the extruded material measured by HPLC was 0%.

4.4.2.2 Run 2

A less aggressive screw design, with one set of 30° forward-kneading elements located at the end of Zone 1, was used in Run 2. With the less aggressive screw design, processing torque decreased significantly to 1,000–1,500 Gm, based on the temperature used. The die pressures, however, were still high and, as expected, die pressure increased with the decrease of processing temperature. Both total residence time and melt residence time were shortened to about 10 min and 7.0 min, respectively. Melt temperature was about 15 ℃ higher than the set processing temperature of the barrels. Unfortunately, with the milder screw design, the drug potency in the extruded material was still extremely low: only the batch 5 sample, processed at 100 ℃, showed 0.2% drug recovery.

4.4.2.3 Run 3

The screw design used in Run 2 was also used in Run 3; however, the die and die connector at the end of the extruder were removed (Figure 4.4). Without the block from the die and the die connector, the processing torque further decreased to 700–1,000 Gm, based on the temperature used. Moreover, total residence time and melt residence time were shortened to about 5 min and 2.5 min, respectively. The melt temperature of the extrudates measured by a calibrated IR thermometer, as shown in Table 4.1, was about the same as the set processing temperature of the barrels. To determine the status of the materials inside the extruder, samples were also taken from ports B, C, and D. XRD, DSC, and potency tests were performed to analyze the samples. GLZ remained in crystalline state at port B. However, for samples taken at port C, which was located after the kneading

element at the end of Zone 1, both DSC and XRD analysis revealed no crystalline signal. Drug recovery values of samples taken at port C were about 92.4–97.3%, and, for samples at port D, the values were about 5.7–25.8%.

4.4.2.4 Run 4

The screw design used in Run 4 is shown in Figure 4.4. Instead of being set at zone 1, the kneading element was placed all the way towards the end of the barrel. The observed processing torque was comparable to Run 3 (700–850 Gm). As for the residence time, since the conversion of GLZ to its amorphous form occurred at the end of the extruder, only total residence time (about 3.0 min) was recorded. The melt temperature measured for the extrudates was about the same as the set processing temperature of the barrels (similar to Run 3). After the redesigning of the screw, ASDs with significantly higher drug recovery rates of 42.6% and 89.4% were achieved at 130 ℃ and 120 ℃, respectively. Processing at 110 ℃ was not successful, as the extrudate emerged in powder form.

4.4.2.5 Run 5

To further optimize the specific mechanical energy input, nine more batches were processed with a varying feed rate (2.3–4.3 g/min) and screw speed (100–300 rpm), as shown Table 4.2, using the same screw design and setup used in Run 4. The drug recovery rates in the extrudates and the calculated specific energy inputs are also shown in Table 4.2. It is clear that the drug recovery rate decreased with the increase in the specific energy input (Figure 4.5). Moreover, when the specific energy inputs were below 1 kW·hr/kg (i.e.,

batches 13, 14, and 21), it was insufficient to fully convert crystalline GLZ to its amorphous form. Therefore, batch 20, with 95.37% drug recovery, was the highest potency amorphous formulation achieved in this study.

4.4.2.6 Energy of Activation Study

Studies using energy of activation were performed to explain the observations in Run 3. Samples of crystalline, ASD, and 1 mg/mL DMSO solution of GLZ were analyzed at several temperatures ranging from 30–120 °C. The degradation constants generated at different temperatures were used to plot the Arrhenius plots shown in Figure 4.6. The activation energies calculated from the linear regression of the plots for the hydrolysis reaction were shown in Table 4.3. Activation energy of crystalline GLZ was determined to be 68.53 kCal/mol, while the values calculated for GLZ ASD and DMSO solution were 27.31 and 29.74 kCal/mol, respectively. Moreover, the extrapolated degradation constants and the corresponding half-lives at the extrusion processing temperatures were also summarized in Table 4.3.

4.5 DISCUSSIONS

Since all batches in this study were processed below the melting point of GLZ (166 °C), the formation of ASDs relied on the solubilization of the drug in the polymer instead of the melting of the drug during extrusion (27). Therefore, the miscibility between GLZ and the selected polymer is crucial. The reader is reffered to the polymer screening method described in our previous paper (9). Briefly, as shown in Supplemental Figure S4.3, better

miscibility between AFFINISOL™ HPMC HME 100LV and GLZ was confirmed as compared to Soluplus and PVP VA64. Also, given that all observations regarding GLZ degradation were similarly observed for extrudates with these polymers, further optimization was done only with AFFINISOL™ HPMC HME 100LV. Successful processing using HME also requires excellent stability at elevated temperatures of the selected drug and polymer combinations. In this work, TGA and DSC data showed the challenges of processing GLZ using HME due to the limited processing window. The thermal degradation onset of GLZ sets the upper limit of the processing window. For pure GLZ, the degradation onset occurs at 165 ℃; however, when blended with AFFINISOL™ HPMC HME 100LV, the good miscibility between the two components as predicted by our model facilitates the solubilization of GLZ in the molten polymer, which depressed the melting point as well as the degradation onset of GLZ to 140 ℃. A recent publication has reported that due to the extruder torque limitation, AFFINISOL™ HPMC HME 100LV is difficult to process by itself at or below 130 ℃ (31). Although the incorporation of small molecule drugs can result in a plasticizing effect to lower the processing torque (32), the optimization window that remains is still very narrow in this study.

The screw used in Run 1, which contains two sets of neutral kneading elements (90°) together with two sets of forward kneading elements (30°), has been reported to be able to provide enough mixing power to improve the dissolution behavior of an amorphous solid dispersion formulation (33). Surprisingly, no drug was recovered in the extrudate processed at 130 ℃, at which temperature GLZ should still be stable, according to the

preformulation studies. Two possible causes for this drug degradation problem are provided: (a) The extremely high torque and melt temperature observed in Run 1 indicates the potential of excess shear provided by the kneading elements (34), and (b) the neutral kneading elements used in Run 1 strongly held back the molten material, resulting in the long residence time (12.6 min) (35). Therefore, a milder screw design was used in Run 2. The decreased processing torque allowed for the application of lower barrel temperatures when extruding. The lowest processing temperature (100 ℃) helped achieve the 0.2% drug recovery rate for Batch 5. Similar to Run 1, both the die pressure and the melt temperature were still high. Given that polymers usually exhibit non-Newtonian shear-thinning viscoelastic properties (36), the high die pressure in this case can be attributed to the significant complex viscosity increase of the melt containing AFFINISOL™ HPMC HME 100LV when it reaches the low-shear die area (31). Todd et al. established an equation that describes the relationship between polymer temperature rise and pressure generation, as shown in Equation 1 (37):

$$\Delta T = \Delta P / \rho C_p E, \quad (1)$$

where ΔT is the temperature rise, ΔP is the pressure rise, ρ is the melt density, C_p is the heat capacity of the melt, and E is the pump efficiency. Under adiabatic conditions, with the assumptions of $\rho = 1.0$, $C_p = 0.5$, and $E = 10\%$:

$$\Delta T\,(K) = \Delta P\,(psi) / 29 \tag{2}$$

Based on Equation 2 and the pressure recorded in Table 4.1, the temperature rise of the material should be around 17 ℃ in the die area, which is in agreement with the discrepancy between the measured melt temperatures and the set processing temperatures (about 15 ℃). Moreover, the high back pressure generated at the die area can also elongate the material residence time (37), thus causing more degradation. When the die and the die connector were removed in Run 3, the melt temperatures measured for all batches were close to the processing temperatures, and this supports the calculated results based on Equation (2).

For hydrolysis reactions in solid state, moisture content has been shown to facilitate the reaction (38). Therefore, the impact of pre-drying the material on drug recovery was also investigated. There was about 1.10% moisture in the 10% GLZ and AFFINISOL™ HPMC HME 100LV physical blend, and the water content was found to be below 0.10% w/w by loss on drying test (105 ℃ for 5 min) after vacuum drying at room temperature for 24 hours. As shown in Table 4.4, after drying the GLZ and AFFINISOL™ HPMC HME 100LV physical blend, the torque of the extrusion process increased, causing a 50–70% specific mechanical energy input increase, according to Equation (4). Moreover, due to the extra mechanical energy input, drug recovery further decreased compared to the drug recovery rate of processing the non-dried blend (Run 3). In this case, the plasticizing effect of water (39) overcame the impact of the water as a reactant. It is believed that this occurs

because the hydrolysis reaction can still continue with the nucleophilic intermediate (as shown in Scheme 4.1) generated after the initiation reaction with water.

Examining Run 3 more closely, it is interesting to note that there was no drug degradation between ports A and B, and even between port A and port C, less than 10% drug degradation was detected. Moreover, the residence time between port A and port C accounted for the first half of the total residence time. However, in the following half of the total residence time, between ports C and D, 70–85% of the drug degraded. Thus degradation kinetics studies were conducted to rationalize this observation. For crystalline GLZ in the solid state, hydrolysis degradation was not observed until the temperature was elevated to 80 ℃, because the energy and mobility of the molecules were so limited at lower temperatures that the reaction rates were too low to measure. On the other hand, the GLZ molecules in DMSO solution and ASD contained sufficient energy and mobility to overcome the reaction energy barrier. Therefore, as shown in Table 4.3, the activation energy of GLZ in amorphous and solution forms were significantly lower (27.31 and 29.74 kCal/mol, respectively) than that of crystalline form (65.40 kCal/mol). Similar values of activation energy in the amide hydrolysis reaction have been reported in the literature (40, 41). This result indicates that GLZ in amorphous and solution forms possesses much higher energy and molecular mobility, which is responsible for the faster degradation rate of GLZ after converting to the amorphous form in the second half of the extruder (42). Furthermore, as shown in Table 4.3, the hydrolysis reaction half-life of ASD at the processing temperatures in Run 3 was in the order of minutes, suggesting an extremely fast

degradation. It is important to point out that for the activation study, we only used the first 15 to 25% of degradation data, where the reaction takes place in one-phase state (amorphous or crystalline) and is not affected by any phase transitions. Moreover, we have (a) expressed the hydrolysis reaction in terms of the first-order rate constant in all cases based on the data fit, same as the method previously reported (22), (b) and assumed the hydrolysis reaction of Scheme 4.1B is the main degradation pathway.

An emerging fusion-based manufacturing technique called KinetiSol® Dispersing has been used successfully to prepare ASDs. KinetiSol® Dispersing utilizes a combination of frictional and shear energies to rapidly produce ASDs (43). By rapidly applying high mixing energy in a short time (less than 30 seconds), materials only briefly achieve elevated temperatures. Because of this, ASDs that contain thermally labile drugs have been successfully processed using KinetiSol® Dispersing (27, 44). The strategy we used in Run 4 to address the GLZ degradation was based in part on KinetiSol® Dispersing. As demonstrated in Run 3, the kneading element played an important role in the amorphous conversion process. And after being moved to the end of the extruder in Run 4, the residence time of the amorphous form of GLZ is notably shortened, resulting in a significant improvement in drug recovery of 89.4% (Batch 11). A similar concept has also been used to avoid water loss and decomposition of nicotine bitartrate by side-feeding the drug downstream (45).

To further improve drug recovery, the specific mechanical energy input was optimized. The specific mechanical energy refers to the amount of power that is contributed by the extruder motor per kilogram of material being processed. A two-step equation has been established for the calculation of specific mechanical energy, as shown below (8, 46):

Applied Power

$$KW(applied) = KW(motor\ rating) \times \%Torque \times \frac{rpm\ running}{rpm\ \max} \times 0.97(gearbox\ efficiency) \quad (3)$$

Specific Mechanical Energy

$$Specific\ Energy(applied) = \frac{KW(applied)}{Feed\ Rate} \quad (4)$$

As mentioned before, we extruded GLZ well below its melting point (166 ℃), at which point the solubilization regime is responsible for the achievement of a single-phase amorphous system (47). Compared to the miscibility regime, a higher amount of shear will be required per unit of mass to adjust the kinetic aspects of the melt materials to maximize the mass transfer rates in the solubilization regime (48). The shear input is especially important for screw design used in Run 4, due to the extremely short solubilization time. However, as shown previously in this paper, excess amounts of shear energy input would cause degradation (Run 1). Therefore, it is critical to provide the proper amount of specific mechanical energy to completely solubilize the drug while avoiding excess mechanical energy that triggers GLZ degradation. In Run 5, different feed rates and screw rpm settings

were applied, resulting in specific mechanical energy inputs that ranged from 0.209–1.397 kW·hr/kg, which is in agreement with previous reported values (49, 50). Moreover, crystalline GLZ was detected in batches with specific mechanical energy less than 1 kW·hr/kg, which is extremely high in comparison to the specific mechanical energy input using sugar alcohol (range from 0.003–0.128 kW·hr/kg) in pharmaceutical melt extrusion (51) and starch (range from 0.107–0.320 kW·hr/kg) for cooking extrusion (52). We believe that the high specific mechanical energy input required for the complete conversion of GLZ from crystalline to amorphous form for the following reasons: (a) The specific mechanical energy input increases with the difference in $\Delta T_{MP\text{-}process}$, which means that the further the processing temperature deviates from the API melting point, the more mechanical energy input is required to produce homogeneous ASD (and in this case, $\Delta T_{MP\text{-}process}$ is more than 36 ℃). And, (b) the conversion occurred at the end of the extruder, which did not leave much time for the kinetics of the solubilization process to complete; therefore, more energy is required at the kneading elements to facilitate the mixing. Batch 20 was chosen, since the single phase ASD was achieved with the minimal specific mechanical energy input, resulting in a 95.37% drug recovery. The optimization method used in Run 5 can result in a potential homogeneity problem (53), since the minimized mechanical energy input required was determined by XRD and DSC results. Although the amorphous form of Batch 20 extrudate was confirmed by the lack of a characteristic peak in XRD and the single T_g detected in DSC, the in vivo performance of the ASD may still be affected due to the limitation of the characterization techniques on ASDs (54).

The LC–MS analysis of thermal forced-degradation studied samples revealed two major degradants with molecular weight of 171 (a major peak in UV) and 278 (a major peak in TIC). As a typical sulfonylurea hydrolysis (55), water or the intermediate nucleophilic agents can attack the carbonyl carbon, hydrolyze GLZ to a sulfonamide and an amine with liberation of CO upon cleavage of the amide linkage as shown in Scheme 4.1. Forced-degradation of GLZ at different conditions were studied previously (56, 57) and confirmed the similar hydrolysis reactions on sulfonylureas (55). Interestingly, the intact GLZ and the sulfonamide degradant (Deg. A) exhibited identical responses when comparing the UV absorption at 227 nm (Figure 4.7). Moreover, both hydrolysis pathways proposed in Scheme 4.1 lead to Deg. A, which means that GLZ molecules will end up with the same amount of Deg. A molecules after hydrolysis. Therefore, when analyzing the 100% degraded sample (Run 1) using a previously reported UV method (measuring drug concentration using UV absorption at 227 nm) (58), a false 100% drug recovery was detected. This observation necessitates the use of liquid chromatography with absorption measurements. Without liquid separation, distinguishing intact drug and degradation products via UV/VIS spectrophotometry cannot be achieved.

4.6 CONCLUSIONS

The application of HME in manufacturing ASDs that contain thermally labile drugs has been limited due to the degradation caused by elevated temperatures, instability nature of amorphous form of drugs, and excess mechanical energy inputs applied during the HME process. In this study, GLZ was used as a model thermally labile drug. After adapting the proper machine setup to reduce the processing pressure, applying the optimal screw design to minimize melt residence time, and selecting the optimized specific mechanical energy input to fulfill the amorphous conversion without providing excess shear force, GLZ ASD with an improved drug recovery rate was successfully manufactured using HME. This study demonstrates that, with proper process optimizations, HME can be used to produce ASDs with a wider range of drugs and polymers.

Acknowledgements

The authors would like to acknowledge The Dow Chemical Company for financial support. The authors would also like to thank Dr. Jordan Dinser and Dr. Ian Riddington for their assistance with the LC/MS experiments.

4.7 REFERENCES

1. Breitenbach J. Melt extrusion: from process to drug delivery technology. European Journal of Pharmaceutics and Biopharmaceutics. 2002;54(2):107-17. doi: http://dx.doi.org/10.1016/S0939-6411(02)00061-9.

2. Maniruzzaman M, Boateng JS, Bonnefille M, Aranyos A, Mitchell JC, Douroumis D. Taste masking of paracetamol by hot-melt extrusion: An in vitro and in vivo evaluation. European Journal of Pharmaceutics and Biopharmaceutics. 2012;80(2):433-42. doi: http://dx.doi.org/10.1016/j.ejpb.2011.10.019.

3. Follonier N, Doelker E, Cole ET. Various ways of modulating the release of diltiazem hydrochloride from hot-melt extruded sustained release pellets prepared using polymeric materials. Journal of Controlled Release. 1995;36(3):243-50. doi: http://dx.doi.org/10.1016/0168-3659(95)00041-6.

4. Maincent JP, Najvar LK, Kirkpatrick WR, Huang S, Patterson TF, Wiederhold NP, et al. Modified release itraconazole amorphous solid dispersion to treat Aspergillus fumigatus: importance of the animal model selection. Drug Development and Industrial Pharmacy. 2016:1-11. doi: 10.1080/03639045.2016.1236811.

5. Brough C, Williams RO. Amorphous solid dispersions and nano-crystal technologies for poorly water-soluble drug delivery. International Journal of

Pharmaceutics. 2013;453(1):157-66. doi: http://dx.doi.org/10.1016/j.ijpharm.2013.05.061.

6. Baronsky-Probst J, Möltgen CV, Kessler W, Kessler RW. Process design and control of a twin screw hot melt extrusion for continuous pharmaceutical tamper-resistant tablet production. European Journal of Pharmaceutical Sciences. 2016;87:14-21. doi: http://dx.doi.org/10.1016/j.ejps.2015.09.010.

7. Gogos CG, Liu H, Wang P. Laminar Dispersive and Distributive Mixing with Dissolution and Applications to Hot-Melt Extrusion. Hot-Melt Extrusion: Pharmaceutical Applications: John Wiley & Sons, Ltd; 2012. p. 261-84.

8. Martin C. Continous Mixing of Solid Dosage Forms via Hot-Melt Extrusion. Pharmaceutical Technology. 2008;32(10):76-86.

9. Huang S, O'Donnell KP, Keen JM, Rickard MA, McGinity JW, Williams RO. A New Extrudable Form of Hypromellose: AFFINISOL™ HPMC HME. AAPS PharmSciTech. 2016;17(1):106-19. doi: 10.1208/s12249-015-0395-9.

10. Hengsawas Surasarang S, Keen JM, Huang S, Zhang F, McGinity JW, Williams RO. Hot melt extrusion versus spray drying: hot melt extrusion degrades

albendazole. Drug Development and Industrial Pharmacy. 2016:1-15. doi: 10.1080/03639045.2016.1220577.

11. Crowley MM, Zhang F, Repka MA, Thumma S, Upadhye SB, Kumar Battu S, et al. Pharmaceutical Applications of Hot-Melt Extrusion: Part I. Drug Development and Industrial Pharmacy. 2007;33(9):909-26. doi: 10.1080/03639040701498759.

12. Hughey JR, DiNunzio JC, Bennett RC, Brough C, Miller DA, Ma H, et al. Dissolution Enhancement of a Drug Exhibiting Thermal and Acidic Decomposition Characteristics by Fusion Processing: A Comparative Study of Hot Melt Extrusion and KinetiSol® Dispersing. AAPS PharmSciTech. 2010;11(2):760-74. doi: 10.1208/s12249-010-9431-y.

13. Blessy M, Patel RD, Prajapati PN, Agrawal YK. Development of forced degradation and stability indicating studies of drugs—A review. Journal of Pharmaceutical Analysis. 2014;4(3):159-65. doi: http://dx.doi.org/10.1016/j.jpha.2013.09.003.

14. Repka MA, Gerding TG, Repka SL, McGinity JW. Influence of Plasticizers and Drugs on the Physical-Mechanical Properties of Hydroxypropylcellulose Films Prepared by Hot Melt Extrusion. Drug Development and Industrial Pharmacy. 1999;25(5):625-33. doi: 10.1081/DDC-100102218.

15. Verreck G, Decorte A, Heymans K, Adriaensen J, Liu D, Tomasko D, et al. Hot stage extrusion of p-amino salicylic acid with EC using CO2 as a temporary plasticizer. International Journal of Pharmaceutics. 2006;327(1–2):45-50. doi: http://dx.doi.org/10.1016/j.ijpharm.2006.07.024.

16. Hovorka SW, Schöneich C. Oxidative degradation of pharmaceuticals: Theory, mechanisms and inhibition. Journal of Pharmaceutical Sciences. 2001;90(3):253-69. doi: 10.1002/1520-6017(200103)90:3<253::AID-JPS1>3.0.CO;2-W.

17. Alsante KM, Huynh-Ba K, Baertschi SW, Reed RA, Landis MS, Kleinman MH, et al. Recent Trends in Product Development and Regulatory Issues on Impurities in Active Pharmaceutical Ingredient (API) and Drug Products. Part 1: Predicting Degradation Related Impurities and Impurity Considerations for Pharmaceutical Dosage Forms. AAPS PharmSciTech. 2014;15(1):198-212. doi: 10.1208/s12249-013-0047-x.

18. Lang B, McGinity JW, Williams RO. Hot-melt extrusion – basic principles and pharmaceutical applications. Drug Development and Industrial Pharmacy. 2014;40(9):1133-55. doi: 10.3109/03639045.2013.838577.

19. Höckerfelt MH, Alderborn G. The crystallinity of cellulose controls the physical distribution of sorbed water and the capacity to present water for chemical

degradation of a solid drug. International Journal of Pharmaceutics. 2014;477(1–2):326-33. doi: http://dx.doi.org/10.1016/j.ijpharm.2014.10.034.

20. Mitchell SM, Ullman JL, Teel AL, Watts RJ. pH and temperature effects on the hydrolysis of three β-lactam antibiotics: Ampicillin, cefalotin and cefoxitin. Science of The Total Environment. 2014;466:547-55. doi: http://dx.doi.org/10.1016/j.scitotenv.2013.06.027.

21. Zaman F, Beezer AE, Mitchell JC, Clarkson Q, Elliot J, Davis AF, et al. The stability of benzoyl peroxide by isothermal microcalorimetry. International Journal of Pharmaceutics. 2001;227(1–2):133-7. doi: http://dx.doi.org/10.1016/S0378-5173(01)00791-8.

22. Guo Y, Byrn SR, Zografi G. Physical characteristics and chemical degradation of amorphous quinapril hydrochloride. Journal of Pharmaceutical Sciences. 2000;89(1):128-43. doi: 10.1002/(SICI)1520-6017(200001)89:1<128::AID-JPS13>3.0.CO;2-Z.

23. Oguchi T, Yonemochi E, Yamamoto K, Nakai Y. Freeze-Drying of Drug-Additive Binary Systems. II. : Relationship between Decarboxylation Behavior and Molecular States of p-Aminosalicylic Acid. Chemical & Pharmaceutical Bulletin. 1989;37(11):3088-91. doi: 10.1248/cpb.37.3088.

24. Boersen N, Brown C, DiNunzio J, Johnson D, Marsac P, Meyer R, et al. Hot-Melt Extrusion: The Process-Product-Performance Interplay. In: Templeton AC, Byrn SR, Haskell RJ, Prisinzano TE, editors. Discovering and Developing Molecules with Optimal Drug-Like Properties. New York, NY: Springer New York; 2015. p. 345-81.

25. Kohlgrüber K. Co-rotating twin-screw extruder: Carl Hanser Verlag GmbH Co KG; 2012.

26. Verreck G. The Influence of Plasticizers in Hot-Melt Extrusion. Hot-Melt Extrusion: Pharmaceutical Applications: John Wiley & Sons, Ltd; 2012. p. 93-112.

27. DiNunzio JC, Brough C, Hughey JR, Miller DA, Williams RO, McGinity JW. Fusion production of solid dispersions containing a heat-sensitive active ingredient by hot melt extrusion and Kinetisol® dispersing. European Journal of Pharmaceutics and Biopharmaceutics. 2010;74(2):340-51. doi: http://dx.doi.org/10.1016/j.ejpb.2009.09.007.

28. Thiry J, Krier F, Evrard B. A review of pharmaceutical extrusion: Critical process parameters and scaling-up. International Journal of Pharmaceutics. 2015;479(1):227-40. doi: http://dx.doi.org/10.1016/j.ijpharm.2014.12.036.

29. Ghosh I, Vippagunta R, Li S, Vippagunta S. Key considerations for optimization of formulation and melt-extrusion process parameters for developing thermosensitive compound. Pharmaceutical Development and Technology. 2012;17(4):502-10. doi: 10.3109/10837450.2010.550624.

30. More SD, Sontakke SB. Solubility Enhancement Of Gliclazide By Solid Dispersion Method. Asian Journal Of Pharmaceutical And Clinical Research. 2013;6(5):91-8.

31. Gupta SS, Solanki N, Serajuddin ATM. Investigation of Thermal and Viscoelastic Properties of Polymers Relevant to Hot Melt Extrusion, IV: Affinisol™ HPMC HME Polymers. AAPS PharmSciTech. 2016;17(1):148-57. doi: 10.1208/s12249-015-0426-6.

32. Li Y, Pang H, Guo Z, Lin L, Dong Y, Li G, et al. Interactions between drugs and polymers influencing hot melt extrusion. Journal of Pharmacy and Pharmacology. 2014;66(2):148-66. doi: 10.1111/jphp.12183.

33. Lang B, McGinity JW, Williams RO. Dissolution Enhancement of Itraconazole by Hot-Melt Extrusion Alone and the Combination of Hot-Melt Extrusion and Rapid Freezing—Effect of Formulation and Processing Variables. Molecular Pharmaceutics. 2014;11(1):186-96. doi: 10.1021/mp4003706.

34. Todd DB. Practical Aspects of Processing in Intermeshing Twin Screw Extruders. Journal of Reinforced Plastics and Composites. 1998;17(18):1607-16. doi: 10.1177/073168449801701802.

35. Seem TC, Rowson NA, Ingram A, Huang Z, Yu S, de Matas M, et al. Twin screw granulation — A literature review. Powder Technology. 2015;276:89-102. doi: http://dx.doi.org/10.1016/j.powtec.2015.01.075.

36. Viridén A, Wittgren B, Larsson A. Investigation of critical polymer properties for polymer release and swelling of HPMC matrix tablets. European Journal of Pharmaceutical Sciences. 2009;36(2–3):297-309. doi: http://dx.doi.org/10.1016/j.ejps.2008.10.021.

37. Todd DB. Plastics compounding: equipment and processing: Hanser Publishers; 1998.

38. Sumie Yoshioka VJS. Chemical Stability of Drug Substances. Stability of Drugs and Dosage Forms. Boston, MA: Springer US; 2002. p. 3-137.

39. Stubberud L, Arwidsson HG, Hjortsberg V, Graffner C. Water-Solid Interactions. III. Effect of Glass Transition Temperature, Tg, and Processing on Tensile Strength of Compacts of Lactose and Lactose/Polyvinyl Pyrrolidone. Pharmaceutical

Development and Technology. 1996;1(2):195-204. doi: 10.3109/10837459609029894.

40. Meloche I, Laidler KJ. Substituent Effects in the Acid and Base Hydrolyses of Aromatic Amides1. Journal of the American Chemical Society. 1951;73(4):1712-4. doi: 10.1021/ja01148a084.

41. Leung SS, Grant DJW. Solid state stability studies of model dipeptides: Aspartame and aspartylphenylalanine. Journal of Pharmaceutical Sciences. 1997;86(1):64-71. doi: 10.1021/js960228d.

42. Yoshioka S, Aso Y. Correlations between molecular mobility and chemical stability during storage of amorphous pharmaceuticals. Journal of Pharmaceutical Sciences. 2007;96(5):960-81. doi: 10.1002/jps.20926.

43. DiNunzio JC, Brough C, Miller DA, Williams RO, McGinity JW. Fusion processing of itraconazole solid dispersions by kinetisol® dispersing: A comparative study to hot melt extrusion. Journal of Pharmaceutical Sciences. 2010;99(3):1239-53. doi: 10.1002/jps.21893.

44. LaFountaine JS, Jermain SV, Prasad LK, Brough C, Miller DA, Lubda D, et al. Enabling thermal processing of ritonavir–polyvinyl alcohol amorphous solid

dispersions by KinetiSol® Dispersing. European Journal of Pharmaceutics and Biopharmaceutics. 2016;101:72-81. doi: http://dx.doi.org/10.1016/j.ejpb.2016.01.018.

45. Bruce C, Manning M. Melt extruded nicotine thin strips. US Patent 20130011462 A1; 2009.

46. Kipping T, Rein H. A new method for the continuous production of single dosed controlled release matrix systems based on hot-melt extruded starch: Analysis of relevant process parameters and implementation of an in-process control. European Journal of Pharmaceutics and Biopharmaceutics. 2013;84(1):156-71. doi: http://dx.doi.org/10.1016/j.ejpb.2012.12.013.

47. DiNunzio JC, Miller DA. Formulation Development of Amorphous Solid Dispersions Prepared by Melt Extrusion. In: Repka MA, Langley N, DiNunzio J, editors. Melt Extrusion: Materials, Technology and Drug Product Design. New York, NY: Springer New York; 2013. p. 161-203.

48. DiNunzio JC, Zhang F, Martin C, McGinity JW. Melt Extrusion. In: Williams Iii RO, Watts AB, Miller DA, editors. Formulating Poorly Water Soluble Drugs. New York, NY: Springer New York; 2012. p. 311-62.

49. Tackenberg MW, Krauss R, Marmann A, Thommes M, Schuchmann HP, Kleinebudde P. Encapsulation of liquids using a counter rotating twin screw extruder. European Journal of Pharmaceutics and Biopharmaceutics. 2015;89:9-17. doi: http://dx.doi.org/10.1016/j.ejpb.2014.11.017.

50. Tackenberg MW, Thommes M, Schuchmann HP, Kleinebudde P. Solid state of processed carbohydrate matrices from maltodextrin and sucrose. Journal of Food Engineering. 2014;129:30-7. doi: http://dx.doi.org/10.1016/j.jfoodeng.2014.01.003.

51. Reitz E, Vervaet C, Neubert RHH, Thommes M. Solid crystal suspensions containing griseofulvin – Preparation and bioavailability testing. European Journal of Pharmaceutics and Biopharmaceutics. 2013;83(2):193-202. doi: http://dx.doi.org/10.1016/j.ejpb.2012.09.012.

52. Valle GD, Boché Y, Colonna P, Vergnes B. The extrusion behaviour of potato starch. Carbohydrate Polymers. 1995;28(3):255-64. doi: http://dx.doi.org/10.1016/0144-8617(95)00111-5.

53. Schenck L, Troup GM, Lowinger M, Li L, McKelvey C. Achieving a Hot Melt Extrusion Design Space for the Production of Solid Solutions. Chemical

Engineering in the Pharmaceutical Industry: John Wiley & Sons, Inc.; 2010. p. 819-36.

54. Berndl G, Degenhardt M, Mäegerlein M, Dispersyn G. Itraconazole compositions with improved bioavailability. US Patent 8,486,456; 2013.

55. Sarmah AK, Sabadie J. Hydrolysis of Sulfonylurea Herbicides in Soils and Aqueous Solutions: a Review. Journal of Agricultural and Food Chemistry. 2002;50(22):6253-65. doi: 10.1021/jf025575p.

56. Bansal G, Singh M, Jindal KC. Forced Degradation Study on Gliclazide and Application of Validated Stability-Indicating HPLC-UV Method in Stability Testing of Gliclazide Tablets. Chromatographia. 2007;66(9):751-5. doi: 10.1365/s10337-007-0394-4.

57. Bansal G, Singh M, Jindal KC, Singh S. Characterization of Mass Ionizable Degradation Products of Gliclazide by LC/ESI-MS. Journal of Liquid Chromatography & Related Technologies. 2008;31(14):2174-93. doi: 10.1080/10826070802225585.

58. Maggi L, Canobbio A, Bruni G, Musitelli G, Conte U. Improvement of the dissolution behavior of gliclazide, a slightly soluble drug, using solid dispersions.

Journal of Drug Delivery Science and Technology. 2015;26:17-23. doi: http://dx.doi.org/10.1016/j.jddst.2015.01.002.

4.8 LIST OF FIGURES

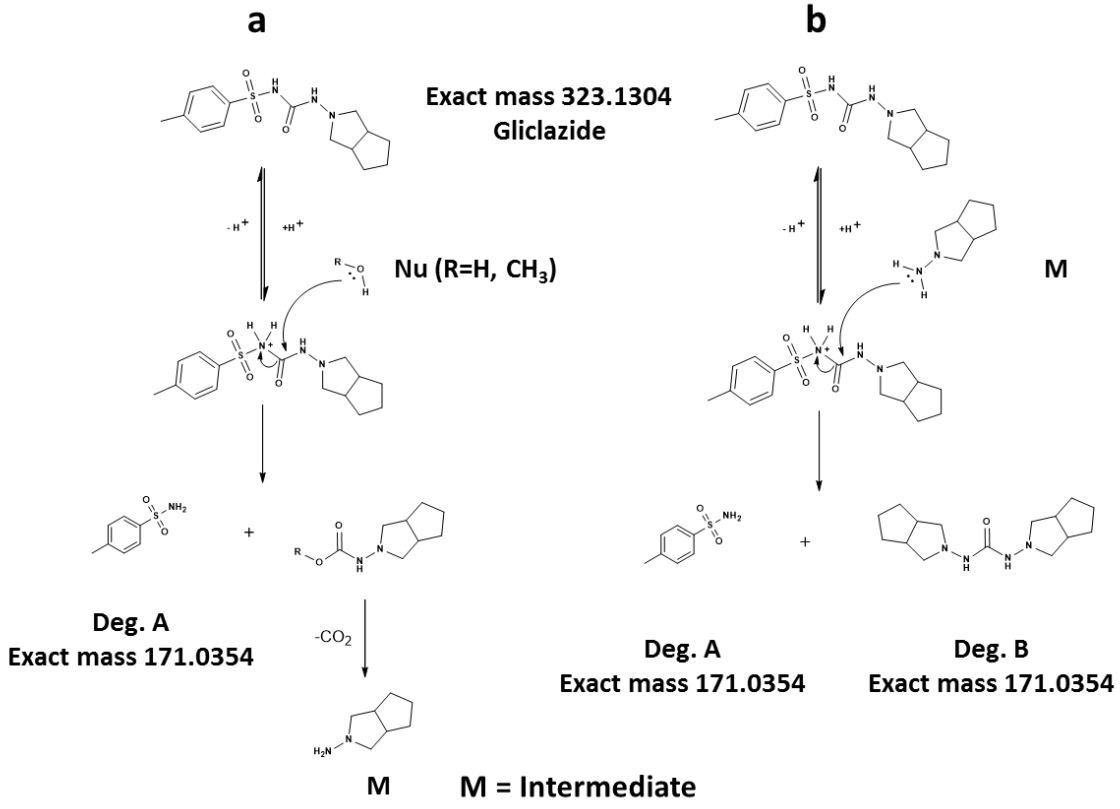

Scheme 4.1 Thermal degradation of GLZ by the hydrolysis of amide group generating two major degradants.

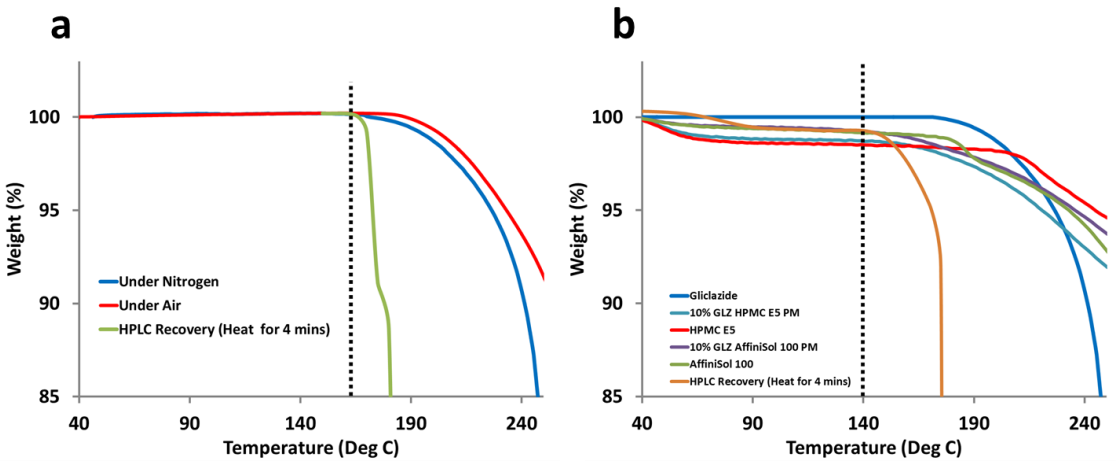

Figure 4.1 Thermogravimetric forced-degradation analysis of: (A) pure GLZ under nitrogen and air purging, and potency result analyzed by HPLC after 4 min heat exposure in air; (B) pure HPMC polymers, a physical mixture of GLZ:METHOCEL™ E5 (1:9), GLZ:AFFINISOL™ HPMC HME 100LV (1:9), and potency result analyzed of GLZ:AFFINISOL™ HPMC HME 100LV physical mixture by HPLC after 4 min heat exposure in air.

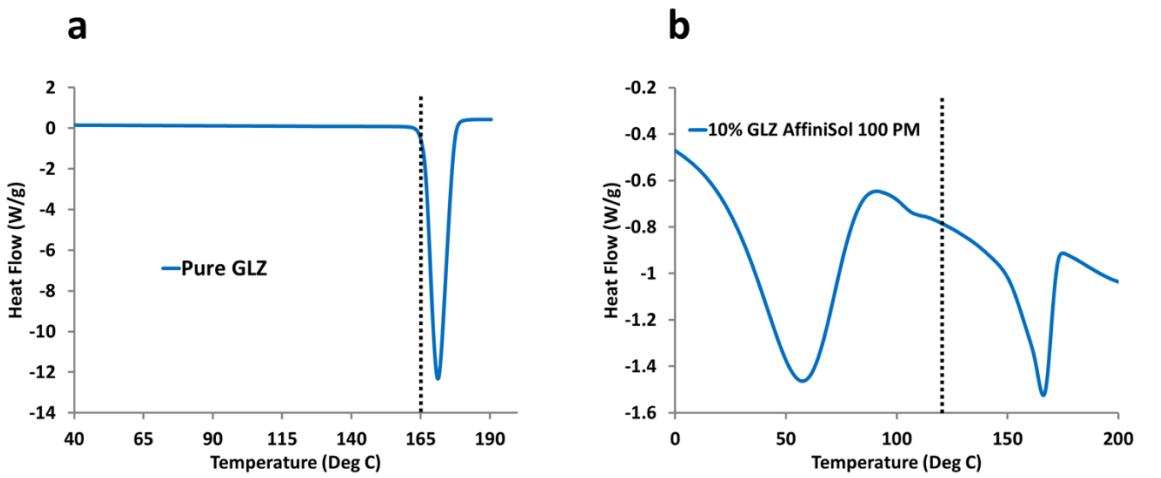

Figure 4.2 DSC analysis of (A) pure GLZ, and (B) physical mixture of 10% GLZ and AFFINISOL™ HPMC HME 100LV GLZ and AFFINISOL™ HPMC HME 100LV (1:9).

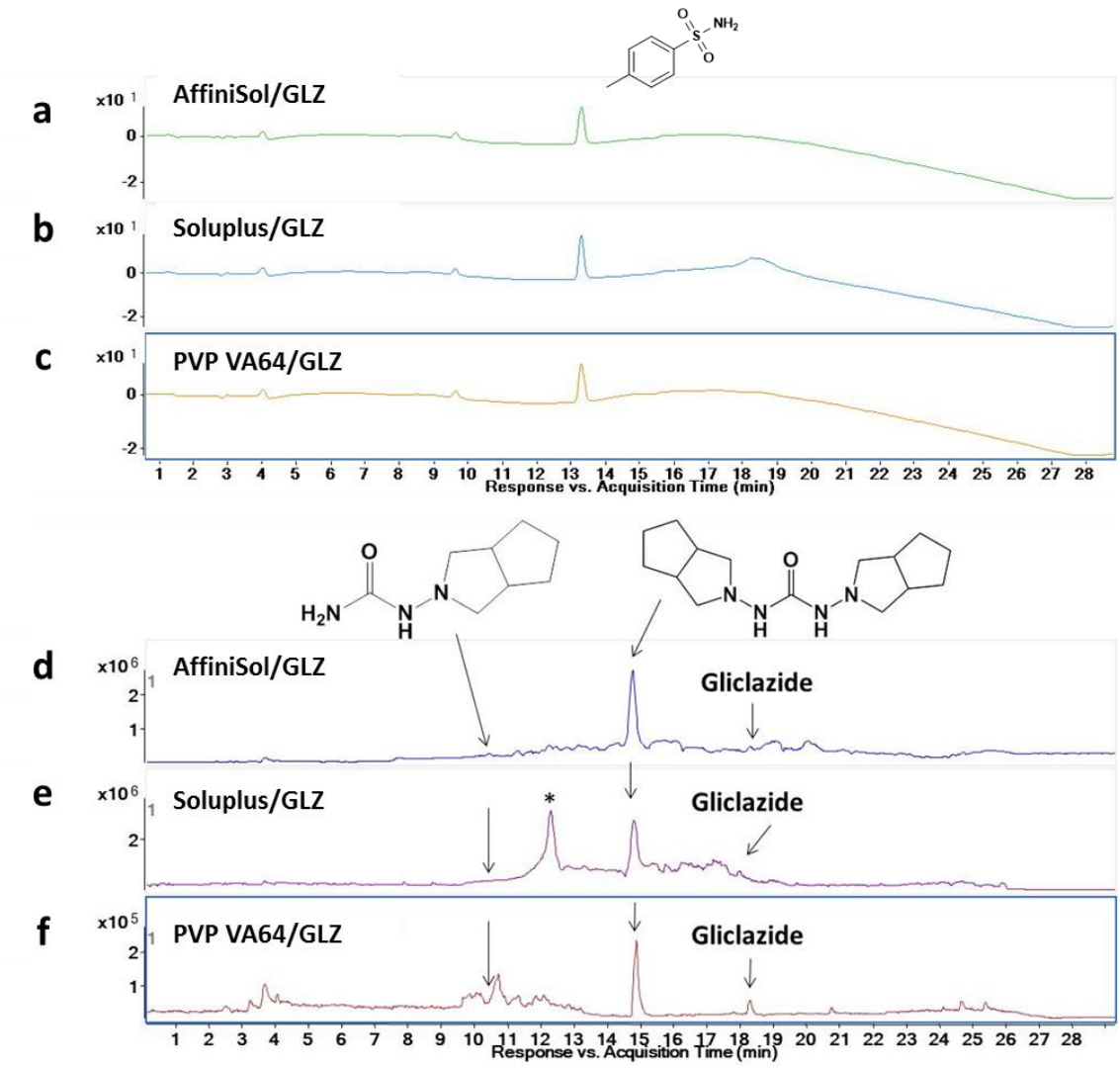

Figure 4.3 LC/UV chromatograms (210–600 nm) from the accurate mass LC–MS/MS analysis of extruded (A) AFFINISOL™ HPMC HME 100LV/GLZ, (B) Solupolus/GLZ, and (C) PVP VA64/GLZ samples. Positive ion mode total ion chromatograms (TIC) from the accurate mass LC–MS/MS analysis of extruded (D) AFFINISOL™ HPMC HME 100LV/GLZ, (E) Solupolus/GLZ, and (F) PVP VA64/GLZ samples. The symbol * represents ion signal from the polymer.

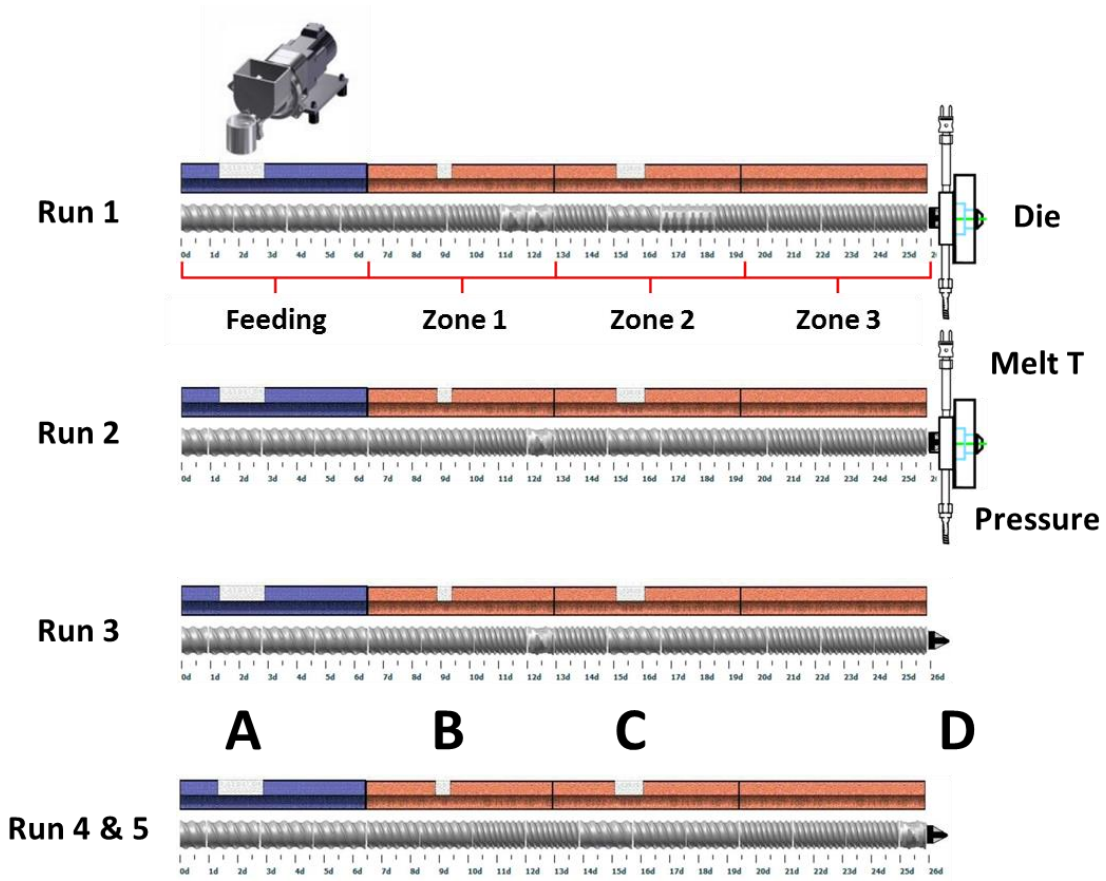

Figure 4.4 The extruder setup and screw design for the five extrusion runs.

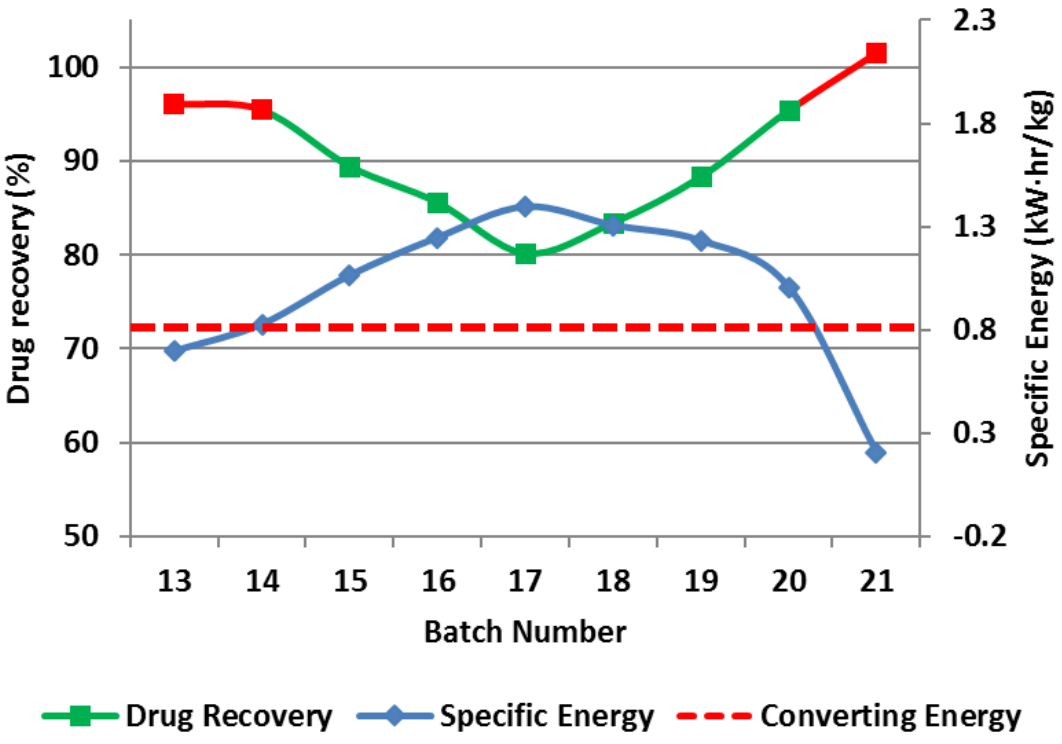

Figure 4.5 GLZ potency in the extrudates and the specific mechanical energy input of the nine batches in Run 5.

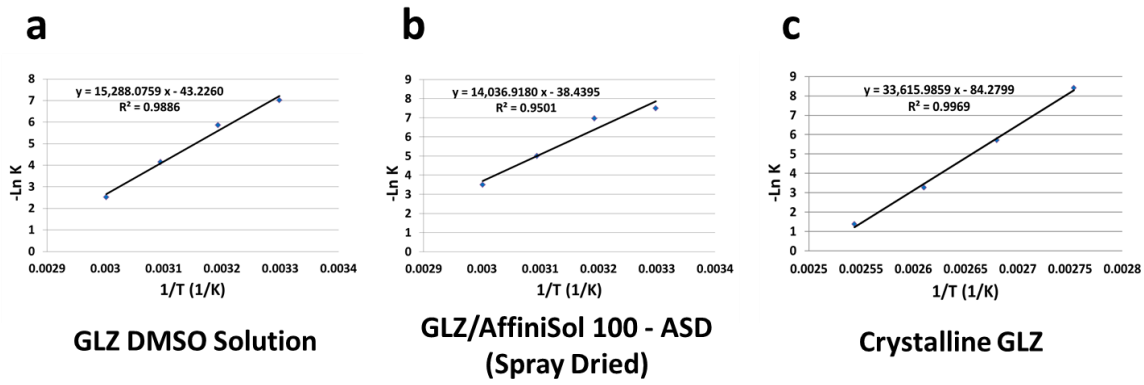

Figure 4.6 Figure Arrhenius plots of the hydrolysis reaction of (a) GLZ DMSO solution, (b) GLZ and AFFINISOL™ HPMC HME 100LV (1:9) spray dried ASD, and (c) crystalline GLZ.

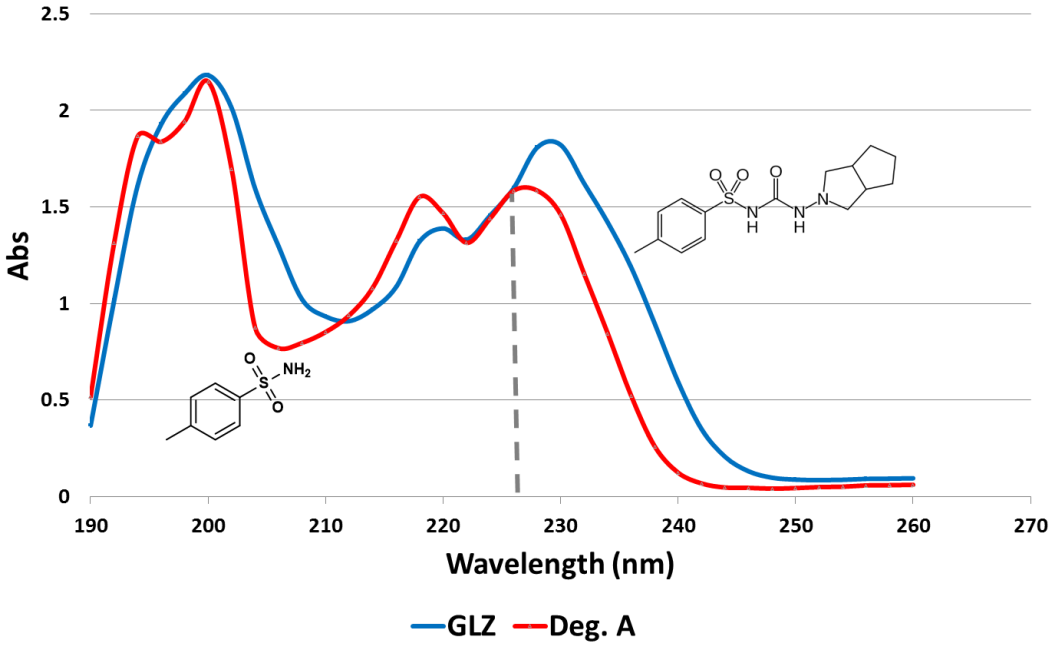

Figure 4.7 UV absorption (190–260 nm) of GLZ and its major hydrolysis degradant A (Deg. A).

4.9 SUPPLEMENTAL FIGURES

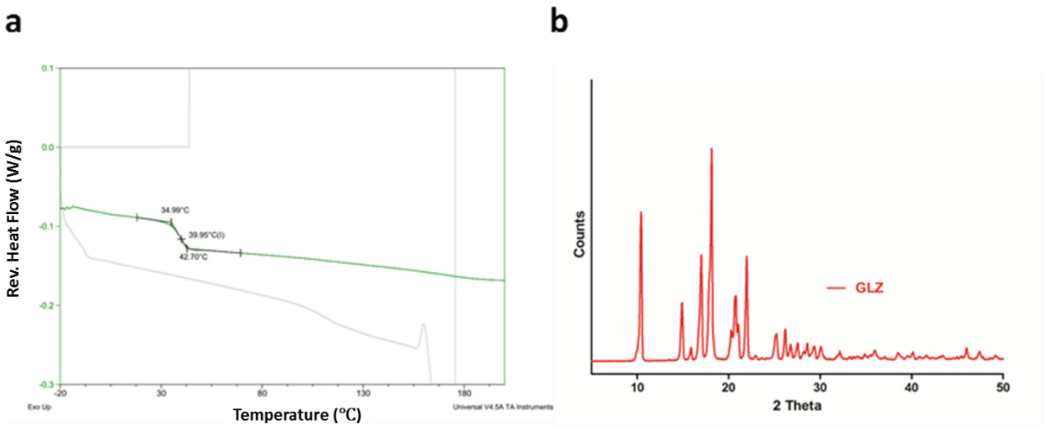

Supplemental Figure S4.1 (A) Second heating cycle of MDSC and (B) XRD analysis of pure GLZ.

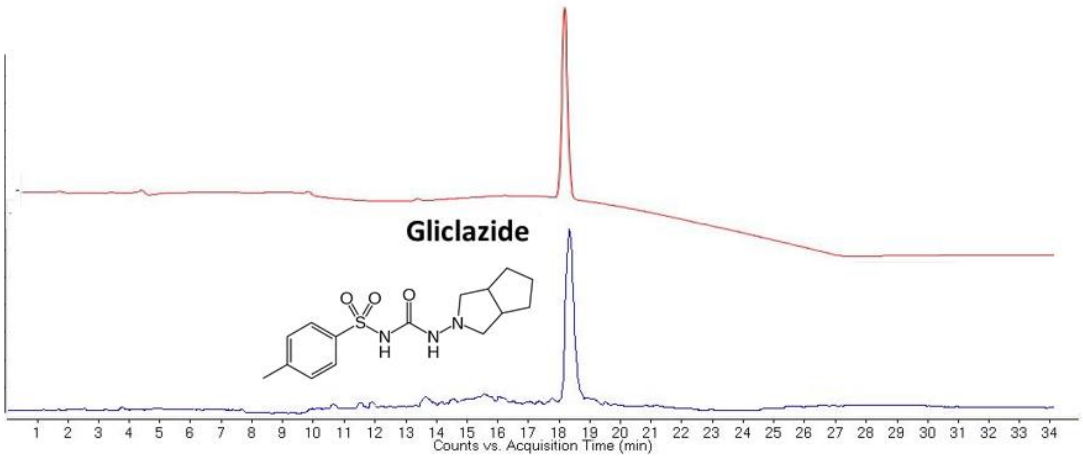

Supplemental Figure S4.2 LC/UV chromatograms (210–600 nm) and positive ion mode total ion chromatograms (TIC) from the accurate mass LC–MS/MS analysis of pure GLZ.

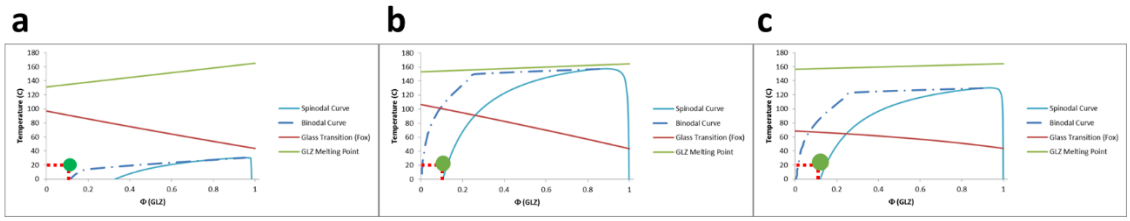

Supplemental Figure S4.3 Thermal phase diagram of GLZ and (A) AFFINISOL™ HPMC HME 100LV (B) PVP VA64 (C) Soluplus system representing the boundaries between thermodynamically unstable, metastable, and stable regions as bounded by the spinodal and binodal curves along with the glass transition boundary.

4.10 LIST OF TABLES

Run	Batch	Processing T (°C)	Torque (Gm)	Pressure (psi)	Melt T (°C)	RT from C to D (min)	Drug recovery @C (%)	RT from A to D (min)	Drug recovery @D (%)
1	**1**	130	1700-2100	500-700	149	9.0	-	12.6	0.0
2	**2**	130	1000-1100	400-600	145	7.0	-	10.0	0.0
	3	120	1150-1250	400-600	137	6.0	-	9.7	0.0
	4	110	1100-1200	400-600	127	6.0	-	9.5	0.0
	5	100	1300-1500	600-950	113	6.2	-	10.0	0.2 [b]
	6	160	400-500	60-80	160	5.1	-	8.5	0.0
3	**7**	130	700-800	-	132 [a]	2.8	92.4 [b]	5.4	5.7 [b]
	8	120	800-900	-	122 [a]	2.7	95.8 [b]	5.5	18.2 [b]
	9	110	900-1000	-	111 [a]	2.3	97.3 [b]	4.8	25.8 [b]
4	**10**	130	700-750	-	127 [a]	2.3	99.5 [c]	3.2	42.6 [b]
	11	120	750-850	-	118 [a]	2.2	99.7 [c]	3.0	89.4 [b]
	12	110	120	-	109 [a]	-	100.0 [c]	0.1	100.0 [c, d]

a) Melt temperature measured by an IR thermometer
b) Sample in amorphous form
c) Sample in crystalline form
d) Extrudate came out as powder

Table 4.1 HME processing conditions and physical-chemical characterizations of the machine setup and screw design optimization batches.

Run	Batch	Temp (°C)	Feed rate (g/min)	RPM	Torque (Gm)	Specific mechanical Energy (kW·hr/kg)	Drug recovery (%)
5	13	120	3.3	100	1,050	0.70	96.1
	14		3.3	150	830	0.83	95.4
	15		3.3	200	800	1.06	89.4
	16		3.3	250	750	1.25	85.6
	17		3.3	300	700	1.40	80.2
	18		2.3	200	650	1.31	83.4
	19		2.8	200	780	1.23	88.3
	20		3.8	200	890	1.01	95.4
	21		4.3	200	210	0.21	101.5

Table 4.2 HME processing conditions and physical-chemical characterizations of the specific mechanical energy input optimization batches.

Temperature	Crystalline		ASD		DMSO solution	
	Degradation Constant (hr^{-1})	Half-life (min)	Degradation Constant (hr^{-1})	Half-life (min)	Degradation Constant (hr^{-1})	Half-life (min)
100	0.0033 [a)]	12600.08	2.28 [b)]	18.28	13.72 [b)]	3.03
110	0.038 [a)]	1088.35	6.07 [b)]	6.85	43.54 [b)]	0.96
120	0.25 [a)]	166.64	15.42 [b)]	2.70	130.34 [b)]	0.32
130	2.45 [b)]	16.97	37.39 [b)]	1.11	369.50 [b)]	0.11
Activation Energy	68.53 kCal/mol		27.31 kCal/mol		29.74 kCal/mol	

a) Data acquired by measurement
b) Data acquired by extrapolation

Table 4.3 Hydrolysis degradation rate of crystalline GLZ, GLZ ASD, and GLZ DMSO solution at extrusion processing temperatures.

Run	Batch	Processing T (℃)	Torque (Gm)	Melt T [a)] (℃)	RT from A to D (min)	Drug recovery @D (%)
3	**7**	130	700-800	132	5.4	5.7 [b)]
	8	120	800-900	122	5.5	18.2 [b)]
	9	110	900-1000	111	4.8	25.8 [b)]
3-Dried	**7D**	130	1000-1200	136	3.2	0
	8D	120	1200-1400	124	3.0	5.7 [b)]
	9D	110	1500-1700	115	0.1	7.8 [b)]

Melt temperature measured by an IR thermometer
Sample in amorphous form

Table 4.4 HME processing conditions and physicochemical characterizations of Run 3 with and without drying the feed materials.

APPENDIX A: Solvent-assist Melt Extrusion

A.1 INTRODUCTION

Poorly water soluble therapeutic compounds typically have low absorption and poor bioavailability when they are present in their crystalline forms. To enhance their dissolution rates and solubility, researchers have sought to prepare formulations, in which drug molecules are present at higher energy states than in crystalline forms. One type of dosage form used to accomplish this higher energy form is a solid dispersion. Solid dispersions can be characterized as a molecular dispersion of the therapeutic compound in an inert carrier in a solid state.

Spray drying and melt extrusion are two common techniques to prepare amorphous solid dispersions in order to improve the biopharmaceutical performance of various classes of therapeutically-active, poorly water soluble agents.

In the spray drying process, a solution containing a therapeutically-active poorly water soluble agent and a polymer are dissolved in organic solvent or solvent mixture along with other additives. A spray dryer is then used to process the solution into a powder form. During the typical spray drying process, the solution is atomized into fine droplets and sprayed into the drying chamber of a spray dryer. This necessitates that the atomized liquids must be of such low viscosity to enable atomization into fine droplets. Therefore, the total

solid contents of the feed solution are typically in the range of 5 to 20%, w/w. Hot gases such as air and nitrogen are commonly used as the drying medium to quickly evaporate the solvent from the fine droplets inside the drying chamber. The dry powder is then carried by the drying gas stream into a collection vessel. Following the primary drying in a spray dryer, the resulted dry powder collected most times undergo secondary drying using a tray drying oven or double-cone dryer to reduce the residual solvent to levels acceptable to health authorities before the spray-dried powder is further processed into various dosage forms. In this process, the solvent is flashed off the droplets so quickly that crystallization of drug is inhibited and drug molecules are "locked" in an amorphous state. After blending with excipients, the either direct compression or dry granulation process is used to process spray dried amorphous solid dispersion into various dosage forms such as tablets and capsules.

The advantage of the spray drying process is the minimal heat exposure. The temperature of the drying gas is typically in the range of 70 °C to 140 °C. However, the actual temperature of the processed formulations is exposed to is much lower than the temperature of the drying gas because of the evaporative cooling effect. The processed formulations are typically exposed to 50°C to 80°C for less than 2 minutes. As a result, the spray drying process avoids degradation problems which are typically associated with conventional melt extrusion process. The other advantage of the spray drying is that solutions homogeneous at molecular levels are initially prepared prior to the spray drying. Both the feed solution composition and processing conditions must be designed to inhibit

potential phase separation during the drying process. However, the spray drying process has several disadvantages over conventional melt extrusion process. Organic solvents must be used as the medium to dissolve poorly water soluble drugs to prepare the solutions for spray drying. There are environmental and health concerns associated with the usage of organic solvents. Depending on the solvent composition and drying kinetics, phase separation between drug and polymer could take place drying the spray drying. Secondary drying is needed to reduce the residual solvent to levels acceptable by health authorities in most cases. Solvent evaporation is very energy consuming and the production rate is quite low given that total solid contents of the feed solution are typically in the range of 5 to 20%, w/w.

Conventional melt extrusion, as an alternative process to prepare amorphous solid dispersions, is a solvent free process. In a typical melt extrusion process, a dry blend containing a therapeutically-active agent, thermoplastic polymer, and other additives, such as antioxidants, is processed using a twin screw melt extruder. During melt extrusion, the active agent, in certain cases, is gradually dissolved into the formulation matrix as the result of the shearing and mixing by the rotating screw and the heat conducted from the barrel, generally in the range of 100 °C to 140 °C, and pressure inside the extruder barrel. In certain cases, drug is at first melted inside the extruder and the molten drug is then further mixed with polymer melt to prepare amorphous solid dispersion. In certain cases, both the "solubilization" and "melting and mixing" mechanisms discussed above are involved. The residency time inside the extruder ranges typically from 15 seconds to 5 minutes. After

being cooled using either compressed air or a chilled-roller, the extrudate is milled into fine granules for further downstream processing into various dosage forms. Due to the high viscosity of the polymeric matrix, drug molecules are “locked” in an amorphous state following the conventional melt extrusion.

As a solvent free and continuous process, melt extrusion is generally considered to be a more efficient manufacturing process than spray drying. The most challenging aspect reported for melt extrusion is the high level of thermal and mechanical energy are required to transform a physical blend of drug and polymer into amorphous solid dispersions homogenous at molecular level. Drug and polymer often degrade during conventional melt extrusion process. As a result, the applicability of the melt extrusion process is limited to active agents and polymers that can withstand these conditions.

Thus, there is a need for a manufacturing process that avoids the degradation problems associated with melt extrusion, facilitates the dispersion of drug molecules in polymer during melt extrusion and the eliminates the problems associated with spray drying resulting from the use of large amounts of solvent.

A.2 METHODS

Solvent-assist HME (SA-HME) overcomes the limits of conventional HME and SD processes. P-aminosalicylic acid (p-ASA) is a poorly water-soluble and thermal-labile drug used in this study to evaluate the SA-HME technology. Its degradation pathway was confirmed by LC-MS, and a thermal forced degradation study was performed to determine the processing conditions. A composition was prepared by geometrically blending 10% wt p-aminosalicylic acid with 90% wt Kollidon VA64 (pre-dried at 70 ℃ for 20 hours) using mortar & pestle. The blend was processed by a twin-screw extruder (Nano 16, Leistriz, Nuremberg, Germany). The extruder used to process the blend was set up with a feeding zone, four heating zones and a die. Feeding zone was cooled with a water jacket to maintain the temperature below 35 ºC. The four heating zones were maintained at various elevated temperatures list in Table A1. Solvent was injected at the second heating zone as shown in Figure A1. Three screw configurations with high, medium and low shear input were used in the extrusion runs as shown in Figure A2, and the screw speed was maintained at 200 rpm in all runs. The extrudates were evaluated for their chemical stabilities, solvent residuals and crystalline properties. The chemical stabilities of the extrudates were analyzed by HPLC (Ultimate 3000, Dionex Corp., Sunnyvale, CA). The solvent residuals were measured by moister analyzer (MF-50, A&D Company, Tokyo, Japan). The crystalline properties were examined by X-ray diffraction (Rigaku MiniFlex 600, Rigaku Americas, Woodlands, TX).

Table A1 showed an overview of the processing conditions varied in the extrusion studies of the p-aminosalicylic acid/Kollidon VA64 blend. Run 1-3, run 9-10, and run 14-15 were control runs without solvent injections. In run 4-8, run 11-13, run 16-20 acetone at 30%-60% wt ratio of the solid feed rate was introduced by a Shimadzu (Kyoto, Japan) HPLC pump during the extrusion runs through an injection nozzle in zone 2.

A.3 RESULTS

By analyzing the forced degradation of p-ASA using LC-MC, the major thermally induced decomposition pathway was identified, as shown in Figure A3. More degradation has also been reported with the increasing temperature, due to which, we managed to keep the processing temperature as low as possible without over-torqueing the extruder during the processing of p-aminosalicylic acid.

As shown in Table A2 run 1 to 9, with the high shear screw configuration, the machine reached the torque limit at 120 ℃ (run 3) without solvent injection, resulting in 21.10% drug recovery rate in the extrudate. The incorporation of acetone in the extrusion runs allowed further decreasing the processing temperature to 100 ℃ with the same screw configuration, bringing the drug recovery rate up to 45.48% (run 8). In run 9 to 18, milder screw configurations were applied in the extrusion runs to minimize drug degradation. In runs without solvent (run 9, 10, 14 and 15), drug degradations were slightly reduced compared to high shear screw configuration. Run 15 at 120 ℃ with the low shear screw configuration achieved the highest drug recovery rate (33.75%) without solvent assist. On the contrary, the presence of acetone in run 11 to 13 and run 16 to 18 significantly improved the drug recovery rate in the extrudates, especially when low shear screw configuration and low temperature conditions were used (run 17), 98.84% drug recovery rate was achieved with the solvent assist extrusion. Furthermore, a higher amount of acetone (2.0 mL/min) injected in the extrusion run further improved the drug recovery rate to 102% (run 20). XRD results indicated drug existed in amorphous form in all extrudates. In summary,

solvent assist extrusion prevented a thermolabile drug p-aminosalicylic acid degradation during extrusion process to manufacture amorphous solid dispersion.

A.4 CONCLUSIONS

The study demonstrated that SA-HME was capable of decreasing the extrusion torque thus minimizing the processing temperature. With the milder energy input applied to the drug and polymer, significantly less degradation was observed. Therefore, SA-HME made thermal processing of thermal-labile compounds by HME possible.

A.5 FIGURES

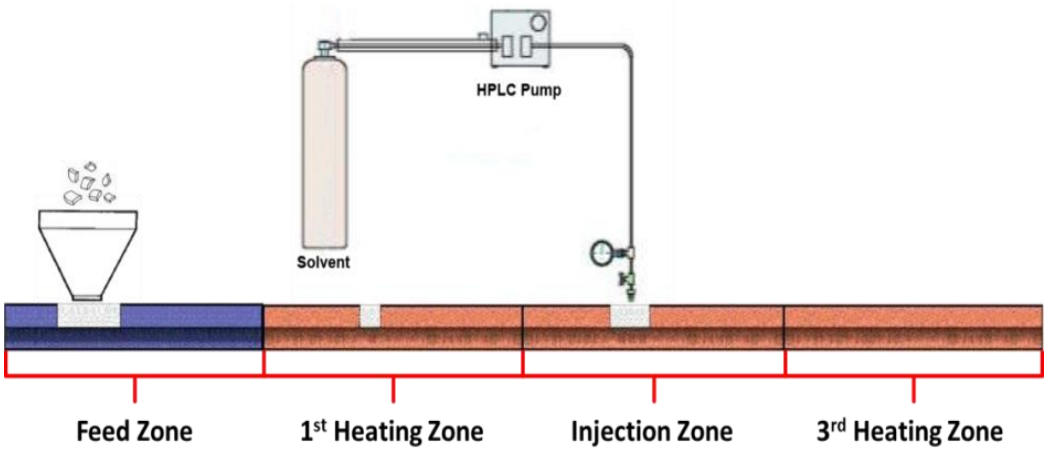

Figure A1 Solvent-assist hot-melt extrusion barrel setup.

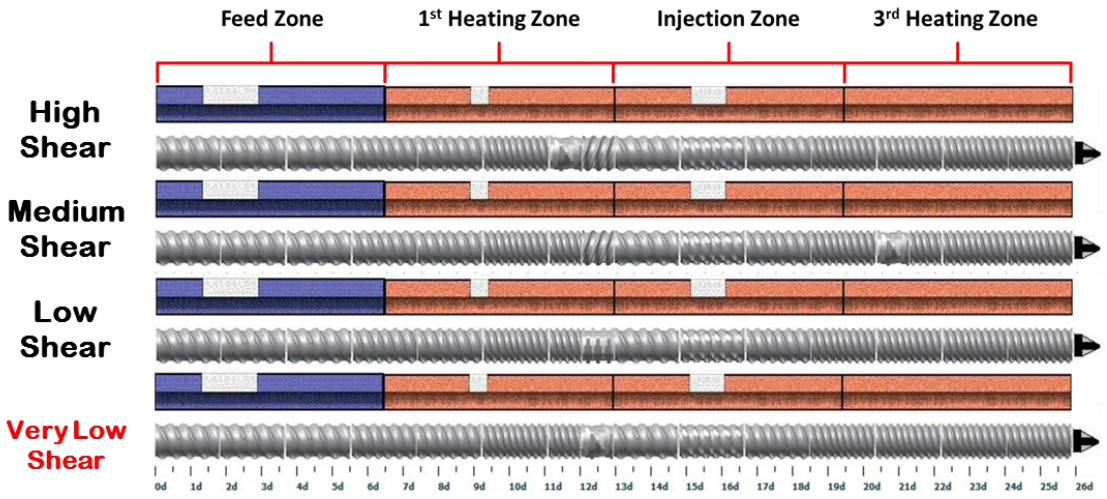

Figure A2 Screw designs for extrusion runs.

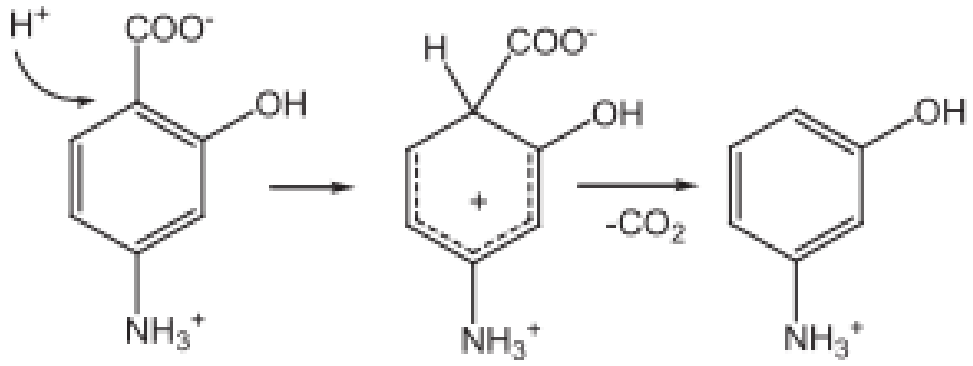

Figure A3 P-aminosalicylic Acid Degradation Pathway.

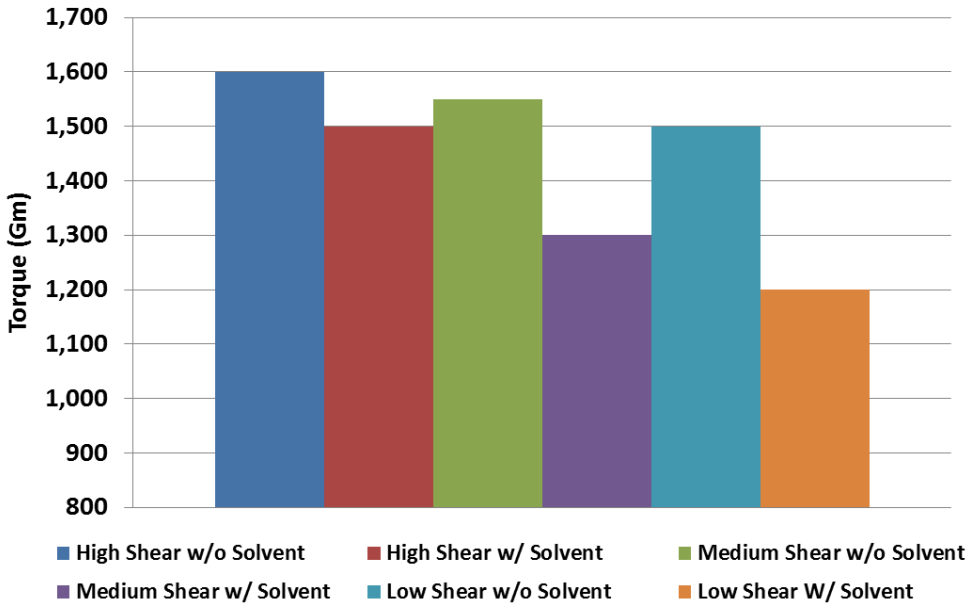

Figure A4 Solvent injection effectively decreased processing torque (@ 130 °C).

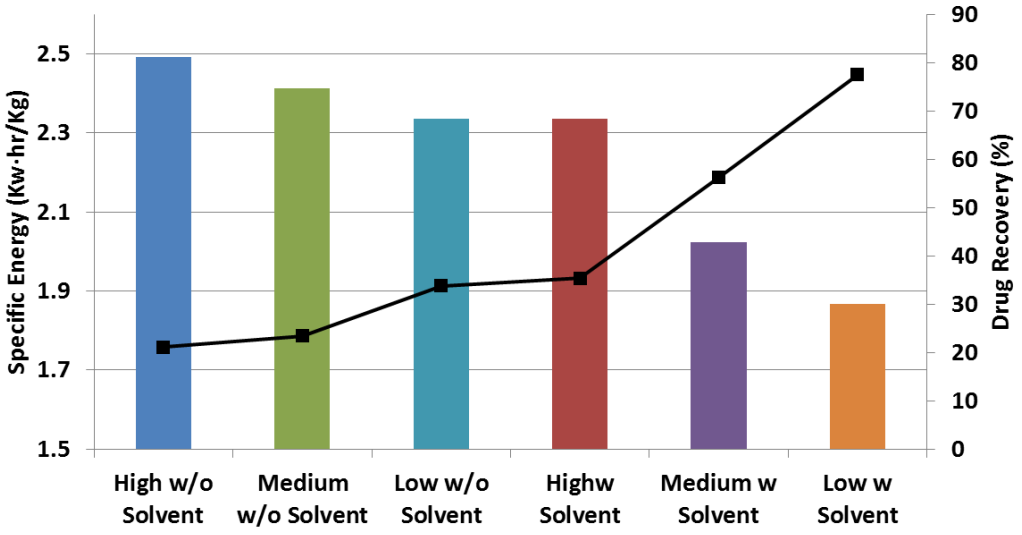

Figure A5 Solvent injection and mild screw design contributed to higher drug recovery (@ 130 °C).

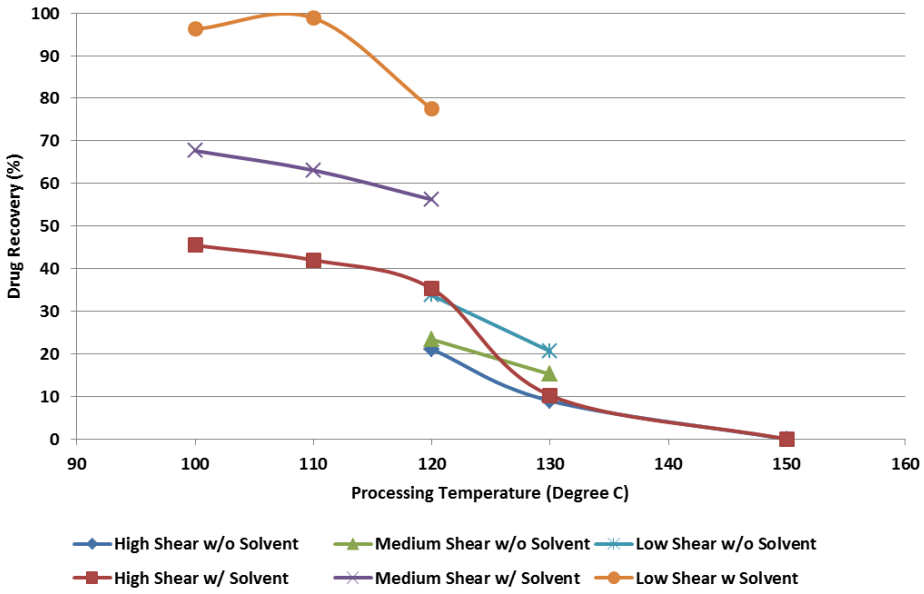

Figure A6 P-aminosalicylic acid recovery rate under different processing conditions.

A.6 TABLES

Extrusion Run	Extrusion Zone Temperature (° C)						Screw Configuration	Screw speed (RPM)	Solvent	Flow rate (ml/min)	Torque (Gm)	Feed rate (g/min)
	Die	4	3	2	1	Melt T						
1	150	150	150	150	150	151	High Shear	200	-	-	800	2.7
2	130	130	130	130	130	135	High Shear	200	-	-	1450	2.7
3	120	120	120	120	120	124	High Shear	200	-	-	1600	2.7
4	150	150	150	150	150	151	High Shear	200	Acetone	1.0	800	2.7
5	130	130	130	130	130	135	High Shear	200	Acetone	1.0	1400	2.7
6	120	120	120	120	120	124	High Shear	200	Acetone	1.0	1500	2.7
7	110	110	110	110	110	115	High Shear	200	Acetone	1.0	1650	2.7
8	100	100	100	100	100	106	High Shear	200	Acetone	1.0	1900	2.7
9	130	130	130	130	130	135	Medium Shear	200	-	-	1350	2.7
10	120	120	120	120	120	126	Medium Shear	200	-	-	1600	2.7
11	120	120	120	120	120	125	Medium Shear	200	Acetone	1.0	1300	2.7
12	110	110	110	110	110	114	Medium Shear	200	Acetone	1.0	1400	2.7
13	100	100	100	100	100	105	Medium Shear	200	Acetone	1.0	1650	2.7
14	130	130	130	130	130	135	Low Shear	200	-	-	1300	2.7
15	120	120	120	120	120	127	Low Shear	200	-	-	1500	2.7
16	120	120	120	120	120	126	Low Shear	200	Acetone	1.0	1200	2.7
17	110	110	110	110	110	115	Low Shear	200	Acetone	1.0	1350	2.7
18	100	100	100	100	100	105	Low Shear	200	Acetone	1.0	1700	2.7
19	100	100	100	100	100	105	Low Shear	200	Acetone	1.5	1800	2.7
20	100	100	100	100	100	105	Low Shear	200	Acetone	2.0	1600	2.7

*Torque limit was considered as 2000 Gm during extrusion to protect the machine

Table A1. Extrusion processing conditions

Extrudate Run	%drug remaining	Solvent or Liquid	Screw Configuration	XRD	Solvent Residual
Blend	100.00	-	-	Crystalline	-
1	0.00	-	High Shear	Amorphous	-
2	9.00	-	High Shear	Amorphous	-
3	21.10	-	High Shear	Amorphous	-
4	0.00	Acetone	High Shear	Amorphous	0.00%
5	10.27	Acetone	High Shear	Amorphous	0.35%
6	35.33	Acetone	High Shear	Amorphous	1.55%
7	42.03	Acetone	High Shear	Amorphous	4.05%
8	45.48	Acetone	High Shear	Amorphous	5.25%
9	15.23	-	Medium Shear	Amorphous	-
10	23.41	-	Medium Shear	Amorphous	-
11	56.23	Acetone	Medium Shear	Amorphous	4.20%
12	63.11	Acetone	Medium Shear	Amorphous	6.80%
13	67.68	Acetone	Medium Shear	Amorphous	7.15%
14	20.63	-	Low Shear	Amorphous	-
15	33.75	-	Low Shear	Amorphous	-
16	77.49	Acetone	Low Shear	Amorphous	1.40%
17	98.84	Acetone	Low Shear	Amorphous	4.10%
18	96.21	Acetone	Low Shear	Amorphous	5.98%
19	95.12	Acetone	Low Shear	Amorphous	5.00%
20	102.00	Acetone	Low Shear	Amorphous	6.65%

Table A2. Percent p-aminosalicylic acid remaining, crystallinity, and Solvent Residual

APPENDIX B: Traditional Chinese Medicine Project

B.1 INTRODUCTION

Breviscapine is a traditional herbal compound extracted from the Chinese herb Erigeron breviscapus. The main active ingredient is Scutellarin, which account for more than 90% content of the extract. Breviscapine has several commercialized products (tablets or injections) on the market in China. The injectable formulation of Breviscapine is clinically used in China to treat ischemic cerebrovascular diseases such as cerebral infarction, apoplexy, coronary heart disease and angina pectoris. However, similar to most flavonoids, a clinical application is limited due to its poor physicochemical properties (low aqueous solubility and poor chemical stability) resulting in a limited bioavailability, despite demonstrated pharmacological effects. Furthermore, the blood-brain-barrier is regulating the molecules access to the brain through many mechanisms such as efflux transport systems as the P-Glycoprotein. Several attempts have been made to develop new delivery systems for this molecule. For example: Polymeric nanoparticles, liposomes, and solid dispersions formulations have been tested with some success. Yet, no attempt was made to formulate amorphous solid dispersions of Breviscapine using the hot melt extrusion technic.

Puerarin is an isoflavone C-Glucoside isolated from a Chinese herbal medicine: Radix Puerariae Lobatae, which is the dried root of Pueraria lobata. According to the Chinese Pharmacopea, it has been reported to have several biological activities such as the

dilation of coronary arteries. It has also been reported as an antioxidant, a hepato-protective, an anticancer and could be used to treat diabetes or cardiovascular diseases. It is currently mostly used to treat cardiovascular diseases such as angina pectoris or myocardial infarction. However, its clinical applications are limited due to its low water solubility and dissolution rate. Moreover, this molecule is very hydrophobic and has a poor liposolubility limiting its absorption in-vivo.

Most of the time, because it was classified as a class IV in Biopharmaceutics Classification System (BCS), Puerarin has to be used by injection and a solubilizer has to be added to increase its solubility. Yet, the addition of cosolvents (that can be sensitizing agents), can lead to side effects such as pruritus, chest tightness or shortness of breath. In addition, the elimination half-life of Puerarin has been shown to be short and frequent injection may be required, leading to a higher risk of side effects. All this factors can explain the interest of researchers for the development of an oral administration form for this drug. Thus, various technics are being studied for this drug such as the preparation of nanocrystals, phospholipids complex, nanoparticles, etc.

B.2 RESULTS AND DISCUSSIONS

I. Characterization of the drug substances:

Before going further in this project, we had to characterize these drugs in order to know more about their characteristics (melting point and glass transition temperature (Tg), thermal degradation profile, crystallinity, etc.)

1. Determination of the drugs' melting point and glass transition temperature:

In order to determine these crucial temperature, we used modulate DSC. Two methods were used: A simple ramping (reach a higher temperature of our chosen at a specific rate) to determine the Tm, and a "Heat-Cool- Heat" method to determine the Tg of the drug.

a) Ramping method:

Based on our research, we found some hypothetical value for the Tm, which were respectively 187°C for Puerarin and 260°C for Breviscapine.

Equilibrate at -20°C; Isothermal for 5 min; Modulate +1°C every 60 second; Ramp 5°C/min from -20°C to 40°C above the Tm value.

b) Heat Cool Heat method:

Cycle 1: Equilibrate at 20°C, Modulate +2°C every 60 sec, Ramp 20°C/min to 20°C above Tm.

Cycle 2: Ramp 40°C/min to -40°CIsothermal for 5 min.

Cycle 3: Modulate +/- 1°C every 60s, -Ramp 5°C/min to 40°C above Tm.

The results showed a Tm around 350°C for Breviscapine (Figure B1, left) and around 210°C for Puerarin (Figure B1, right). Furthermore, the Heat Cool Heat results seemed to indicate a change in the crystalline form for Breviscapine around 200°C (melting followed by crystallization). Both drugs also showed a big "drop" of the Heat Flow and Non Reverse Heat flow Curve around 100°C, this is probably a simple solvent/water evaporation. However, additional tested will be perform to confirm this hypothesis.

The Heat Cool Heat method was used to determine the Glass transition temperature since the drug was heat above its melting point and then cooled allowing the drug to reach the Tg. The values were respectively 102°C for Breviscapine and 144°C for Puerarin (Figure B2). As expected by the high Tm values the Tg values are relatively high as well.

The pure drugs were analysed using Polarized Light Microscopy (PLM) to confirm the values obtained with DSC and determine the thermal profile of each drug.

In order to do that, the melting of the drugs was studied throught Hot-Stage PLM. The method was made to reach the melting point of the drug throught a simple ramping. Breviscapine was heat to 350°C (above its Tm value) as follows: Ramp 10°C/min to 100°C and then ramp 5°C/min to 350°C. Similarly, Puerarin was heat above the Tm value found with DSC: Ramp 10°C/min to 100°C and then ramp 5°C/min to 250°C. Pictures were taken automatically by the software in order to monitor any modifications very carefully. The images taken confirmed the values and events found using DSC. Indeed, Breviscapine showed an interesting behavior with the appearance of needle shapes around 220°C (Figure B3) that could confirm the "recrystallization" event seen on the DSC results. A clear melting was hard to see since Breviscapine has a wide melting point (as seen on the DSC results) that starts around 340 °C and ends at 351 °C. This relatively broad melting could explain that it is harder and longer to observe on PLM. (Figure B4). Regarding Puerarin, the events observed perfectly fitted those observed throught DSC: The crystals started to melt around 220°C (more clearly around 230 °C) and the melting was complete at 240 °C (drug was then liquid). (Figure B5 and Figure B6). It should be noted that, for both drugs, nothing noticeable happens around 100 °C, this seems to confirm that the drop around this temperature is probably not a melting but a solvent evaporation.

But, in order to confirm this, both samples of pure drug were heated with a LOD to 150°C for 3 min, the weight loss was calculated for both drugs, showing respectively a loss of 5,95% for Puerarin and 10,15% for Breviscapine. The samples were then directly analyzed with XRD to check the cristallinity of the samples when compared to pure

unheated drugs. The objective was to prove that the drugs are still crystalline at these temperatures and that it is not the drug melting. For both drugs, the peaks were perfectly identical to the pure unheated drug's crystalline peaks. This confirms that the drop visible in DSC around 100°C is probably moisture evaporation and not a melting point.

2. Characterization of the crystallinity:

XRD analysis was conducted to identify the 2-theta angle of the diffraction peaks. Those 2-theta angles will be monitored in the hot-melt extrusion formulations to identify any residual crystals or crystallization of the drug substance.

3. Characterization of the degradation profile using TGA

The thermal degradation temperature of each drug substance was identified using TGA with both nitrogen (N2) and O2 gas. The results were used to confirm the previous results obtained with DSC and Hot stage PLM and to help determine the processing temperature of the hot-melt extrusion process.

Breviscapine was analyzed from 45°C to 400°C with a constant heating rate of 10°C/min and under a gas flow of N2 or air (both at a 65ml/min rate).The data (Figure B7) are comparable to those obtain with DSC: We can see solvent evaporation from 100°C to 200°C, then weight loss (drop) around 210°C due to the recrystallization and finally

another drop at the Tm value (340°C). The drug is probably degrading. Puerarin was analyzed from 45°C to 325°C with a constant heating-rate of 10°Cmin and under a gas flow of N2 or air (both at a 65mL/min rate). The curve obtained for Puerarin (Figure B8), shows the weight loss (%) of the drug in function of the temperature. From 0 to 100°C about 5% of the sample weight is lost; this can be explained by the loss of solvent/water. This result is similar to the result previously obtain with the LOD showing a loss of 5,95% after heating the sample for 3 min at 150°C. The weight loss is then stabilizing from 100°C to the Tm value (210°C). This is in accordance with the result obtained with DSC. Above the Tm temperature, the drug starts degrading (probably by hydrolysis) and the weight loss starts increasing again. It must be noted that the curves obtained with the N2 environment and the air are similar until higher temperatures where they start to separate: The weight loss of the sample at the end of the analysis is less important in the air environment (25% loss) than in nitrogen environment (35% loss). This could be due to oxidation of the sample at high temperature; the reaction of the drug with oxygen atoms contained in the air leading to the addition of oxygen atoms on the drug could compensate the weight loss.

As detected, the melting points temperatures of the two drugs are high which could be an issue to obtain amorphous solid dispersions using hot melt extrusion. In order to successfully convert crystalline into amorphous form, the drug must be heated above its melting point and above the polymer's Tg to induce plasticity during the extrusion process. When the drug's Tm is high, it can induce the drug and/or polymer's degradation. Fortunately, by choosing the right polymer for each drug in good proportion, it is possible

to lower the melting temperature of the drug and consequently prevent any degradation during the process.

II. Miscibility with polymers:

1. Preparation of the physical mixtures:

The 2 drugs were blended with 6 different polymers: EPO®, HPMC-AS, PVPK12, Affinisol®, Soluplus® and PVPVA64. First, the drug loading tested was 30%. Hot stage PLM was used to determine the miscibility of the drug with each polymer and their effect on the drug Tm (diminution of the melting temperature).

The method used for the heating was as following:

Ramp 20°C above the polymer's Tg to induce its melting, hold this temperature for 10 minutes, ramp 10°C to 185°C, hold for 10 minutes.

Pictures were taken during the entire experiment in order to detect any changes in the drug's aspect.

As it can be seen in Table B1 and Table B2, PVPK12 was by far the polymer showing the best miscibility with Breviscapine while Soluplus was one of the best polymers for Puerarin. Based on these results, physical mixtures were made this time using

different drug loading, and analyse using DSC to study the effect of the different drug loading and the polymer's effect on the thermal profile of each drug. The method used for DSC was the same ramping than previously.

As we can see on Figure B9, Breviscapine's Tm (usually around 350°C) disappears with high polymer content, but is still visible with the lowest polymer content (10%). The disappearance of the drug Tm on the DSC results is a sign of good miscibility between drug and polymer. The recrystallization phenomenon happening around 200°C decreases with a high polymer content however without completely disappearing. These results suggest the 15% drug loading to be used for the extrusion runs. Regarding Puerarin, the results were satisfying as well (Figure B10). As seen previously, the pure drug only had one melting peak around 210 °C but with high polymer content another peak appears later (this is probably due to degradation). The miscibility is satisfying for the higher content in polymer since the melting peak of the drug is no longer visible on the curve. (Figure B4)This polymer can thus be used for a low drug loading (lower than 50%).

III. Hot melt extrusion:

The hot melt extrusion technic was then used to obtain amorphous solid dispersions of these drugs in polymers. 200g of each physical mixture was prepared by mixing the polymer and the API with a mortar and pestle. First, equal quantity of drug and polymer powders were mixed (in a 50:50 ratio) to ensure a homogeneous mixing. More polymer

was then added to reach a final ratio of 15% of drug with 85% of polymer. The extruder used was a Leistriz Nano 16 with a Brebender twin screw feeder.

For Breviscapine:

The feeder was calibrated to 300rpm to obtain a feeding rate of 3,33g/min. The time necessary for extrudates to come out of the extruder was 7minutes and 2 seconds. Screw design were shown in Figure B11. The screw can be divided in 4 zones from the left to the right (die). Zone 1 (in blue), is the feeding zone, zone 2 is the venting zone, zone 3 is where the mixing takes place (particularly with screws 13 and 14) and finally zone 4 is a mixing and ejection zone.

Based on the PLM and DSC results regarding the melting temperatures of the drug with polymer, 3 different temperatures were used to run Breviscapine (Table B3): First, 150 °C, the aspect of the extrudates was satisfying so it was decided to try to decrease the run temperature in the extruder to 130°C for each zone. But at this temperature, the torque needed is excessive (exceeding 2200 Gm).

Following these results, we tried the intermediate temperature (140 °C) which was also satisfying. It must be noted that we use lower temperature than the real Tm because, in the extruder, beside the thermal energy input that is provided there also is the impact of

the mechanical energy of the screws that will help dissolve the drug. Aspect of the extrudates (150°C and 140°C) can be seen on Figure B12 and Figure B13.

For Puerarin, the feeder was calibrated in order to reach a feed rate close to 3g/min: At 220rpm the feed rate was 3,7g/min. This was the setting used during the entire process. However it must be noted that this feed rate decreased to 2,5g/min at the end of the run due to the decreasing of the amount of powder remaining in the feeder (decreased the pressure at the entrance of the feeding zone). The screw design was similar to the one used for the Breviscapine sample. As presented in Table B4, the temperatures were set to 150°C and 170°C. The extrudates obtained (Figure B14) are clear which is a good sign of amorphization.

IV. Characterization of the extrudates:

First, the extrudates were grinded into very fine powder in order to be analyzed through different technics and prove that the samples obtained through extrusion were indeed amorphous.

1. Polarized Light Microscopy:

The images obtained with PLM (Figure B15 and Figure B16) seem to confirm the amorphization of both drugs after extrusion. The images obtained with the microscope

(figure 51) clearly indicated that the Breviscapine is now in its amorphous state especially if we compare to the previous aspect of pure Breviscapine (Figure B16). Similarly, the images obtained through PLM demonstate the amorphization of Puerarin (Before processing Figure B17, after processing Figure B18). Indeed, the extrudates did not show any birefringence properties and had a “glassy” aspect. (Figure B18).

2. XRD analysis

The XRD spectra of Breviscapine show typical results: Very characteristics crystalline peaks for the pure drug, once mixed with polymer most of these peaks disappear and the curve is a mix between an amorphous “halo” and a few crystalline peaks. And finally, the extrudates are proven to be amorphous since no crystalline peaks are visible. (Figure B19). Results are similar with XRD analysis of Puerarin and confirm amorphization of the drug after HME. (Figure B20).

3. DSC analysis

The DSC analysis of the extrudates confirmed these previous results showing the lack of a Tm on the Non-reverse heat flow curve (Figure B21 and Figure B22). This is a sign that the drug is now in its amorphous state and no longer crystalline.

4. FTIR analysis:

For Breviscapine:

The FTIR analysis of Breviscapine shows a good interaction of the polymer with the drug. Indeed, if we compare the spectra between them, we can see that the spectrum of the physical mixture attenuates the drug's and polymer's peaks and is a mix between the two spectra. (Figure B23). FTIR analysis was then run on the extrudates (Figure B24), and shows amorphization of the drug indeed, the drug's peaks disappeared and the spectra of the extrudates are flatter, showing mostly the polymer's peaks around 3500 and 3000 cm^{-1}.

For Puerarin:

Similar to Breviscapine, the FTIR results show a good interaction between the drug and the polymer (Figure B25). The second figure (Figure B26) also confirms amorphization of Puerarin with disappearance on the main drug's peaks while still some polymer's peaks on the extrudates spectra.

B.3 CONCLUSIONS

With this work we have shown that it is possible to produce amorphous solid dispersions of high melting temperature's drugs using HME. This can be facilitated by choosing the right polymer with the right ratio. But this work is still unfinished, the in vitro dissolution studies and in vivo tests be further conducted in China.

B.4 FIGURES

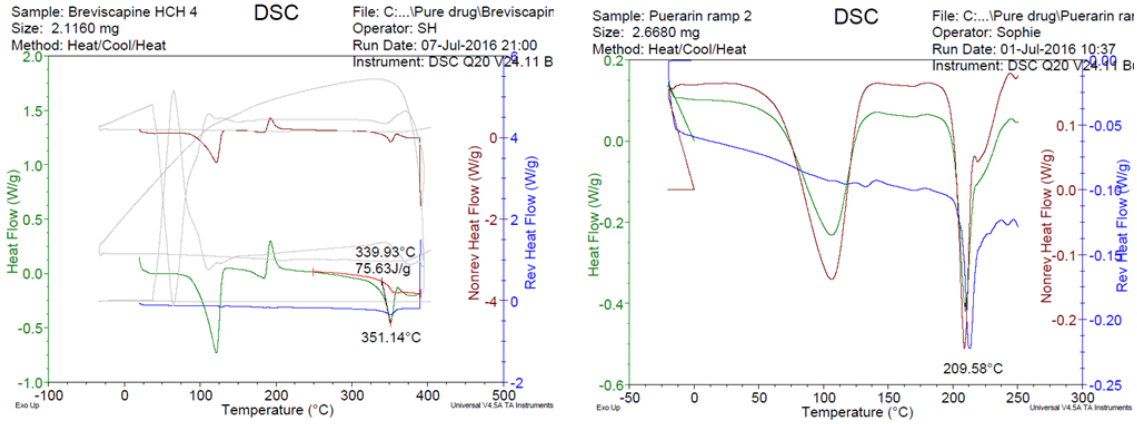

Figure B1 Tm values of Breviscapine (left) and Puerarin (right).

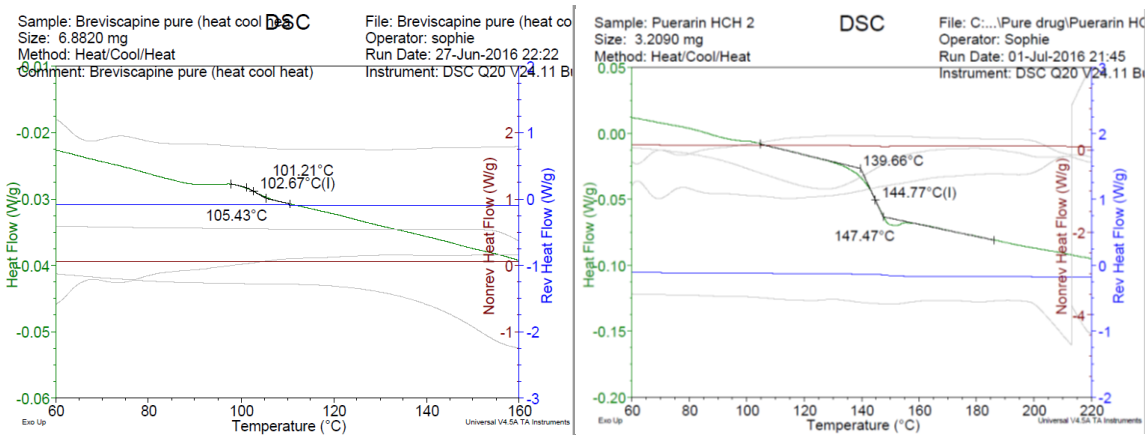

Figure B2 Tg values of Breviscapine (left) and Puerarin (right).

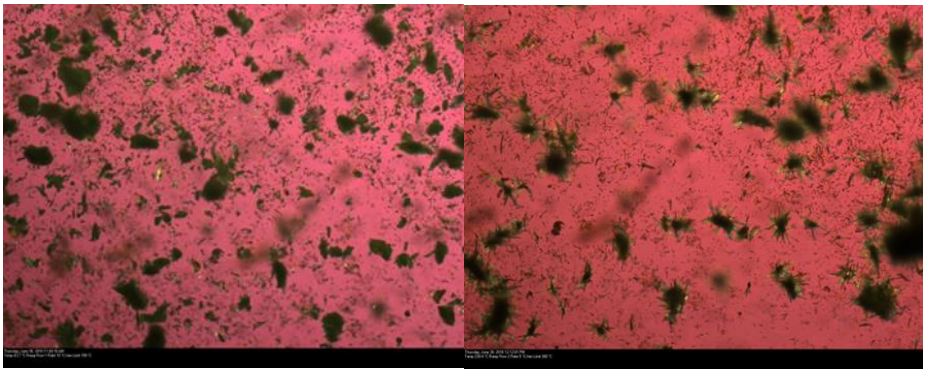

Figure B3 Breviscapine at T_0 and 230 °C. Needles are clearly visible at 230 °C.

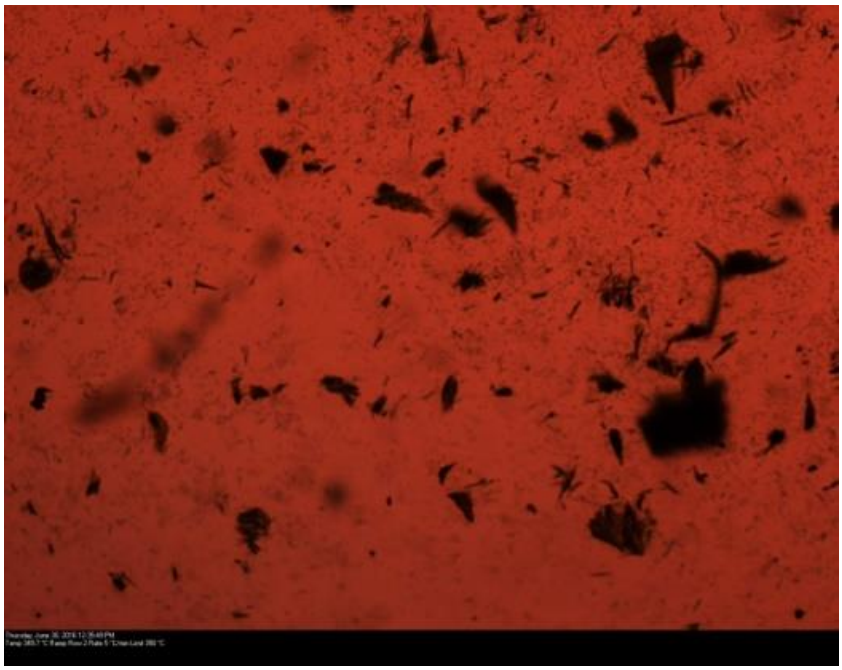

Figure B4 Breviscapine at 350°C.

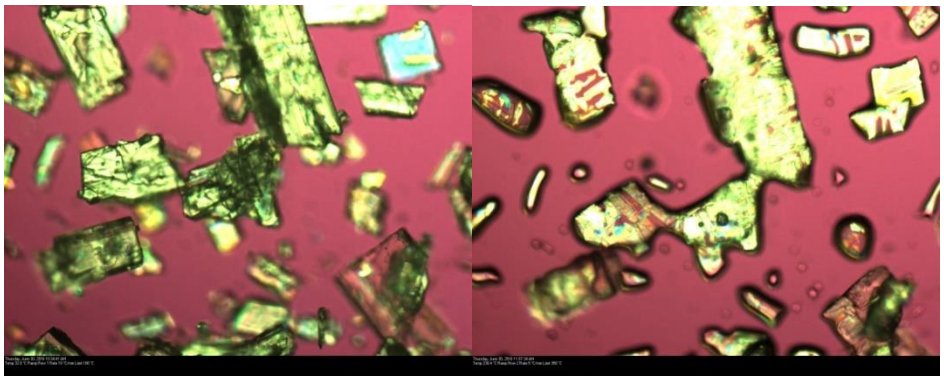

Figure B5 Puerarin at T_0 and 230 °C.

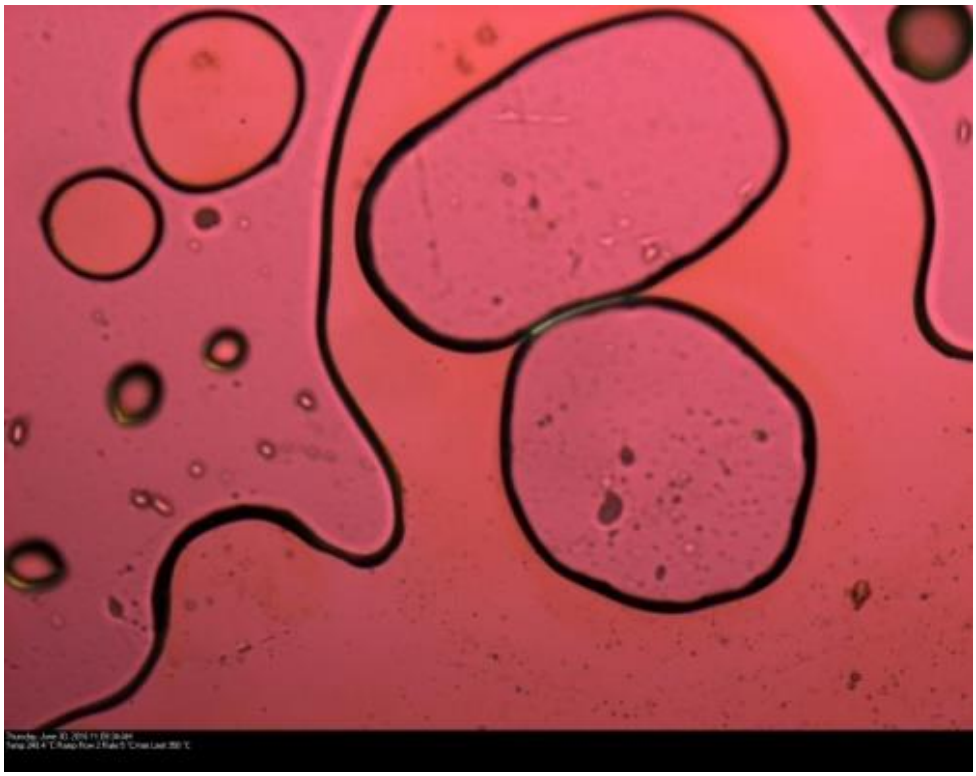

Figure B6 Puerarin at 240 °C.

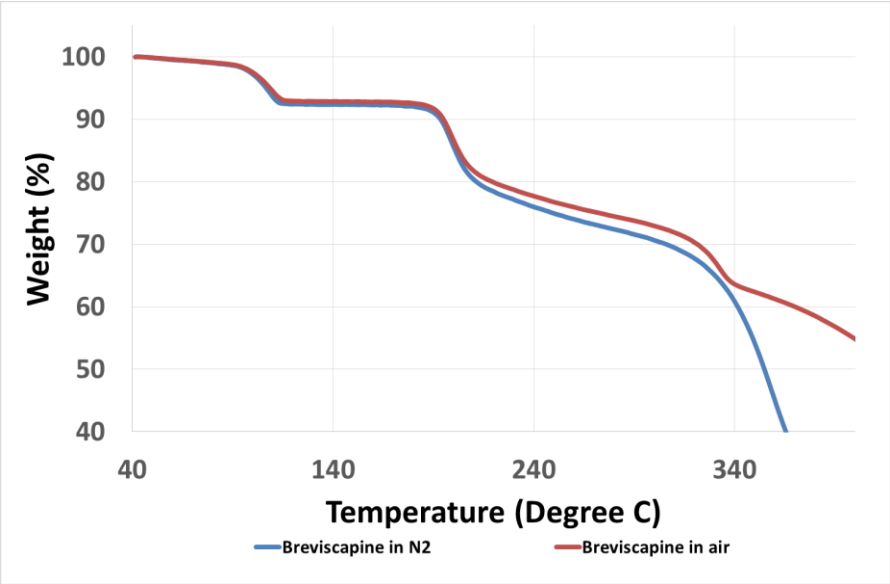

Figure B7 TGA analysis of Breviscapine in air and N2.

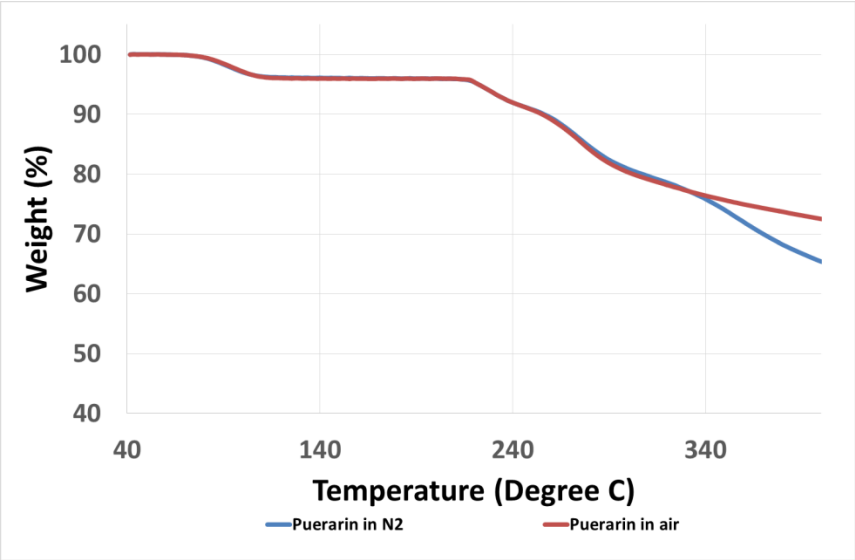

Figure B8 TGA analysis of Puerarin in air and N2.

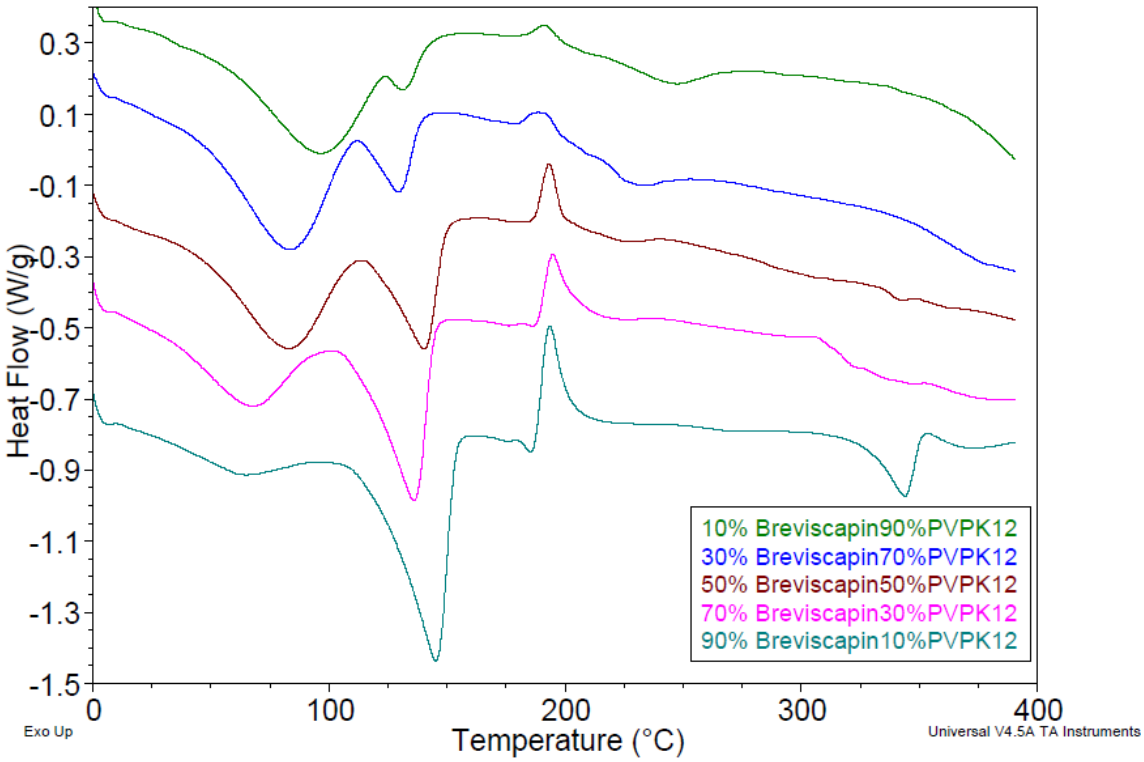

Figure B9 DSC results of different drug loading of Breviscapine with PVP K12.

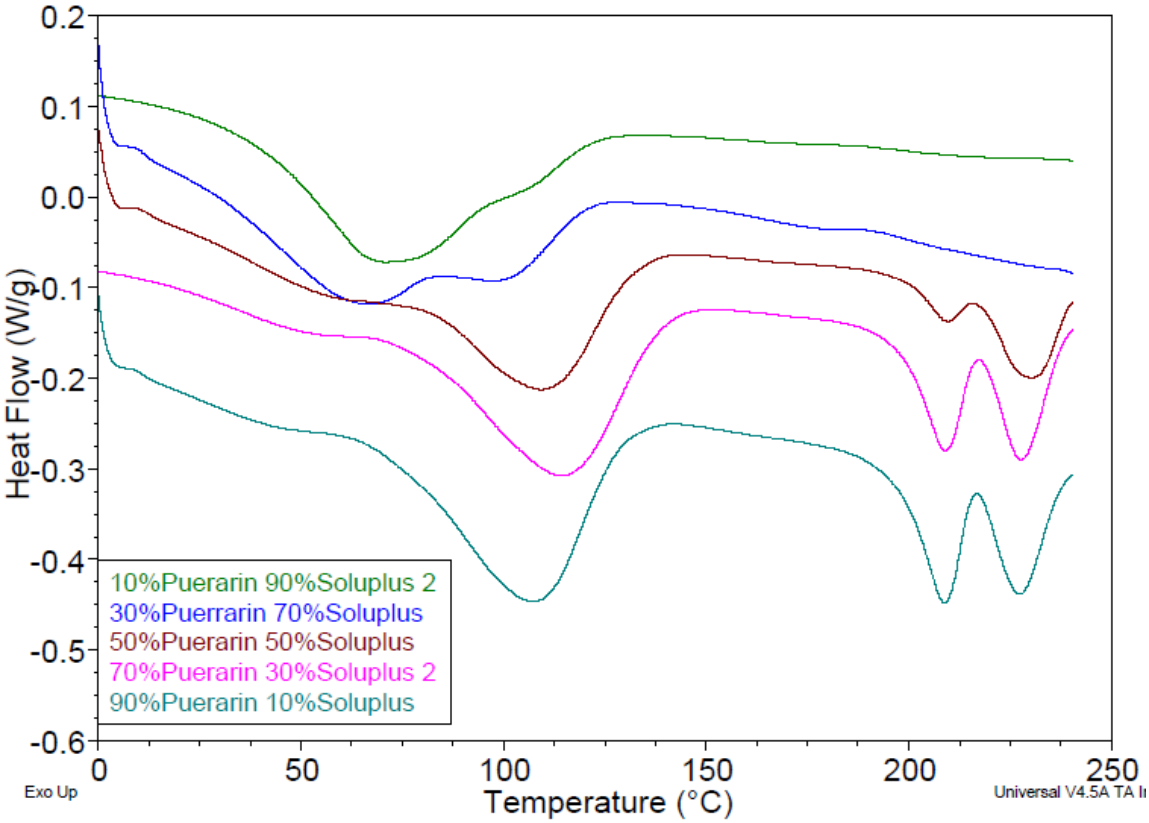

Figure B10 DSC results of different drug loading of Puerarin with Soluplus.

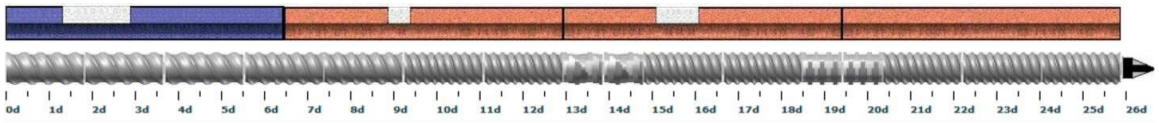

Figure B11 Screw design used for the extrusion.

Figure B12 Breviscapine extrudates after a 150 °C run.

Figure B13 Breviscapine extrudates after the 140 °C run.

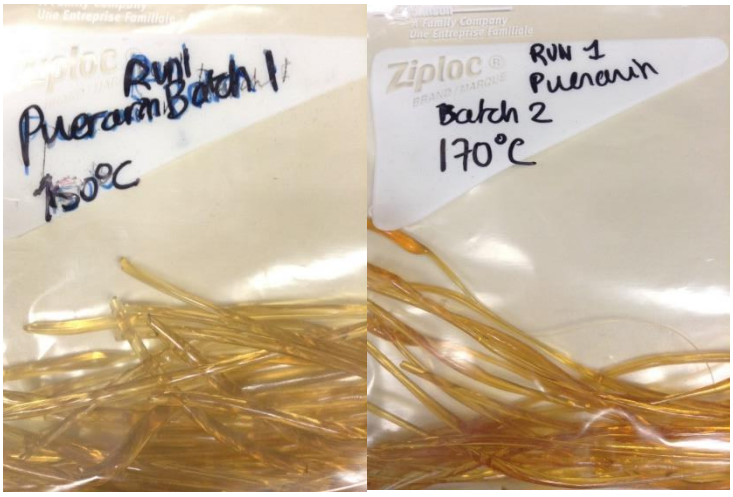

Figure B14 Aspect of the Puerarin extrudates (150 °C and 170 °C).

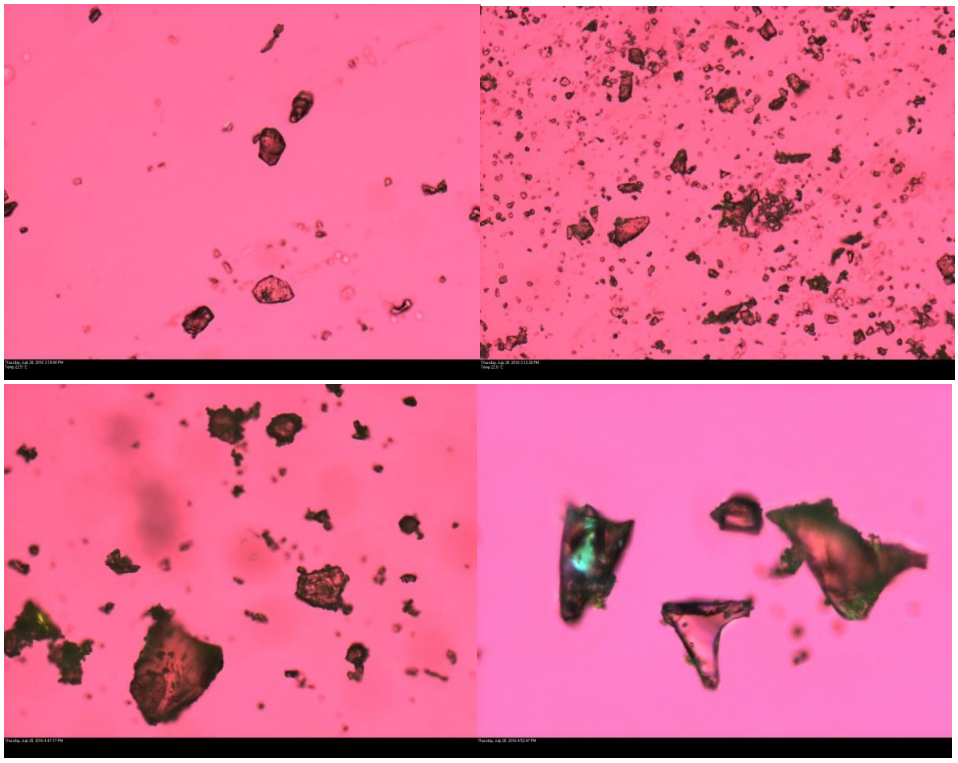

Figure B15 Breviscapine samples extruded at 140 °C (top images) and samples extruded at 150 °C (bottom).

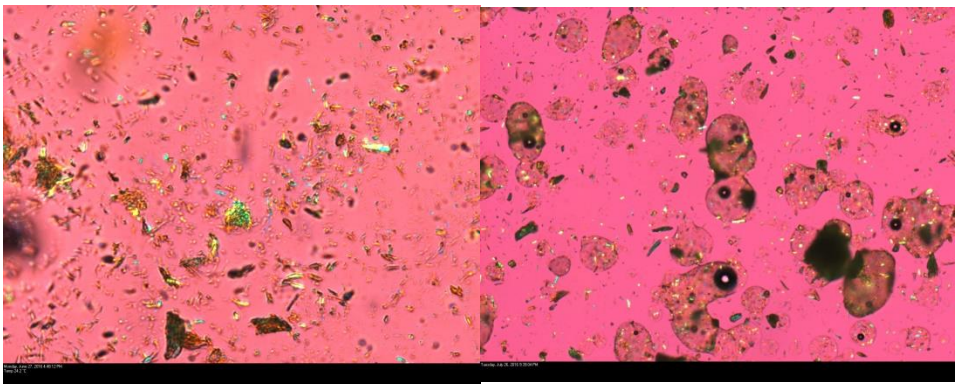

Figure B16 Breviscapine before extrusion (left) and physical mixture of 15% Breviscapine with 85% PVP K12 before extrusion (right).

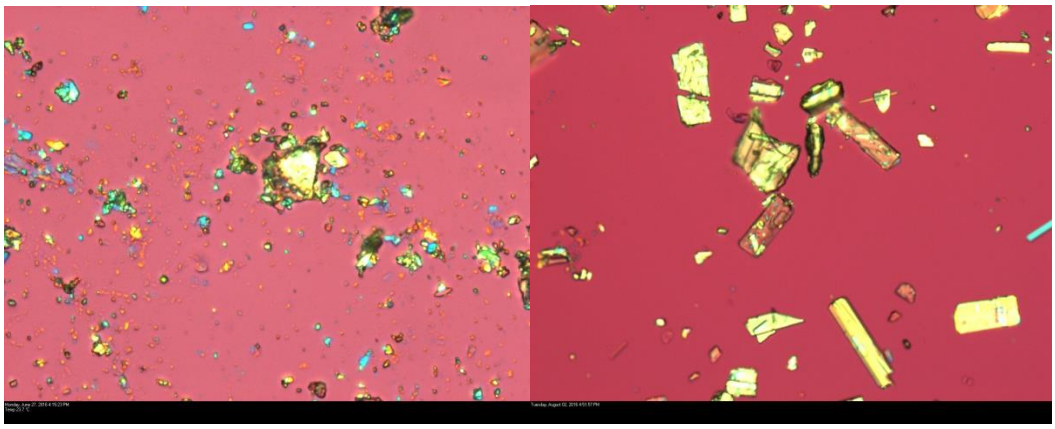

Figure B17 Pure Puerarin (left) and physical mixture of Puerarin with Soluplus (15% and 85%) on the right.

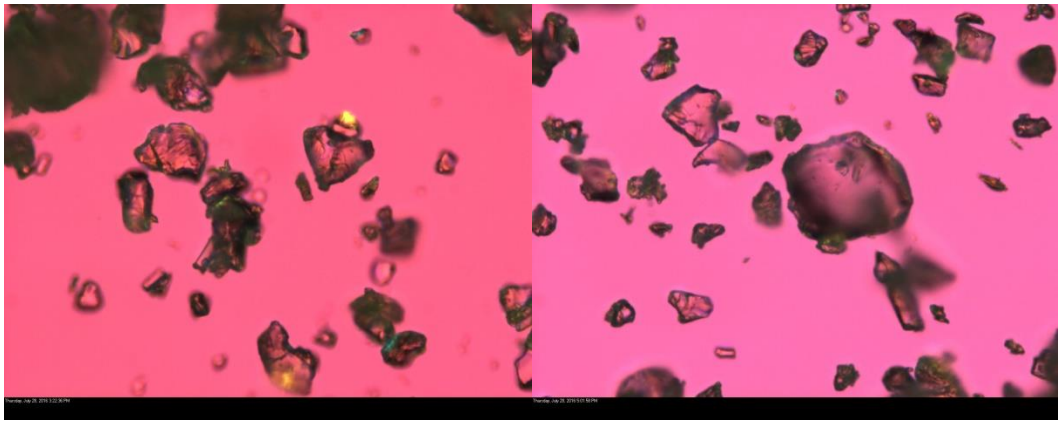

Figure B18 From left to right: Puerarin extrudates at 150 °C and 170 °C.

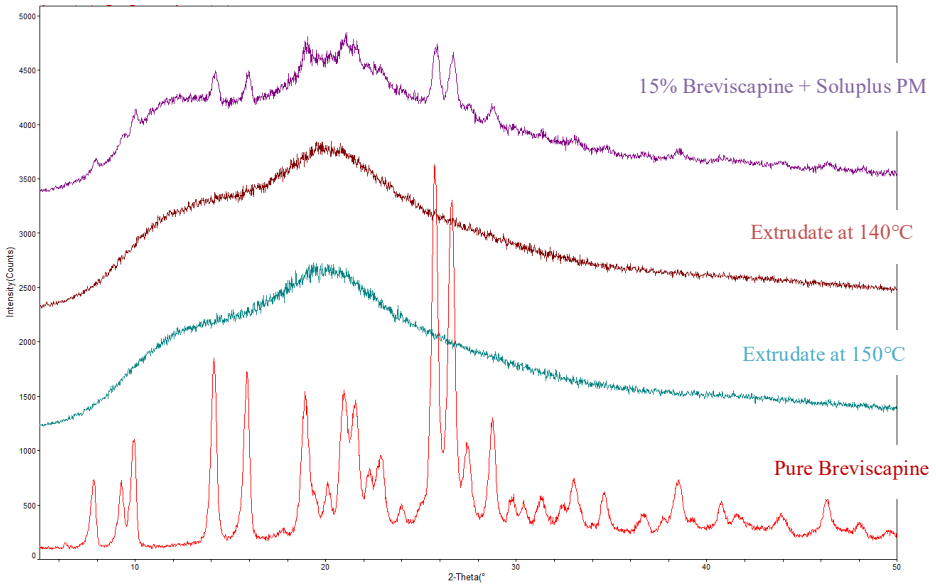

Figure B19 XRD spectra of pure Breviscapine, physical mixture and extrudates.

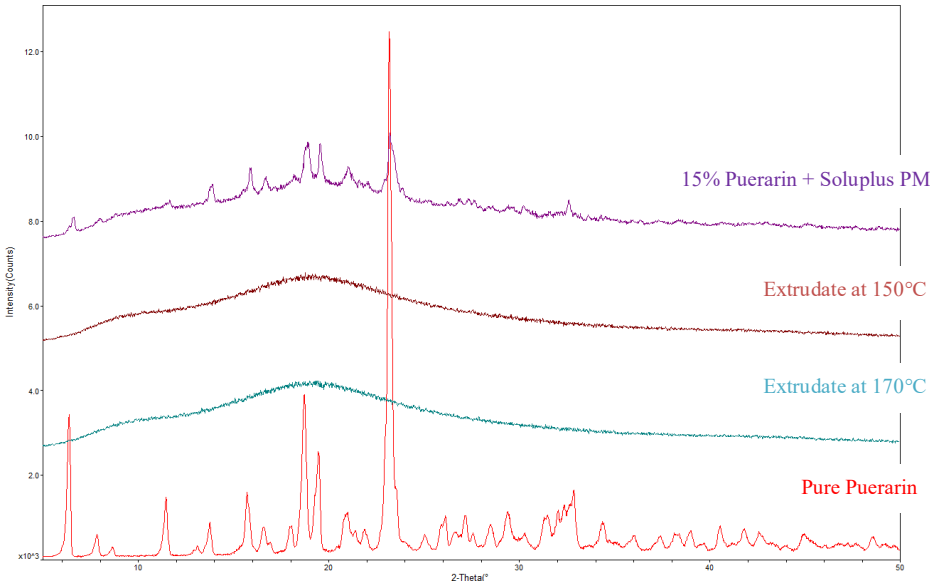

Figure B20 XRD spectra for Pure Puerarin, physical mixture and extrudates.

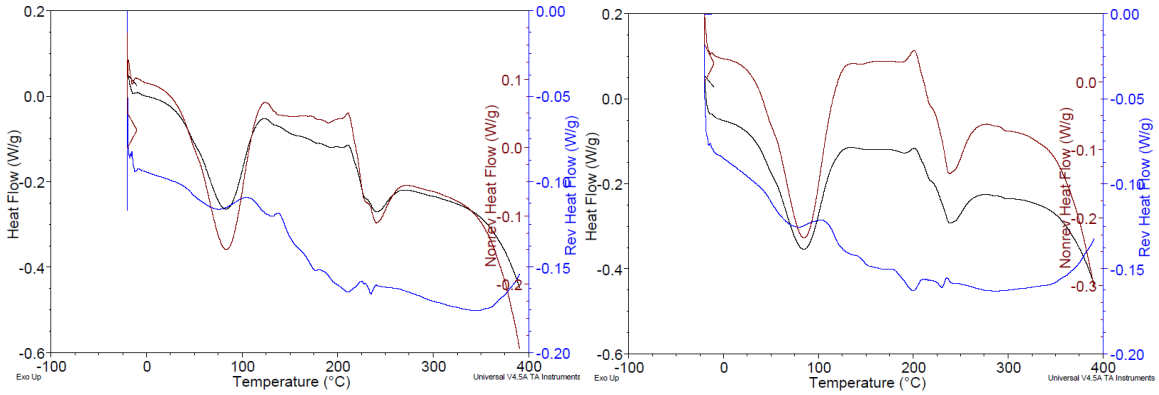

Figure B21 DSC spectra of the Breviscapine extrudates 140 °C and 150 °C.

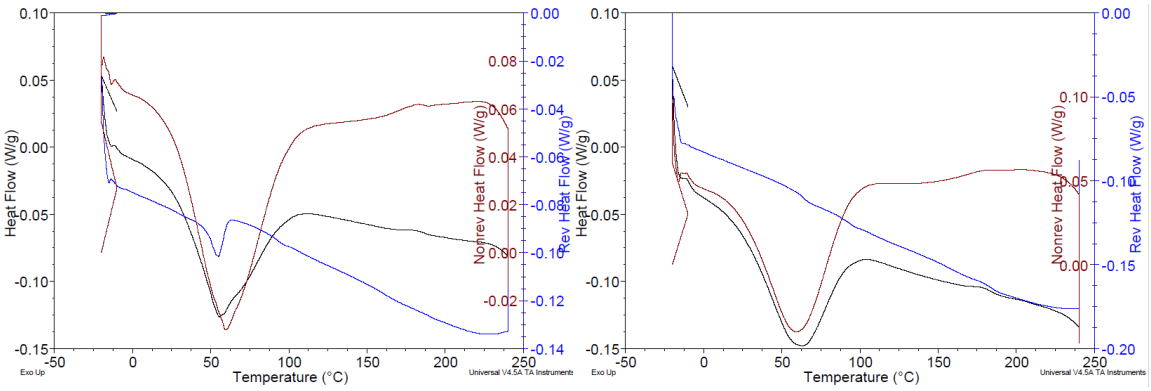

Figure B22 DSC analysis of Puerarin extrudates at 150 °C and 170°C.

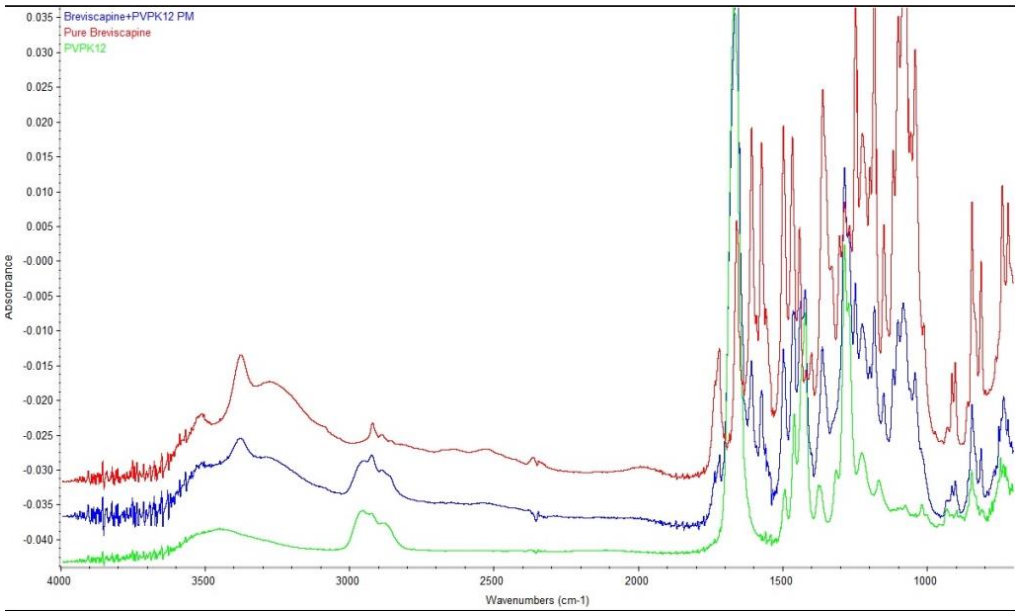

Figure B23 Spectra of Breviscapine (blue), PVPK12 (purple) and physical mixture (red).

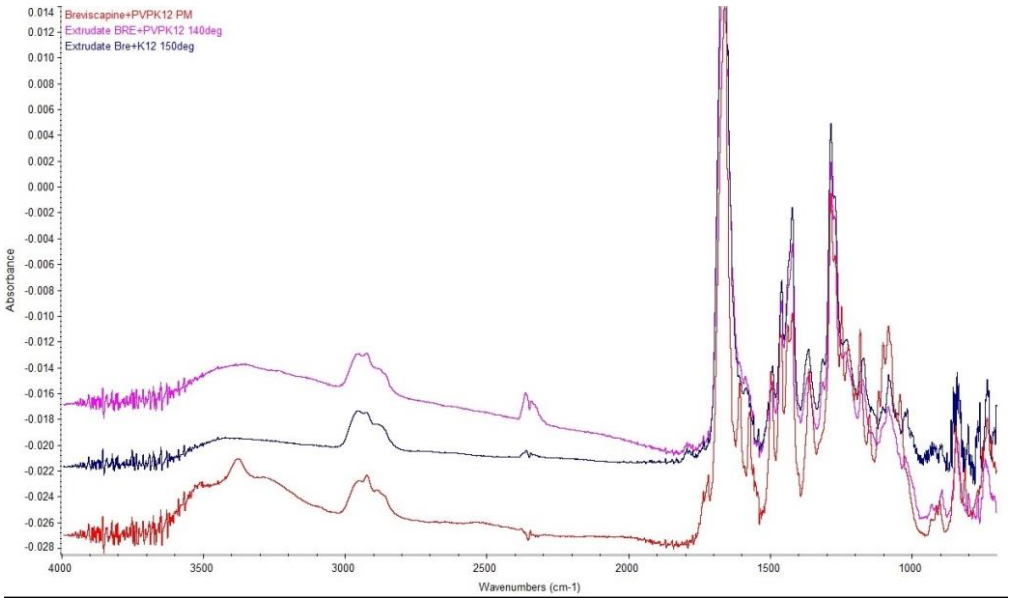

Figure B24 Spectra of physical mixture (blue) and the extrudates at 140 °C (purple) and 150 °C (red).

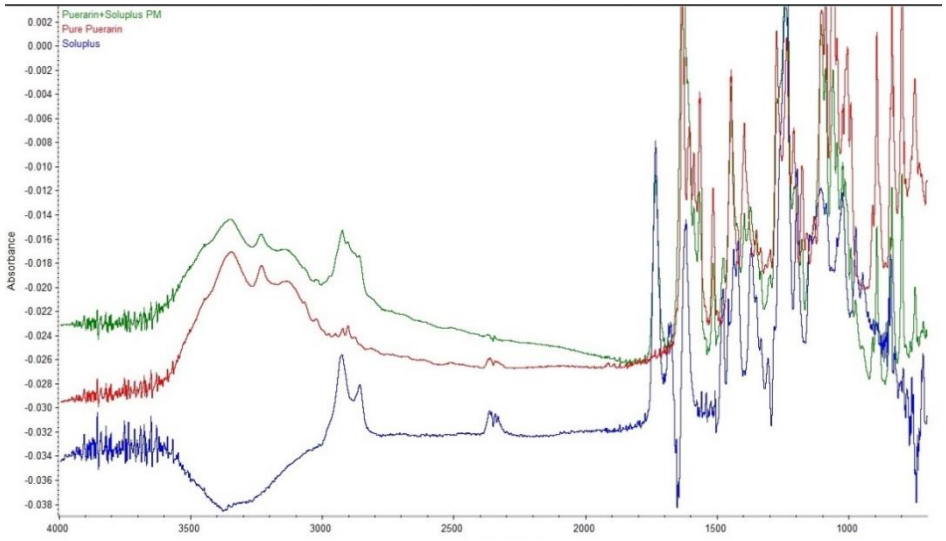

Figure B25 Spectra of Puerarin (green), Soluplus (blue) and physical mixture (red).

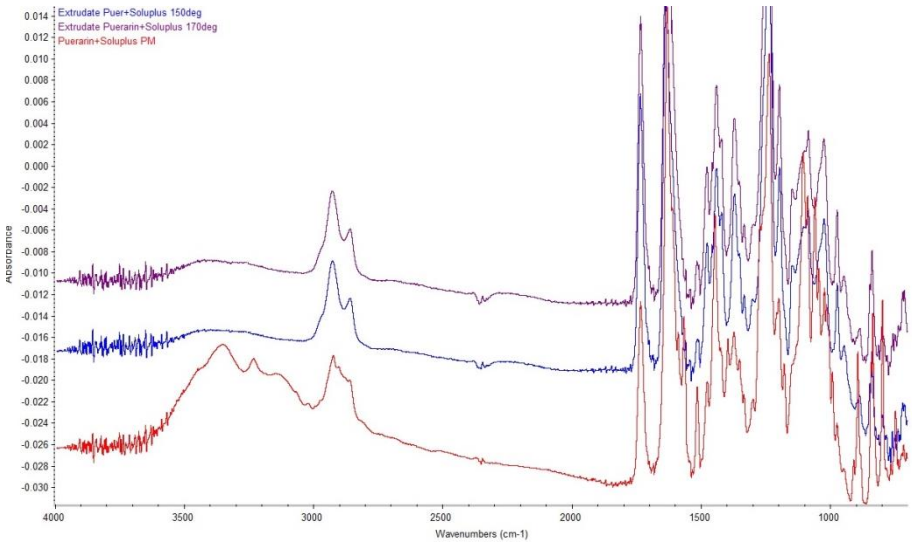

Figure B26 Spectra of the physical mixture (red) and the extrudates at 150 °C (purple) and 170 °C (green).

B.5 TABLES

Polymer	Before heating	After holding 10 min 60 °C above drug Tg	Before holding at 185 °C	After holding 10 min at 185 °C
PVP K12	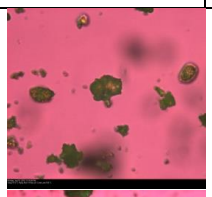	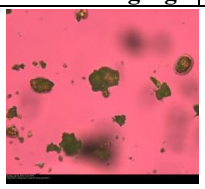	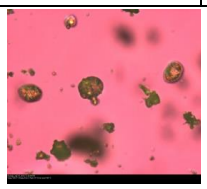	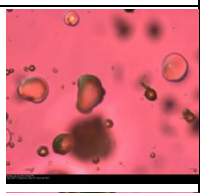
Affinisol		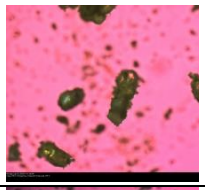	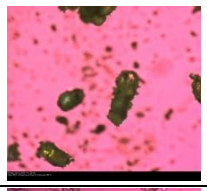	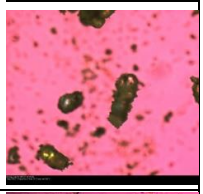
EPO	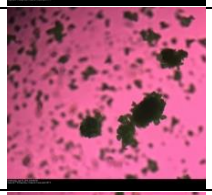	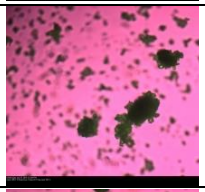	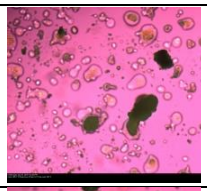	
Soluplus	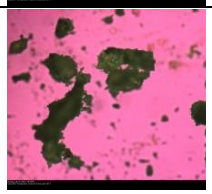	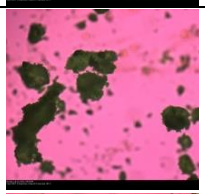	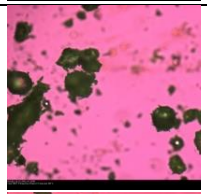	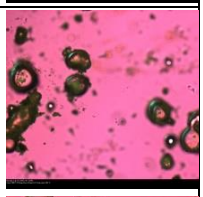
VA 64	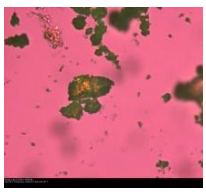	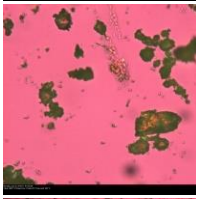	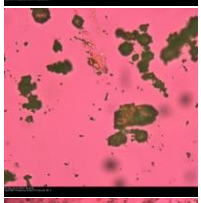	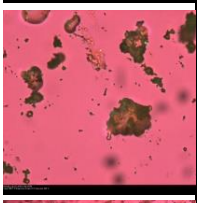
HPMC AS	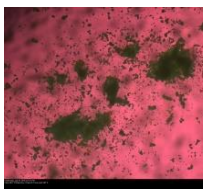	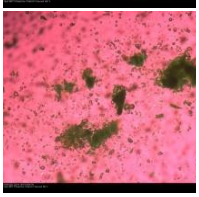	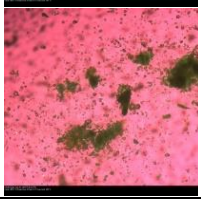	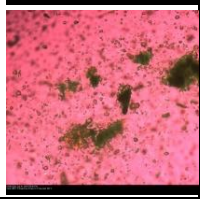

Table B1 Polymers miscibility study with Breviscapine.

Polymer	Before heating	After holding 10 min 60 °C above polymer Tg	Before holding 10 min at 185 °C	After holding 10 min at 185 °C
PVP K12	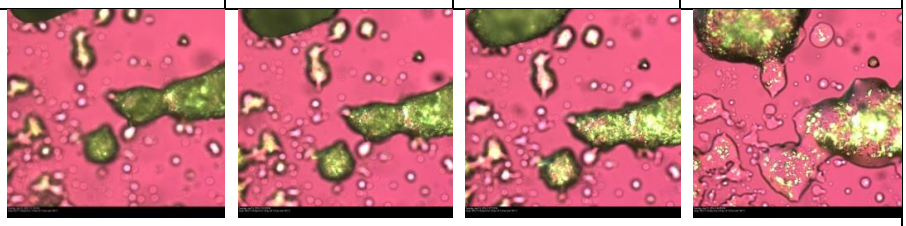			
Affinisol	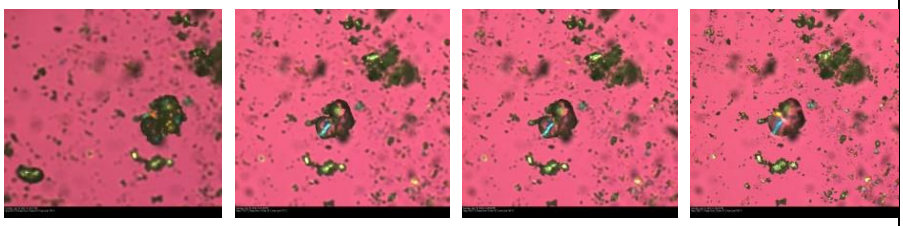			
EPO	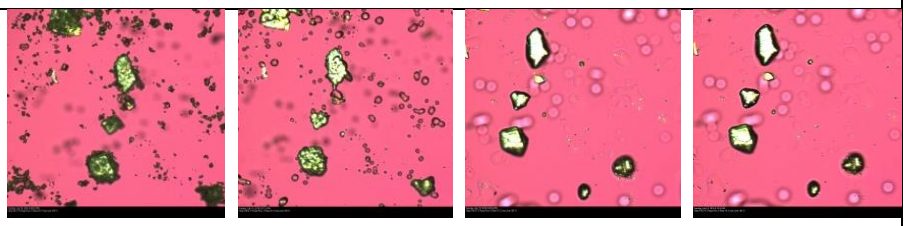			
Soluplus	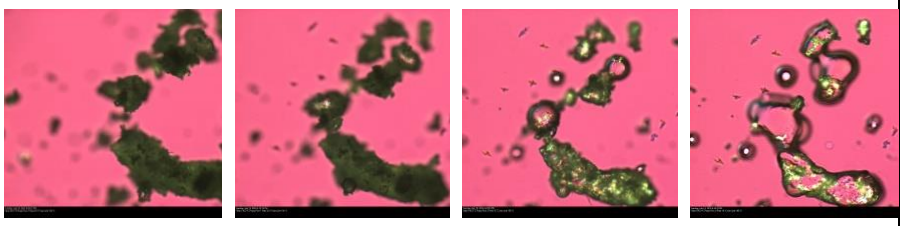			
VA64	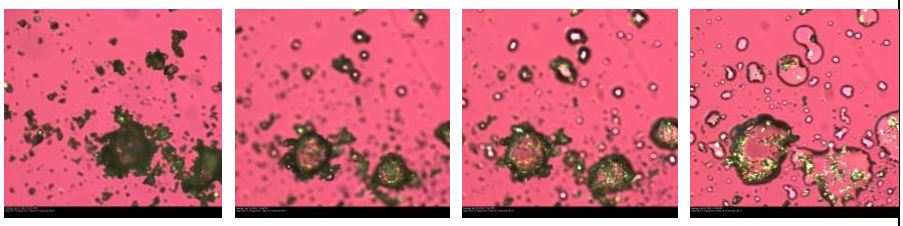			

Table B2 Polymer miscibility study with Puerarin.

Batch	Condition	Zone 1	Zone 2	Zone 3	Zone 4	Die	Torque (Gm)	Pressure (psi)	Melting T (℃)
1	Set	150	150	150	150	150	1300	0	165
	Real	150	151	151	150	150			
2	Set	130	130	130	130	130	Excessive (>2200)		
	Real	/	/	/	/	/			
3	Set	140	140	140	140	140	1600	0	154
	Real	140	143	143	140	140			

Table B3 Extrusion conditions for Breviscapine.

Batch	Condition	Zone 1 (°C)	Zone 2 (°C)	Zone 3 (°C)	Zone 4 (°C)	Die (°C)	Torque (Gm)	Pressure (psi)	Melt T°C
1	Set	150°	150	150	150	150	1600	0	166
	Real	150	154	155	150	150			
2	Set	170	170	170	170	170	1100	0	189
	Real	170	170	170	170	170			

Table B4 Extrusion conditions for Puerarin.

APPENDIX C: Investigating the Cation-π Interaction in a Drug-polymer Complex

C.1 INTRODUCTION

Numerous studies have shown the strong interactions between polymer and drug are important not only to maintain physical stabilities of amorphous solid dispersion (ASD) during and storage, and to achieve enhanced and sustained transient solubility of ASDs in aqueous medium. Other interactions have been studied. Cation–π interaction, which plays an important role in protein–ligand, protein-DNA interactions as well as maintaining protein structures, however, has not been studied in solid dispersions. This study was designed to investigate the effect of cation-π interaction on dissolution performance of solid

C.2 METHODS

Solid dispersions of 30% and 15% Carbamazepine (CBZ) and 70% EUDRAGIT® EPO were prepared using a NANO-16 twin screw extruder (Leistritz Advanced Technologies Corp.). Crystallinity in the HME extrudates was evaluated using differential scanning calorimetry (DSC) and powder X-ray diffraction (XRD). Dissolution testing was conducted under both sink and non-sink conditions using USP Apparatus II. FTIR and Raman spectroscopy were used to characterize drug-polymer interactions before and after polymer ionization. Discovery Studio (Accelrys Inc.) was used docking compound with polymers to predict molecular interactions.

C.3 RESULTS

XRD and DSC results indicated the existence of crystalline form of CBZ in the extrudates. Sink dissolution testing in neutral media revealed that the unprocessed carbamazepine was completely dissolved in 60 minutes, but the CBZ-EPO extrudate released only 40% at 2 hrs. Non-sink dissolution in acidic media testing revealed that 30% CBZ-EPO and 15% CBZ-EPO extrudate rapid released 55% and 80% of CBZ in solution at 15 minutes, respectively, reaching a 1.5 and 2.5-fold increase in drug concentration compared to equilibrium solubility. The concentration was maintained through 360 minutes. However, bulk CBZ reached its equilibrium concentration (30% CBZ released) at 2 hrs. The computational docking results suggested the existence Cation-π interaction between CBZ and EUDRAGIT® EPO, and the interaction was confirmed by FTIR and Raman spectroscopy.

C.4 CONCLUSIONS

Cation-π interaction has been observed between CBZ and EUDRAGIT® EPO, resulting in an increased dissolution rate and apparent solubility of the drug. Based on the results, this interaction between alkali metal or nitrogenous cation groups and the aromatic π system can be further studied and used to broaden drug candidate pool in the formulation screening process.

Bibliography

Administration, U.F.D., 2016. Orange book: approved drug products with therapeutic equivalence evaluations. Silver Spring, MD: US FDA.

Agrawal, A.M., Dudhedia, M.S., Patel, A.D., Raikes, M.S., 2013. Characterization and performance assessment of solid dispersions prepared by hot melt extrusion and spray drying process. International Journal of Pharmaceutics 457, 71-81.

Alderman, D.A., Wolford, T.D., 1987. Sustained release dosage form based on highly plasticized cellulose ether gels. US Patent 4,678,516.

Alexy, P., Káchová, D., Kršiak, M., Bakoš, D., Šimková, B., 2002. Poly(vinyl alcohol) stabilisation in thermoplastic processing. Polymer Degradation and Stability 78, 413-421.

Alonzo, D., Zhang, G.Z., Zhou, D., Gao, Y., Taylor, L., 2010. Understanding the Behavior of Amorphous Pharmaceutical Systems during Dissolution. Pharm Res 27, 608-618.

Alsante, K.M., Huynh-Ba, K., Baertschi, S.W., Reed, R.A., Landis, M.S., Kleinman, M.H., Foti, C., Rao, V.M., Meers, P., Abend, A., Reynolds, D.W., Joshi, B.K., 2014. Recent Trends in Product Development and Regulatory Issues on Impurities in

Active Pharmaceutical Ingredient (API) and Drug Products. Part 1: Predicting Degradation Related Impurities and Impurity Considerations for Pharmaceutical Dosage Forms. AAPS PharmSciTech 15, 198-212.

Amidon, G.L., Lennernäs, H., Shah, V.P., Crison, J.R., 1995. A Theoretical Basis for a Biopharmaceutic Drug Classification: The Correlation of in Vitro Drug Product Dissolution and in Vivo Bioavailability. Pharmaceutical Research 12, 413-420.

Andrews, G.P., Abu-Diak, O., Kusmanto, F., Hornsby, P., Hui, Z., Jones, D.S., 2010. Physicochemical characterization and drug-release properties of celecoxib hot-melt extruded glass solutions. Journal of Pharmacy and Pharmacology 62, 1580-1590.

Andronis, V., Zografi, G., 2000. Crystal nucleation and growth of indomethacin polymorphs from the amorphous state. Journal of Non-Crystalline Solids 271, 236-248.

ASTM, E1269-11. Standard test method for determining specific heat capacity by differential scanning calorimetry. ASTM International, West Conshohocken, PA, USA.

Babu, N.J., Nangia, A., 2011. Solubility Advantage of Amorphous Drugs and Pharmaceutical Cocrystals. Crystal Growth & Design 11, 2662-2679.

Baert, L.E.C., Verreck, G., Thoné, D., 2003. Antifungal compositions with improved bioavailability. US 6509038.

Baird, J.A., Taylor, L.S., 2012. Evaluation of amorphous solid dispersion properties using thermal analysis techniques. Advanced Drug Delivery Reviews 64, 396-421.

Banik, M., Gopi, S.P., Ganguly, S., Desiraju, G.R., 2016. Cocrystal and Salt Forms of Furosemide: Solubility and Diffusion Variations. Crystal Growth & Design 16, 5418-5428.

Bansal, G., Singh, M., Jindal, K.C., 2007. Forced Degradation Study on Gliclazide and Application of Validated Stability-Indicating HPLC-UV Method in Stability Testing of Gliclazide Tablets. Chromatographia 66, 751-755.

Bansal, G., Singh, M., Jindal, K.C., Singh, S., 2008. Characterization of Mass Ionizable Degradation Products of Gliclazide by LC/ESI-MS. Journal of Liquid Chromatography & Related Technologies 31, 2174-2193.

Baronsky-Probst, J., Möltgen, C.V., Kessler, W., Kessler, R.W., 2016. Process design and control of a twin screw hot melt extrusion for continuous pharmaceutical tamper-resistant tablet production. European Journal of Pharmaceutical Sciences 87, 14-21.

Bellantone, R.A., Patel, P., Sandhu, H., Choi, D.S., Singhal, D., Chokshi, H., Malick, A.W., Shah, N., 2012. A method to predict the equilibrium solubility of drugs in solid polymers near room temperature using thermal analysis. Journal of Pharmaceutical Sciences 101, 4549-4558.

Benet, L.Z., 2010. Predicting Drug Disposition via Application of a Biopharmaceutics Drug Disposition Classification System. Basic & Clinical Pharmacology & Toxicology 106, 162-167.

Bennett, R.C., Brough, C., Miller, D.A., O'Donnell, K.P., Keen, J.M., Hughey, J.R., Williams, R.O., McGinity, J.W., 2015. Preparation of amorphous solid dispersions by rotary evaporation and KinetiSol Dispersing: approaches to enhance solubility of a poorly water-soluble gum extract. Drug Development and Industrial Pharmacy 41, 382-397.

Berndl, G., Degenhardt, M., Mäegerlein, M., Dispersyn, G., 2013. Itraconazole compositions with improved bioavailability. US Patent 8,486,456.

Bhardwaj, S.P., Suryanarayanan, R., 2012. Molecular Mobility as an Effective Predictor of the Physical Stability of Amorphous Trehalose. Molecular Pharmaceutics 9, 3209-3217.

Bhugra, C., Pikal, M.J., 2008. Role of thermodynamic, molecular, and kinetic factors in crystallization from the amorphous state. Journal of Pharmaceutical Sciences 97, 1329-1349.

Bhugra, C., Rambhatla, S., Bakri, A., Duddu, S.P., Miller, D.P., Pikal, M.J., Lechuga-Ballesteros, D., 2007. Prediction of the onset of crystallization of amorphous sucrose below the calorimetric glass transition temperature from correlations with mobility. Journal of Pharmaceutical Sciences 96, 1258-1269.

Birtalan, E., Hoelig, P., Lindley, D.J., Sanzgiri, Y.D., Tong, P., 2012. Melt-extruded solid dispersions containing an apoptosis-inducing agent. US 20120108590.

Blessy, M., Patel, R.D., Prajapati, P.N., Agrawal, Y.K., 2014. Development of forced degradation and stability indicating studies of drugs—A review. Journal of Pharmaceutical Analysis 4, 159-165.

Boersen, N., Brown, C., DiNunzio, J., Johnson, D., Marsac, P., Meyer, R., McKelvey, C., 2015. Hot-Melt Extrusion: The Process-Product-Performance Interplay, in: Templeton, A.C., Byrn, S.R., Haskell, R.J., Prisinzano, T.E. (Eds.), Discovering and Developing Molecules with Optimal Drug-Like Properties. Springer New York, New York, NY, pp. 345-381.

Breitenbach, J., 2002. Melt extrusion: from process to drug delivery technology. European Journal of Pharmaceutics and Biopharmaceutics 54, 107-117.

Brough, C., Williams, R.O., 2013. Amorphous solid dispersions and nano-crystal technologies for poorly water-soluble drug delivery. International Journal of Pharmaceutics 453, 157-166.

Bruce, C., Manning, M., 2009. Melt extruded nicotine thin strips. US Patent 20130011462 A1.

Childs, S.L., Kandi, P., Lingireddy, S.R., 2013. Formulation of a Danazol Cocrystal with Controlled Supersaturation Plays an Essential Role in Improving Bioavailability. Molecular Pharmaceutics 10, 3112-3127.

Childs, S.L., Rodriguez-Hornedo, N., Reddy, L.S., Jayasankar, A., Maheshwari, C., McCausland, L., Shipplett, R., Stahly, B.C., 2008. Screening strategies based on solubility and solution composition generate pharmaceutically acceptable cocrystals of carbamazepine. CrystEngComm 10, 856-864.

Cohen, C., Tanny, G.B., Prager, S., 1979. Diffusion-controlled formation of porous structures in ternary polymer systems. Journal of Polymer Science: Polymer Physics Edition 17, 477-489.

Coppens, K., Hall, M., Larsen, P., Mitchell, S., Nguyen, P., Read, M., Shrestha, U., Walia, P., 2004. Thermal and rheological evaluation of pharmaceutical excipients for hot melt extrusion, AAPS Annual Meeting and Exposition, Baltimore, MD.

Coppens, K.A., Hall, M.J., Mitchell, S.A., Read, M.D., 2006. Hypromellose, ethylcellulose, and polyethylene oxide use in hot melt extrusion: hot melt extrusion (HME) formulation development depends heavily on choosing the appropriate polymers. This article reviews HME process parameters and highlights three polymers in HME: polyethylene oxide, ethylcellulose, and hypromellose, Pharmaceutical Technology, p. 62+.

Crowley, K.J., Zografi, G., 2002. Water vapor absorption into amorphous hydrophobic drug/poly(vinylpyrrolidone) dispersions. Journal of Pharmaceutical Sciences 91, 2150-2165.

Crowley, M.M., Zhang, F., Repka, M.A., Thumma, S., Upadhye, S.B., Kumar Battu, S., McGinity, J.W., Martin, C., 2007. Pharmaceutical Applications of Hot-Melt Extrusion: Part I. Drug Development and Industrial Pharmacy 33, 909-926.

Curatolo, W.J., Niantic, C., 1999. Solid pharmaceutical dispersions with enhanced bioavailability. EP 0901786 A2.

De Jaeghere, W., De Beer, T., Van Bocxlaer, J., Remon, J.P., Vervaet, C., 2015. Hot-melt extrusion of polyvinyl alcohol for oral immediate release applications. International Journal of Pharmaceutics 492, 1-9.

DiNunzio, J.C., Brough, C., Hughey, J.R., Miller, D.A., Williams III, R.O., McGinity, J.W., 2010. Fusion production of solid dispersions containing a heat-sensitive active ingredient by hot melt extrusion and Kinetisol® dispersing. European Journal of Pharmaceutics and Biopharmaceutics 74, 340-351.

DiNunzio, J.C., Brough, C., Miller, D.A., Williams III, R.O., McGinity, J.W., 2010c. Applications of KinetiSol® Dispersing for the production of plasticizer free amorphous solid dispersions. European Journal of Pharmaceutical Sciences 40, 179-187.

DiNunzio, J.C., Brough, C., Miller, D.A., Williams, R.O., McGinity, J.W., 2010d. Fusion processing of itraconazole solid dispersions by kinetisol® dispersing: A comparative study to hot melt extrusion. Journal of Pharmaceutical Sciences 99, 1239-1253.

DiNunzio, J.C., Miller, D.A., 2013. Formulation Development of Amorphous Solid Dispersions Prepared by Melt Extrusion, in: Repka, M.A., Langley, N., DiNunzio,

J. (Eds.), Melt Extrusion: Materials, Technology and Drug Product Design. Springer New York, New York, NY, pp. 161-203.

DiNunzio, J.C., Zhang, F., Martin, C., McGinity, J.W., 2012. Melt Extrusion, in: Williams III, R.O., Watts, A.B., Miller, D.A. (Eds.), Formulating Poorly Water Soluble Drugs. Springer New York, New York, NY, pp. 311-362.

Djuris, J., Nikolakakis, I., Ibric, S., Djuric, Z., Kachrimanis, K., 2013. Preparation of carbamazepine–Soluplus® solid dispersions by hot-melt extrusion, and prediction of drug–polymer miscibility by thermodynamic model fitting. European Journal of Pharmaceutics and Biopharmaceutics 84, 228-237.

Dong, Z., Chatterji, A., Sandhu, H., Choi, D.S., Chokshi, H., Shah, N., 2008. Evaluation of solid state properties of solid dispersions prepared by hot-melt extrusion and solvent co-precipitation. International Journal of Pharmaceutics 355, 141-149.

El-Egakey, M.A., Soliva, M., Speiser, P., 1971. Hot extruded dosage forms. I. Technology and dissolution kinetics of polymeric matrices. Pharmaceutica Acta Helvetiae 46, 31-52.

Flory, P.J., 1942a. Thermodynamics of high polymer solutions. Journal of Chemical Physics 10, 51-61.

Flory, P.J., 1953. Principles of polymer chemistry. Cornell University Press, Ithaca, New York, NY.

Follonier, N., Doelker, E., Cole, E.T., 1995. Various ways of modulating the release of diltiazem hydrochloride from hot-melt extruded sustained release pellets prepared using polymeric materials. Journal of Controlled Release 36, 243-250.

Forster, A., Hempenstall, J., Rades, T., 2001. Characterization of glass solutions of poorly water-soluble drugs produced by melt extrusion with hydrophilic amorphous polymers. Journal of Pharmacy and Pharmacology 53, 303-315.

Fountain, A.W., Vickers, T.J., Mann, C.K., 1998. Factors that Affect the Accuracy of Raman Shift Measurements on Multichannel Spectrometers. Appl. Spectrosc. 52, 462-468.

Frank, K.J., Rosenblatt, K.M., Westedt, U., Hölig, P., Rosenberg, J., Mägerlein, M., Fricker, G., Brandl, M., 2012. Amorphous solid dispersion enhances permeation of poorly soluble ABT-102: True supersaturation vs. apparent solubility enhancement. International Journal of Pharmaceutics 437, 288-293.

Furfine, E.S., Baker, C.T., Hale, M.R., Reynolds, D.J., Salisbury, J.A., Searle, A.D., Studenberg, S.D., Todd, D., Tung, R.D., Spaltenstein, A., 2004. Preclinical

pharmacology and pharmacokinetics of GW433908, a water-soluble prodrug of the human immunodeficiency virus protease inhibitor amprenavir. Antimicrobial agents and chemotherapy 48, 791-798.

Ghebremeskel, A.N., Vemavarapu, C., Lodaya, M., 2007. Use of surfactants as plasticizers in preparing solid dispersions of poorly soluble API: Selection of polymer–surfactant combinations using solubility parameters and testing the processability. International Journal of Pharmaceutics 328, 119-129.

Ghosh, I., Vippagunta, R., Li, S., Vippagunta, S., 2012. Key considerations for optimization of formulation and melt-extrusion process parameters for developing thermosensitive compound. Pharmaceutical Development and Technology 17, 502-510.

Gogos, C.G., Liu, H., Wang, P., 2012. Laminar Dispersive and Distributive Mixing with Dissolution and Applications to Hot-Melt Extrusion, Hot-Melt Extrusion: Pharmaceutical Applications. John Wiley & Sons, Ltd, pp. 261-284.

Gordon, M., Taylor, J.S., 1952. Ideal copolymers and the second-order transitions of synthetic rubbers. i. non-crystalline copolymers. Journal of Applied Chemistry 2, 493-500.

Grzesiak, A.L., Lang, M., Kim, K., Matzger, A.J., 2003. Comparison of the four anhydrous polymorphs of carbamazepine and the crystal structure of form I. Journal of Pharmaceutical Sciences 92, 2260-2271.

Guns, S., Dereymaker, A., Kayaert, P., Mathot, V., Martens, J.A., Van den Mooter, G., 2011. Comparison Between Hot-Melt Extrusion and Spray-Drying for Manufacturing Solid Dispersions of the Graft Copolymer of Ethylene Glycol and Vinylalcohol. Pharmaceutical Research 28, 673-682.

Guo, Y., Byrn, S.R., Zografi, G., 2000. Physical characteristics and chemical degradation of amorphous quinapril hydrochloride. Journal of Pharmaceutical Sciences 89, 128-143.

Gupta, S.S., Solanki, N., Serajuddin, A.T.M., 2016. Investigation of Thermal and Viscoelastic Properties of Polymers Relevant to Hot Melt Extrusion, IV: Affinisol™ HPMC HME Polymers. AAPS PharmSciTech 17, 148-157.

Hancock, B.C., Parks, M., What is the True Solubility Advantage for Amorphous Pharmaceuticals? Pharmaceutical Research 17, 397-404.

Hancock, B.C., Shamblin, S.L., Zografi, G., 1995. Molecular Mobility of Amorphous Pharmaceutical Solids Below Their Glass Transition Temperatures. Pharmaceutical Research 12, 799-806.

Hancock, B.C., Zografi, G., The Use of Solution Theories for Predicting Water Vapor Absorption by Amorphous Pharmaceutical Solids: A Test of the Flory–Huggins and Vrentas Models. Pharmaceutical Research 10, 1262-1267.

Hauss, D.J., 2007. Oral lipid-based formulations. Advanced Drug Delivery Reviews 59, 667-676.

Hengsawas Surasarang, S., Keen, J.M., Huang, S., Zhang, F., McGinity, J.W., Williams, R.O., 2016. Hot melt extrusion versus spray drying: hot melt extrusion degrades albendazole. Drug Development and Industrial Pharmacy, 1-15.

Ho, R., Naderi, M., Heng, J.Y.Y., Williams, D.R., Thielmann, F., Bouza, P., Keith, A.R., Thiele, G., Burnett, D.J., 2012. Effect of Milling on Particle Shape and Surface Energy Heterogeneity of Needle-Shaped Crystals. Pharmaceutical Research 29, 2806-2816.

Höckerfelt, M.H., Alderborn, G., 2014. The crystallinity of cellulose controls the physical distribution of sorbed water and the capacity to present water for chemical degradation of a solid drug. International Journal of Pharmaceutics 477, 326-333.

Hovorka, S.W., Schöneich, C., 2001. Oxidative degradation of pharmaceuticals: Theory, mechanisms and inhibition. Journal of Pharmaceutical Sciences 90, 253-269.

Huang, S., O'Donnell, K.P., Keen, J.M., Rickard, M.A., McGinity, J.W., Williams, R.O., 2016. A New Extrudable Form of Hypromellose: AFFINISOL™ HPMC HME. AAPS PharmSciTech 17, 106-119.

Huang, S., Mao, C., Williams, R. O., Yang, C. Y. Solubility Advantage (and Disadvantage) of Pharmaceutical Amorphous Solid Dispersions. Journal of Pharmaceutical Sciences 105, 3549-3561.

Huggins, M.L., 1942. THERMODYNAMIC PROPERTIES OF SOLUTIONS OF LONG-CHAIN COMPOUNDS. Annals of the New York Academy of Sciences 43, 1-32.

Hughey, J.R., DiNunzio, J.C., Bennett, R.C., Brough, C., Miller, D.A., Ma, H., Williams, R.O., McGinity, J.W., 2010. Dissolution Enhancement of a Drug Exhibiting Thermal and Acidic Decomposition Characteristics by Fusion Processing: A

Comparative Study of Hot Melt Extrusion and KinetiSol® Dispersing. AAPS PharmSciTech 11, 760-774.

Hughey, J.R., Keen, J.M., Brough, C., Saeger, S., McGinity, J.W., 2011. Thermal processing of a poorly water-soluble drug substance exhibiting a high melting point: The utility of KinetiSol® Dispersing. International Journal of Pharmaceutics 419, 222-230.

Hughey, J.R., Keen, J.M., Miller, D.A., Brough, C., McGinity, J.W., 2012. Preparation and characterization of fusion processed solid dispersions containing a viscous thermally labile polymeric carrier. International Journal of Pharmaceutics 438, 11-19.

Janssens, S., Van den Mooter, G., 2009. Review: physical chemistry of solid dispersions. Journal of Pharmacy and Pharmacology 61, 1571-1586.

Javeer, S.D., Patole, R., Amin, P., 2013. Enhanced solubility and dissolution of simvastatin by HPMC-based solid dispersions prepared by hot melt extrusion and spray-drying method. Journal of Pharmaceutical Investigation 43, 471-480.

Jayasankar, A., Reddy, L.S., Bethune, S.J., Rodríguez-Hornedo, N., 2009. Role of Cocrystal and Solution Chemistry on the Formation and Stability of Cocrystals with Different Stoichiometry. Crystal Growth & Design 9, 889-897.

Jung, J.-Y., Yoo, S.D., Lee, S.-H., Kim, K.-H., Yoon, D.-S., Lee, K.-H., 1999. Enhanced solubility and dissolution rate of itraconazole by a solid dispersion technique. International Journal of Pharmaceutics 187, 209-218.

Keseru, G.M., Makara, G.M., 2009. The influence of lead discovery strategies on the properties of drug candidates. Nat Rev Drug Discov 8, 203-212.

Kestur, U.S., Ivanesivic, I., Alonzo, D.E., Taylor, L.S., 2013. Influence of particle size on the crystallization kinetics of amorphous felodipine powders. Powder Technology 236, 197-204.

Kim, M.-S., Jin, S.-J., Kim, J.-S., Park, H.J., Song, H.-S., Neubert, R.H.H., Hwang, S.-J., 2008. Preparation, characterization and in vivo evaluation of amorphous atorvastatin calcium nanoparticles using supercritical antisolvent (SAS) process. European Journal of Pharmaceutics and Biopharmaceutics 69, 454-465.

Kipping, T., Rein, H., 2013. A new method for the continuous production of single dosed controlled release matrix systems based on hot-melt extruded starch: Analysis of

relevant process parameters and implementation of an in-process control. European Journal of Pharmaceutics and Biopharmaceutics 84, 156-171.

Kobayashi, Y., Ito, S., Itai, S., Yamamoto, K., 2000. Physicochemical properties and bioavailability of carbamazepine polymorphs and dihydrate. International Journal of Pharmaceutics 193, 137-146.

Kohlgrüber, K., 2012. Co-rotating twin-screw extruder. Carl Hanser Verlag GmbH Co KG.

Kolter, K., Karl, M., Gryczke, A., Ludwigshafen am Rhein, B., 2012. Hot-melt extrusion with BASF pharma polymers: extrusion compendium. BASF.

Koningsveld, R., Stockmayer, W.H., Nies, E., 2001. Polymer Phase Diagrams. Oxford University Press, New York, NY, USA.

Konno, H., Handa, T., Alonzo, D.E., Taylor, L.S., 2008. Effect of polymer type on the dissolution profile of amorphous solid dispersions containing felodipine. European Journal of Pharmaceutics and Biopharmaceutics 70, 493-499.

LaFountaine, J.S., Jermain, S.V., Prasad, L.K., Brough, C., Miller, D.A., Lubda, D., McGinity, J.W., Williams III, R.O., 2016a. Enabling thermal processing of ritonavir–polyvinyl alcohol amorphous solid dispersions by KinetiSol® Dispersing. European Journal of Pharmaceutics and Biopharmaceutics 101, 72-81.

Lakshman, J.P., Cao, Y., Kowalski, J., Serajuddin, A.T.M., 2008. Application of Melt Extrusion in the Development of a Physically and Chemically Stable High-Energy Amorphous Solid Dispersion of a Poorly Water-Soluble Drug. Molecular Pharmaceutics 5, 994-1002.

Lang, B., Liu, S., McGinity, J.W., Williams, R.O., 2016. Effect of hydrophilic additives on the dissolution and pharmacokinetic properties of itraconazole-enteric polymer hot-melt extruded amorphous solid dispersions. Drug Development and Industrial Pharmacy 42, 429-445.

Lang, B., McGinity, J.W., Williams, R.O., 2014a. Dissolution Enhancement of Itraconazole by Hot-Melt Extrusion Alone and the Combination of Hot-Melt Extrusion and Rapid Freezing—Effect of Formulation and Processing Variables. Molecular Pharmaceutics 11, 186-196.

Lang, B., McGinity, J.W., Williams, R.O., 2014b. Hot-melt extrusion – basic principles and pharmaceutical applications. Drug Development and Industrial Pharmacy 40, 1133-1155.

Law, D., Schmitt, E.A., Marsh, K.C., Everitt, E.A., Wang, W., Fort, J.J., Krill, S.L., Qiu, Y., 2004. Ritonavir–PEG 8000 amorphous solid dispersions: In vitro and in vivo evaluations. Journal of Pharmaceutical Sciences 93, 563-570.

Lee, K.W.Y., Porter, C.J.H., Boyd, B.J., 2013. The effect of administered dose of lipid-based formulations on the In Vitro and In Vivo performance of cinnarizine as a model poorly water-soluble drug. Journal of Pharmaceutical Sciences 102, 565-578.

Leuner, C., Dressman, J., 2000. Improving drug solubility for oral delivery using solid dispersions. European Journal of Pharmaceutics and Biopharmaceutics 50, 47-60.

Leung, S.S., Grant, D.J.W., 1997. Solid state stability studies of model dipeptides: Aspartame and aspartylphenylalanine. Journal of Pharmaceutical Sciences 86, 64-71.

Li, Y., Pang, H., Guo, Z., Lin, L., Dong, Y., Li, G., Lu, M., Wu, C., 2014. Interactions between drugs and polymers influencing hot melt extrusion. Journal of Pharmacy and Pharmacology 66, 148-166.

Lin, D., Huang, Y., 2010. A thermal analysis method to predict the complete phase diagram of drug–polymer solid dispersions. International Journal of Pharmaceutics 399, 109-115.

Lipinski, C.A., 2000. Drug-like properties and the causes of poor solubility and poor permeability. Journal of Pharmacological and Toxicological Methods 44, 235-249.

Lipinski, C.A., Lombardo, F., Dominy, B.W., Feeney, P.J., 2012. Experimental and computational approaches to estimate solubility and permeability in drug discovery and development settings. Advanced Drug Delivery Reviews 64, Supplement, 4-17.

Liu, J., Cao, F., Zhang, C., Ping, Q., 2013. Use of polymer combinations in the preparation of solid dispersions of a thermally unstable drug by hot-melt extrusion. Acta Pharmaceutica Sinica B 3, 263-272.

Liu, X., Lu, M., Guo, Z., Huang, L., Feng, X., Wu, C., 2012. Improving the Chemical Stability of Amorphous Solid Dispersion with Cocrystal Technique by Hot Melt Extrusion. Pharm Res 29, 806-817.

Lu, X., Weiss, R.A., 1992. Relationship between the glass transition temperature and the interaction parameter of miscible binary polymer blends. Macromolecules 25, 3242-3246.

Madsen, C.M., Boyd, B., Rades, T., Müllertz, A., 2016. Supersaturation of zafirlukast in fasted and fed state intestinal media with and without precipitation inhibitors. European Journal of Pharmaceutical Sciences 91, 31-39.

Maggi, L., Canobbio, A., Bruni, G., Musitelli, G., Conte, U., 2015. Improvement of the dissolution behavior of gliclazide, a slightly soluble drug, using solid dispersions. Journal of Drug Delivery Science and Technology 26, 17-23.

Mahmah, O., Tabbakh, R., Kelly, A., Paradkar, A., 2014. A comparative study of the effect of spray drying and hot-melt extrusion on the properties of amorphous solid dispersions containing felodipine. Journal of Pharmacy and Pharmacology 66, 275-284.

Maincent, J.P., Najvar, L.K., Kirkpatrick, W.R., Huang, S., Patterson, T.F., Wiederhold, N.P., Peters, J.I., Williams, R.O., 2016. Modified release itraconazole amorphous solid dispersion to treat Aspergillus fumigatus: importance of the animal model selection. Drug Development and Industrial Pharmacy, 1-11.

Maniruzzaman, M., Boateng, J.S., Bonnefille, M., Aranyos, A., Mitchell, J.C., Douroumis, D., 2012. Taste masking of paracetamol by hot-melt extrusion: An in vitro and in vivo evaluation. European Journal of Pharmaceutics and Biopharmaceutics 80, 433-442.

Marsac, P., Li, T., Taylor, L., 2009. Estimation of Drug–Polymer Miscibility and Solubility in Amorphous Solid Dispersions Using Experimentally Determined Interaction Parameters. Pharm Res 26, 139-151.

Marsac, P., Shamblin, S., Taylor, L., 2006. Theoretical and Practical Approaches for Prediction of Drug–Polymer Miscibility and Solubility. Pharm Res 23, 2417-2426.

Marsac, P.J., Li, T., Taylor, L.S., 2008. Estimation of Drug–Polymer Miscibility and Solubility in Amorphous Solid Dispersions Using Experimentally Determined Interaction Parameters. Pharmaceutical Research 26, 139-151.

Marsac, P.J., Rumondor, A.C.F., Nivens, D.E., Kestur, U.S., Stanciu, L., Taylor, L.S., 2010. Effect of temperature and moisture on the miscibility of amorphous dispersions of felodipine and poly(vinyl pyrrolidone). Journal of Pharmaceutical Sciences 99, 169-185.

Martin, C., 2008. Continous Mixing of Solid Dosage Forms via Hot-Melt Extrusion. Pharmaceutical Technology 32, 76-86.

Matsumoto, T., Zografi, G., 1999. Physical Properties of Solid Molecular Dispersions of Indomethacin with Poly(vinylpyrrolidone) and Poly(vinylpyrrolidone-co-vinyl-acetate) in Relation to Indomethacin Crystallization. Pharm Res 16, 1722-1728.

McGinity, J.W., Felton, L.A., 2013. Aqueous polymeric coatings for pharmaceutical dosage forms. CRC Press.

Mehuys, E., Vervaet, C., Gielen, I., Van Bree, H., Remon, J.P., 2004. In vitro and in vivo evaluation of a matrix-in-cylinder system for sustained drug delivery. Journal of Controlled Release 96, 261-271.

Meloche, I., Laidler, K.J., 1951. Substituent Effects in the Acid and Base Hydrolyses of Aromatic Amides1. Journal of the American Chemical Society 73, 1712-1714.

Mijatovic, D., Eijkel, J., Van Den Berg, A., 2005. Technologies for nanofluidic systems: top-down vs. bottom-up—a review. Lab on a Chip 5, 492-500.

Miller, D.A., Keen, J.M., 2014. KinetiSol®-Based Amorphous Solid Dispersions, in: Shah, N., Sandhu, H., Choi, D.S., Chokshi, H., Malick, A.W. (Eds.), Amorphous Solid Dispersions: Theory and Practice. Springer New York, New York, NY, pp. 567-577.

Miller, D.A., Keen, J.M., Brough, C., Kucera, S.U., Ellenberger, D.J., 2016. Improved formulations of vemurafenib and methods of making the same WO 2016073421 A1.

Mitchell, S.M., Ullman, J.L., Teel, A.L., Watts, R.J., 2014. pH and temperature effects on the hydrolysis of three β-lactam antibiotics: Ampicillin, cefalotin and cefoxitin. Science of The Total Environment 466, 547-555.

Mizoe, T., Ozeki, T., Okada, H., 2008. Application of a Four-fluid Nozzle Spray Drier to Prepare Inhalable Rifampicin-containing Mannitol Microparticles. AAPS PharmSciTech 9, 755-761.

More, S.D., Sontakke, S.B., 2013. Solubility Enhancement Of Gliclazide By Solid Dispersion Method. Asian Journal Of Pharmaceutical And Clinical Research 6, 91-98.

Morishita, M., Peppas, N.A., 2006. Is the oral route possible for peptide and protein drug delivery? Drug Discovery Today 11, 905-910.

Mujumdar, A.S., 2014. Handbook of industrial drying. Crc Press.

Murdande, S.B., Pikal, M.J., Shanker, R.M., Bogner, R.H., 2010a. Solubility advantage of amorphous pharmaceuticals: I. A thermodynamic analysis. Journal of Pharmaceutical Sciences 99, 1254-1264.

Murdande, S.B., Pikal, M.J., Shanker, R.M., Bogner, R.H., 2010b. Solubility Advantage of Amorphous Pharmaceuticals: II. Application of Quantitative Thermodynamic Relationships for Prediction of Solubility Enhancement in Structurally Diverse Insoluble Pharmaceuticals. Pharmaceutical Research 27, 2704-2714.

Murdande, S.B., Pikal, M.J., Shanker, R.M., Bogner, R.H., 2011. Solubility advantage of amorphous pharmaceuticals, part 3: Is maximum solubility advantage experimentally attainable and sustainable? Journal of Pharmaceutical Sciences 100, 4349-4356.

Naima, Z., Siro, T., Juan-Manuel, G.-D., Chantal, C., René, C., Jerome, D., 2001. Interactions between carbamazepine and polyethylene glycol (PEG) 6000: characterisations of the physical, solid dispersed and eutectic mixtures. European Journal of Pharmaceutical Sciences 12, 395-404.

Nair, R., Nyamweya, N., Gönen, S., Martínez-Miranda, L.J., Hoag, S.W., 2001. Influence of various drugs on the glass transition temperature of poly(vinylpyrrolidone): a thermodynamic and spectroscopic investigation. International Journal of Pharmaceutics 225, 83-96.

Nandiyanto, A.B.D., Okuyama, K., 2011. Progress in developing spray-drying methods for the production of controlled morphology particles: From the nanometer to submicrometer size ranges. Advanced Powder Technology 22, 1-19.

Newman, A., Knipp, G., Zografi, G., 2012. Assessing the performance of amorphous solid dispersions. Journal of Pharmaceutical Sciences 101, 1355-1377.

Newman, A., Zografi, G., 2014. Critical Considerations for the Qualitative and Quantitative Determination of Process-Induced Disorder in Crystalline Solids. Journal of Pharmaceutical Sciences 103, 2595-2604.

Nishi, T., Wang, T.T., 1975. Melting Point Depression and Kinetic Effects of Cooling on Crystallization in Poly(vinylidene fluoride)-Poly(methyl methacrylate) Mixtures. Macromolecules 8, 909-915.

Noyes, A.A., Whitney, W.R., 1897. THE RATE OF SOLUTION OF SOLID SUBSTANCES IN THEIR OWN SOLUTIONS. Journal of the American Chemical Society 19, 930-934.

O'Donnell, K.P., Cai, Z., Schmerler, P., Williams, R.O., 3rd, 2012. Atmospheric freeze drying for the reduction of powder electrostatics of amorphous, low density, high surface area pharmaceutical powders. Drug Development and Industrial Pharmacy.

O'Brien, L.E., Timmins, P., Williams, A.C., York, P., 2004. Use of in situ FT-Raman spectroscopy to study the kinetics of the transformation of carbamazepine polymorphs. Journal of Pharmaceutical and Biomedical Analysis 36, 335-340.

Oguchi, T., Yonemochi, E., Yamamoto, K., Nakai, Y., 1989. Freeze-Drying of Drug-Additive Binary Systems. II. : Relationship between Decarboxylation Behavior and

Molecular States of p-Aminosalicylic Acid. Chemical & Pharmaceutical Bulletin 37, 3088-3091.

Olabisi, O., Robeson, L.M., Shaw, M.T., 1979. Polymer-polymer miscibility. Academic Press, New York, NY.

Overhoff, K.A., Engstrom, J.D., Chen, B., Scherzer, B.D., Milner, T.E., Johnston, K.P., Williams III, R.O., 2007. Novel ultra-rapid freezing particle engineering process for enhancement of dissolution rates of poorly water-soluble drugs. European Journal of Pharmaceutics and Biopharmaceutics 65, 57-67.

Pajula, K., Taskinen, M., Lehto, V.-P., Ketolainen, J., Korhonen, O., 2010. Predicting the Formation and Stability of Amorphous Small Molecule Binary Mixtures from Computationally Determined Flory−Huggins Interaction Parameter and Phase Diagram. Molecular Pharmaceutics 7, 795-804.

Patterson, J.E., James, M.B., Forster, A.H., Lancaster, R.W., Butler, J.M., Rades, T., 2005. The influence of thermal and mechanical preparative techniques on the amorphous state of four poorly soluble compounds. Journal of Pharmaceutical Sciences 94, 1998-2012.

Patterson, J.E., James, M.B., Forster, A.H., Lancaster, R.W., Butler, J.M., Rades, T., 2007. Preparation of glass solutions of three poorly water soluble drugs by spray drying, melt extrusion and ball milling. International Journal of Pharmaceutics 336, 22-34.

Patterson, J.E., James, M.B., Forster, A.H., Rades, T., 2008. Melt Extrusion and Spray Drying of Carbamazepine and Dipyridamole with Polyvinylpyrrolidone/Vinyl Acetate Copolymers. Drug Development and Industrial Pharmacy 34, 95-106.

Paudel, A., Nies, E., Van den Mooter, G., 2012. Relating Hydrogen-Bonding Interactions with the Phase Behavior of Naproxen/PVP K 25 Solid Dispersions: Evaluation of Solution-Cast and Quench-Cooled Films. Molecular Pharmaceutics 9, 3301-3317.

Paudel, A., Van Humbeeck, J., Van den Mooter, G., 2010. Theoretical and Experimental Investigation on the Solid Solubility and Miscibility of Naproxen in Poly(vinylpyrrolidone). Molecular Pharmaceutics 7, 1133-1148.

Petit, S., Coquerel, G., 2006. The amorphous state, in: Hilfiker, R. (Ed.), Polymorphism. Wiley-VCH, Weinheim, Germany, pp. 259-285.

Pinto, E., Dürig, T., 2013. Cellulose Ethers for Extrusion Applications, in: Repka, M.A., Langley, N., DiNunzio, J. (Eds.), Melt Extrusion. Springer New York, pp. 123-144.

Powell, C.T., Xi, H., Sun, Y., Gunn, E., Chen, Y., Ediger, M.D., Yu, L., 2015. Fast Crystal Growth in o-Terphenyl Glasses: A Possible Role for Fracture and Surface Mobility. The Journal of Physical Chemistry B 119, 10124-10130.

Qian, F., Huang, J., Zhu, Q., Haddadin, R., Gawel, J., Garmise, R., Hussain, M., 2010. Is a distinctive single Tg a reliable indicator for the homogeneity of amorphous solid dispersion? International Journal of Pharmaceutics 395, 232-235.

Rao, R.N., Ramachandra, B., Vali, R.M., Raju, S.S., 2010. LC–MS/MS studies of ritonavir and its forced degradation products. Journal of Pharmaceutical and Biomedical Analysis 53, 833-842.

Raw, A.S., Furness, M.S., Gill, D.S., Adams, R.C., Holcombe Jr, F.O., Yu, L.X., 2004. Regulatory considerations of pharmaceutical solid polymorphism in Abbreviated New Drug Applications (ANDAs). Advanced Drug Delivery Reviews 56, 397-414.

Reitz, E., Vervaet, C., Neubert, R.H.H., Thommes, M., 2013. Solid crystal suspensions containing griseofulvin – Preparation and bioavailability testing. European Journal of Pharmaceutics and Biopharmaceutics 83, 193-202.

Repka, M.A., Gerding, T.G., Repka, S.L., McGinity, J.W., 1999. Influence of Plasticizers and Drugs on the Physical-Mechanical Properties of Hydroxypropylcellulose Films

Prepared by Hot Melt Extrusion. Drug Development and Industrial Pharmacy 25, 625-633.

Repka, M.A., Majumdar, S., Kumar Battu, S., Srirangam, R., Upadhye, S.B., 2008. Applications of hot-melt extrusion for drug delivery. Expert Opinion on Drug Delivery 5, 1357-1376.

Roberts, A.D., Zhang, H., 2013. Poorly water-soluble drug nanoparticles via solvent evaporation in water-soluble porous polymers. International Journal of Pharmaceutics 447, 241-250.

Rumondor, A.C.F., Marsac, P.J., Stanford, L.A., Taylor, L.S., 2009. Phase Behavior of Poly(vinylpyrrolidone) Containing Amorphous Solid Dispersions in the Presence of Moisture. Molecular Pharmaceutics 6, 1492-1505.

Rumondor, A.C.F., Taylor, L.S., 2010. Effect of Polymer Hygroscopicity on the Phase Behavior of Amorphous Solid Dispersions in the Presence of Moisture. Molecular Pharmaceutics 7, 477-490.

Rustichelli, C., Gamberini, G., Ferioli, V., Gamberini, M.C., Ficarra, R., Tommasini, S., 2000. Solid-state study of polymorphic drugs: carbamazepine. Journal of Pharmaceutical and Biomedical Analysis 23, 41-54.

Sacchetti, M., 1998. Thermodynamic analysis of moisture sorption isotherms. Journal of Pharmaceutical Sciences 87, 982-986.

Sacchetti, M., 2001. The General Form of the Gibbs-Duhem Equation for Multiphase/Multicomponent Systems and Its Application to Solid-State Activity Measurements. Journal of Chemical Education 78, 260.

Sarmah, A.K., Sabadie, J., 2002. Hydrolysis of Sulfonylurea Herbicides in Soils and Aqueous Solutions: a Review. Journal of Agricultural and Food Chemistry 50, 6253-6265.

Schenck, L., Troup, G.M., Lowinger, M., Li, L., McKelvey, C., 2010. Achieving a Hot Melt Extrusion Design Space for the Production of Solid Solutions, Chemical Engineering in the Pharmaceutical Industry. John Wiley & Sons, Inc., pp. 819-836.

Schroers, J., Masuhr, A., Johnson, W.L., Busch, R., 1999. Pronounced asymmetry in the crystallization behavior during constant heating and cooling of a bulk metallic glass-forming liquid. Physical Review B 60, 11855-11858.

Seem, T.C., Rowson, N.A., Ingram, A., Huang, Z., Yu, S., de Matas, M., Gabbott, I., Reynolds, G.K., 2015. Twin screw granulation — A literature review. Powder Technology 276, 89-102.

Serajuddin, A.T.M., 1999. Solid dispersion of poorly water-soluble drugs: Early promises, subsequent problems, and recent breakthroughs. Journal of Pharmaceutical Sciences 88, 1058-1066.

Shah, N., Iyer, R.M., Mair, H.-J., Choi, D.S., Tian, H., Diodone, R., Fähnrich, K., Pabst-Ravot, A., Tang, K., Scheubel, E., Grippo, J.F., Moreira, S.A., Go, Z., Mouskountakis, J., Louie, T., Ibrahim, P.N., Sandhu, H., Rubia, L., Chokshi, H., Singhal, D., Malick, W., 2013. Improved human bioavailability of vemurafenib, a practically insoluble drug, using an amorphous polymer-stabilized solid dispersion prepared by a solvent-controlled coprecipitation process. Journal of Pharmaceutical Sciences 102, 967-981.

Shah, N., Sandhu, H., Choi, D.S., Chokshi, H., Malick, A.W., 2014. Amorphous Solid Dispersions, Theory and Practice. Springer.

Shah, N., Sandhu, H., Phuapradit, W., Pinal, R., Iyer, R., Albano, A., Chatterji, A., Anand, S., Choi, D.S., Tang, K., Tian, H., Chokshi, H., Singhal, D., Malick, W., 2012. Development of novel microprecipitated bulk powder (MBP) technology for manufacturing stable amorphous formulations of poorly soluble drugs. International Journal of Pharmaceutics 438, 53-60.

Shamblin, S.L., Tang, X., Chang, L., Hancock, B.C., Pikal, M.J., 1999. Characterization of the Time Scales of Molecular Motion in Pharmaceutically Important Glasses. The Journal of Physical Chemistry B 103, 4113-4121.

Six, K., Berghmans, H., Leuner, C., Dressman, J., Van Werde, K., Mullens, J., Benoist, L., Thimon, M., Meublat, L., Verreck, G., 2003. Characterization of solid dispersions of itraconazole and hydroxypropylmethylcellulose prepared by melt extrusion, part II. Pharm Res 20, 1047-1054.

Soh, Y.S., Kim, J.H., Gryte, C.C., 1995. Phase behaviour of polymer/solvent/ non-solvent systems. Polymer 36, 3711-3717.

Stillinger, F.H., 1995. A topographic view of supercooled liquid and glass formation. Science 267, 1935-1939.

Stubberud, L., Arwidsson, H.G., Hjortsberg, V., Graffner, C., 1996. Water-Solid Interactions. III. Effect of Glass Transition Temperature, Tg, and Processing on Tensile Strength of Compacts of Lactose and Lactose/Polyvinyl Pyrrolidone. Pharmaceutical Development and Technology 1, 195-204.

Sumie Yoshioka, V.J.S., 2002. Chemical Stability of Drug Substances, Stability of Drugs and Dosage Forms. Springer US, Boston, MA, pp. 3-137.

Sun, D.D., Lee, P.I., 2015. Probing the mechanisms of drug release from amorphous solid dispersions in medium-soluble and medium-insoluble carriers. Journal of Controlled Release 211, 85-93.

Sun, Y., Tao, J., Zhang, G.G.Z., Yu, L., 2010. Solubilities of crystalline drugs in polymers: An improved analytical method and comparison of solubilities of indomethacin and nifedipine in PVP, PVP/VA, and PVAc. Journal of Pharmaceutical Sciences 99, 4023-4031.

Sunderland, T., Kelly, J.G., Ramtoola, Z., 2015. Application of a novel 3-fluid nozzle spray drying process for the microencapsulation of therapeutic agents using incompatible drug-polymer solutions. Archives of Pharmacal Research 38, 566-573.

Surana, R., Pyne, A., Suryanarayanan, R., 2004a. Effect of Aging on the Physical Properties of Amorphous Trehalose. Pharmaceutical Research 21, 867-874.

Surana, R., Pyne, A., Suryanarayanan, R., 2004b. Effect of Preparation Method on Physical Properties of Amorphous Trehalose. Pharmaceutical Research 21, 1167-1176.

Swarbrick, J., Boylan, J.C., 2000. Encyclopedia of Pharmaceutical Technology: Volume 20-Supplement 3. CRC Press.

Tackenberg, M.W., Krauss, R., Marmann, A., Thommes, M., Schuchmann, H.P., Kleinebudde, P., 2015. Encapsulation of liquids using a counter rotating twin screw extruder. European Journal of Pharmaceutics and Biopharmaceutics 89, 9-17.

Tackenberg, M.W., Thommes, M., Schuchmann, H.P., Kleinebudde, P., 2014. Solid state of processed carbohydrate matrices from maltodextrin and sucrose. Journal of Food Engineering 129, 30-37.

Tanno, F., Nishiyama, Y., Kokubo, H., Obara, S., 2004. Evaluation of Hypromellose Acetate Succinate (HPMCAS) as a Carrier in Solid Dispersions. Drug Development and Industrial Pharmacy 30, 9-17.

Tawa, M., Almarsson, O., Remenar, J., 2004. Pharmaceutical salts of zafirlukast. Google Patents.

Taylor, L.S., 2010. Physical Stability and Crystallization Inhibition, Pharmaceutical Sciences Encyclopedia. John Wiley & Sons, Inc.

Taylor, L.S., Zografi, G., 1998. Sugar–polymer hydrogen bond interactions in lyophilized amorphous mixtures. Journal of Pharmaceutical Sciences 87, 1615-1621.

Thiry, J., Krier, F., Evrard, B., 2015. A review of pharmaceutical extrusion: Critical process parameters and scaling-up. International Journal of Pharmaceutics 479, 227-240.

Tian, Y., Booth, J., Meehan, E., Jones, D.S., Li, S., Andrews, G.P., 2012. Construction of Drug–Polymer Thermodynamic Phase Diagrams Using Flory–Huggins Interaction Theory: Identifying the Relevance of Temperature and Drug Weight Fraction to Phase Separation within Solid Dispersions. Molecular Pharmaceutics 10, 236-248.

Tian, Y., Caron, V., Jones, D.S., Healy, A.-M., Andrews, G.P., 2014. Using Flory–Huggins phase diagrams as a pre-formulation tool for the production of amorphous solid dispersions: a comparison between hot-melt extrusion and spray drying. Journal of Pharmacy and Pharmacology 66, 256-274.

Timko, R.J., Bradway, R.J., Clements, A., 1999. Pharmaceutical agents. Google Patents.

Todd, D.B., 1998a. Plastics compounding: equipment and processing. Hanser Publishers.

Todd, D.B., 1998b. Practical Aspects of Processing in Intermeshing Twin Screw Extruders. Journal of Reinforced Plastics and Composites 17, 1607-1616.

Tsukushi, I., Yamamuro, O., Suga, H., 1994. Heat capacities and glass transitions of ground amorphous solid and liquid-quenched glass of tri-O-methyl-ß-cyclodextrin. Journal of Non-Crystalline Solids 175, 187-194.

Tsuzuki, S., Yoshida, M., Uchimaru, T., Mikami, M., 2001. The Origin of the Cation/π Interaction: The Significant Importance of the Induction in Li+ and Na+ Complexes. The Journal of Physical Chemistry A 105, 769-773.

Valle, G.D., Boché, Y., Colonna, P., Vergnes, B., 1995. The extrusion behaviour of potato starch. Carbohydrate Polymers 28, 255-264.

Van den Mooter, G., 2012. The use of amorphous solid dispersions: A formulation strategy to overcome poor solubility and dissolution rate. Drug Discovery Today: Technologies 9, e79-e85.

Vasconcelos, T., Marques, S., das Neves, J., Sarmento, B., 2016. Amorphous solid dispersions: Rational selection of a manufacturing process. Advanced Drug Delivery Reviews 100, 85-101.

Vasconcelos, T., Sarmento, B., Costa, P., 2007. Solid dispersions as strategy to improve oral bioavailability of poor water soluble drugs. Drug Discovery Today 12, 1068-1075.

Verreck, G., 2012. The Influence of Plasticizers in Hot-Melt Extrusion, Hot-Melt Extrusion: Pharmaceutical Applications. John Wiley & Sons, Ltd, pp. 93-112.

Verreck, G., Decorte, A., Heymans, K., Adriaensen, J., Liu, D., Tomasko, D., Arien, A., Peeters, J., Van den Mooter, G., Brewster, M.E., 2006. Hot stage extrusion of p-amino salicylic acid with EC using CO2 as a temporary plasticizer. International Journal of Pharmaceutics 327, 45-50.

Verreck, G., Six, K., Van den Mooter, G., Baert, L., Peeters, J., Brewster, M.E., 2003. Characterization of solid dispersions of itraconazole and hydroxypropylmethylcellulose prepared by melt extrusion—part I. International journal of pharmaceutics 251, 165-174.

Viridén, A., Wittgren, B., Larsson, A., 2009. Investigation of critical polymer properties for polymer release and swelling of HPMC matrix tablets. European Journal of Pharmaceutical Sciences 36, 297-309.

Wegiel, L.A., Mauer, L.J., Edgar, K.J., Taylor, L.S., 2013. Crystallization of amorphous solid dispersions of resveratrol during preparation and storage—Impact of different polymers. Journal of Pharmaceutical Sciences 102, 171-184.

West, D.R.F., Saunders, N., 2002. Ternary Phase Diagrams in Materials Science. Maney Publishing, London, UK.

Wood, J.H., Syarto, J.E., Letterman, H., 1965. Improved holder for intrinsic dissolution rate studies. Journal of Pharmaceutical Sciences 54, 1068-1068.

Yalkowsky, S.H., Banerjee, S., 1992. Aqueous Solubility: methods of estimation for organic compounds. Marcel Dekker, New York, NY.

Yang, W., Johnston, K.P., Williams III, R.O., 2010. Comparison of bioavailability of amorphous versus crystalline itraconazole nanoparticles via pulmonary administration in rats. European Journal of Pharmaceutics and Biopharmaceutics 75, 33-41.

Yonemochi, E., Inoue, Y., Buckton, G., Moffat, A., Oguchi, T., Yamamoto, K., 1999. Differences in Crystallization Behavior Between Quenched and Ground Amorphous Ursodeoxycholic Acid. Pharmaceutical Research 16, 835-840.

Yoshioka, S., Aso, Y., 2007. Correlations between molecular mobility and chemical stability during storage of amorphous pharmaceuticals. Journal of Pharmaceutical Sciences 96, 960-981.

Zaman, F., Beezer, A.E., Mitchell, J.C., Clarkson, Q., Elliot, J., Davis, A.F., Willson, R.J., 2001. The stability of benzoyl peroxide by isothermal microcalorimetry. International Journal of Pharmaceutics 227, 133-137.

Zhang, T., Huang, P., Shi, L., Su, Y., Zhou, L., Zhu, X., Yan, D., 2015. Self-Assembled Nanoparticles of Amphiphilic Twin Drug from Floxuridine and Bendamustine for Cancer Therapy. Molecular Pharmaceutics 12, 2328-2336.

Zhao, Y., Inbar, P., Chokshi, H.P., Malick, A.W., Choi, D.S., 2011. Prediction of the thermal phase diagram of amorphous solid dispersions by flory–huggins theory. Journal of Pharmaceutical Sciences 100, 3196-3207.

Zhou, D., Zhang, G.G.Z., Law, D., Grant, D.J.W., Schmitt, E.A., 2008. Thermodynamics, Molecular Mobility and Crystallization Kinetics of Amorphous Griseofulvin. Molecular Pharmaceutics 5, 927-936.

Vita

Siyuan Huang was born on December 19, 1989 in China. He graduated from Shuguang High School in 2008. After graduation, he was enrolled by Sun Yat-sen University (Guangzhou, China), and majored in Pharmaceutical Sciences. While pursuing his degree, he also served as an undergraduate research assistant in Professor Chuanbin Wu's laboratory from 2010 to 2012, investigating the mesoporous silica nanoparticle as a target drug delivery carrier. He was awarded "Outstanding Undergraduate Thesis" by Guangdong province based on his study in Professor Wu's group. As an undergraduate research assistant, he was also co-authored in two research articles. In 2012, he received his B.S. degree from Sun Yat-sen University, and determined to continue his study in the US. In August of 2012, he came to The University of Texas at Austin and joined the research lab of Dr. Robert O. Williams III in Pharmaceutics Program, specializing in the oral delivery of poorly water-soluble drug. As a graduate student, he has authored/co-authored 10 publications which have been submitted to or published in many leading journals, presented 6 abstracts describing his research at international conferences and also is a co-inventor on one patent application. He has also given one invited presentations at an international conference. Following graduation, he will continue his career at Eli Lilly and Company in Indianapolis, IN as a Formulation Scientist.

Email: Hsy_08@utexas.edu

This dissertation was typed by the author.